

**EFFICIENCY ENHANCEMENT OF SOLUTION PROCESSED  
ORGANIC LIGHT EMITTING DIODES (OLEDs)**

**YEOH KEAT HOE**

**THESIS SUBMITTED IN FULFILLMENT OF THE  
REQUIREMENTS FOR THE DEGREE OF  
DOCTOR OF PHILOSOPHY**

**DEPARTMENT OF PHYSICS  
FACULTY OF SCIENCE  
UNIVERSITY OF MALAYA  
KUALA LUMPUR**

**2014**



# UNIVERSITY MALAYA

## ORIGINAL LITERARY WORK DECLARATION

Name of Candidate: YEOH KEAT HOE

(I.C/Passport No:820108-08-5725)

Registration/Matric No: SHC110032

Name of Degree: DOCTOR OF PHILOSOPHY

Title of ~~Project Paper/Research Report/Dissertation~~/Thesis ("this Work"):

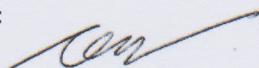
EFFICIENCY ENHANCEMENT OF SOLUTION PROCESSED ORGANIC LIGHT EMITTING DIODES (OLEDs)

Field of Study: ORGANIC ELECTRONICS

I do solemnly and sincerely declare that:

- (1) I am the sole author/writer of this Work;
- (2) This Work is original;
- (3) Any use of any work in which copyright exists was done by way of fair dealing and for permitted purposes and any excerpt or extract from, or reference to or reproduction of any copyright work has been disclosed expressly and sufficiently and the title of the Work and its authorship have been acknowledged in this Work;
- (4) I do not have any actual knowledge nor do I ought reasonably to know that the making of this work constitutes an infringement of any copyright work;
- (5) I hereby assign all and every rights in the copyright to this Work to the University of Malaya ("UM"), who henceforth shall be owner of the copyright in this Work and that any reproduction or use in any form or by any means whatsoever is prohibited without the written consent of UM having been first had and obtained;
- (6) I am fully aware that if in the course of making this Work I have infringed any copyright whether intentionally or otherwise, I may be subject to legal action or any other action as may be determined by UM.

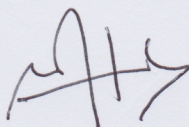
Candidate's Signature:



Date: 1/7/2014

Subscribed and solemnly declared before,

Witness's Signature:



Date: 11/7/14

Name:

Professor Dr. Wan Haliza Abdul Majid

Designation:

Labatan Fizik  
Universiti Malaya  
50603 Kuala Lumpur



## ABSTRACT

This research aims at improving the efficiency of solution processed organic light emitting diodes (OLEDs). The first part of this research work involved investigating the effects of Triton X-100 in a single layer solution processed blue phosphorescent OLED (PHOLED) with poly(vinylcarbazole) (PVK) and 1,3-bis[(4-tertbutylphenyl)-1,3,4-oxadiazolyl] phenylene (OXD-7) as host and bis(4,6-difluorophenylpyridinato-N,C2)picolinateiridium (FIrpic) act as guest. Results indicate that the addition of Triton X-100 into the emissive layer (EML) can provide spatial separation between the guest-host which reduces the back energy transfer from the high triplet FIrpic to the low triplet PVK. The addition of Triton X-100 also increased the EML film roughness which is beneficial for electron injection at the cathode as evidenced from the Atomic Force Microscopy (AFM) images, single carrier devices characteristics and photovoltaic measurements. Blue PHOLED with efficiency 8.5 lm/W at 1000 cd/m<sup>2</sup> was achieved by adding Triton X-100 into the EML. This efficiency is comparable to the best efficiency of a single layer solution processed blue PHOLED reported to date.

The effects of perfluorinated ionomer (PFI) doped poly(ethylenedioxythiophene):polystyrenesulfonate (PEDOT:PSS) as hole injection layer (HIL) in a single layer solution processed blue PHOLED was investigated. A systematic study on the interplay of PFI concentrations, device efficiency, PEDOT:PSS thin film conductivity and transparency were carried out to determine the optimum amount of PFI to yield the best blue PHOLED efficiency. Compared to the control device, the optimized device efficiencies improved from 7.3 lm/W and 5.9 lm/W to 9.4 lm/W and 7.9 lm/W at 100 cd/m<sup>2</sup> and 1000 cd/m<sup>2</sup> respectively.

We successfully demonstrated that the efficiency of a single layer solution processed yellow fluorescent OLED can be increased markedly by treating the EML surface with fluorinated alcohol. The fluorinated alcohol treatment improves the device efficiency to 19.3 lm/W at 1000 cd/m<sup>2</sup> which corresponds to ~74% increment compared to the control device. To the best of our knowledge, this power efficiency is one of the best reported to date for a solution processed yellow fluorescent OLED. The improvement is attributed to the formation of a surface dipole layer induced by the fluorinated alcohol which effectively lowered the cathodic injection barrier. It was further shown that solvent with higher dipole moment is better in passivating traps on the EML surface. This could be another reason for the high efficiency yellow OLED achieved using fluorinated alcohol treatment.

The final part of this research work involved the developments of high efficiency double layer solution processed blue PHOLED. The first emissive layer consists of PVK and FIrpic mixed with 4,4',4''-tris(N-carbazolyl)-triphenylamine (TCTA) or OXD-7. The second layer consists of an alcohol-soluble 2,7-bis(diphenylphosphoryl)-9,9'-spirobi(fluorene) (SPP013) and FIrpic. The incorporation of OXD-7 into PVK blurs the interface between the emissive layers heterojunction and widens the recombination zone while blending TCTA into PVK reduces the hole injection barrier from PEDOT:PSS to the first emissive layer. The best blue device gave an acceptable power efficiency of 11 lm/W at 1000 cd/m<sup>2</sup>, which is comparable to the best reported fully solution processed multi layer blue PHOLED reported to date.



## ABSTRAK

Objektif penyelidikan dalam tesis ini adalah untuk meningkatkan kecekapan organik diod pemancar cahaya (OLED). Bahagian pertama penyelidikan ini melibatkan kajian kesan Triton X-100 dalam fosforesen OLED (PHOLED) biru. Peranti ini berlapisan tunggal dan difabrikasi melalui kaedah pemprosesan basah. Peranti ini menggunakan poly(vinylcarbazole) (PVK) dan 1,3-bis[(4-tertbutylphenyl)-1,3,4-oxadiazolyl] phenylene (OXD-7) sebagai hos yang didop dengan bis(4,6-difluorophenylpyridinato-N,C2)picolinatoiridium (FIrpic). Penambahan Triton X-100 ini memisahkan hos dari FIrpic. Pemisahan ini mengurangkan pemindahan tenaga dari FIrpic yang bertenaga triplet tinggi ke PVK yang tenaga tripletnya rendah. Selain itu, Triton X-100 juga menyebabkan morfologi lapisan aktif OLED menjadi lebih kasar. Ini secara langsung menyenangkan proses penyuntikan electron dari katod peranti OLED. Kesan ini boleh diperhatikan dari imej Mikroskopi Tenaga Atomik (AFM), ketumpatan arus (J) – voltan (V) bagi peranti arus tunggal dan keputusan pencirian fotovoltik. Melalui kaedah ini, PHOLED biru dengan kecekapan 8.5 lm /W ( $1000\text{cd/m}^2$ ) berjaya diperoleh. Kecekapan ini setanding dengan kecekapan tertinggi yang pernah direkod sebelum ini bagi PHOLED biru berlapisan tunggal yang dihasilkan melalui kaedah pemprosesan basah.

Kesan penambahan perfluorinated ionomer (PFI) ke dalam poly(ethylenedioxythiophene):polystyrenesulfonate (PEDOT:PSS) telah dikaji sebagai lapisan penyuntikan lohong (HIL) dalam OLED. Kajian terhadap interaksi di antara kuantiti PFI, konduktiviti dan tahap ketelusan filem nipis PEDOT:PSS telah dijalankan secara bersistematik bagi menentukan kuantiti PFI yang optimum bagi menghasilkan kecekapan PHOLED biru yang tertinggi. Berbanding dengan peranti kawalan, peranti

yang telah dioptimum melihatkan penaingkatan kecekapan dari 7.3 lm/W dan 5.9 lm/W ke 9.4 lm/W dan 7.9 lm/W pada 100 cd/m<sup>2</sup> dan 1000 cd/m<sup>2</sup>.

Di samping itu, kami berjaya menghasilkan fluorezen OLED kuning yang mempunyai kecekapan yang tinggi dengan merawat lapisan aktif pemancar (EML) dengan menggunakan alkohol berfluorin. Peranti ini berlapisan tunggal dan dihasilkan melalui kaedah pemprosesan basah. Teknik ini berjaya memberikan kecekapan 19.3 lm/W pada 1000 cd/m<sup>2</sup>, iaitu peningkatan sebanyak ~74% berbanding dengan peranti kawalan. Kecekapan ini adalah antara yang tertinggi pernah dilaporkan bag fluorezen OLED kuning yang difabrikasi melalui kaedah pemprosesan basah. Peningkatan ini disebabkan oleh pembentukan permukaan dipol pada EML oleh alkohol berfluorin. Melalui permukaan dipol ini, tenaga penghalang di katod peranti dapat direndahkan dan ini memudahkan penyuntikan electron. Tambahan pula, kami mendapati bahawa alkohol yang berdipol momen tinggi adalah lebih efektif dalam mengurangkan perangkap pada permukaan EML. Ini juga merupakan salah satu faktor yang menyebabkan peningkatan kecekapan pada OLED yang dirawat dengan alkohol berfluorin.

Bahagian terakhir dalam kerja penyelidikan ini melibatkan rekabentuk PHOLED biru yang terdiri daripada dua lapisan aktif pemancar. Peranti ini difabrikasi melalui kaedah pemprosesan basah. Lapisan aktif pemancar pertama terdiri daripada PVK dan FIrpic dicampur dengan 4,4',4''-tris(N-carbazolyl)-triphenylamine (TCTA) atau OXD-7. Lapisan kedua pula terdiri daripada alkohol boleh-larut 2,7-bis(diphenylphosphoryl)-9,9'-spirobi(fluorine) (SPP013) dan FIrpic. Penambahan OXD-7 ke dalam PVK mengaburkan simpang hetero di antara lapisan pemancar yang akan melebarkan zon rekombinasi. Penambahan TCTA ke dalam PVK pula mengurangkan tenaga penghalang bagi penyuntikan lohong dari PEDOT:PSS ke PVK. Peranti terbaik kami memberikan kecekapan 11 lm/W pada 1000 cd/m<sup>2</sup>. Nilai ini adalah standing dengan

nilai terbaik yang pernah dilaporkan bagi PHOLED biru berlapisan kembar yang difabrikasi melalui kaedah pemprosesan basah.



## ACKNOWLEDGEMENT

I take great joy in acknowledging the following people who have contributed throughout my studies in University Malaya (UM).

Dr. Woon Kai Lin, my research supervisor who has gave me a lot of freedom to run my experiment. I appreciate his financial assistance, trust and confidence given to me during my stay here in UM. I thank him for his suggestions and helps in going through the obstacles in paper publications.

Prof Wan Haliza is another person I must thank. Her role during my last stage of my doctoral program has been very essential and instrumental to the sucess of this thesis. This thesis would not have been in this present form without many constructive feedback and inputs from Prof Wan Haliza, Prof Mary O' Neill and Prof Masahiro Funahashi. I am especially thankful to Prof Saadah, Prof Sithi Muniandy and Prof Halijah for serving my thesis commitee.

Dr. Li Jingqi who is currently attached to King Abdullah University of Technology (KAUST), Saudi Arabia deserves a lot of credits for his guidance and assistance given to me when I was in Prof Zhang's group (NTU). I am indebted to Prof Zhang for giving me a wonderful opportunity to join his research team and learn under Dr. Li Jingqi. I thank Dr. Li Jingqi for willing to spend some of his time in training me to become an experimentalist. I admire his superb intuitive mind picking up the right materials and the right experimental methods to prove his concept.

I am very grateful to Prof Ong Duu Sheng (MMU) and Dr. Yoon Tiem Leong (USM). They have helped me a lot when I decided to leave the industry to pursue my doctoral studies. I appreciate all the encouragement and support from Prof Ong over these years.

I would like to thank my collaborator, Assoc Prof Azhar Ariffin in chemistry department UM for giving me free access to FTIR measurement and some of his labs facilities.

I would like to extend my thanks to our collaborators, Prof Prayoon Songsiriritthigul (NANOTEC-SUT, Thailand), Dr. Hideki Nakajima and his BL3.2a beamline team in Synchrotron Light Research Institute (SLRI, Thailand) for their professional service and advice on the XPS/UPS characterizations.

Prof Chen Chin-Ti from Academia Sinica, Taiwan whom I met in EL 2012, HKBU, Hong Kong has been a great help to me. I thank him for answering all my fundamental questions on OLED fabrication patiently.

I am thankful to my research group members, past and present that I have spent a great amount of time with them during my stay in UM. It was a good experience to work with Dr. Thomas Whitcher who has helped me in XPS/UPS measurements. I thank Chua for the efficient glovebox management and maintenance. A big thank you goes to Azrina and Calvin for assisting me in device fabrication and characterizations. Thank you to Karwei for providing me some of the chemical that I need for device fabrication. I am thankful to Lih Wei, Boon Ki, Faisal, Ga Sing and Malcom for being great friends during these years and also not forgetting Wah Seng and Siew Yoong, two highly talented new member in our research group.

I must also thank Pn Norlela for taking care of the lab and ensuring all the invoices are paid promptly. I acknowledge the generous funding from MOSTI e-science (16-02-03-6030), ItraMAS Corporation and Postgraduate Research Fund– PPP (PG112-2012B).

I am indebted to my parents support throughout my doctoral studies. Without their support, my PhD studies would not have been possible.

Lastly, I would like to dedicate the virtue arising from this work to the long life of my Nyingmapa guru and all the great spiritual masters who uphold the pure teachings of the Buddha for the benefits of others. I bow to them.

*Keat Hoe*

*Kuala Lumpur, 2014*



## TABLE OF CONTENTS

ABSTRACT .....	ii
ABSTRAK .....	v
ACKNOWLEDGEMENT .....	viii
TABLE OF CONTENTS .....	xi
LIST OF FIGURES .....	xvi
LIST OF TABLES .....	xxi
LIST OF ABBREVIATIONS .....	xxii
LIST OF SYMBOLS .....	xxv
CHAPTER 1: Introduction .....	1
1.1    Introduction .....	1
1.2    History of organic electroluminescence .....	2
1.3    Motivations and objectives .....	3
1.4    Organisation of the thesis .....	4
CHAPTER 2: Literature review .....	7
2.1    Organic light emitting diode (OLED) device physics .....	7
2.1.1    What is CT states? .....	8
2.2    Fluorescence vs Phosphorescence .....	9
2.2.1    Quantum efficiency .....	12

2.2.2	Efficiency roll-off in OLED .....	13
2.3	Exciton formation model .....	15
2.4	Energy transfer process between a host doped with phosphorescent dye ....	19
2.5	OLED fabrication process .....	21
2.5.1	Vacuum deposition method.....	22
2.5.2	Wet process .....	23
2.5.2.1	Spin coating method .....	24
2.5.2.2	Blade-spin method .....	25
2.5.2.3	Blade-only method.....	27
2.5.2.4	Inkjet printing .....	27
2.6	Small molecule vs polymer OLED .....	28
2.7	Multilayer vs single layer OLED.....	31
2.7.1	Anode .....	34
2.7.2	Hole injection layer (HIL) .....	37
2.7.3	Hole transport layer (HTL).....	39
2.7.4	Emissive layer (EML) .....	40
2.7.5	Electron transport layer (ETL) .....	40
2.7.6	Electron injection layer (EIL) / cathode interfacial material.....	41
2.7.7	Cathode.....	43

CHAPTER 3: Experimental methods.....	45
3.1    Introduction.....	45
3.2    OLED fabrication process .....	45
3.3    Current density-voltage-luminance (J-V-L) measurement.....	48
3.3.1    Photovoltaic measurement of OLED.....	50
3.4    Fourier transforms infrared (FTIR) spectroscopy.....	52
3.5    Ultraviolet-visible (UV-Vis) absorption spectroscopy .....	53
3.6    Surface profiler .....	56
3.7    Atomic force microscopy (AFM) .....	57
3.8    4-point probe.....	60
3.9    Photoluminescence (PL) measurement .....	61
3.10    X-Ray Photoelectron Spectroscopy (XPS).....	62
 CHAPTER 4: Efficiency enhancement of a single layer solution processed blue phosphorescent organic light emitting diode (PHOLED) by using Triton X-100 .....	 64
4.1    Introduction.....	64
4.2    Experimental.....	67
4.3    J- V –L and efficiency characteristics.....	68
4.4    Shielding of triplet energy transfer by Triton X-100.....	71
4.5    Effects of surface morphology in device efficiency enhancement.....	74
4.6    Summary.....	80



CHAPTER 5: Efficiency enhancement of a single layer solution processed phosphorescent organic light emitting diodes via hole injection layer modification..... 82

5.1	Introduction.....	82
5.2	Experimental.....	84
5.3	J-V-L and efficiency characteristics .....	86
5.4	Conductivity characterizations. ....	90
5.5	Optical characterizations .....	91
5.6	Surface morphology characterizations.....	92
5.7	Summary.....	94

CHAPTER 6: High efficiency solution processed single layer fluorescent yellow OLED through fluorinated alcohol treatment at the emissive layer/cathode interface..... 95

6.1	Introduction.....	95
6.2	Experimental.....	97
6.3	J-V-L and efficiency characteristics .....	98
6.4	Photovoltaic measurement and single carrier devices .....	103
6.5	XPS characterizations .....	106
6.6	Optical characterizations .....	108
6.7	Surface morphology.....	109
6.8	Summary .....	110

CHAPTER 7: High efficiency double emissive solution processed blue PHOLED ....	111
7.1    Introduction.....	111
7.2    Experimental.....	114
7.3    J-V-L characteristics and efficiencies of the TCTA doped devices .....	115
7.4    J-V -L characteristics and efficiencies of the OXD-7 doped devices.....	118
7.5    Blurring effects and reduction of hole injection barrier .....	121
7.6    Photovoltaic measurement and single carrier devices .....	123
7.7    Validation of orthogonal film formation .....	126
7.8    Optical characterizations .....	127
7.9    Summary.....	128
CHAPTER 8: Summary and future works .....	129
8.1    Summary .....	129
8.2    Future works .....	132
REFERENCES.....	134
LIST OF PUBLICATIONS AND PAPERS PRESENTED .....	152

## LIST OF FIGURES

<b>Figure 2.1:</b> (a) Simplified diagram of a basic OLED device structure. (b) OLED energy level diagram during operation. Figure 2.1b is adapted from (Pereira, 2012).	8
<b>Figure 2.2:</b> Formation of excitons via CT states. $r_c$ and $r_k$ is temperature dependent. ISC denotes intersystem crossing which will be discussed in section 2.2. Adapted from (Segal et al., 2003).	9
<b>Figure 2.3:</b> Simplified Jablonski Diagram showing fluorescent and phosphorescent OLED system.	12
<b>Figure 2.4:</b> Exciton dissociation in guest due to presence of electric field. Adapted from (Luo et al., 2006)	14
<b>Figure 2.5:</b> Exciton formation model for the following condition: (a) No mixing occur, (b) exciton mixing, producing phosphorescence emission due to spin-orbit coupling (SOC), (c) thermal activation delay fluorescence process and (d) mixing occur at the CT states. $\eta$ denotes quantum efficiency whereas $k_s$ , $k_T$ and $k_m$ denotes singlet and triplet excitons formation rate and CT states mixing rate respectively. Adapted from (Reineke & Baldo, 2012).	16
<b>Figure 2.6:</b> Schematic diagram of TDAF in enhancing the fluorescence emission.	17
<b>Figure 2.7:</b> Exciton formation model based on CT state mixing. The formation rate of singlet CT states is given as $G$ . $k_{TS}$ and $k_{ST}$ denote the mixing rate from triplet to singlet and singlet to triplet respectively. $^3CT$ , $^1CT$ , $k_s$ , $k_T$ , $k_{ISC}$ , $S_1$ and $T_1$ denote triplet CT state, singlet CT state, singlet exciton formation rate, triplet exciton formation rate, inter system crossing rate, singlet state and triplet state respectively. Adapted from (Segal et al., 2007).	18
<b>Figure 2.8:</b> (a) Förster energy transfer and (b) Dexter energy transfer. (c) Energy diagram showing Förster and Dexter energy transfer process for a fluorescent/phosphorescent guest-host system. The singlet excited state, ground state and triplet excited state are denoted as $S_1$ , $S_0$ and $T_1$ respectively.	20
<b>Figure 2.9:</b> Light emission induced by charge trapping mechanism in a guest/host system.	21
<b>Figure 2.10:</b> Schematic diagram of the vacuum deposition method for OLED thin film deposition.	23
<b>Figure 2.11:</b> Schematic diagram of the spin coating process for OLED thin film deposition.	25

<b>Figure 2.12:</b> Blade-spin method for OLED thin film deposition. Adapted from (C. Y. Chen et al., 2011).	26
<b>Figure 2.13:</b> Schematic diagram of the blade-only coating process.	27
<b>Figure 2.14:</b> Schematic diagram of the inkjet printing process.	28
<b>Figure 2.15:</b> Thin film formation using (a) polymer and (b) small molecule solution. Adapted from (Duan et al., 2010a).	30
<b>Figure 2.16:</b> Schematic diagram of a (a) multilayer and (b) single layer OLED.	33
<b>Figure 2.17:</b> Workfunction ( $e\phi_m$ ) enhancement of ITO induced by In-Cl surface dipole. From (Helander et al., 2011).	36
<b>Figure 3.1:</b> (a) Photolithography mask and the ITO pattern dimensions. (b) Development of ITO in AZ developer diluted with DI water. (c) ITO substrate after HCl etch and (d) ITO after photoresist stripping.	46
<b>Figure 3.2:</b> (a) OLED fabrication process. (b) Photograph of an actual device. The device consists of six active areas, denoted by P1 –P6. (c) Simplified diagram indicating the cross section of a single pixel. (d) An actual light up blue device.	47
<b>Figure 3.3:</b> I-V-L measurement setup. DUT denotes device under test.	49
<b>Figure 3.4:</b> An example of the photovoltaic measurement results of a OLED.	51
<b>Figure 3.5:</b> (a) Schematic diagram of FTIR spectroscopy setup and (b) FTIR ATR operation principles. Adapted from (S. Zhang et al., 2009) and ( <a href="http://www.piketech.com/information.html">http://www.piketech.com/information.html</a> ).	53
<b>Figure 3.6:</b> Possible electronic transitions of organic compound.	54
<b>Figure 3.7:</b> Schematic diagram of a UV-Vis spectroscopy setup. Adapted from ( <a href="http://www2.chemistry.msu.edu/faculty/reusch/virttxtjml/spectrpy/uv-vis/uvspec.htm">http://www2.chemistry.msu.edu/faculty/reusch/virttxtjml/spectrpy/uv-vis/uvspec.htm</a> )	55
<b>Figure 3.8:</b> Simplified schematic diagram of a surface profiler. Adapted from ( <a href="http://www.ptb.de/cms/en/fachabteilungen/abt5/fb-51/ag515/tastschnittverfahren0.html">www.ptb.de/cms/en/fachabteilungen/abt5/fb-51/ag515/tastschnittverfahren0.html</a> )	56
<b>Figure 3.9:</b> Schematic diagram of a AFM setup.	57
<b>Figure 3.10:</b> (a) Variation of the atomic force as a function of tip separation. (b) Height detection by AFM cantilever tip operated in contact mode. Adapted from ( <a href="http://www.nanoscience.com/education/afm.html">www.nanoscience.com/education/afm.html</a> )	58
<b>Figure 3.11:</b> Step profile detection through the changes of cantilever tip oscillation amplitude.	59
<b>Figure 3.12:</b> Phase imaging by AFM. Adapted from ( <a href="http://www.bruker.jp/axs/nano/imgs/pdf/AN011.pdf">www.bruker.jp/axs/nano/imgs/pdf/AN011.pdf</a> )	59
<b>Figure 3.13:</b> Schematic diagram of a 4-point probe setup.	60

<b>Figure 3.14:</b> Typical setup of a photoluminescence spectrometer. Adapted from ( <a href="http://www.chemistry.adelaide.edu.au/external/soc-rel/content/mol-fluo.htm">www.chemistry.adelaide.edu.au/external/soc-rel/content/mol-fluo.htm</a> ).....	62
<b>Figure 3.15:</b> Simplified diagram of the XPS setup. ....	63
<b>Figure 4.1:</b> Some of the best single layer solution processed blue PHOLED reported to date. The efficiencies are benchmarked at 1000 cd/m <sup>2</sup> .....	65
<b>Figure 4.2:</b> Schematic diagram of (a) device architecture (b) energy level diagram and (c) molecular structure of the materials used. ....	68
<b>Figure 4.3:</b> J-V-L characteristics of the blue devices with different concentrations of Triton X-100. ....	69
<b>Figure 4.4 :</b> (a) Current efficiency and (b) power efficiency vs brightness of blue PHOLEDs doped with different concentrations Triton X-100. ....	70
<b>Figure 4.5:</b> Normalized PL spectra of PVK:OXD-7:Flrpic thin film doped with different concentration of Triton X-100. Inset is the expanded view of PL in region of 320 nm to 400 nm. ....	72
<b>Figure 4.6:</b> FTIR absorbance spectra on (a) PVK, OXD-7, Flrpic, Triton X-100, and (b) PVK:OXD-7:Flrpic (100:40:10 wt/wt/wt) and PVK:OXD-7:Flrpic:Triton X-100 (100:40:10:3.2 wt/wt/wt/wt). ....	73
<b>Figure 4.7:</b> AFM topographical height images and cross-sectional line profile of the solution processed EML film doped with: (a)-(c) 0 wt% (d)-(f) 0.8 wt%, (g)-(i) 3.2 wt% and (j)- (l) 10 wt% of Triton X-100. The surface roughness of the EML films for 0 wt%, 0.8 wt%, 3.2 wt% and 10 wt% is 0.443 nm rms, 0.64 nm rms, 0.703 nm rms and 3.23 nm rms respectively. The white line in (b), (e), (h), (k) indicate the location where the cross sectional line profile is taken. Inset in (c), (f), (i) is the expanded view of the corresponding graphs. ....	75
<b>Figure 4.8:</b> 2D PSD curves of the EL film doped with Triton X-100. Arrows indicate the slope of the PSD curves. ....	77
<b>Figure 4.9:</b> Photovoltaic characteristics of the blue devices with different concentrations of Triton X-100 in the EMLs. ....	79
<b>Figure 4.10:</b> Current density-voltage characteristics of electron dominated and hole dominated devices of the blue PHOLEDs with 0 wt% and 3.2 wt% of Triton X-100. ..	80
<b>Figure 5.1:</b> Some of the best single layer solution processed blue PHOLED reported to date. The efficiencies are benchmarked at 1000 cd/m <sup>2</sup> .....	83
<b>Figure 5.2:</b> Schematic diagram of (a) device architecture (b) energy level diagram and (c) molecular structure of the materials used. ....	85

<b>Figure 5.3:</b> J-L-V characteristics of the blue devices with different amount of PFI doped into PEDOT:PSS. ....	86
<b>Figure 5.4:</b> (a) Current efficiency and (b) power efficiency of the blue devices. ....	87
<b>Figure 5.5:</b> J-V characteristics of hole dominated devices of the blue PHOLEDs with different concentrations of PFI doping in the PEDOT:PSS. ....	89
<b>Figure 5.6:</b> Conductivity of pristine PEDOT:PSS and PEDOT:PSS blended with different amount of PFI. The thin film conductivity was measured using 4-point probe. ....	90
<b>Figure 5.7:</b> Transmittance spectra of pristine PEDOT:PSS film, PFI film and PFI doped PEDOT:PSS film. ....	91
<b>Figure 5.8:</b> PL and absorption (Abs) spectra of the devices EML which consists of PVK (60 wt%):OXD-7 (30 wt%):FIrpic (10 wt%). ....	92
<b>Figure 5.9:</b> AFM phase images of the PEDOT: PSS:PFI (wt/wt/wt) film. ....	93
<b>Figure 6.1:</b> Some of the best solution processed yellow fluorescent OLED reported to date. The efficiencies are benchmarked at 1000 cd/m <sup>2</sup> ....	96
<b>Figure 6.2:</b> (a) Device structure, (b) energy level diagram of the yellow device and (c) molecular structure of 2,2,3,3,4,4,5,5-Octafluoro-1-pentanol and SY-PPV. ....	98
<b>Figure 6.3:</b> J-V-L characteristics of the yellow OLEDs. ....	99
<b>Figure 6.4:</b> (a) Current efficiency and (b) power efficiency of the SY-PPV devices. .	100
<b>Figure 6.5:</b> Energy level diagram at the SY-PPV/cathode interface for (a) device without treatment and (b) device with ethanol or fluorinated alcohol treatment. $\Delta$ and $\phi$ denotes the vacuum level shift and cathode work function respectively. ....	102
<b>Figure 6.6:</b> Photovoltaic response of the yellow OLED devices. ....	103
<b>Figure 6.7:</b> J-V characteristics of the electron/hole current dominated devices. Hollow symbols denote hole current dominated devices whereas solid symbols denote electron current dominated devices. ....	104
<b>Figure 6.8:</b> J-V characteristics of the electron current dominated devices. Inset is the slope calculated from the device J-V curves plotted on the double logarithmic scale. Red lines are only guide to eyes only. ....	105
<b>Figure 6.9:</b> XPS spectra of the SY-PPV thin samples. Inset is the expanded view of the spectra in the region of 680 eV to 698 eV. The F 1s can be detected for the samples treated with fluorinated alcohol. ....	107
<b>Figure 6.10:</b> Absorption (hollow symbol) and PL (filled symbol) of the SY-PPV thin film. ....	108

<b>Figure 6.11:</b> AFM images of the (a) pristine, (b) ethanol treated and (c) fluorinated alcohol treated SY-PPV thin film. ....	109
<b>Figure 7.1:</b> Efficiencies of fully solution processed multi layer blue PHOLED reported to date. The efficiencies are benchmarked at 1000 cd/m <sup>2</sup> .....	113
<b>Figure 7.2:</b> Schematic diagram of (a) device architecture (b) energy level diagram and (c) molecular structure of the materials used. ....	115
Figure 7.3: J-L-V characteristics of the blue devices doped with different concentrations of TCTA. ....	116
<b>Figure 7.4:</b> (a) Power efficiency and (b) current efficiency vs brightness of blue PHOLED with different concentrations of TCTA. ....	117
<b>Figure 7.5:</b> J-L-V characteristics of the blue devices doped with different concentrations of OXD-7. ....	119
<b>Figure 7.6:</b> (a) Power efficiency and (b) current efficiency vs brightness of blue PHOLED with different concentrations of OXD-7. ....	120
<b>Figure 7.7:</b> Energy level diagram (a) of the control devices, (b) device with 40 wt% TCTA doped into the first emissive layer. The effective hole barrier height is reduced due to the favourable HOMO level alignment. (c) The addition of 40 wt% of OXD-7 provides an additional path for electron to hop into the first emissive layer. Black dotted line in (b) and (c) indicate HOMO/LUMO level of TCTA and OXD-7 respectively. The HOMO/LUMO of FIrpic is denoted by blue dotted line.....	122
<b>Figure 7.8:</b> Photovoltaic response of the blue devices.....	124
<b>Figure 7.9:</b> Current density characteristics of the hole-dominated (empty symbols) ITO/PEDOT:PSS/first EML/second EML/Au and electron-dominated ITO/LiF/first EML/second EML/LiF/Al (filled symbols) devices. ....	125
<b>Figure 7.10:</b> Comparison of the thin films absorbance and thickness after being washed with IPA. The film consists of (a) PVK:FIrpic (100:10 wt/wt) (b) PVK:TCTA:FIrpic (100:40:10 wt/wt/wt) and (c) PVK:OXD-7:FIrpic (100:40:10 wt/wt/wt). ....	127
<b>Figure 7.11:</b> Absorption (hollow symbols) and PL (filled symbols) spectra of control, 40 wt% TCTA and 40 wt% blue PHOLEDs.....	128

## LIST OF TABLES

<b>Table 4.1:</b> Blue PHOLEDs performances at different concentrations of Triton X-100 doping.....	71
<b>Table 5.1:</b> PEDOT:PSS work function with different concentrations of PFI. Taken from (T. W. Lee et al., 2007). .....	84
<b>Table 5.2:</b> Blue PHOLEDs performances with different amount of PFI blended into PEDOT:PSS. ....	88
<b>Table 6.1:</b> Yellow OLEDs performances with different type of alcohol treatment. ....	100
<b>Table 7.1:</b> Blue PHOLEDs performances with different concentrations of TCTA. ....	118
<b>Table 7.2:</b> Blue PHOLEDs performances with different concentrations of OXD-7. ..	121
<b>Table 7.3:</b> Comparison of the first layer film thickness after being washed by IPA ...	126
<b>Table 8.1:</b> Summary of the OLED devices performance and optimization techniques carried out in this research work. The efficiency are benchmarked at 1000 cd/m <sup>2</sup> . ....	131



## LIST OF ABBREVIATIONS

AFM	Atomic force microscopy
Al	Aluminium
ATR	Attenuated total reflection
Au	Aurum
BPhen	4,7-diphenyl-1,10-phenanthroline
CBP	4,4'-bis(carbazol-9-yl)biphenyl
CE	Current efficiency
CFL	Compact fluorescent lamp
Cl	Chlorine
Cs	Caesium
Cs <sub>2</sub> CO <sub>3</sub>	Caesium carbonate
CsF	Caesium fluoride
CT	Charge transfer
DI	Deionized
DUT	Device under test
EIL	Electron injection layer
EL	Electroluminescence
EML	Emissive layer
EQE	External quantum efficiency
ETL	Electron transport layer
ETM	Electron transport material
FIrpic	Bis(4,6-difluorophenylpyridinato-N,C2)picolinateiridium
FTIR	Fourier transforms infrared
HCl	Hydrochloric acid
HIL	Hole injection layer
HOMO	Highest occupied molecular orbital
HTL	Hole transport layer
IQE	Internal quantum efficiency

Ir	Iridium
IR	Infrared
ISC	Intersystem crossing
ITO	Indium tin oxide
LiF	Lithium fluoride
LUMO	Lowest unoccupied molecular orbital
OLED	Organic light emitting diode
OXD-7	1,3-bis[(4-tertbutylphenyl) -1,3,4 oxidiazolyl] phenylene
PE	Power efficiency
PEDOT:PSS	Poly(ethylenedioxythiophene):polystyrenesulfonate
PEG	Polyethylene glycol
PFI	Perfluorinated ionomer
PHOLED	Phosphorescent organic light emitting diode
PL	Photoluminescence
PLED	Polymer light emitting diode
PO	Phosphine oxide
PPV	Poly(p-phenylene vinylene)
PSD	Power spectral density
Pt	Platinum
PVK	Poly(vinylcarbazole)
RGBY	Red green blue yellow
RSIC	Reverse intersystem crossing
SLRI	Synchrotron Light Research Institute
SMU	Source measuring unit
SOC	Spin orbit coupling
SPP013	2,7-bis(diphenylphosphoryl)-9,9'-spirobi(fluorine)
SY-PPV	Super yellow poly(p-phenylene vinylene)
TAPC	1-Bis[4-[ N , N -di(4-tolyl)amino]phenyl]-cyclohexane
TCTA	4,4',4''-tris(N-carbazolyl)triphenylamine
TDAF	Thermally activated delayed fluorescence
TFV	Trifluorovinyl ether

TMO	Transition metal oxide
TPA	Triplet polaron annihilation
TTA	Triplet-triplet annihilation
UHV	Ultra high vacuum
UV-Vis-NIR	Ultraviolet - visible - near infrared
WOLED	White organic light emitting diode
XPS	X-ray photoelectron spectroscopy

## LIST OF SYMBOLS

$\Delta E_{ST}$	Splitting energy
$\eta_c$	Light output coupling efficiency
$\eta_{ex}$	Fractions of fluorescent of phosphorescent excitons formed
$\eta_{ext}$	External quantum efficiency
$\eta_{FL}$	Density of fluorescent excited state
$\eta_{int}$	Internal quantum efficiency
$\eta_{PL}$	Density of phosphorescence excited state
$\gamma$	Charge balance factor
$\mu$	Electrochemical potential
$\phi$	Radiative decay efficiency
$\phi_m$	Work function
$\tau$	Exciton lifetime
$^1CT$	Singlet charge transfer state
$^3CT$	Triplet charge transfer state
$g_a$	Photogenerated hole at the anode
$g_c$	Photogenerated hole at the cathode
$J$	Current density
$J_{DIF}$	Forward diffusion current density
$J_{RD}$	Reversed drift current density
$k$	Boltzmann constant
$k_{ISC}$	Intersystem crossing rate
$k_M$	Mixing rate
$k_{TPAc}$	Triplet polaron annihilation rate for negative polaron
$k_{TPAh}$	Triplet polaron annihilation rate for positive polaron
$k_S$	Singlet exciton formation rate
$k_{ST}$	Mixing rate from singlet to triplet
$k_T$	Triplet exciton formation rate
$k_{TS}$	Mixing rate from triplet to singlet

$k_{\text{TTA}}$	Triplet-triplet annihilation rate
$L$	Brightness
$M_w$	Molecular weight
$P^+$	Positive polaron
$P^-$	Negative polaron
$r_c$	Capture radius
$S$	Total spin
$S_0$	Ground state
$S_1$	First excited singlet state
$T$	Temperature
$T_1$	First excited triplet state
$V$	Voltage
$V_f$	Forward bias voltage
$V_{\text{OC}}$	Open circuit voltage
$V_{\text{ON}}$	Turn on voltage

## **CHAPTER 1: Introduction**

### **1.1 Introduction**

Over the past decades, huge efforts have been dedicated in searching for a new light source and organic light emitting diodes (OLEDs) are expected to be the next generation of light source for display and lighting applications. For lighting applications, the efficiency of incandescent bulb efficiency is very poor where 90% of the power is dissipated as heat rather than visible light (M. M.-Y. Chan, Tao, & Yam, 2010) whereas the widely used energy saving compact fluorescent lamp (CFL) contains mercury which complicates their disposal. In contrast to CFL, OLED are made from carbon based material and mercury free thus meeting the requirement of EU WEEE& RoHS (Yersin, Rausch, Czerwieniec, Hofbeck, & Fischer, 2011). OLED is glare free, light weight and emit light across all the surface (Tyan, 2011) . However the commercialization of OLED lighting panel is relatively slow mainly hampered by the high fabrication cost. Most of this light panel does not have very high efficiency (15lm/W to 50lm/W). In 2008, OSRAM introduced the first OLED base lighting application in the form of desk light (Chino, 2008). For the first time in 2009, Philip under the brand name of Lumiblade commercialized the first OLED light panel (Mertens, 2012). In 2012, Fraunhofer Institute produced the first transparent OLED panel under the Tabola brand. To date the largest OLED light panel are from Lumioteq which measured 15cm x15cm. Currently the main challenge for OLED as SSL application is the price. Cheap and efficient manufacturing process is still not available to date.

On the other hand, for display applications OLEDs device has successfully entered the market after nearly 20 years of research and development. Compared with

LCD technology, OLED offers many advantages. It has fast response time, light weight, low power consumption, wide viewing angle and good contrast. The commercialization of OLED display began when Kodak introduced the first digital camera (LS633) using 2.2" OLED display in 2003. In late 2007, Sony announced XEL-1 TV the first OLED TV with 11" screen.

## **1.2 History of organic electroluminescence**

Electroluminescence (EL) in organic material was first reported by Helfrich & Schneider in 1965. They observed EL from anthracene crystal of 1 mm to 5 mm thick by applying several hundred volts across it (Helfrich & Schneider, 1964). At that time, their discovery did not generate much interest due to the high voltage required. In 1987 C.W. Tang and VanSlyke from Kodak Eastman have made breakthrough in OLED research by reporting the first bilayer OLED. The device active layers consist of thermal evaporated small molecule diamine and 8-hydroxyquinoline. The device yielded power efficiency of 1.5 lm/W and brightness exceeded 1000 cd/m<sup>2</sup> below 10V (Tang & Vanslyke, 1987). Following that in 1988, Adachi et. al. (Adachi, Tokito, Tsutsui, & Saito, 1988) demonstrated a stable multilayer OLED with electron transport layer (ETL) and hole transport layer (HTL) between the electrode.

The first polymer LED (PLED) was successfully fabricated by Burroughes et. al. in 1990. The device active layer consist of poly-(para-phenylene vinylene) (PPV) spin coated on indium tin oxide (ITO) on glass substrate (Burroughes et al., 1990). Their discovery marks the beginning of OLED fabrication using wet process. Wet processing methods e.g. spin coating, blade coating and inkjet printing are cheaper and does not required complex vacuum deposition system. The first white OLED (WOLED) was demonstrated by Kido et. al. in 1995. White emission with efficiency of 0.5 lm/W (300 cd/m<sup>2</sup>) was generated by a tri-layer device with each layer producing red, blue and

green emission (Kido, Kimura, & Nagai, 1995). The device was fabricated using vacuum deposition method. In 1998, Forrest group reported the first phosphorescence OLED (PHOLED) by incorporating phosphorescent organometallic dopants (M. A. Baldo et al., 1998). The presence of heavy metal in organometallic dopant leads to efficient intersystem crossing. This allows triplet to be harvested thus opening the possibility of achieving 100% internal quantum efficiency (IQE) (Chopra, Lee, Xue, & So, 2010). Lu group reported a unique light output coupling method that boost the efficiency of a green OLED to a record high of 290 lm/W (Z. B. Wang et al., 2011). Another breakthrough in WOLED was achieved by Leo group in 2012. By using light output coupling and careful design of the active layers, for the first time WOLED has reached the power efficiency comparable to a fluorescent tube. The reported OLED gave 90 lm/W at brightness of 1000 cd/m<sup>2</sup> (Reineke et al., 2009).

### **1.3 Motivations and objectives**

OLED is one of the most promising technologies for the next generation of display and lighting. In fact OLEDs have already successfully penetrated consumer market for display applications such as television, digital camera and mobile phone display. Especially for lighting applications, OLED is very attractive considering its outstanding features such as light weight, non-glaring, easy integrated to flexible electronics and mercury free (Chang & Lu, 2013; Yersin et al., 2011). These features offer flexibility in integrating OLED into different lighting module which is one of the main criteria for successful market penetration. In fact, high efficiency white OLED on par with the widely used fluorescent tube has already been demonstrated by (Reineke et al., 2009). Nevertheless it can only be realized using high cost vacuum deposition method. Solution processed method is another alternative way of producing affordable OLED. Unfortunately, OLED fabricated using current wet process technology has very



poor efficiency. This is because wet process is limited by number of functional layer it can deposit (Duan et al., 2010b). The research work presented in this thesis is focused on enhancing the efficiency of solution processed OLED through careful device design, fabrication and characterization. The objectives of this thesis are as follows:

- To enhance the efficiency of a single layer solution processed blue PHOLED through: (a) cathode engineering and (b) reducing excitons quenching at the emissive layer caused by back energy transfer.
- To fabricate and characterize solution processed single layer blue PHOLED based on perfluorinated ionomer (PFI) doped Poly(3,4-ethylenedioxythiophene): poly(strenesulfonate) (PEDOT:PSS) as hole injection layer (HIL).
- To study the effects of polar solvent treatment on a single layer solution processed yellow fluorescent OLED. The impact of the solvents treatment on yellow devices efficiency and current injection shall be studied.
- To design, fabricate and characterize high efficiency solution processed multi layer blue solution processed blue PHOLED.

#### **1.4 Organisation of the thesis**

Chapter 1 begins with the overview of OLED followed by a brief discussion on the history of organic electroluminescence. Then the motivations and objectives of this research are highlighted and then ended with the overview of this thesis.

Chapter 2 serves to provide basic theoretical background on OLED devices and fabrication process. It begins with a brief introduction on OLED operation principles followed by an over view on the fluorescence and phosphorescence emission of OLED. Next, the excitons formation model and energy transfer process are discussed. The general overview of the OLED fabrication process is also presented followed by a write

up on the comparison between polymer and small molecule OLED. Considering the importance of the OLED device architecture in designing high efficiency OLED, the final section of this chapter is dedicated in explaining each functional layer in a single and multi layer OLED.

Chapter 3 consists of two major parts. The first part gives an over view on the OLED fabrication process while the second parts details the device characterization methods used in this research works. The background theory of each experimental probes and techniques will be briefly discussed.

Chapter 4 intends to demonstrate the effects of Triton X-100 in enhancing the efficiency of a single layer solution processed blue PHOLED. The influence of Triton X-100 concentrations on the energy transfer mechanism between host and dye is compared and discussed. In addition to that, the effects of Triton X-100 on the emissive layer (EML) surface morphology are also investigated.

Chapter 5 examines the effects of PFI doped PEDOT:PSS on a single layer solution processed blue PHOLED. The effects of PFI concentrations in PEDOT:PSS on the blue device performances are compared and discussed. The conductivity measurements help to identify the optimum PFI concentrations to give the best device efficiency. The change of the PFI doped PEDOT:PSS film surface morphology are also investigated.

Chapter 6 reports a high efficiency solution processed single layer fluorescent yellow OLED by treating the EML/cathode interface with polar solvent. Devices treated with polar solvents of different dipole moment are studied and compared. This chapter also presents one of the highest efficiency solution processed single layer yellow fluorescent OLED reported to date.

Chapter 7 focuses on the development of high efficiency multi layer blue PHOLED fabricated using wet process. The efficiency improvement is achieved by controlling the charge transport at the first emissive layer and at the heterojunction. It presents blue device with considerable high power efficiency compared to the best power efficiency reported to date for a multi layer solution processed blue PHOLED.

Chapter 8 summarises the research works that have been presented in this thesis. Possible future works in efficiency enhancement of solution processed OLED are proposed at the end of this chapter.

## CHAPTER 2: Literature review

### 2.1 Organic light emitting diode (OLED) device physics

Generally OLED are organic device that produce light when electricity is applied across it. OLED device structure resembles a p-i-n structure as shown in Figure 2.1a. It consists of a few organic thin film sandwiched between two electrodes where one of the electrodes has to be transparent. The EL process in an OLED operation involves 4 process (Figure 2.1b) namely carrier injection, carrier transport and excitons formation and light emission (Gray, 2010). When DC bias is applied to the device, electron and hole are injected from the cathode and anode respectively (process 1). The charge transport mechanism is an intermolecular process where charges hop between two adjacent molecules or along the polymer chains due to the thermoactivated lattice vibrations (process 2 (Tse, Cheung, & So, 2010)). Under the presence of electric field and at separation of few nanometers, electron-hole is bounded together by Coulombic interaction. The Coulombic attraction is stronger for organic material than the inorganic counterpart. This is because the dielectric constant of organic material  $\epsilon_r \sim 3$  which is relatively smaller compared to most of the inorganic semiconductor, for example silicon with  $\epsilon_r \sim 11.7$ . Usually the electrons and holes are captured in a form known as charge transfer (CT) state before excitons are formed in a single molecule (Reineke & Baldo, 2012). Subsequently, electron-hole pair in CT state relaxed into exciton at a single molecule or polymer chain (process 3) (Monkman, 2013). If these excitons recombine radiatively, light is produced (process 4). The light output energy is given as  $h\nu$  where  $h$  is the Plank constant and  $\nu$  is the light frequency. The emission colour is depending on the properties of the organic material used.

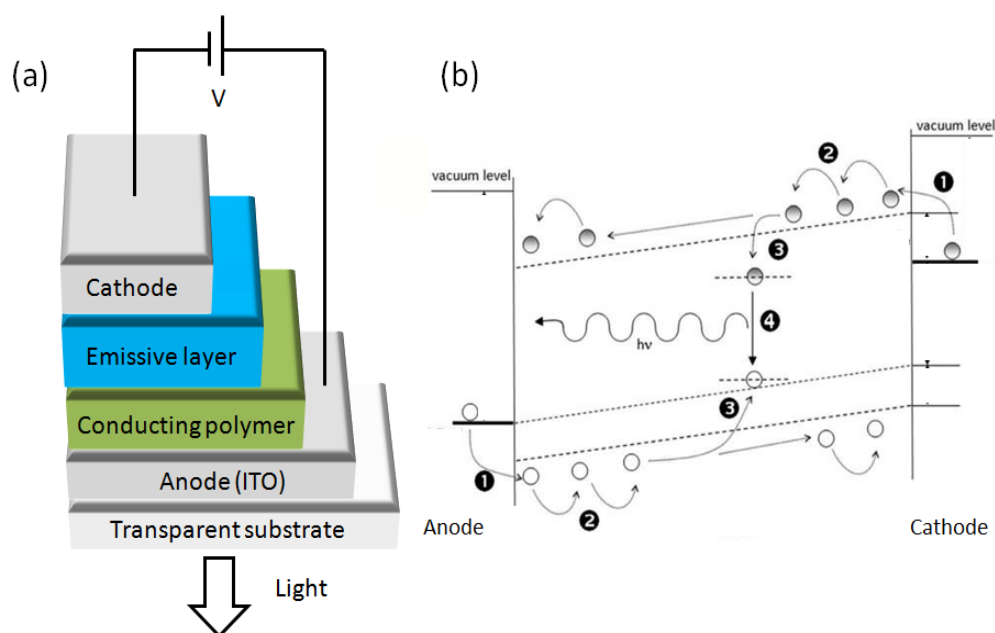


**Figure 2.1:** (a) Simplified diagram of a basic OLED device structure. (b) OLED energy level diagram during operation. Figure 2.1b is adapted from (Pereira, 2012).

### 2.1.1 What is CT states?

In OLED, excited species in the form of electron-hole pair can be considered as a two-electron system. In this system, one electron is in a partially filled highest occupied molecular orbital (HOMO) and another in a partially filled lowest unoccupied molecular orbital (LUMO). The total spin,  $S$  of a two-electron system can be either  $S=0$  (singlet) or  $S=1$  (triplet). The triplet state is usually lower than the singlet state by  $2K$ , where  $K \sim 0.5$  eV for organic molecule (Segal, Baldo, Holmes, Forrest, & Soos, 2003). Here,  $K$  is the exchange integral involving the HOMO and LUMO. During electrical excitation, injected carrier (electron and hole) forms extended  $^1$ polaron pair and subsequently collapse to form CT states. Relaxation from CT states will form excitons as illustrated in Figure 2.2. At large charge separation,  $r > 100$  Å, the positive and negative polaron are not correlated. Therefore the spin states are randomly oriented with respect to each other and  $K=0$ .

<sup>1</sup>Carrier (electron or hole) in a solid will interact with the surrounding ion, for example an electron will slightly attract to the positive ions. Carrier together with this self induced polarization is known as polaron. Polaron is a good way to visualize carrier in organic semiconductor since organic material are soft and deformable.

The charge separation limit that is used to define this independent polaron is termed as critical radius,  $r_c$ . On the other hand, CT states occur from  $r_c$  down to  $r_k$  i.e. nearest neighbouring molecule pair. Typically  $r_k$  is in the order of molecular dimension  $\sim 10$  Å (Segal et al., 2003). In some literature, CT states are commonly described as an intermediate state which consists of bounded electron-hole pair on neighbouring molecules (Ford, Ohkita, Cook, Durrant, & Greenham, 2008; Segal et al., 2007).

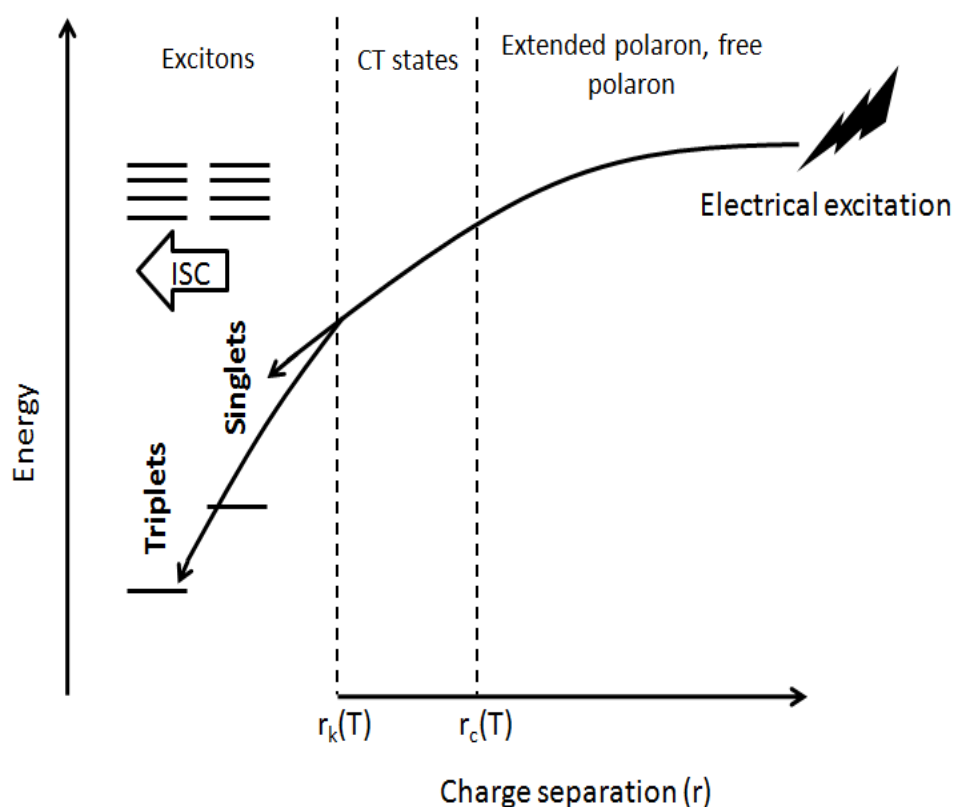


**Figure 2.2:** Formation of excitons via CT states.  $r_c$  and  $r_k$  is temperature dependent. ISC denotes intersystem crossing which will be discussed in section 2.2. Adapted from (Segal et al., 2003).

## 2.2 Fluorescence vs Phosphorescence

The Pauli Exclusion Principle states that no two electrons in an atom can have the same quantum states. As mention in section 2.1.1, a two electron system may have total spin either  $S=0$  or  $S=1$ . State  $S=0$  is antisymmetric, known as singlet whereas  $S=1$

consists of three possible symmetric states known as triplet (Atkins & Friedman, 1997). Radiative decay of singlet exciton produces luminescence known as fluorescence with lifetime in the range of nanoseconds (M. A. Baldo, Thompson, & Forrest, 1999). On the other hand, radiative decay of triplet exciton is termed as phosphorescence. In pure organic compounds, radiative decay of triplet exciton is forbidden by spin selection rules (Kohler & Bassler, 2009). Therefore, the triplet emission is very weak and tends to undergo deactivation processes which lead to non-radiative decay. Due to that, radiatively phosphorescence emission is usually not observed in room temperature (Hong, 2007).

All the excitons produced by photo-excitation process are singlet and subsequently the radioactively recombination to the ground state will results in 100% photoluminescence quantum yield in theory. On the other hand for electroluminescence process, the injected carriers have random spin. The formation of excitons have four possible states namely, one singlet and three triplet states (Perepichka, Meng, & Ling, 2007). From the quantum mechanical spin statistics, only 1/4 of the excitons formed can emit light when the singlet recombines radiatively thus limiting the internal quantum efficiency (IQE) of the fluorescent OLED to an upper limit of 25%. In view of this, it is not a surprise that during the early stage of fluorescent OLED research, OLEDs suffered from very low efficiency. In 1998, Forrest group demonstrated that triplet excitons can be harvested by introducing phosphorescent dye (henceforth called the guest) which contains heavy metal with organic ligand doped into an appropriate organic material (henceforth called the host) (M. A. Baldo et al., 1998). The presence of heavy metal compound such as Platinum (Pt) or Iridium (Ir) enhances spin orbit coupling (SOC) in a molecule (M. A. Baldo, Lamansky, Burrows, Thompson, & Forrest, 1999). SOC mixes the triplet and singlet states in such a way that the triplet gain some singlet characteristics allowing it to recombine radiatively to ground state in

room temperature (M. Baldo & Segal, 2005). At the same time, the intersystem crossing (ISC) rate i.e. radiationless transition between singlet state ( $S_1$ ) to triplet state ( $T_1$ ) become highly probable. Due to the high ISC rate, singlet excitons created by electrical excitation are depopulated into triplet states and decay radiatively to ground state. By using phosphorescent guest-host system, triplet excitons can be harvested and theoretically 100% IQE can be achieved.

The possible electronic transitions for fluorescent and phosphorescent OLED are summarized in Figure 2.3. For fluorescent/phosphorescent system, upon absorption of a photon, electron is excited from ground state  $S_0$  to excited singlet state  $S_1$  as shown in arrow 1. Radiative recombination from  $S_1$  to  $S_0$  produces fluorescence emission (transition 2). Simultaneously  $S_1 \rightarrow S_0$  (transition 2) has to compete with ISC (transition 3) which can depopulate excitons in  $S_1$ . However, the ISC rate for  $S_1 \rightarrow T_1$  is very low for fluorescent OLED. Due to the long lifetime, triplet excitons undergo deactivation process and decay non-radiatively (transition 4). For phosphorescent OLED, due to SOC, ISC rate is efficient allowing high transition rate from  $S_1$  to  $T_1$  (transition 6), thus singlet emission is not observed. Radiative decay rate from  $T_1$  to  $S_0$  (transition 7) is high and phosphorescence emission can be observed at room temperature. Finally, the non-radiative transition (transition 5, 8 and 9) will compete with the radiative fluorescence and phosphorescence emission (Mikhnenko, 2012).



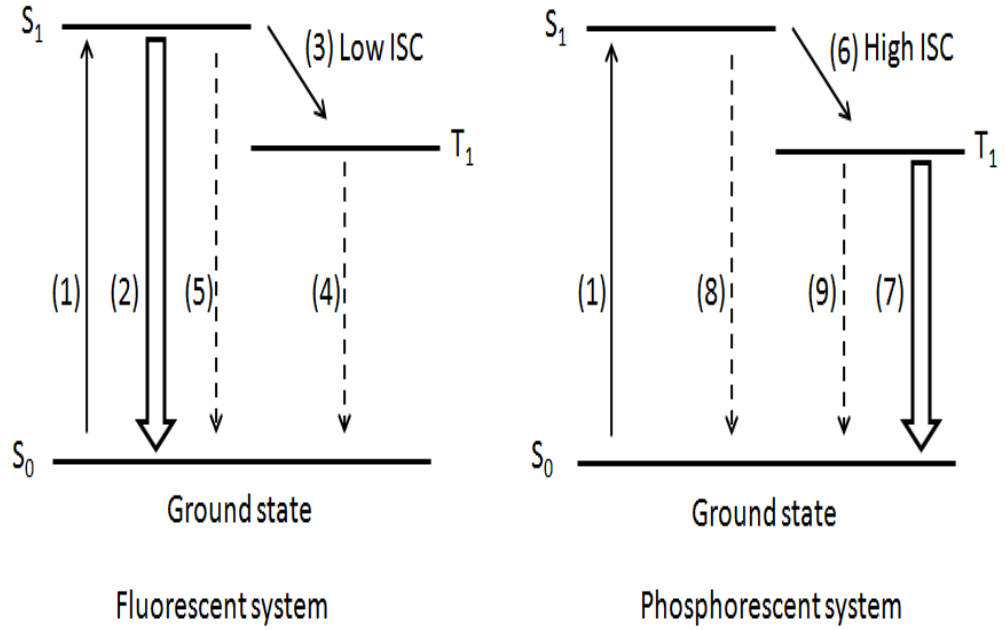


**Figure 2.3:** Simplified Jablonski Diagram showing fluorescent and phosphorescent OLED system.

### 2.2.1 Quantum efficiency

The quantum efficiency of the OLED can be characterized using two parameters namely external quantum efficiency  $\eta_{\text{ext}}$  (EQE) and internal quantum efficiency (IQE). EQE is the ratio of the number of photons extracted into the air to the number of electrons injected into the device. On the other hand, IQE is defined as the number of photons generated per electron injected into the device (Krummacher, Mathai, So, Choulis, & Choong, 2007). EQE ( $\eta_{\text{ext}}$ ) can be described using the following equation (Gray, 2010; Kido & Iizumi, 1998; Tsutsui, 1997):

$$\eta_{\text{ext}} = \eta_c \cdot \eta_{\text{int}} = \eta_c \cdot \gamma \cdot \phi \cdot \eta_{\text{ex}} \quad (2.1)$$

where  $\eta_{\text{int}}$  is the IQE,  $\eta_c$  is the light output coupling efficiency,  $\gamma$  is the charge balance factor,  $\phi$  is the efficiency of the radiative decay process and  $\eta_{\text{ex}}$  is the fraction of the excitons formed i.e.  $\eta_{\text{ex}} = 0.25$  and 1 for fluorescent and phosphorescent OLED respectively.

### 2.2.2 Efficiency roll-off in OLED

When OLED operated at high brightness, its efficiency tends to decrease. In PHOLED, the efficiency roll-off is more severe compared to fluorescent OLED. This efficiency roll-off are due to three mechanism: triplet-triplet annihilation (TTA) (Adachi et al., 2001; M. A. Baldo et al., 1998; C. L. Li et al., 2005; Song et al., 2004), triplet polaron annihilation (TPA) (Reineke, Walzer, & Leo, 2007) and electric field induced quenching (Kalinowski et al., 2002; Kohler & Bassler, 2009).

TTA process occurs either through Dexter or Förster energy transfer and the possible pathways for this mechanism can be expressed as (C. Murawski, K. Leo, & M.C. Gather, 2013b):



where  $k_{TT}$ ,  $S_0$ ,  $S_1$  and  $T_1$  denotes TTA rate, ground state, singlet and triplet excited state respectively. TTA is beneficial to fluorescent system, due to the creation of singlet excitons upon the annihilation of triplet excitons. For phosphorescent system, TTA either eliminates both of the triplet excitons or at least one triplet exciton remains after the process.

TPA is caused by the charge carrier induced exciton quenching. The process can be described as follows (Gesquiere, Park, & Barbara, 2005; Murawski et al., 2013b):



The TPA induced by positive and negative polaron is distinguished by process (2.3) and (2.4). Here  $P^-$  and  $P^+$  denotes negative and positive polaron respectively whereas asterisk (\*) indicates polaron with excess energy.  $S_0$ ,  $T_1$ ,  $k_{TPAh}$  and  $k_{TPAe}$  are ground

state, triplet excited state, TPA rate for positive polaron and TPA rate for negative polaron respectively. It is worth mentioning that TPA also quenches singlet excitons but because of the relative short lifetime of singlet excitons, TPA is more efficient in annihilating triplet excitons.

The third mechanism is the exciton dissociation under high electric field. Exciton dissociation is also influenced by exciton lifetime, active layer thickness, device operating temperature, exciton binding energy and the separation of electron hole pair. For example in guest-host system, electric field induced exciton quenching depends on the position of the HOMO/LUMO level of the guest relative to the HOMO/LUMO level of the host as proposed by (Luo, Aziz, Popovic, & Xu, 2006). If the HOMO/LUMO level of guest lie deep inside the HOMO/LUMO level of host, the dissociation becomes difficult due to the energetic barrier of  $\Delta \text{HOMO}/\Delta \text{LUMO}$  that the coulombically bounded electron-hole pair needs to overcome as shown in Figure 2.4.

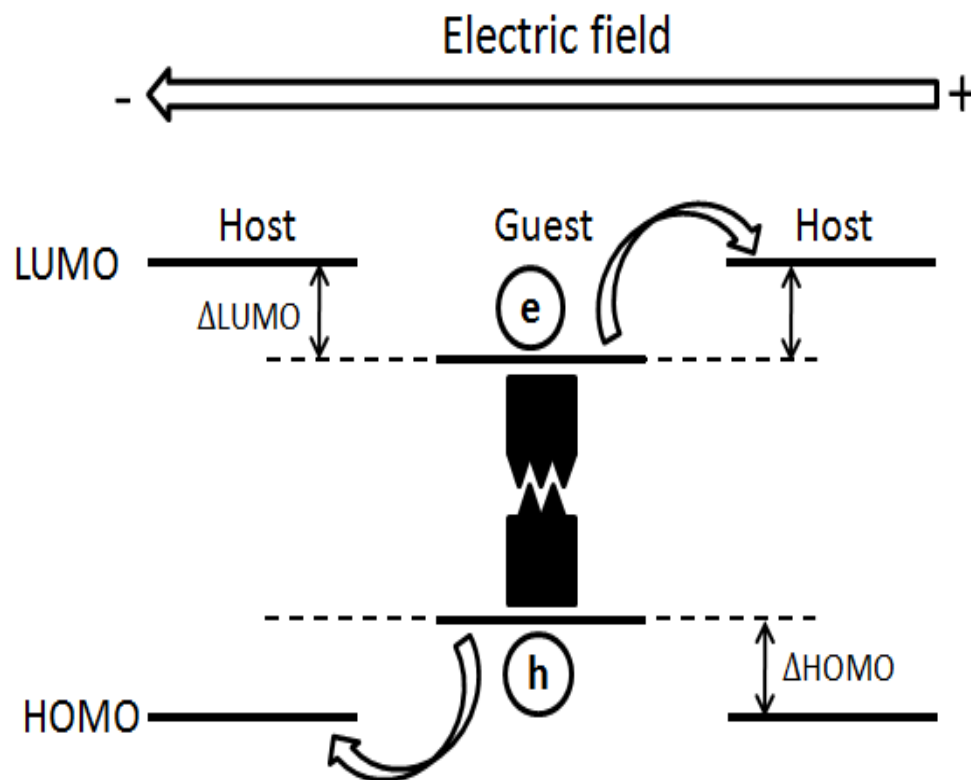


**Figure 2.4:** Exciton dissociation in guest due to presence of electric field. Adapted from (Luo et al., 2006)

The next question is why efficiency roll-off is more severe in phosphorescent OLED compared to fluorescent OLED. Consider the following: The brightness ( $L$ ) of an OLED is inversely proportional to the singlet/triplet exciton lifetime ( $\tau$ ) and proportional to the density of the excited state ( $n$ ). Taking into the account of spin statistics for singlet/triplet excitons formation, the brightness of OLED can be estimated as (Reineke et al., 2007):

$$L_{FL} \sim \frac{n_{FL}/4}{\tau_{FL}} \quad \text{and} \quad L_{PH} \sim \frac{n_{PH}}{\tau_{PH}} \quad (2.5)$$

where the subscript  $FL$  and  $PH$  denote fluorescent and phosphorescent system respectively. Typically the lifetime of the OLED phosphorescent triplet is 2 orders higher than fluorescent singlet (Reineke et al., 2007; Sokolik, Priestley, Walser, Dorsinville, & Teng, 1996). Hence, the ratio of the phosphorescent to fluorescent excited state density can be written as:

$$\frac{n_{PH}}{n_{FL}} \sim \frac{\tau_{PH}}{4\tau_{FL}} \sim 25 \quad (2.6)$$

From (2.6), it can be observed that to achieve the same brightness, phosphorescent system need 25 times of excitons compared to the fluorescent counterpart. This causes severe roll-off in phosphorescent OLED operating at high brightness as high density of triplet is required to generate higher brightness which at the same time lead to higher TTA and TPA.

### 2.3 Exciton formation model

Figure 2.4 shows the schematic diagram of the possible exciton formation model in OLED. (Reineke & Baldo, 2012; Wohlgenannt, Tandon, Mazumdar, Ramasesha, & Vardeny, 2001). When voltage is applied across OLED, electrons and holes are injected into the cathode and anode respectively. Electron-hole pairs are captured by Coulombic

interaction in the form of CT state. Relaxation from the CT state forms exciton in a molecule or polymer. From the exciton formation model in Figure 2.5a, it is clear that without a mixing process only 25% of the excitons can emit light when radiative recombination occurs.

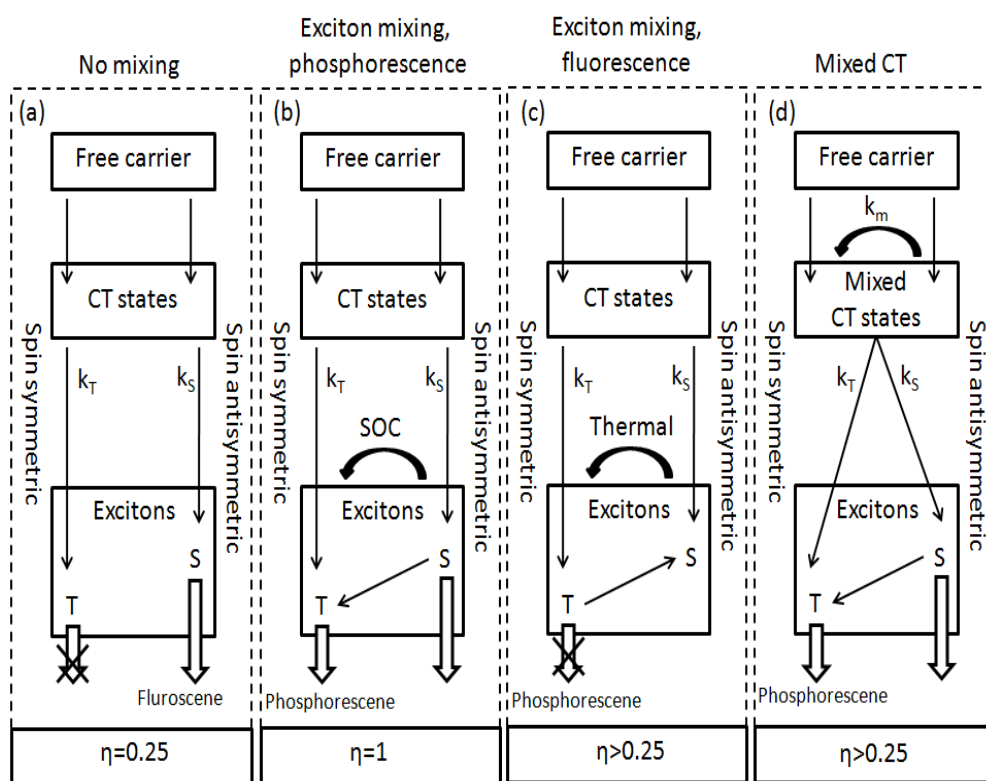


**Figure 2.5:** Exciton formation model for the following condition: (a) No mixing occur, (b) exciton mixing, producing phosphorescence emission due to spin-orbit coupling (SOC), (c) thermal activation delay fluorescence process and (d) mixing occur at the CT states.  $\eta$  denotes quantum efficiency whereas  $k_s$ ,  $k_T$  and  $k_m$  denotes singlet and triplet excitons formation rate and CT states mixing rate respectively. Adapted from (Reineke & Baldo, 2012).

Mixing process is a process that converts carrier in singlet state to triplet state or vice versa (Segal et al., 2007). The mixing process can occur either at exciton level or CT state (Reineke & Baldo, 2012). There are two methods for mixing process that occurs at exciton level. The first one is through SOC (Figure 2.5b) which already discussed in section 2.2. Briefly, the mixing process is enabled by the presence of heavy metal (e.g. Ir or Pt) in a molecule that promotes SOC which enhances ISC from singlet to triplet. Therefore triplet excitons can be harvested, opening up the possibility

of achieving quantum efficiencies of 100%. The second method is through thermal process, widely known as thermally activated delayed fluorescence (TADF) as shown in Figure 2.5c. This approach can be used to enhance the quantum efficiency of fluorescent OLED above the upper limit of 25% where non-radiative triplets are channelled back to the singlet through thermal activation process (Goushi, Yoshida, Sato, & Adachi, 2012; B. S. Kim & Lee, 2014; J. Lee et al., 2013; S. Y. Lee, Yasuda, Nomura, & Adachi, 2012; Méhes, Goushi, Potscavage Jr., & Adachi, 2014; Nakagawa, Ku, Wong, & Adachi, 2012; Nakanotani, Masui, Nishide, Shibata, & Adachi, 2013; Tanaka, Shizu, Miyazaki, & Adachi, 2012; Uoyama, Goushi, Shizu, Nomura, & Adachi, 2012; H. Wang et al., 2014; Q. Zhang et al., 2014; Q. S. Zhang et al., 2012). To obtain efficient TADF, the splitting energy ( $\Delta E_{ST}$ ) between singlet and triplet state must be as low as possible and ideally lower than carrier thermalization energy to ensure fast reversed intersystem crossing (RISC) (see Figure 2.6). If the RISC is slow, triplet excitons that pile up will cause TTA (Kepler, Caris, Avakian, & Abramson, 1963) which lead to severe efficiency roll-off at high current density.

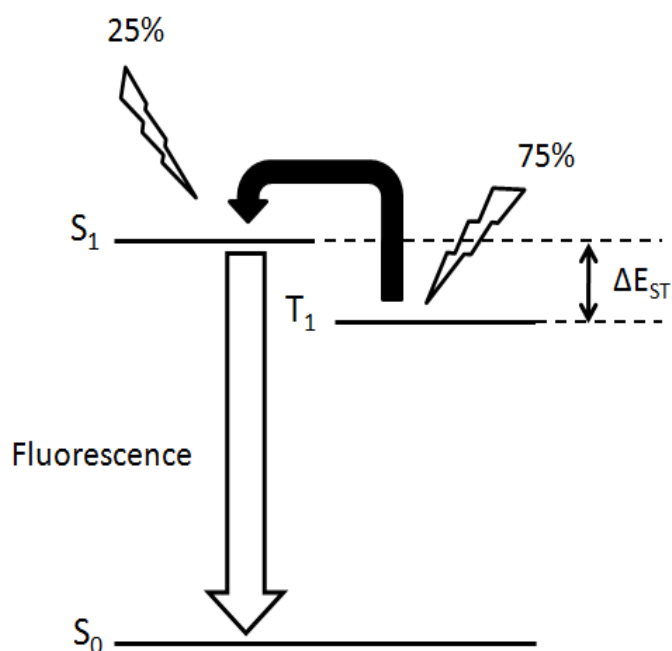


**Figure 2.6:** Schematic diagram of TADF in enhancing the fluorescence emission.

Mixing can occur at CT states and the process are summarized in Figure 2.5d and Figure 2.7. This idea was initially proposed by (Segal et al., 2007), aimed at breaking the 25% upper limit of fluorescent OLED. During electrical bias, the formation rate of triplet CT states is 3 times higher than the singlet CT states. Without any mixing at the CT states, these charge-pairs will relax into excitons with 25% of the excitons are singlet while the remaining are triplets. If mixing happens at the CT states and the mixing rate from triplet to singlet ( $k_{TS}$ ) is larger than the singlet exciton formation rate ( $k_S$ ), then the theoretical 25% limit can be broken (see Figure 2.7). To ensure “extra fluorescent” luminescence, the mixing rate from singlet to triplet ( $k_{ST}$ ) need to be reduced and this can be accomplished by ensuring the triplet CT state ( $CT^3$ ) is higher than the singlet CT state ( $CT^1$ ).

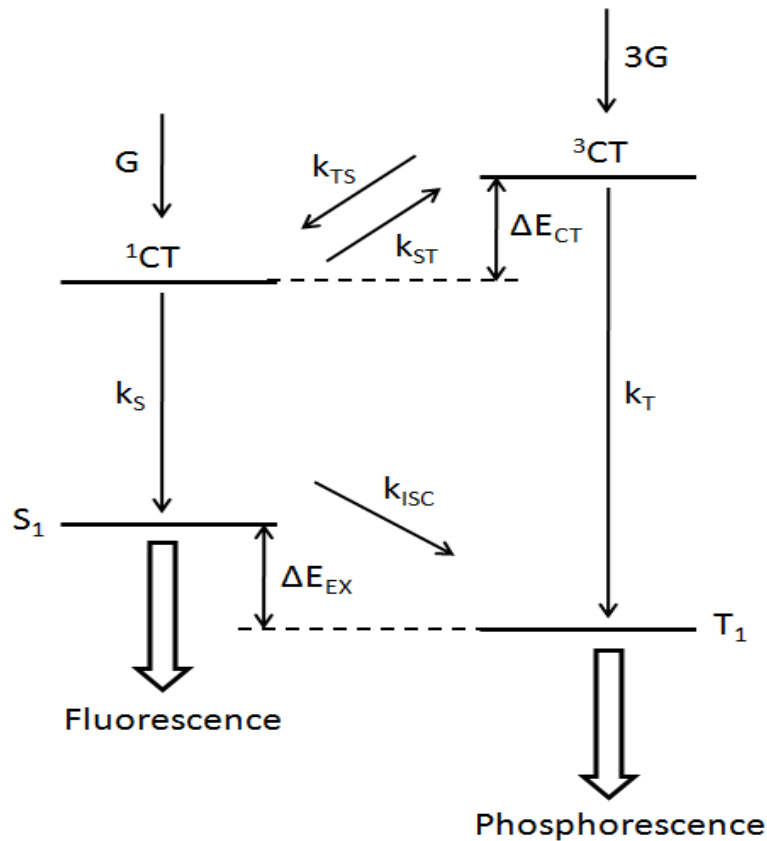


**Figure 2.7:** Exciton formation model based on CT state mixing. The formation rate of singlet CT states is given as  $G$ .  $k_{TS}$  and  $k_{ST}$  denote the mixing rate from triplet to singlet and singlet to triplet respectively.  $^3CT$ ,  $^1CT$ ,  $k_S$ ,  $k_T$ ,  $k_{ISC}$ ,  $S_1$  and  $T_1$  denote triplet CT state, singlet CT state, singlet exciton formation rate, triplet exciton formation rate, inter system crossing rate, singlet state and triplet state respectively. Adapted from (Segal et al., 2007).

## 2.4 Energy transfer process between a host doped with phosphorescent dye

In phosphorescent OLED, heavy metal based organometallic complexes dye (guest) are doped into an organic host. During OLED operation, the excitation energy is transferred from host to guest. There are three types of energy transfer involved, namely long range Förster energy transfer, short range Dexter energy transfer and direct generation of excitons in the guest. Figure 2.8 shows the schematic diagram of Förster and Dexter energy transfer leading to the generation of fluorescent and phosphorescent emission.

Förster energy transfer is based on dipole-dipole coupling between guest and host (Förster, 1959; W. S. Jeon et al., 2009; Scholes, 2003). It occurs when there is a strong overlap of guest absorption spectrum with the emission spectrum of the host. The efficiency of this energy transfer decreases when the guest-host separation ( $r$ ) increases and the efficiency of Förster mechanism is a function of  $1/r^6$ . Efficient Förster energy transfer occurs for a separation of guest-host up to 10 nm. In contrast to Förster mechanism, Dexter energy transfer (Dexter, 1953; Jain, Willander, & Kumar, 2007) is a short range energy transfer process as it involves the overlapping of molecular orbital between adjacent molecule. Typically, for Dexter mechanism to happen the distance of the guest-host need to be within 0.6 nm to 2 nm. Dexter energy transfer rate is a function of  $e^{-2r/L}$  where  $r$  is the guest-host separation and  $L$  is the sum of van der Waals radius.



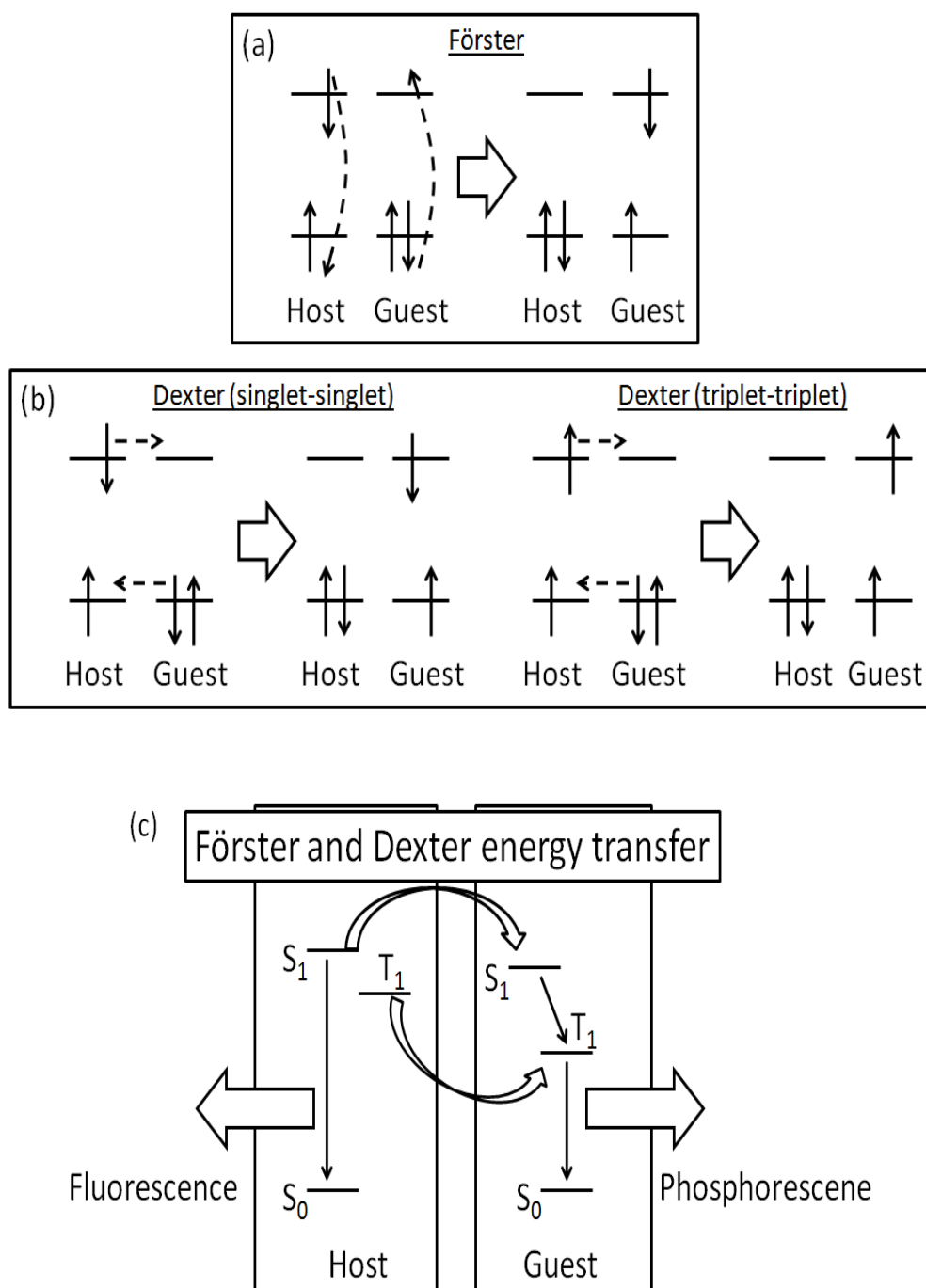


**Figure 2.8:** (a) Förster energy transfer and (b) Dexter energy transfer. (c) Energy diagram showing Förster and Dexter energy transfer process for a fluorescent/phosphorescent guest-host system. The singlet excited state, ground state and triplet excited state are denoted as  $S_1$ ,  $S_0$  and  $T_1$  respectively.

Direct generation of excitons in guest is also known as charge trap mechanism (Mi, Gao, Liao, Huang, & Chen, 2010). The HOMO/LUMO level of the host must be below/above the HOMO/LUMO of the guest (see Figure 2.9). In this case, the energy level of the guest acts as charge trapping sites, thus forming excitons directly in guest.

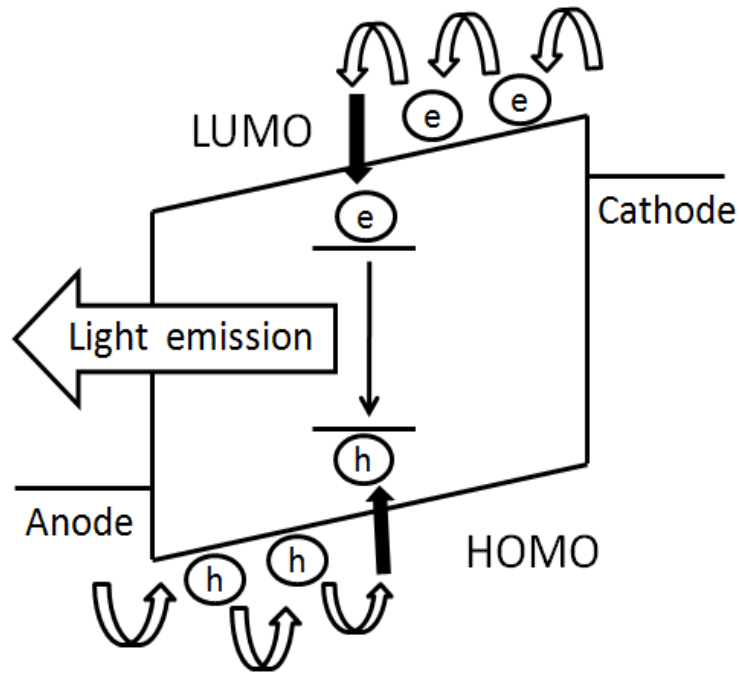


**Figure 2.9:** Light emission induced by charge trapping mechanism in a guest/host system.

## 2.5 OLED fabrication process

OLED can be fabricated either using vacuum deposition method or wet process such as spin coating method, blade coating and ink-jet printing. Generally, the fabrication process of OLED can be summarized as follow:

1. *Substrates:* For non-inverted OLED, the substrate must be transparent in order to allow light to pass through. Usually, ITO on glass or transparent plastic is used as the substrate. The ITO is patterned using standard lithography method.
2. *Active material deposition:* OLED material is deposited on top of the substrate using vacuum deposition method or wet process. Following that, low work function metal alloy is deposited as cathode. Typically, the work function of this metal is in the range of 2.9 eV - 4 eV (Kalyani & Dhoble, 2012). The cathode layer must be transparent for inverted OLED.

3. *Encapsulation:* Encapsulation is carried out to protect the OLED from ambient moisture and oxygen which will degrade the device performance. For example, UV curable epoxy is one of the approaches to encapsulate the device.

### **2.5.1 Vacuum deposition method**

For high performance OLED, it is crucial to balance the hole/electron injection. In addition to that it is important to confine excitons in the emissive layer in order to minimize excitons quenching. This can be easily achieved using vacuum deposition method because it allows deposition of multilayer functional layer to improve the device performance (Divayana, Liu, Kyaw, & Sun, 2011; Reineke et al., 2009; Y. R. Sun et al., 2006). However the vacuum deposition system is expensive and the consumption of the OLED material is very high during the vacuum deposition method. It is estimated that 80% of the OLED material is wasted during the deposition process (H. Kim, Byun, Das, Choi, & Ahn, 2007). In addition to that, this approach is very challenging for high resolution process and scalability due to pixelation of vacuum deposition mask (Sonoyama et al., 2008). Therefore, the fabrication of large lighting panel and display is hindered by this method. Figure 2.10 shows the simplified schematic diagram of the vacuum deposition process.

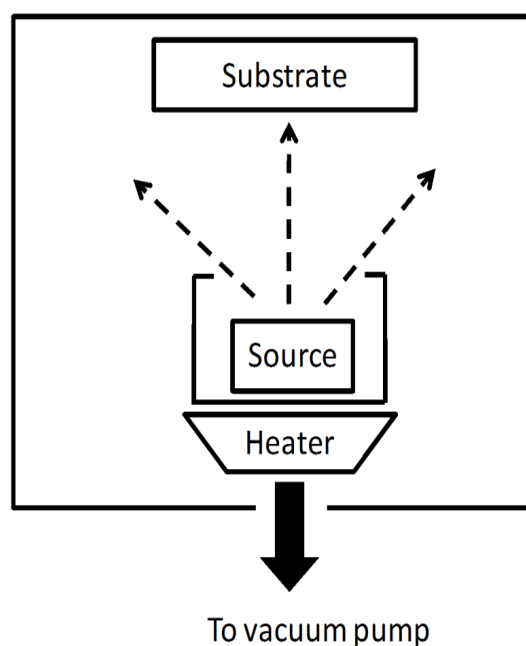


**Figure 2.10:** Schematic diagram of the vacuum deposition method for OLED thin film deposition.

### 2.5.2 Wet process

Wet process OLED fabrication is fast gaining popularity. It does not required high cost vacuum deposition system setup and OLED fabrication can be done in ambient environment. More important it allows large area, low cost and roll-to-roll manufacturing process (So et al., 2007). This method involves dispensing OLED solution on to the substrate followed by formation of thin film using spin-coating, blade-spin process, blade only process and inkjet printing. Subsequently the substrates undergo annealing process to remove the solvent. There are two important criteria needed to be met in order to use the wet process. First, the OLED material must dissolved well in solvent. Second, OLED material used must have high glass transition temperature,  $T_g$ , ideally above  $100^\circ\text{C}$  (Schroegel et al., 2011). When low  $T_g$  material is used, it tends to crystallize resulting in reliability issues. Crystallization of OLED thin film can cause electric field inhomogeneity leading to thermal breakdown and catastrophic failure (E. M. Han, Do, Yamamoto, & Fujihira, 1996; X. Zhou et al., 2000).

To date, the performance of wet processed OLED is lagging compared to OLED fabricated using vacuum deposition method. The main reason is that it is very difficult to form a multilayer OLED using wet process. Almost all OLED organic material dissolve in organic solvent therefore the top layer will dissolved the under layer resulting in intermixing. To overcome this problem, several solutions have been proposed. For instance, several research groups have tried using UV or thermal crosslinkable OLED material (Aizawa, Pu, Sasabe, & Kido, 2012; Liaptsis & Meerholz, 2013; Yook & Lee, 2012; Zuniga et al., 2013) while for the top-most layer, alcohol or formic acid/water soluble OLED material can be used (Earmme & Jenekhe, 2012a; J. H. Lu et al., 2011; Yook, Jang, Jeon, & Lee, 2010). Other methods are to use blade-spin and blade only coating which will be discussed in section 2.5.2.2 and 2.5.2.3.

#### **2.5.2.1 Spin coating method**

The simplest OLED wet process method is the spin coating approach as illustrated in Figure 2.11. Due to its cheap and simple setup, this method is often use in research laboratory. In this method, OLED in solution is dispensed onto the substrate. By controlling the spinning speed, spinning time, concentration of the solution and the boiling point of the solvent, the thickness of the thin film formed can be controlled. The major drawback is that high mount of OLED material are wasted in this process. More important, without using cross-linkable, non-organic solvent soluble OLED material or orthogonal sovent it is impossible to form a multi layer OLED device structure solely using this method.

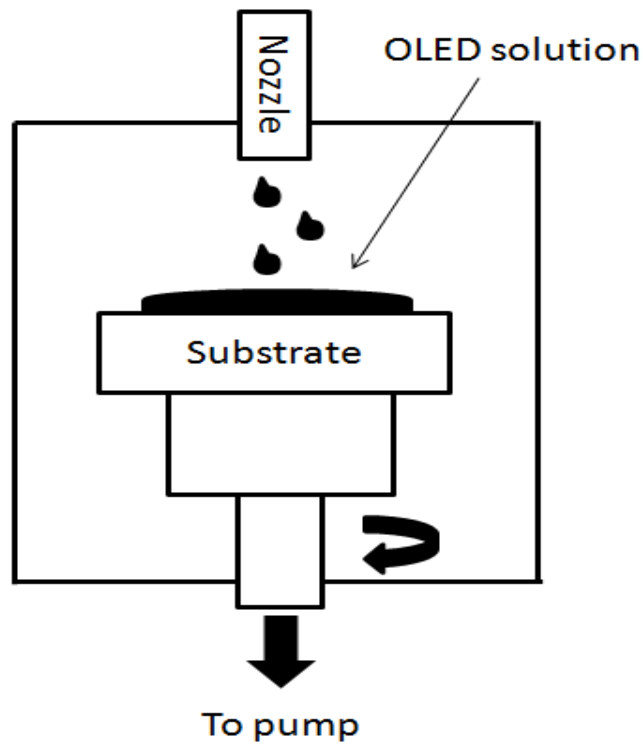


**Figure 2.11:** Schematic diagram of the spin coating process for OLED thin film deposition.

#### 2.5.2.2 Blade-spin method

Multilayer OLED can be fabricated using blade-spin process (You et al., 2009), a combination of blade coating and spin coating process. In contrast to spin coating method, most of the dispensed OLED solution remain on the substrate after blade coating. The method is as follows: First solution is dispensed at the edge of the substrates mounted on the spin coater chuck. Immediately after this, wet thin film is form by moving the blade coater rapidly across the substrate (see Figure 2.12a). The wet film is dried by spinning the substrate using a spin coater as shown in Figure 2.12b. The circulating air generated by the motion of the spin coater chuck effectively removed the residue solvent. The next layer can be deposited using the same procedure. The fast movement of the blade coating bar can dry the top layer as it moves across the substrate rapidly (C. Y. Chen et al., 2011). By doing so, the dissolution of the underlying layer can be minimized. The film thickness can be controlled by the gap between the blade

coater and the substrate, solution concentration and the chuck spinning speed. It has been demonstrated that the performance of OLED fabricated using blade-spin method is 30% lower compared to the vacuum deposition method (You et al., 2009). The inferior performance is attributed to the small amount of layers intermixing and microscopic crystallites formation on the film (Z. Y. Liu et al., 2011). The disadvantages of this method lie in the spinning process. First, the presence of the spin drying process slows down the fabrication process as the blade coating process cannot proceed continuously. Second, it limits the size of the substrate to be fabricated because poor mounting of the large substrate on the spinning chuck (C. Y. Chen et al., 2011).

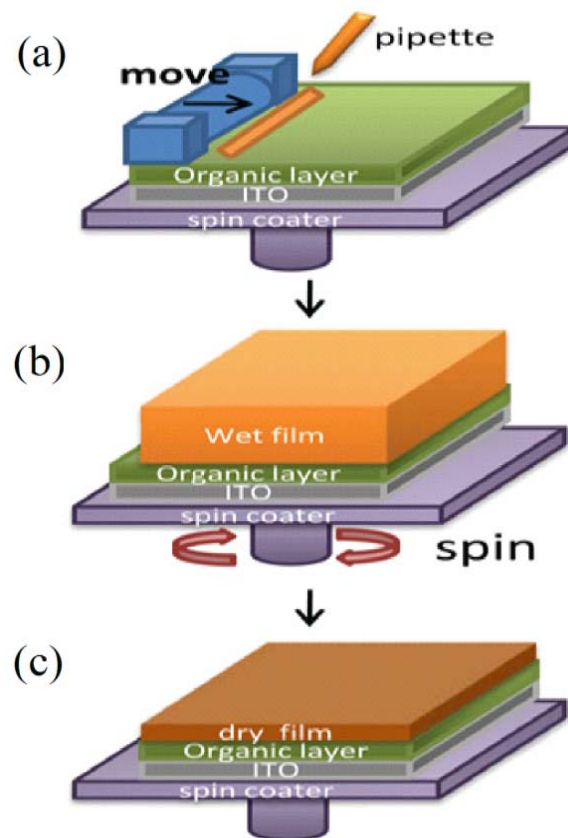


**Figure 2.12:** Blade-spin method for OLED thin film deposition. Adapted from (C. Y. Chen et al., 2011).

### 2.5.2.3 Blade-only method

Compared with blade-spin method, blade-only method eliminates the spinning process. Blade-only method has been successfully demonstrated in coating polymer film (Syu et al., 2010; Tseng, Meng, Lee, & Horng, 2008) and small molecule film (Chao et al., 2011; Ko et al., 2010; Z. Y. Liu et al., 2011) for multi layer OLED. In this approach, substrate is placed on the hotplate. The hotplate is adjusted to temperature within 70°C to 80°C. Solution is dispensed on the edge of the substrate and then thin film is formed by moving the blade coater across the surface. Subsequent layer is deposited using the similar method. By heating the substrate, the wet film will dry rapidly as the blade coater is moved across the substrate surface thus preventing the dissolution of the underlying layer. The whole process is summarized in Figure 2.13.

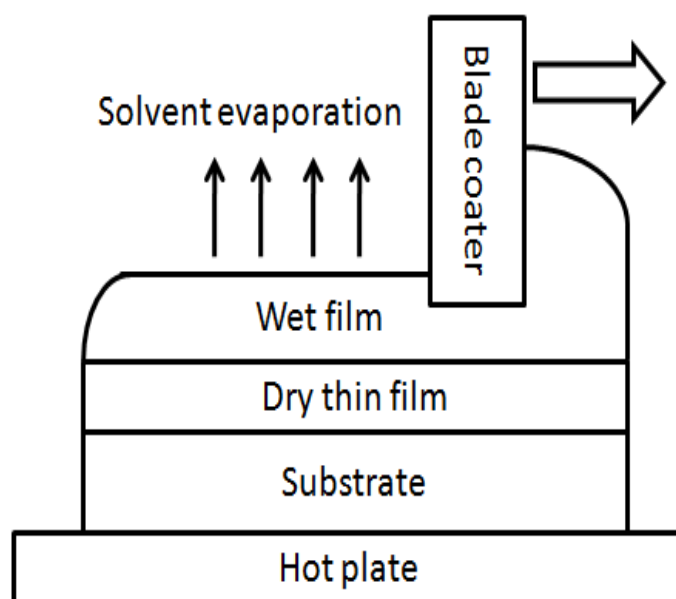


**Figure 2.13:** Schematic diagram of the blade-only coating process.

### 2.5.2.4 Inkjet printing

Figure 2.14 illustrates the concept of inkjet printing. Solution is dispensed through the nozzle of the print head as the substrate is passed beneath the print head. The main advantage of inkjet printing is it allows small pixel printing (C. Y. Chen et al.,



2011). Similar to spin coating method, inkjet printing does not allow the fabrication of multi layer OLED. In addition to that, the cost of the inkjet system is higher due to the complicated design of the print head.

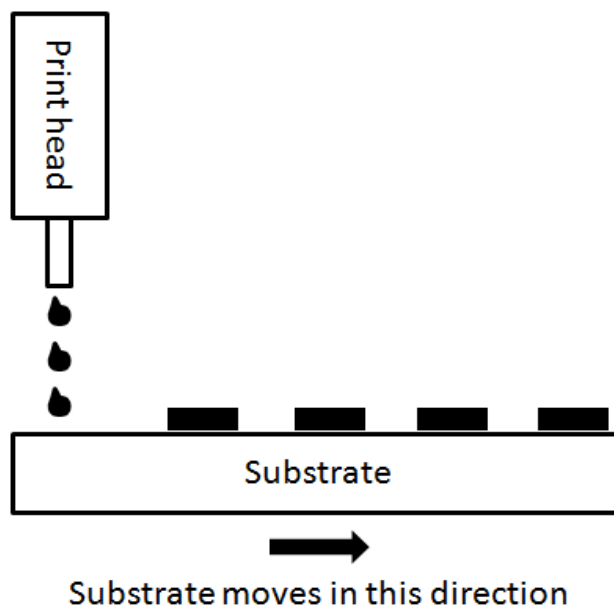


**Figure 2.14:** Schematic diagram of the inkjet printing process.

## 2.6 Small molecule vs polymer OLED

The film formation process using polymer is shown in Figure 2.15a. In solution, polymer chains are extended. The polymer chains starts to entangle as the wet thin film dried out. It is worth noting that even the film completely dried, there are still space between the polymer chains thus allowing the relaxation of the polymer chain (Duan et al., 2010b). Polymer material is widely used in fluorescent OLED. Some of the examples are polyphenylene vinylene (PPV) (Remmers et al., 1996; Spreitzer et al., 1998) and polyfluorene (PFO) (Bernius, Inbasekaran, Woo, Wu, & Wujkowski, 2000; W. S. Wu et al., 2004) based materials. Polymer is widely known to be able to form excellent film from solution processed method thanks to its high molecular weight and the presence of alkyl group. It has high glass transition temperature,  $T_g$ , which prevents the crystallization of the thin film when annealing process is carried out. Despite the

high quality and stability of the film formed by polymer material, controlling batch-to-batch variation in its molecular weight and the purification of polymer is a not an easy task (Walker, Tamayo, Yang, Brzezinski, & Nguyena, 2008).

The film formation using solution processed small molecule is depicted in Figure 2.15b. For small molecule, instead of entanglement the packing density plays an important role in forming good quality solution process thin film (Duan et al., 2010b). The formation of thin film is made possible by physical entanglement and hydrogen bonding between molecules. Therefore, it is very important to control the intermolecular interaction in order to ensure pin-hole free solution processed thin film. The solubility of small molecule in organic solvent can be improved by decorating the small molecule with alkoxy or alkyl group. Compared to polymer it is easier to purify, making it an excellent candidate for OLED material. Nevertheless, most of the OLED small molecules available to date form poor film morphology as they prone to crystallize when wet process is used (Duan et al., 2010a). Crystallization of solution processed small molecule thin film can be avoided by increasing its  $T_g$ . One way is by enlarging the small molecule size such as dendrimers. Other methods are by introducing structurally twisted molecule, rigid/bulky such as carbazole, naphthalene, fluorene, phenothiazine and biphenyl (Shirota, 2005; Tsai et al., 2007).

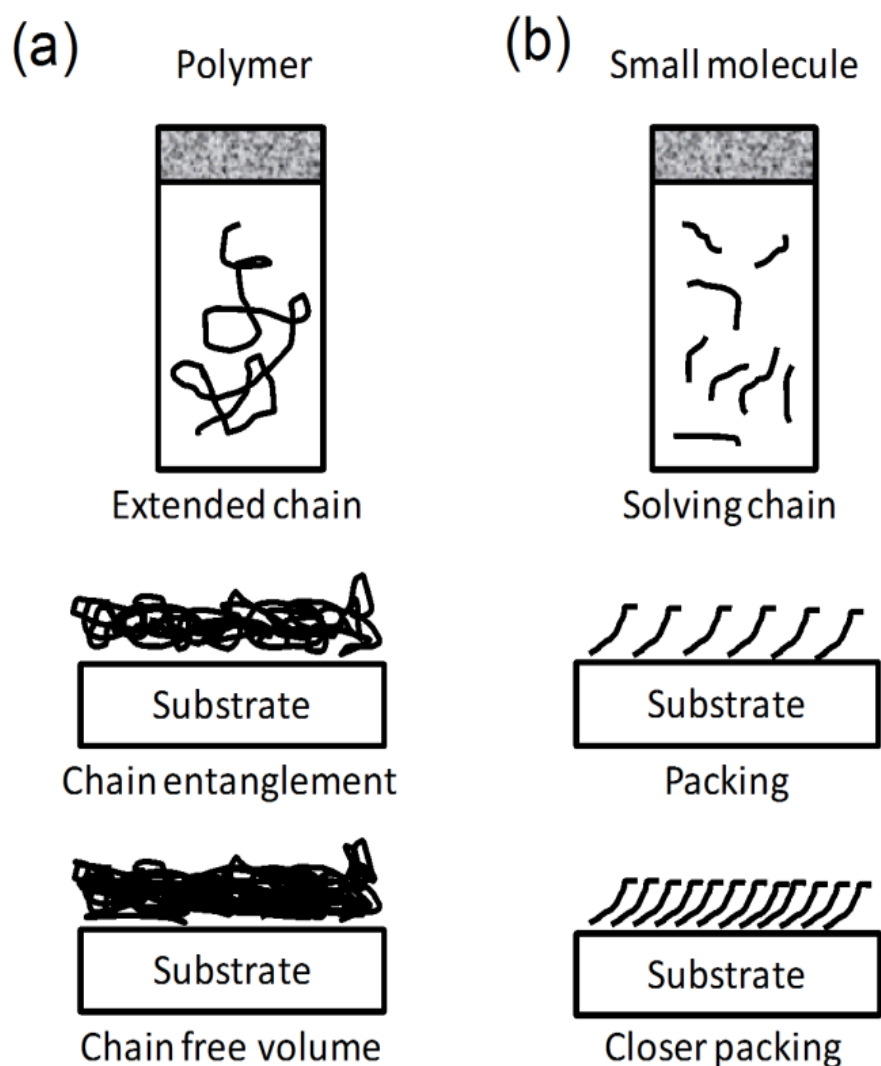


**Figure 2.15:** Thin film formation using (a) polymer and (b) small molecule solution. Adapted from (Duan et al., 2010a).

A compromise is often reached by blending polymer and small molecule together (J. S. Huang, Hou, Li, Li, & Yang, 2006). One of the most commonly used polymer for this purpose is polyvinyl carbazole (PVK) which favours hole transport. PVK is usually blended with electron transporting small molecule compound such as phosphine oxide or oxidiazole based material to achieve balance charge injection (Lu Li, Liu, Yu, & Pei, 2013; Mathai, Choong, Choulis, Krummacher, & So, 2006; X. H. Yang, Jaiser, Klinger, & Neher, 2006; X. H. Yang, Muller, Neher, & Meerholz, 2006). The blend of polymer and small molecule can produce high quality film using solution

process method. Furthermore, it also allows the usage of a wide range of small molecule material available in the market.

## 2.7 Multilayer vs single layer OLED

The complexity of the OLED device architecture is heavily depending on the number of functional layer. The presence of the functional layers helps to balance the electron/hole injection, confine excitons in the emissive layer and prevent excitons quenching at the device anode/cathode. Based on this multi-layer concept, white OLED with ground-breaking efficiency up to 90 lm/W at 1000 cd/m<sup>2</sup> has been reported (Reineke et al., 2009). This efficiency already exceed the typical efficiency of fluorescent tube i.e. 60 lm/W to 70 lm/W. Even though multi layer OLED is very attractive in terms of device performance, this multi stack device is very difficult to be implemented using wet process. The main reason is the intermixing between the top and bottom layer. In a single layer device, compound with different functionalities, for example hole/electron transport compound, host, small molecule dye are blended into a single layer. It is worth mentioning that most OLED device incorporate multilayer design in their anode/cathode architecture to improve carrier injection. Some of the widely used combinations are PEDOT:PSS on ITO (Jou, Shen, et al., 2010; Zhong, Duan, Huang, Wu, & Cao, 2011; Zhu et al., 2011) for anode and alkali metal fluoride (e.g. LiF/Al, CsF/Al) or alkali metal carbonate (e.g. Cs<sub>2</sub>CO<sub>3</sub>/Al) for cathode. However the presence of this active layer on the electrodes is not considered as an additional layer to the device.

Due to the simplicity of the single layer device, it is not surprising that its performance is always inferior compared to the multilayer counterpart. To overcome this, several groups have developed high efficiency double layer OLED by combining

solution processed and vacuum deposition method. In this type of design, the emissive (EML) is deposited using wet process whereas the top layer is the vacuum deposited electron transport layer (ETL) (J. S. Chen et al., 2012; J. H. Jou et al., 2013; Jou, Wang, et al., 2010; C. W. Lee & Lee, 2013; C. W. Lee, Yook, & Lee, 2013; B. Liu et al., 2013; B. H. Zhang et al., 2012). Such device can cut down fabrication cost and improves the device efficiency by reducing excitons quenching at the cathode and promotes excitons confinement at the EML/ETL heterojunction.

Figure 2.16a and Figure 2.16b show the device architecture of a typical multilayer and single layer OLED respectively. A multilayer OLED may have more than one similar functional layer stack together, for example some device may have up to three or more HTL stack on top of each other (S. E. Jang, Joo, & Lee, 2010; J. Lee, Lee, Lee, & Chu, 2009; Seo & Lee, 2011). Also, some of the functional layers can combine into a single layer. The functions of each layer discussed in the following sections. On the other hand, in single layer OLED, HTL and ETL are combined in a single EML layer.

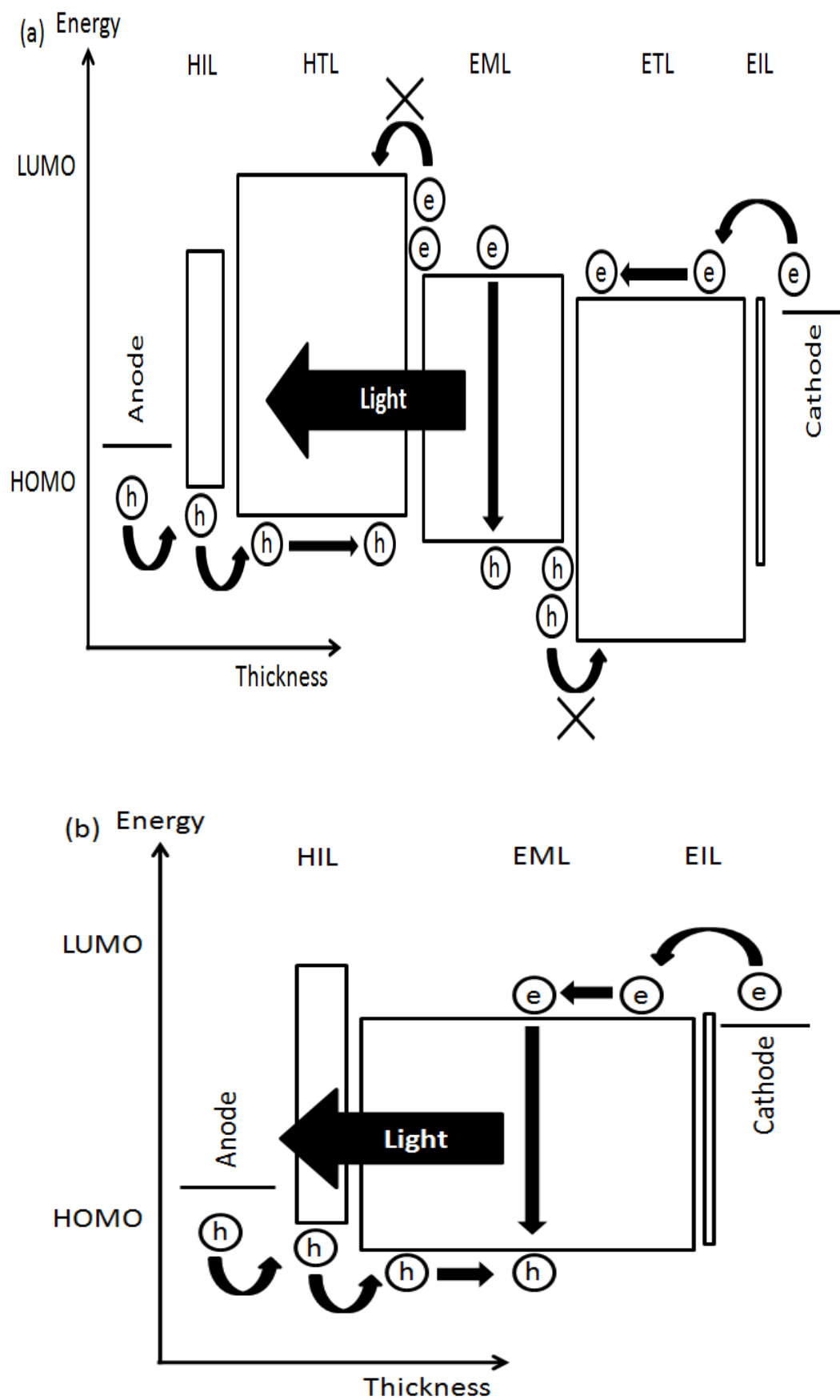


**Figure 2.16:** Schematic diagram of a (a) multilayer and (b) single layer OLED.

### 2.7.1 Anode

The anode for OLED should meet the following criteria:

1. Excellent thermal and chemical stability.
2. Highly transparent. In the case of inverted OLED, it should be highly reflective.
3. High work-function, preferably  $>5\text{eV}$ , to reduce the barrier height for hole injection.
4. Low resistivity to minimize contact resistance.
5. Good wetting properties and adhesion for organic materials.

ITO is commonly used as transparent anode for OLED due to its high transparency (90% in visible region) and low resistivity ( $1 \times 10^{-4} \Omega\cdot\text{cm}$ ). By definition, the surface work function  $q\phi_m$  of a conductor is defined as the energy difference between the electron potential energy in vacuum ( $q\phi_{\text{vac}}$ ) just outside the conductor surface and the electrochemical potential ( $\bar{\mu}$ ) of the electrons in the bulk (Helander et al., 2011), given as:

$$q\phi_m = q\phi_{\text{vac}} - \bar{\mu} \quad (2.7)$$

The work function of pristine ITO is about 4.3 eV (Y. Park, Choong, Gao, Hsieh, & Tang, 1996) which is low compared with the highest occupied molecular orbital (HOMO) level of most of the OLED material ( $\sim 5.5\text{ eV}$ - $6\text{ eV}$ ). In this case, energy barrier exist for hole to transport from ITO to the first organic layer of the device. Much effort has been spent on research in reducing the barrier height for hole injection. One of the widely used methods is treating the ITO with oxygen plasma (I. M. Chan, Cheng, & Hong, 2002; Ding et al., 2000; Irfan, Graber, So, & Gao, 2012; S. Jang, Chae, Jung, Kim, & Kim, 2007; J. S. Kim, Cacialli, Cola, Gigli, & Cingolani, 1999; K. H. Lee, Jang, Kim, Tak, & Lee, 2004; H. T. Lu & Yokoyama, 2004; C. C. Wu, Wu, Sturm,

& Kahn, 1997). Recently, So and co-worker reported the ITO work function can be increased from 4.3 eV to 6.1 eV after oxygen plasma treatment (Irfan et al., 2012).

It is well known that ITO is an n-type degenerate semiconductor, rich with oxygen vacancies. These vacancies contribute to the high carrier concentration on ITO (Irfan et al., 2012; C. C. Wu et al., 1997). During oxygen plasma, these vacancies are passivated and as a result Fermi level is shifted away from the conduction band. This increases the ITO work function but at the same time making the ITO more intrinsic (I. M. Chan et al., 2002; Irfan et al., 2012; K. H. Lee et al., 2004). In addition to that, oxygen plasma helps to clean ITO surface from carbon contaminant which can enhance OLED lifetime and improves the device efficiency (I. M. Chan et al., 2002).

Very recently Helander et. al. reported that the work function of ITO can be increased up to ~6 eV by treating the substrate with dichlorobenzene and UV light (Helander et al., 2011). In this method, few drops of dichlorobenzene was dispensed on to the ITO surface and immediately after this, the sample was illuminated with UV light. The UV light breaks the Chlorine (Cl) from dichlorobenzene and bond Cl with Indium (In). The formation of In-Cl creates a layer of dipole layer across the ITO surface which increased the ITO work function (see Figure 2.17)



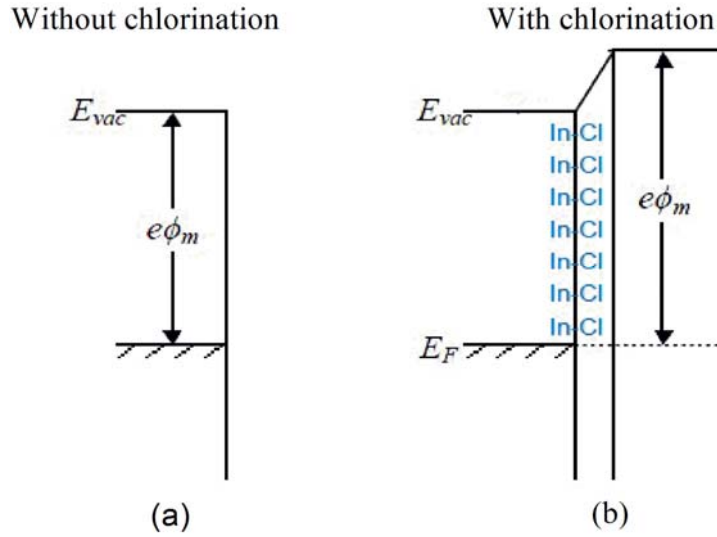


**Figure 2.17:** Workfunction ( $e\phi_m$ ) enhancement of ITO induced by In-Cl surface dipole. From (Helander et al., 2011).

Following the same concept, various groups have tried increased the ITO work function by halogenating the ITO surface. For example by using Cl plasma, ITO with work function  $\sim 6.1$  eV was reported by Zhang's group (Cao & Zhang, 2012). Zheng et. al. used a series of halogenated solvent precursor namely 1,2-difluobenzene, 1,2-dibromobenzene and 1,2-diiodobenzene to improve the ITO work function. The fluorinated, brominated and iodinated ITO gave work function of 5.45 eV, 5.72 eV and 5.47 eV respectively (Zheng & Wong, 2013). By dipping the ITO into chloroform and without any UV light treatment, Xu and co workers have improved the ITO work function from 4.58 eV to 4.86 eV (Z. Q. Xu et al., 2011). Realizing the fact that In-Cl can enhanced the ITO work function significantly, (Gao et al., 2012) vacuum deposited a layer of ultra thin  $\text{InCl}_3$  onto the ITO surface. By doing so, the work function of ITO can be increased by 0.48 eV.

### 2.7.2 Hole injection layer (HIL)

In OLED device, holes are injected from the anode, for example ITO to the HOMO of the organic semiconductor. To reduce the barrier injection, usually HIL is inserted between the anode and the first layer of the device. In general the HIL should meet the following requirements:

1. The HOMO level of the HIL should be positioned between the work function of the anode and the HOMO of the first organic layer of the device to prevent energetic mismatches at the anode/organic semiconductor interfaces.
2. High hole mobility.
3. Excellent thermal and chemical stability.
4. Good transparency.

One of the widely used HIL is PEDOT:PSS. PEDOT:PSS with work function  $\sim 5.1$  eV to  $5.3$  eV is a water soluble conducting polymer that exhibits high transparency in visible range and excellent thermal stability (Xia & Ouyang, 2010; Xia, Sun, & Ouyang, 2012). It is commonly used as HIL in OLED to assist hole injection and smoothen the ITO surface. Therefore the ability to tune the PEDOT:PSS work function to match the HOMO level of the next organic layer is technologically important to improve the device hole injection. One good example is the work done by Lee and co-workers where they blend PFI with PEDOT:PSS (T. H. Han, Choi, et al., 2012; T. H. Han, Lee, et al., 2012; T. W. Lee, Chung, Kwon, & Park, 2007; T. W. Lee et al., 2005). The surface work function of the PEDOT:PSS can be tuned from  $5.55$  eV to  $5.95$  eV by controlling the amount of PFI. More interesting, the PFI concentration in the PEDOT:PSS film tends to increase from ITO to the film surface thus creating a gradient work function profile with maximum work function at the film surface (T. W. Lee et al., 2007). This is due to the different surface energy between PFI and PEDOT:PSS.

The work function and resistivity of PEDOT:PSS can be altered by using UV-ozone treatment (Benor, Takizawa, Chen, Perez-Bolivar, & Anzenbacher, 2009; Helander et al., 2009; Lin et al., 2007; Nagata, Oha, Chikyow, & Wakayama, 2011). Details on the effects of UV-ozone on PEDOT:PSS film was carried out by (Nagata et al., 2011). The UV light in a UV-ozone cleaner consists of two major wavelengths i.e. 184.9 nm and 253.7 nm. These energetic UV wavelength provide sufficient energy to break chemical bonds in PEDOT:PSS film. This process not only causes film etching but also increase the PEDOT:PSS film resistivity. Simultaneously, oxygen are absorbed on to the PEDOT:PSS surface during the ozone treatment. Oxygen, having higher electron affinity tend to withdraw electron form the PEDOT:PSS results in a negatively charge surface which lead to the formation of surface dipole. This effect shifts the PEDOT:PSS HOMO to higher binding energy which effectively increase the work function. Using UV-ozone treatment, PEDOT:PSS work function enhancement from 5.16 eV to 5.68 eV has been reported (Nagata et al., 2011).

PEDOT:PSS has been successfully used as HIL in OLED for the past decade. Unfortunately, the residual moisture in the aqueous dispersed PEDOT:PSS film can caused severe reliability issues and degrades the device lifetime (Jorgensen et al., 2012; So & Kondakov, 2010). Furthermore the acidic nature of PEDOT:PSS etches ITO, causing In diffusion into the organic layers (de Jong, van IJzendoorn, & de Voigt, 2000; Duan et al., 2010a). Transition metal oxides (TMO) such as Molybdenum oxide ( $\text{MoO}_3$ ), Wolfram oxide ( $\text{WO}_3$ ) and Vanadium oxide ( $\text{V}_2\text{O}_5$ ) has been identified as the alternative of PEDOT:PSS. TMO, depending on the processing conditions has shown to exhibit very high work function, up to 7 eV for  $\text{V}_2\text{O}_5$  thin film (Meyer, Zilberberg, Riedl, & Kahn, 2011). In addition to this, it has low optical absorption in visible range and excellent thermal stability (Meyer et al., 2012). These properties make TMO an excellent alternative to PEDOT:PSS. Initially, TMO is vacuum deposited but recently

solution processed TMO is slowly gaining momentum (Zilberberg, Meyer, & Riedl, 2013). For instance, (Hofle et al., 2013) demonstrated blue OLED using solution processed MoO<sub>3</sub> as HIL with post-heat treatment at 150°C only. Very recently for the first time, room-temperature solution processed MoO<sub>3</sub> thin films as HIL was demonstrated on a green PHOLED (Fu, Chen, Shi, & Ma, 2013). The device efficiency was comparable to the device using PEDOT:PSS. More important the device lifetime is 2 order higher than the PEDOT:PSS device. These exciting works show that TMO is a promising approach in realizing practical applications for long-lifetime flexible OLED.

### **2.7.3 Hole transport layer (HTL)**

HTL provides a pathway for hole to transport from anode into the EML and prevents electron reaching the anode which can lead to excitons quenching. A good HTL should meet the following requirements:

1. Good hole mobility and retards electron transport.
2. HTL material must have electron-donating moieties to form fairly stable radical-cation.
3. The HOMO level of HTL should higher than the EML and preferably isoenergetic with HIL.
4. High thermal stability to prevent crystallization during device operation due to Joule heating.
5. A high LUMO to block the electron transport.
6. The triplet energy of HTL need to be sufficient high to reduces excitation quenching.

For phosphorescent OLED, the triplet energy of the HTL need to be higher than the triplet energy of the dye. This is very important to prevent back triplet energy transfer which can reduce the device efficiency. HTL can be doped to improved carrier injection and charge transport (Blochwitz, Pfeiffer, Fritz, & Leo, 1998; Walzer, Maennig, Pfeiffer, & Leo, 2007; Yamamori, Adachi, Koyama, & Taniguchi, 1998).

#### **2.7.4 Emissive layer (EML)**

This layer emits light. Ideally all the excitons should be confined in this layer. In guest-host system, it consists of dye doped in a small percentage into a host material. The host provide spatial separations for the guest to prevent severe excitons quenching due to TTA while the emission wavelength is guest dependent. A good host should have the following properties:

1. Exhibits good electron and hole conduction.
2. Thermally and chemically stable.
3. Phase compatible with guest materials
4. Triplet energy of the guest need to be lower than the triplet energy of the host to ensure exothermic energy transfer from host to guest (Sasabe & Kido, 2011; Tokito et al., 2003).

For non guest-host system, the EML is fluorescent emissive materials.

#### **2.7.5 Electron transport layer (ETL)**

The functions of ETL follow the same principles with HTL. In addition of providing a pathway for electron to transfer into the EML, it also assists excitons confinement in ETL. It should meet the following criteria:

1. Good electron mobility and exhibits very poor hole transporting characteristic.
2. ETL material must have electron-withdrawing moieties to form fairly stable radical-anion.
3. Ideally, the lowest unoccupied molecular orbital (LUMO) of the ETL should be isoenergetic with the work function of EIL/cathode to reduce the barrier height for electron injection.
4. High thermal stability to prevent crystallization during device operation due to Joule heating.

#### **2.7.6 Electron injection layer (EIL) / cathode interfacial material**

Low work function metals are highly desirable for the OLED cathode in order to minimize electron injection barrier to the organic semiconductor LUMO. Unfortunately, low work function metals are very easily oxidized. Initially, this problem was circumvented by capping high work function metal such as Ca (Parker, Cao, & Yang, 1999) or Ba (Braun & Heeger, 1991) with Al. Although it solves the problem, these metals are highly reactive which make the fabrication process very challenging. One solution to this problem is to insert a very thin layer (~1nm) of alkali metal fluoride or alkali metal carbonate in the interface between Al and the organic layer. This thin cathode interfacial layer is known as EIL (Chiba et al., 2012; Hatwar & Spindler, 2008). Some of the well-known buffer layers are LiF (Hung, Tang, & Mason, 1997; Hung, Tang, Mason, Raychaudhuri, & Madathil, 2001; Mason et al., 2001), CsF (Brown et al., 2003; Jabbour, Kippelen, Armstrong, & Peyghambarian, 1998; Lai, Chan, Lee, & Lee, 2003) and Cs<sub>2</sub>CO<sub>3</sub> (J. S. Huang, Xu, & Yang, 2007; Rao, Su, & Huang, 2013; C. I. Wu et al., 2006). When Al is deposited onto Cs<sub>2</sub>CO<sub>3</sub>, chemical reaction takes place producing Al-O-Cs complex which can reduce the cathode work function to 2.1

eV (J. S. Huang et al., 2007). For CsF, (Piromreun et al., 2000) proposed that the deposition of Al dissociate CsF, forming  $\text{AlF}_3$  and liberating Cs. Cs having a low function of 1.9 eV is beneficial for electron injection. On the other hand, the mechanism of LiF in lowering the OLED cathode work function is controversial (Brown et al., 2003). The first proposed mechanism is similar to the case of CsF and  $\text{Cs}_2\text{CO}_3$  where the deposition of Al dissociate LiF to liberate Li (Heil et al., 2001; Le et al., 2000). These Li atoms dope the organic material /cathode interfacial region and create low work function contact for electron injection. The other mechanism is LiF does not dissociate, instead work function change is caused by surface dipole, shifting the vacuum level between the organic layer and metal electrode, resulting in lower cathodic barrier height (Brown et al., 2003; Schlaf et al., 1998). It was found that this dipole originates from the chemisorption of water molecule on the LiF due to the hygroscopic nature of LiF and the water molecules are not properly pumped out during vacuum deposition of LiF (Schlaf et al., 1998). Heil et. al. showed that the dissociation of LiF is only possible with the presence of water molecule (Heil et al., 2001). This is further proved by (Greczynski, Fahlman, & Salaneck, 2000) where they showed that when cathode deposition was carried out in Ultra High Vacuum (UHV) ( $10^{-9}$  -  $10^{-10}$  mbar), no significant LiF dissociation nor dipole effect was observed. The third proposed mechanism is that the presence of a ultra thin LiF layer will induce sufficient band bending at the organic layer next to the LiF. When the LiF is thin enough to allowed large voltage drop, it will induce sufficient band bending to initiate tunnelling process from the Al to the organic layer (Hung et al., 1997; Parker & Kim, 1994).

### 2.7.7 Cathode

The cathode for OLED should have the following properties:

1. Good stability
2. Highly reflective. In the case of inverted OLED, it should be highly transparent.
3. Low work-function to reduce the barrier height for electron injection into the LUMO level of the adjacent organic semiconductor
4. Low resistivity to minimize contact resistance.
5. Good wetting properties and adhesion with the adjacent organic materials.

OLED cathode engineering usually aims to reducing the barrier height for electron injection. Low barrier height for electron injection is crucial in reducing the OLED operating voltage and improves the device efficiency. One of the widely use method is by inserting a thin layer of alkali metal fluoride or alkali metal carbonate between the organic layer and Al as already discussed in section 2.7.6.

Another widely adopted strategy is to increase the roughness of the organic layer/Al interface which effectively increases the contact area and promotes electric field localization. For example, Liu et. al. incorporated multiwall carbon nanotube (CNT) on top of the OLED EML layer before the deposition of Al (D. Liu et al., 2009). The presence of CNT caused upward shift of the EML LUMO by 0.3 eV thus lowering the electron injection barrier. In addition to this, CNT promotes electric field localization which helps electron injection. Peng's group reported on a simple method in improving the OLED efficiency by spin coating methanol or ethanol on top of the EML before cathode deposition (Q. Wang et al., 2011). This simple concept increased the quantum efficiency of the OLED by 58%. The efficiency improvement was



attributed to the formation of dipole on the interface between EML and cathode induced by the alcohol solvent.

Another very attractive concept reported recently by Jenekhe's group is spin coating a highly concentrated electron transport materials (ETM) dissolved in formic acid and deionized water prior to the deposition of Al (Ahmed, Earmme, & Jenekhe, 2011; Earmme, Ahmed, & Jenekhe, 2010; Earmme & Jenekhe, 2012a). High densities of vertical nanopillars were observed on the surface of the ETM thin films which can maximize the Al/ETM contact area and promotes electrical field localization. This effects help electron injection in the vertical direction. Using this method, efficiency improvement up to 40% was reported for a green PHOLED (Earmme & Jenekhe, 2012a).

Wong's group reported on a simple single layer poly (phenylene vinylene) (PPV) based OLED blended with polymer oxide surfactant i.e. poly(ethylene glycol) (PEG) which improves the device efficiency by two order (Deng et al., 2004). The PEG phase segregated to the PPV film surface (F. C. Chen & Chien, 2009) and reaction took place between Al and the lone pair electrons in the PEG, which results in the formation of  $Al^{3+}$ . Electrons released during this process doped the surface of the PPV film forming a thin interfacial n-type layer. This interfacial layer helps electron injection by lowering the work function of Al. This reported work generated much interest and subsequently (F. C. Chen, Chien, & Lee, 2008; L. Li, Liu, Yu, & Pei, 2011; Niu, Ma, Xu, & Jen, 2005) found out that the polymer oxide surfactant also roughened the organic film surface. The rough surface is beneficial in improving the device performance. First, rough surface promotes electric field localization. Second, the effective area of the cathode increases with rougher surface. Both of these attributes assist electron injection.

## **CHAPTER 3: Experimental methods**

### **3.1 Introduction**

In this work OLEDs were fabricated using wet process and the devices were evaluated using different characterization techniques. The following sections consist of two major parts. The first part describes the OLEDs fabrication process whereas the second part presents the characterization techniques carried out to extract useful information related to the OLED performances.

### **3.2 OLED fabrication process**

The OLED fabrication process begins with patterning of ITO using standard lithography method. Bare ITO deposited on polished soda lime glass was used as substrate. The ITO/glass substrates were purchased from Luminescence Technology Corporation, Taiwan. The thickness of the ITO and glass was 120 nm and 1.1mm respectively. The size of the substrates was 15 mm X 20 mm. The substrates were cleaned sequentially using deionised water (DI), acetone, isopropyl alcohol, and DI water again for 10 minutes. Photoresist (AZ5214E) was spin casted on to the substrate at 4000 rpm ( $\sim 1.4 \mu\text{m}$ ) and then baked at 105°C for 105 seconds to remove the residual solvent in the photoresist. Next using Oriel 87431 contact mask aligner, the substrates were exposed by mercury lamp with i-line (365nm) output through a chrome photo mask. AZ developer diluted with DI water in 1:2 of volumetric ratio was used to develop the substrates. Development in DI water diluted AZ developer for 1 minute creates the desired pattern on the photoresist. Following that, the substrates were baked in the oven at 110°C for 10 minutes to harden the photoresist. Using

photoresist as a protective layer, the exposed ITO was etched using hydrochloric acid (HCl) diluted in DI water in 1:1 volumetric ratio at 80°C. Finally the photoresist was stripped using in 10% sodium hydroxide (NaOH) solution. The substrates were rinsed thoroughly using DI water and cleaned in a sonicator bath using IPA, acetone and DI water again for 20 minutes. Figure 3.1a shows the lithography mask and the ITO pattern dimensions.

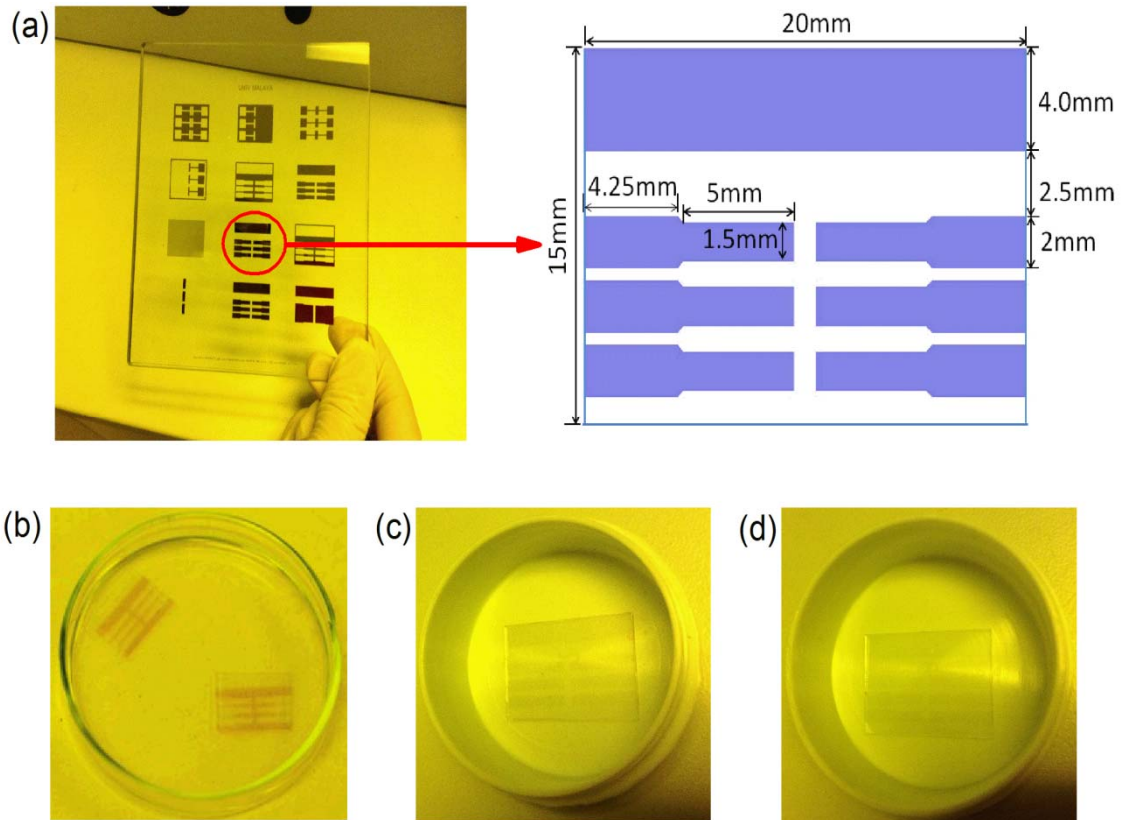


**Figure 3.1:** (a) Photolithography mask and the ITO pattern dimensions. (b) Development of ITO in AZ developer diluted with DI water. (c) ITO substrate after HCl etch and (d) ITO after photoresist stripping.

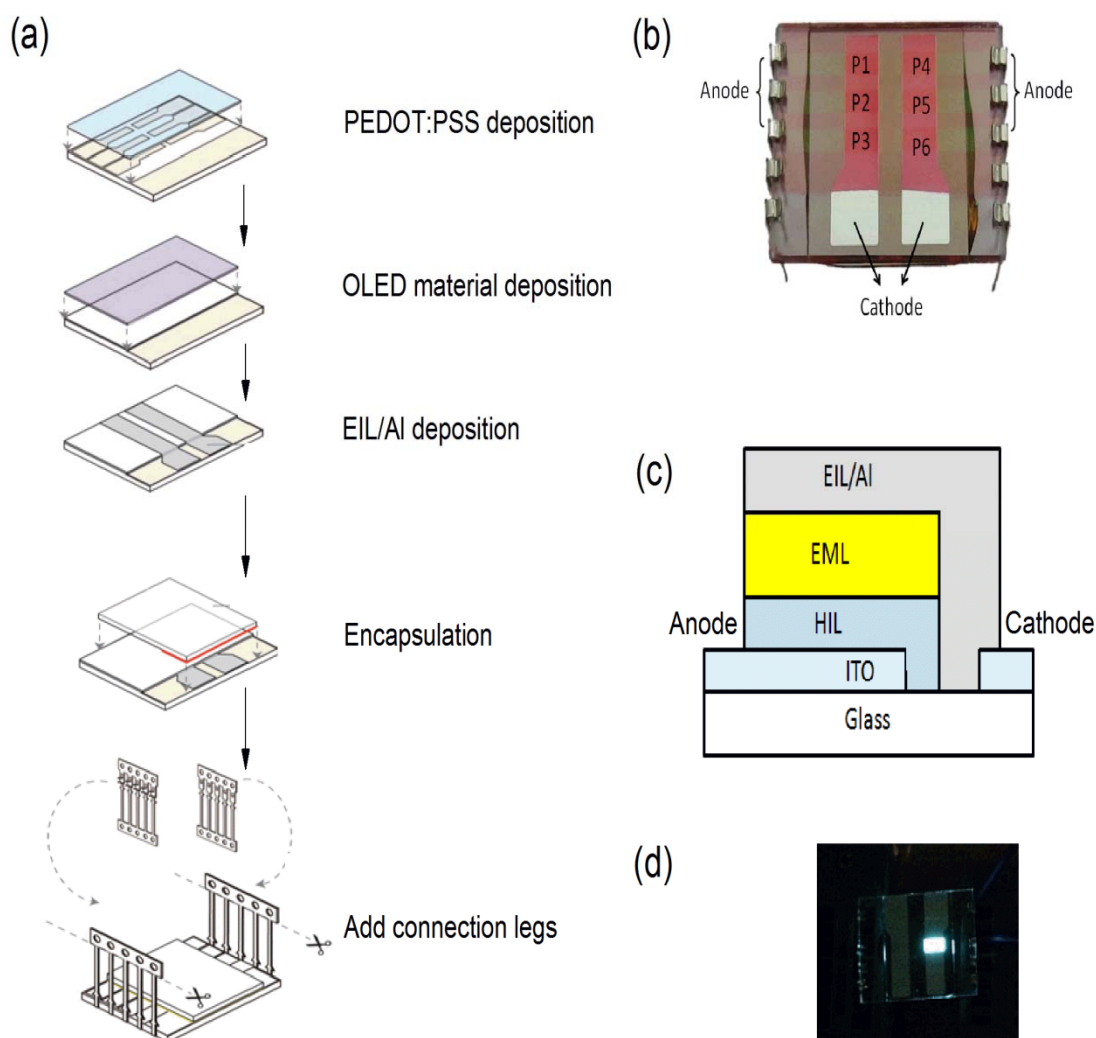


**Figure 3.2:** (a) OLED fabrication process. (b) Photograph of an actual device. The device consists of six active areas, denoted by P1 –P6. (c) Simplified diagram indicating the cross section of a single pixel. (d) An actual light up blue device.

The OLED fabrication process is summarized in Figure 3.2. To fabricate OLEDs, patterned ITO substrates were treated using oxygen plasma at 35 W for 5 minutes. The oxygen plasma treatment is crucial. First it removes organic contaminants through chemical reaction of highly reactive oxygen radicals. Second it increases the ITO work function. More important, it promotes surface hydroxylation which improves the surface wettability. Immediately after the oxygen plasma treatment, aqueous dispersion of PEDOT:PSS was spin coated on to the substrates to form a 40 nm film. The substrates were annealed at 150°C in N<sub>2</sub> environment to remove water residual. Next OLED material dissolved in organic solvent was spin

coated on top of the PEDOT:PSS, followed by annealing process to remove the residual solvent. The OLED material, choice of organic solvent and annealing temperature are depending on the device architecture and the organic material properties. After that, the device cathode which consists of EIL/AL were sequentially evaporated at base pressure of  $2.5 \times 10^{-6}$  mbar through a shadow mask. Lastly, the devices were encapsulated using UV (Ossila) curable epoxy and glass lid. All the fabrication process except the PEDOT:PSS film deposition was carried out in a glovebox with oxygen less than 100 ppm and moisture below 40 ppm. The OLED device consists of six active areas defined by the overlapping of the cathode and anode. The active area of the device was  $4.5 \text{ mm}^2$ .

### 3.3 Current density-voltage-luminance (J-V-L) measurement

The most basic and important measurement for OLED is the J-V-L measurement. The J-V-L measurements were carried out using Konica Minolta CS-200 chroma meter integrated with a Keithley 236 source-measuring-unit (SMU). The measurement was carried out in a dark enclosure to avoid stray light. Voltage from the SMU was applied across the OLED and simultaneously the current, luminance of the device were captured by the chroma meter. OLED efficiency is commonly characterized by current efficiency and power efficiency. These efficiencies can be easily calculated from the J-V-L data. Current efficiency (cd/A) is the luminance (L) generated by the device per unit current (I). Current efficiency from luminance in forward direction can be calculated using:

$$\eta_{CE} = L/I \quad (3.1)$$

with L and I is the measured brightness and operating current respectively.

On the other hand, power efficiency or luminous efficacy (lm/W) of the device in forward direction can be described as (Reineke, Thomschke, Lussem, & Leo, 2013):

$$\eta_{PE} = \eta_{CE} \cdot \pi \cdot f_D / V \quad (3.2)$$

where

$$f_D = \frac{1}{\pi I_0} \int_0^{\pi/2} \int_{-\pi}^{+\pi} I(\theta, \phi) \sin \theta \, d\phi d\theta \quad (3.3)$$

The  $f_D$  factor takes into the consideration of the light intensity distribution in forward hemisphere.  $I_0$  is measured light intensity in forward direction and  $V$  is the operating voltage. The J-V-L measurement setup is shown in Figure 3.3.

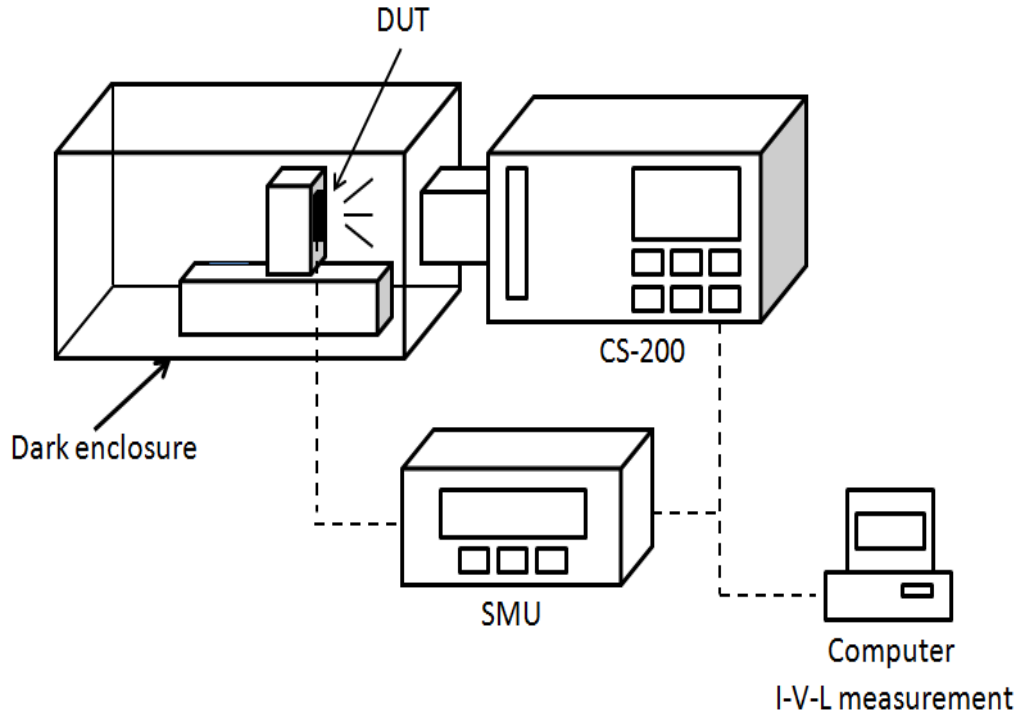


**Figure 3.3:** I-V-L measurement setup. DUT denotes device under test.

### 3.3.1 Photovoltaic measurement of OLED

Photovoltaic measurement is an extension of the device I-V measurement as discussed in section 3.3. The device is illuminated with AM1.5 light source (Newport 67005) at  $100 \text{ mW/cm}^2$  in a dark enclosure and the device I-V characteristics is obtained using Keithley 236 SMU. It is a simple yet powerful technique in studying the changes of the device built-in-potential,  $V_{bi}$ .

The basic concept of photovoltaic measurement can be understood with the following explanation. Consider a simple OLED active layer sandwiched between anode and cathode. Due to the difference between the work function of these two electrodes, a built-in field exist inside the device at equilibrium. In dark condition, when the forward bias,  $V_f$  is less than the built-in potential i.e.  $V_f < V_{bi}$ , hole/electron injection at the anode/cathode takes place via thermionic emission process. The resultant current is the competition between the reverse drift and forward diffusion with the later being the dominant mechanism in the dark condition (Malliaras, Salem, Brock, & Scott, 1998). The reverse drift component is attributed to the effect of the  $V_{bi}$ .

When the sample is irradiated with light, additional carriers are generated inside the device by photoexcitation process. It is widely known that excitons in organic materials are strongly bounded. Therefore the dissociation of the excitons formed by photo excitation process into free carriers is highly not probable. The free charge generation mechanism involved here is the dissociation of excited state through charge transfer to the metallic electrode, leaving the other free charge inside the organic materials (Malliaras et al., 1998). When the applied voltage is less than  $V_{bi}$ , these carriers will drift under the influence of the built-in field (Ray, Patankar, Periasamy, & Narasimhan, 2005). During photovoltaic measurement, the external applied voltage are gradually increased and when the forward bias compensated  $V_{bi}$  i.e.  $V_f = V_{bi}$ , the measured current drops to minimum as illustrated in Figure 3.4. The voltage at this

point is known as the open-circuit voltage,  $V_{OC}$  and it provides an indication on the device  $V_{bi}$ .

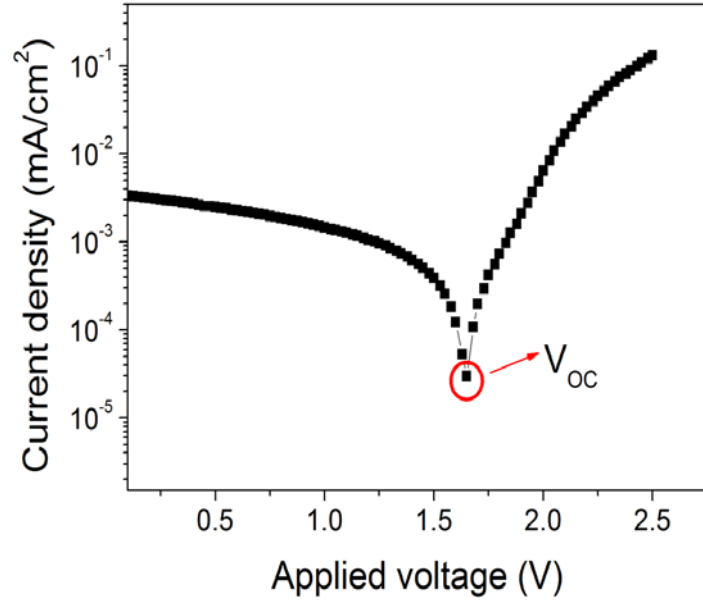


**Figure 3.4:** An example of the photovoltaic measurement results of a OLED.

A higher  $V_{OC}$  indicates that the injection barrier either at the cathode or anode has reduced. Experimentally obtained  $V_{OC}$  is lowered than the actual  $V_{bi}$ . It is because the  $V_{OC}$  is temperature dependent. The relation of  $V_{OC}$  and  $V_{bi}$  can be simplified as follows (Kouki, Karsi, Lang, Horowitz, & Bouchriha, 2012):

$$V_{OC} = V_{bi} - \frac{kT}{q} \ln \left( \frac{g_a}{g_c} \right) \quad (3.4)$$

where  $k$  is Boltzmann constant,  $T$  is the temperature,  $q$  is the elementary charge,  $g_a$  and  $g_c$  are the density of the photogenerated holes at the anode and cathode respectively. Therefore unless the measurement is carried at very low temperature,  $V_{OC}$  obtained is usually lower than  $V_{bi}$  (Malliaras et al., 1998). Another possible reason is the presence of a substantial space-charge near the injecting electrodes at voltages well below  $V_{bi}$  which can result in the difference between  $V_{OC}$  and  $V_{bi}$  (Kemerink, Kramer, Gommans, & Janssen, 2006). Finally, the Fermi-level pinning of the electrodes also can lead to the deviation of the experimentally obtained  $V_{OC}$  from  $V_{bi}$ .



### 3.4 Fourier transforms infrared (FTIR) spectroscopy

FTIR is a fast and efficient technique in indentifying an unknown compound and detect the presence of certain chemical groups in a sample. In FTIR, infrared (IR) beam consists of frequencies in the range of  $625\text{ cm}^{-1}$  to  $4000\text{ cm}^{-1}$  is passed through a interferometer. The interferometer consists of a beam splitter which splits the incoming IR beam into two optical beams. One of the beams is reflected by a fixed mirror back to the beam splitter. The other optical beam will be directed to a moving mirror. Due to the motion of the mirror, the total path of the second beam is constantly varied. The difference of the beams path length results in interference when these beams recombine at the beam splitter again. The resulting beam is known as interferogram (S. Zhang, Li, & Kumar, 2009). By using this method, all the IR wavelengths from a polychromatic light source can be scanned. When the interferogram is irradiated on to the sample, it can initiate a molecular bond to vibrate if its frequency matches the natural frequency of the bonding atom (Williams & Fleming, 2008). This is because the vibrational energy of a molecular bond is quantized. Therefore parts of the IR wavelengths are absorbed if the selection rule is met. The interferogram that pass through the sample are analyzed and decoded into frequency domain via Fourier Transform. Figure 3.5a shows the schematic diagram of a FTIR setup.

If the sample is not transparent, FTIR can be performed on reflective mode. One widely adopted method is the Attenuated Total Reflection (ATR) (Ulman, 2010). In ATR mode, IR beams passed through a high reflective index crystal and reflected by the surface of the crystal. The evanescent wave generated on the crystal surface project orthogonally to towards the sample as shown in Figure 3.5b. Parts of the IR wavelength are absorbed and the rest will be reflected by sample and captured by the detector. The samples in this work were characterized using FTIR ATR mode i.e. Perkin Elmer Spectrum 400 spectrometer with 1 nm resolution.

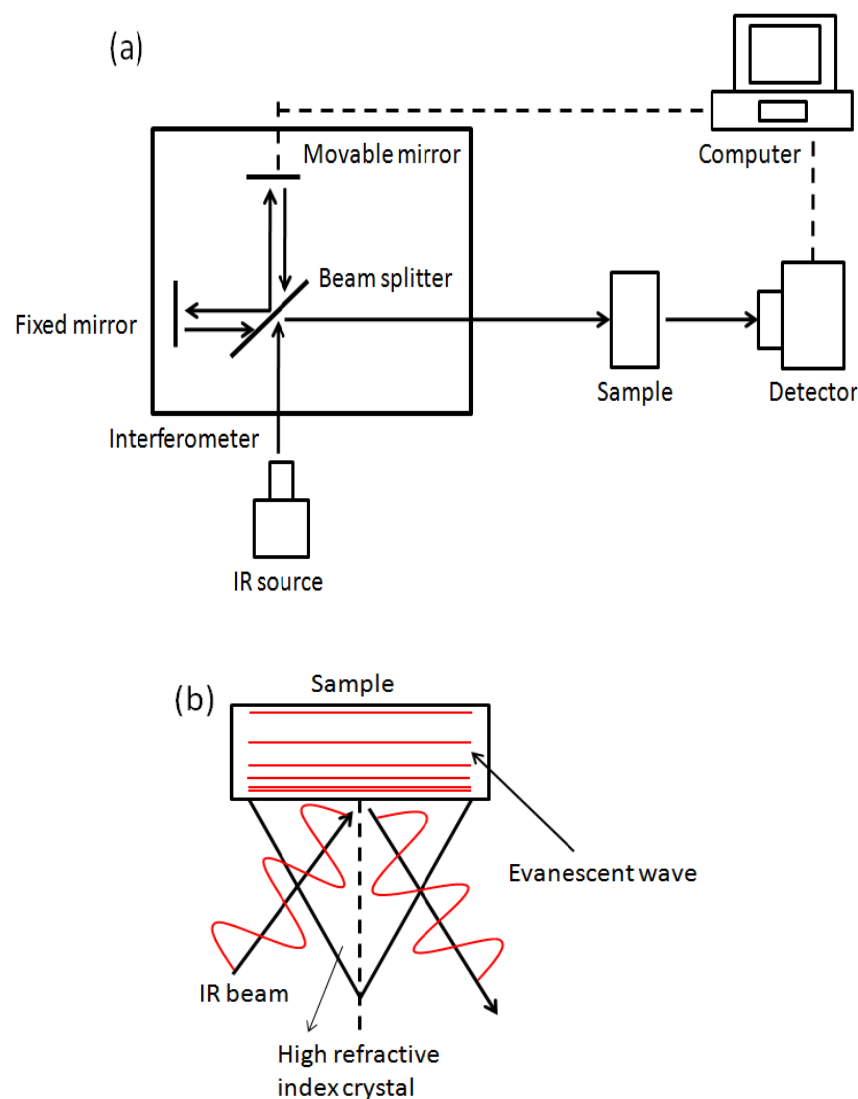


**Figure 3.5:** (a) Schematic diagram of FTIR spectroscopy setup and (b) FTIR ATR operation principles. Adapted from (S. Zhang et al., 2009) and (<http://www.piketech.com/information.html>).

### 3.5 Ultraviolet-visible (UV-Vis) absorption spectroscopy

The operation principle of UV-Vis spectroscopy is based on the selective light absorption in the range of 200 nm – 800 nm by a material. The absorbed energy will cause electronic transition from lower energy orbital (ground state) to higher energy orbital if the wavelength of the absorption is correspond to the energy difference between these orbitals. The absorbance ( $A$ ) of a compound is defined as:

$$A = \log_{10} \frac{I_0}{I} \quad (3.5)$$

where  $I_0$  and  $I$  is the intensity of the incident and transmitted light respectively.

On the other hand, absorbance is proportional to three variables i.e path length ( $l$ ), concentration of the absorption species ( $c$ ) and molar extinction coefficient ( $\epsilon$ ) as stated by Beer-Lambert laws (S. Zhang et al., 2009) :

$$A = \epsilon \cdot l \cdot c \quad (3.6)$$

where the  $l$ ,  $c$  and  $\epsilon$  is expressed in cm, molL<sup>-1</sup> and Lmol<sup>-1</sup>cm<sup>-1</sup> respectively. The molar extinction coefficient is substance dependent. A substance with high molar extinction coefficient absorbs more light (of the appropriate wavelength) and thus can be easily detected by UV-Vis spectroscopy.  $I_0$  and  $I$  is a function of wavelength ( $\lambda$ ) and therefore the plot of  $A$  vs  $\lambda$  gives the absorbance spectrum.

For organic compound, the possible electronic transitions are shown in Figure 3.6. Among these transitions only  $\pi \rightarrow \pi^*$  and  $n \rightarrow \pi^*$  can be realized by light absorption in the UV-Vis region. This is because absorption in these transitions fall between 200 nm - 800 nm. Functional groups that strongly absorbed light in UV-Vis region are known as chromophores.

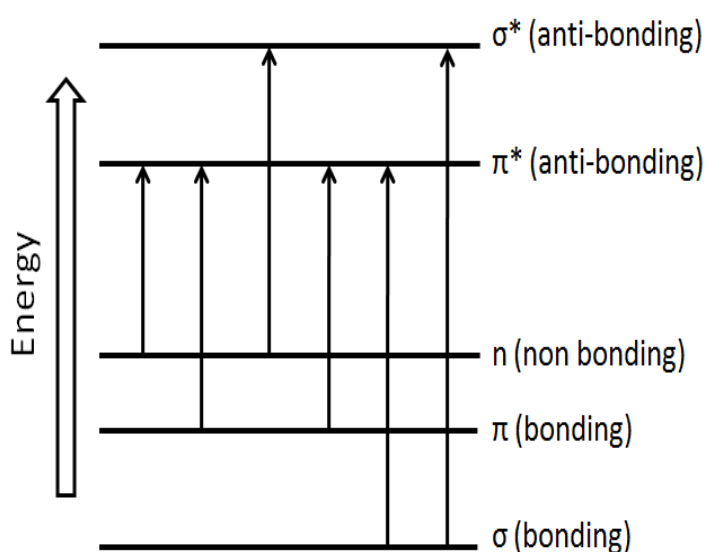


**Figure 3.6:** Possible electronic transitions of organic compound.

The schematic diagram of the UV-Vis spectroscopy setup is shown in Figure 3.7. UV and visible light sources are directed to a diffraction grating where the components of the wavelength are separated. Each light with single wavelength are split into two optical beams with equal intensities. One of the beams is the reference beam, will pass through the reference sample. The second beam passes through the sample and finally both beams intensities are measured and compared by the detectors. The spectroscopy scans the wavelength in UV (200-400 nm) and visible (400-800 nm) region in a very short period of time. Finally the computer output the sample absorbance plotted across the UV- Vis wavelength. The UV-Vis characterizations in this research work were carried using Perkin Elmer PE750 UV-Vis, with resolution of 1nm.

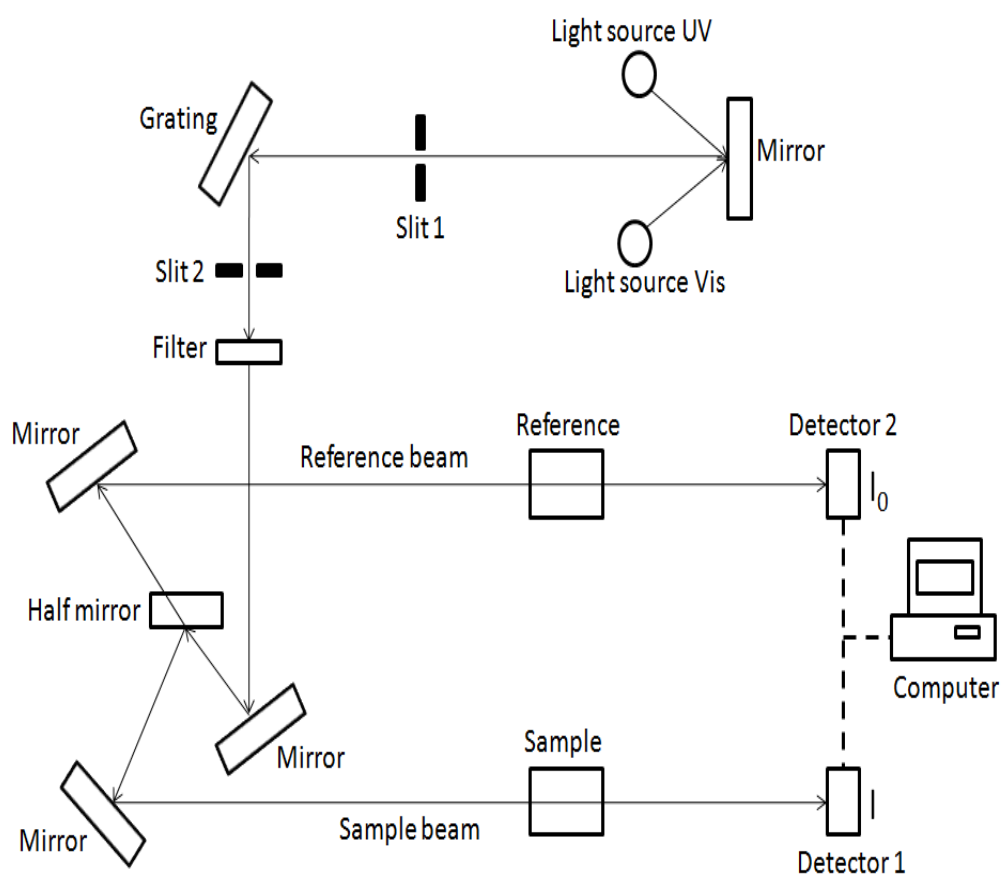


**Figure 3.7:** Schematic diagram of a UV-Vis spectroscopy setup. Adapted from (<http://www2.chemistry.msu.edu/faculty/reusch/virttxtjml/spectrpy/uv-vis/uvspec.htm>)

### 3.6 Surface profiler

Surface profiler is capable of measuring the step height of thin film and provides analysis of the surface roughness and waviness in the form of 3D or 2D scan. Figure 3.8 shows the simplified schematic diagram of a surface profiler. During scanning, the stylus is moved across the sample surface at a constant velocity while maintaining a constant applied stylus force (Poon & Bhushan, 1995). As the stylus is moved, the contact force between the stylus and the sample surface is sensed by a displacement capacitance sensor. This information is feed back to the computer and the surface profile can be modelled. Selecting the appropriate constant applied stylus force is very important. If the force is too low, it will lose contact with the sample surface when it encounters a high aspect ratio feature. On the other hand, a high stylus force may damage the sample during the scanning process. Generally the recommended stylus load is in between 1 mg – 2 mg. In this work, surface profiler P-6 (KLA Tencor) was used to check the thickness of spin coated organic thin film. The sylus load was set at 1 mg with the tip radius of 2  $\mu\text{m}$ .

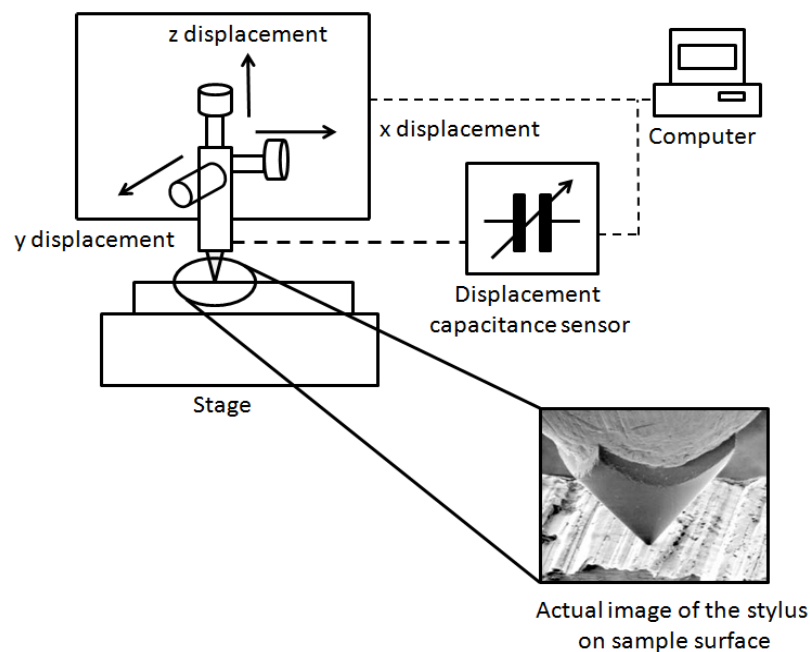


**Figure 3.8:** Simplified schematic diagram of a surface profiler. Adapted from ([www.ptb.de/cms/en/fachabteilungen/abt5/fb-51/ag515/tastschnittverfahren0.html](http://www.ptb.de/cms/en/fachabteilungen/abt5/fb-51/ag515/tastschnittverfahren0.html))

### 3.7 Atomic force microscopy (AFM)

In OLED research, AFM is primarily used for surface imaging at nanoscale region. The schematic diagram of an AFM setup is shown in Figure 3.9. Its operation principle is based on the detection of laser beam on a cantilever as it moves across the sample surface. The cantilever tip is usually made of silicon or silicon nitride tip with radius of curvature in several tenths of nm. AFM imaging, as its name implies, relies on the force interaction between the cantilever tip and the sample surface. These forces will deflect the cantilever as it raster scans across the sample corrugation, which results in changes in the reflected laser beam intensities. The differences in the signal intensities are then converted into surface topography.

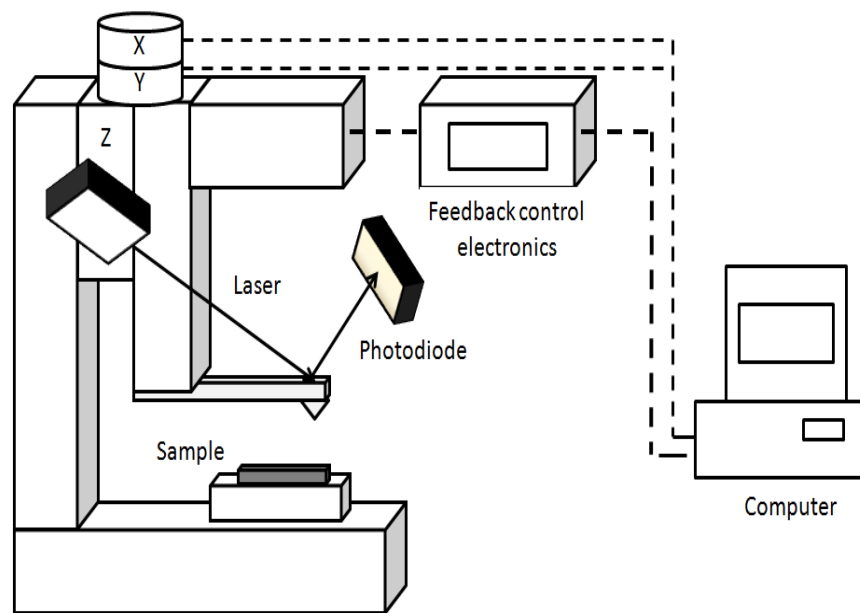


**Figure 3.9:** Schematic diagram of a AFM setup.

Two commonly used imaging modes in AFM are contact mode and tapping mode. In contact mode, cantilever tip with low spring constant is in permanent contact with the sample surface and constantly deflected as the scanning progress (L. Yang, 2008). It is based on the Lennard-Jones interaction potential between two atoms as shown in Figure 3.10a. When the tip is very close or in hard contact with the surface, due to atomic force the cantilever will be repelled from the sample surface. However as the tip starts

to move away from the sample the interaction forces are attractive. The surface morphology can be determined from the cantilever deflection. The disadvantage of this technique is the shear force applied by the tip on to the sample during scanning process.

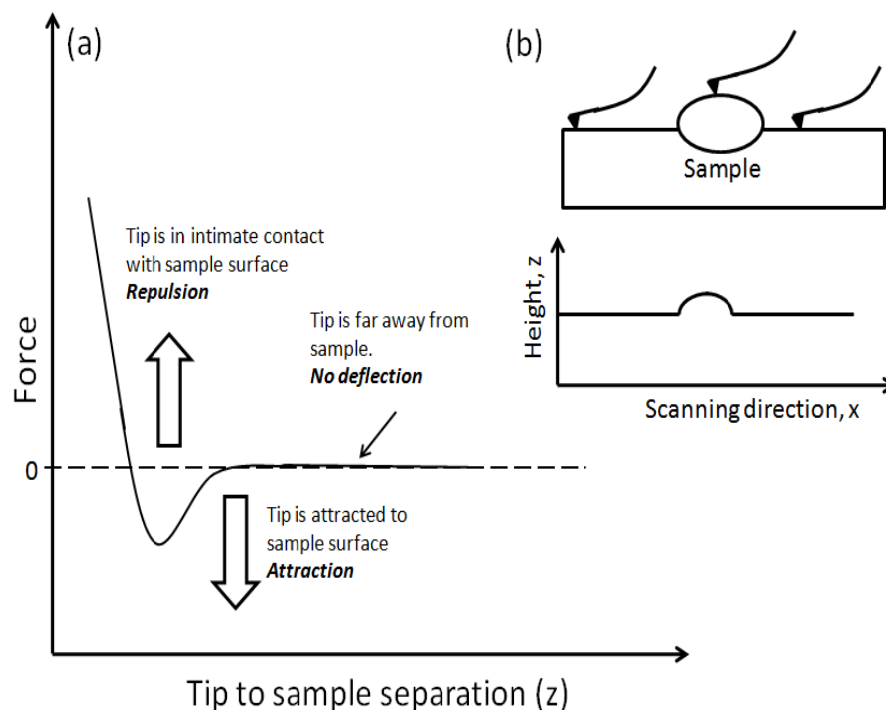


**Figure 3.10:** (a) Variation of the atomic force as a function of tip separation. (b) Height detection by AFM cantilever tip operated in contact mode. Adapted from ([www.nanoscience.com/education/afm.html](http://www.nanoscience.com/education/afm.html))

In this research work, the AFM measurements were done on NT-MDT NTEGRA-Prima and NX10 (Park Systems) operating at tapping mode. In this mode, the tip of the cantilever is oscillating at high frequency ( $\sim 50\text{k}-500\text{ kHz}$ ) and intermittently taps the sample surface. The amplitude of the tip oscillation changes when there are differences on the surface topography (see Figure 3.11). For instance, when the tip encounters a bump its oscillation amplitude decreases. Conversely, the amplitude increases when the tip passes a cavity because it has more room to oscillate. These changes are feedback to the computer and the surface morphology can be computed. These forces deflect the cantilever and by measuring the cantilever deflection, the image of the samples surface can be mapped out. By using tapping mode, lateral drag force on the sample surface is

eliminated, making it a suitable method for specimen that has poor adhesion on the substrate. In addition to that, tip-sample adhesion can be reduced.

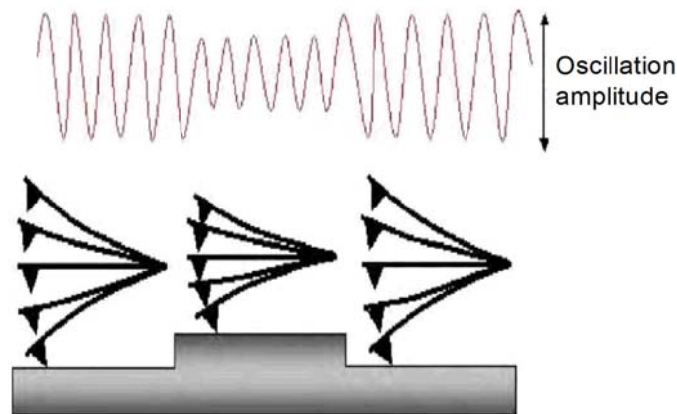


**Figure 3.11:** Step profile detection through the changes of cantilever tip oscillation amplitude.

Phase measurement is a powerful extension of AFM operating in tapping mode. It measures the phase differences of the vibrating cantilever (see Figure 3.12) when the tip comes across surfaces with different adhesion, friction, composition or elasticity. The phase shift is proportional to the inelastic energy transferred from the cantilever tip to the sample surface (N. F. Martinez & Garcia, 2006; L. Yang, 2008).

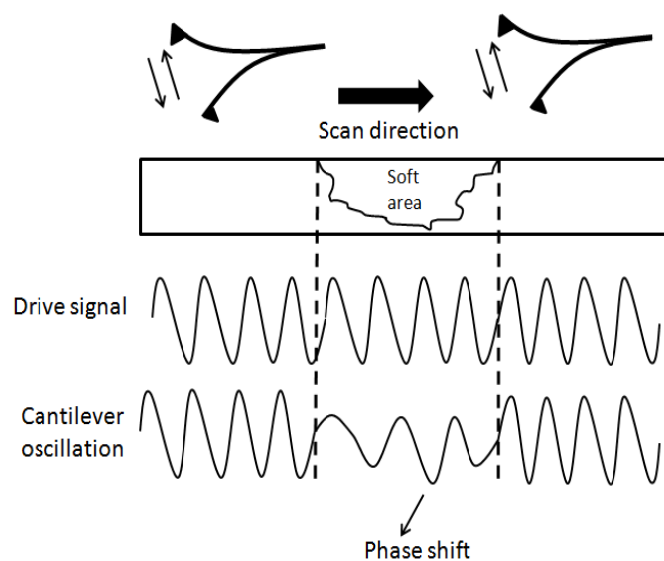


**Figure 3.12:** Phase imaging by AFM. Adapted from ([www.bruker.jp/axs/nano/imgs/pdf/AN011.pdf](http://www.bruker.jp/axs/nano/imgs/pdf/AN011.pdf))



### 3.8 4-point probe

. In our research, Jandel Universal 4-point probe powered by Keithley 236 SMU was used to measure the conductivity of a thin film. The 4-point probe setup is shown in Figure 3.13. It consists of 4 tungsten carbide probes equally spaced at 1 mm. Current is supplied through the outer two probes by a Keithley 236 SMU and simultaneously the voltage across the inner two probes is measured. The other ends of the probes are supported by spring to eliminate any damage on the sample during probing. If the probe spacing ( $s$ ) is much larger than the film thickness ( $t$ ) i.e.  $t \ll s$ , then the conductivity of the thin film can be computed as follows (Schroder, 2006):

$$\sigma = \frac{\ln 2}{\pi \cdot t} \cdot \left( \frac{I}{V} \right) \quad (3.7)$$

with  $\frac{I}{V}$  obtained from the SMU measurement.

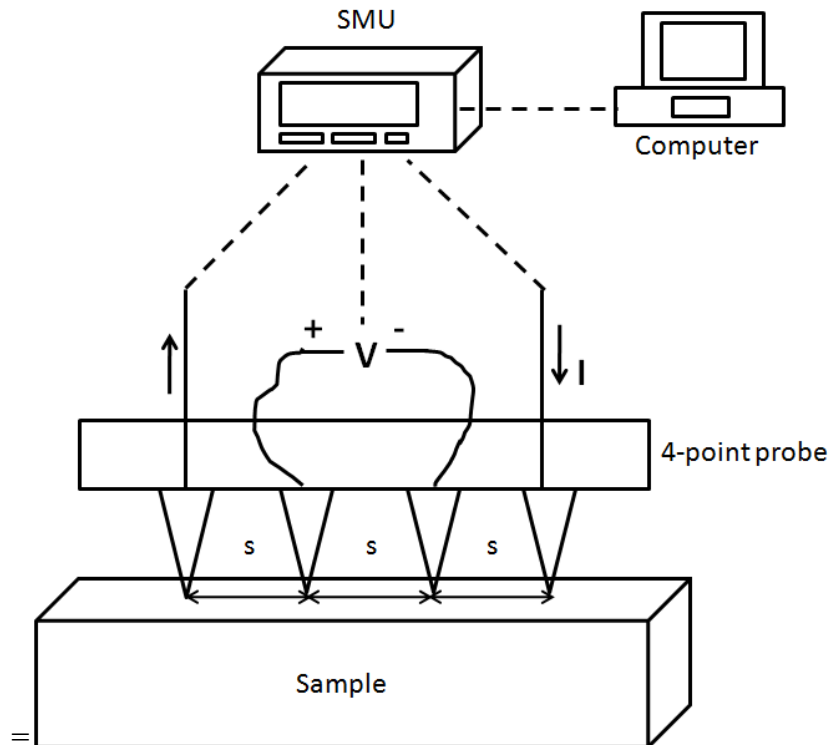


**Figure 3.13:** Schematic diagram of a 4-point probe setup.

### 3.9 Photoluminescence (PL) measurement

Electron in a chemical compound will vibrate and/or be excited to higher energy state if it absorbed sufficient energy. For this transition to occur, the excitation energy must be equal to the energy difference between the initial state and the next higher energy state (Guilbault, 1973). This excitation energy usually express in wavelength. Fluorescence emission occurs when electron absorbs energy in the UV-Vis range (200 nm-800 nm), excited to the higher energy state with life time of  $\sim 10^{-9}$  s and emit photon when it relax to the initial state. The emission energy is always less than the excitation energy because some of the energy is lost through phonon and heat. PL measurement is the measurement of the fluorescence emission given known excitation energy.

In this research, photoluminescence measurement was carried out using Perkin Elmer LS50B fluorescence spectrometer. The spectrophotometer uses Xenon as light source. Equipped with two monochromators, it can provide excitation and emission in the range of 200 nm to 800 nm and 200 nm to 900 nm respectively. The typical setup for a fluorescene spectrometer is shown in Figure 3.14. Broad band light from Xenon light source is passed through the excitation monochromator where only the selected wavelength will pass through the monochromator. The slit controls the amount of light incident onto the sample and into the detector. It also helps to reduce stray light and control the specimen surface area sampled by the spectrometer. The output beam from the excitation chromator is used to excite the sample. The emission is passed through the emission monochromator and the signal is enchanced by a amplifier. By scanning the emission monochromator the emission spectrum can be obtained.

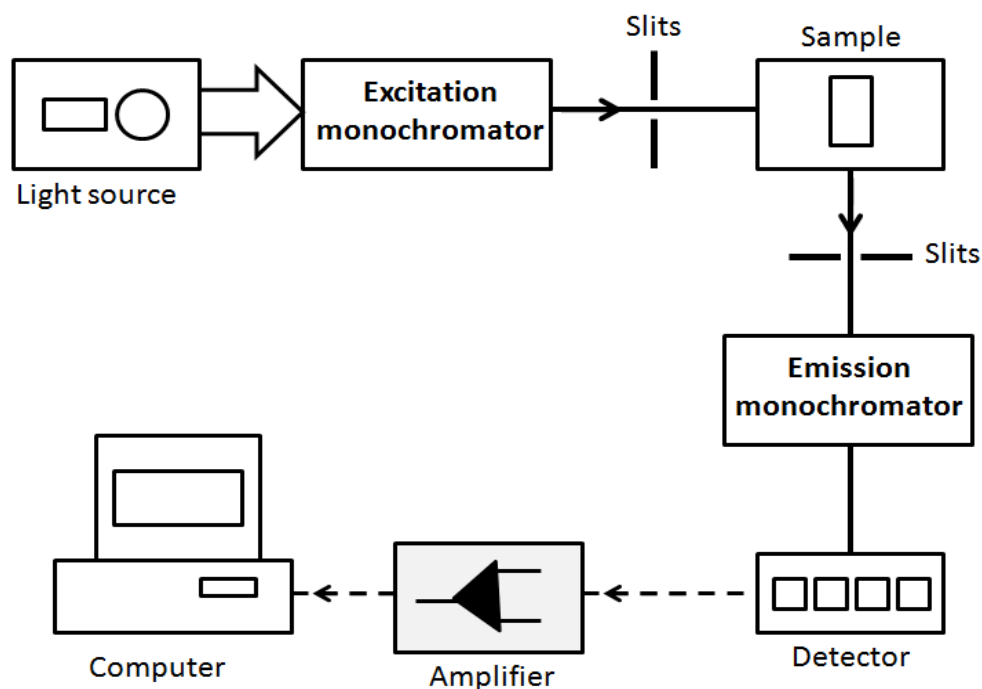


**Figure 3.14:** Typical setup of a photoluminescence spectrometer. Adapted from ([www.chemistry.adelaide.edu.au/external/soc-rel/content/mol-fluo.htm](http://www.chemistry.adelaide.edu.au/external/soc-rel/content/mol-fluo.htm))

### 3.10 X-Ray Photoelectron Spectroscopy (XPS)

In XPS characterization, sample surface is irradiated with x-ray photons. The highly energetic x-ray photons ( $h\nu$ ) can knock out core electron of the atoms, for example from the atom K's shell. This core electron that is ejected from the sample surface with kinetic energy  $E_k$  is known as photoelectron. By knowing the electron kinetic energy, the binding energy  $E_{BE}$  of the atom can be determined using the following:

$$E_{BE} = h\nu - E_k - \Phi \quad (3.8)$$

The parameter  $\Phi$  is depending on the material and spectrometer. It represents the energy that is required by the electron to escape from the material surface. Generally, the x-ray can penetrate deep into the material. However, photoelectrons that are free from inelastic scattering can only be obtained not more than 10 nm from the sample surface. XPS characterizations need to be carried out in Ultra High Vacuum with

pressure ranging from  $10^{-8}$  to  $10^{-10}$  mbar. If the vacuum is not sufficiently high, the ejected electron from the samples will be scattered by the residue gas molecules. Due to this, the detected signal intensity is reduced and the background noise in the XPS spectra will be increased (L. Yang, 2008). Also, UHV condition can reduce the possibility of the sample surface being contaminated by gas molecules since XPS is a very surface-sensitive characterization method. Figure 3.15 illustrate the simplified schematic diagram of the XPS.

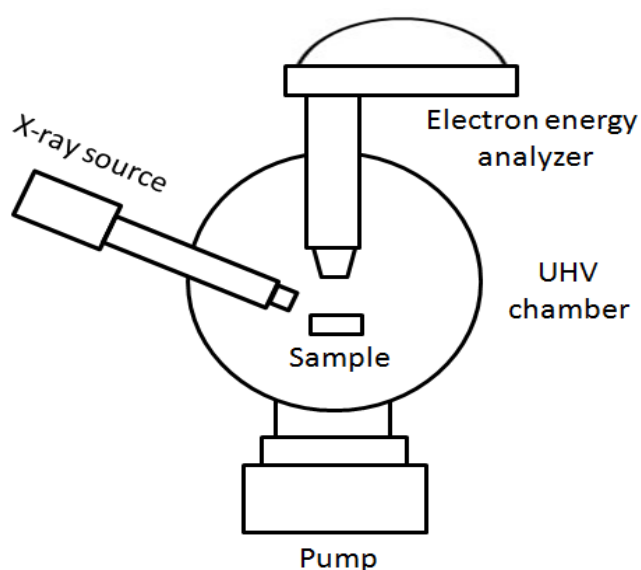


**Figure 3.15:** Simplified diagram of the XPS setup.

The XPS spectrum is a plot of the detected photoelectron intensity vs binding energy. The binding energy of the atom is in turn a fingerprint of the emitting element. Therefore XPS is a good method in element identification and chemical bond investigation on the sample surface. Our XPS characterizations were carried out by our collaborator from Synchrotron Light Research Institute (Thailand) (Nakajima et al., 2013). The photon energy of the excitation was 771.6 eV.

## **CHAPTER 4: Efficiency enhancement of a single layer solution processed blue phosphorescent organic light emitting diode (PHOLED) by using Triton X-100**

### **4.1 Introduction**

In recent years, significant efforts have been dedicated in developing high efficiency red, green and blue (RGB) emission PHOLED to cater for full colour display and lighting applications. In particular, the development of PHOLED is currently bottle necked at blue emission which is very crucial to realize high efficiency white PHOLED for lighting applications. It is widely known that to achieve high efficiency PHOLED, the triplet energy of the dye must be lower than the triplet of the host to prevent excitons quenching. In the case of blue PHOLED, this prove to be very challenging due to high triplet energy of the commonly used blue dopant, e.g. bis(4,6-difluorophenylpyridinato-N,C2)picolinatoiridium (FIrpic). Reducing the conjugation length of the host can help to increase the triplet energy but simultaneously it will widen the bandgap of the host which in turn increases the device operating voltage (S. E. Jang, Yook, & Lee, 2010; Padmaperuma, Sapochak, & Burrows, 2006). This may adversely effects the device lifetime and stability.

Several groups have developed multi layer solution processed blue PHOLED with power efficiency more than 15 lm/W. These multi layer device structures consist of an electron transport layer (ETL) layer formed on top of the EML. The ETL is deposited either by vacuum deposition method (Doh, Park, Jeon, Pode, & Kwon, 2012; Fu, Chen, Shi, & Ma, 2012; Jou, Wang, et al., 2010; Jou et al., 2011) or wet process (Ahmed et al., 2011; Earmme & Jenekhe, 2012b; Yook, Jang, et al., 2010) which increases the process complexity and fabrication cost. The development of solution processed single layer PHOLED is fairly slow. For lighting application, the power

efficiency of the OLED is usually benchmarked at 1000 cd/m<sup>2</sup>. Some of the best solution processed single layer blue PHOLED devices reported to date are demonstrated by So and co-workers (Mathai et al., 2006) which gave maximum power efficiency of 14 lm/W at about 35 cd/m<sup>2</sup> and dropped to 8 lm/W at 1000 cd/m<sup>2</sup> and by Pei's group (L. Li et al., 2011) which gave 9 lm/W at 1000 cd/m<sup>2</sup>. Chen's group has reported a single layer solution processed blue PHOLED with power efficiency up to 11 lm/W but at 1000 cd/m<sup>2</sup> the efficiency dropped to 7.5 lm/W (S. W. Liu et al., 2011). Very recently for the first time, (S. W. Liu et al., 2013) demonstrated a solution processed single layer blue PHOLED by using only small molecule. The blue device exhibits 8 lm/W and 4.3 lm/W at 600 cd/m<sup>2</sup> and 1000 cd/m<sup>2</sup> respectively. The efficiencies of some of the best single layer solution processed blue PHOLEDs reported to date are summarized in Figure 4.1.

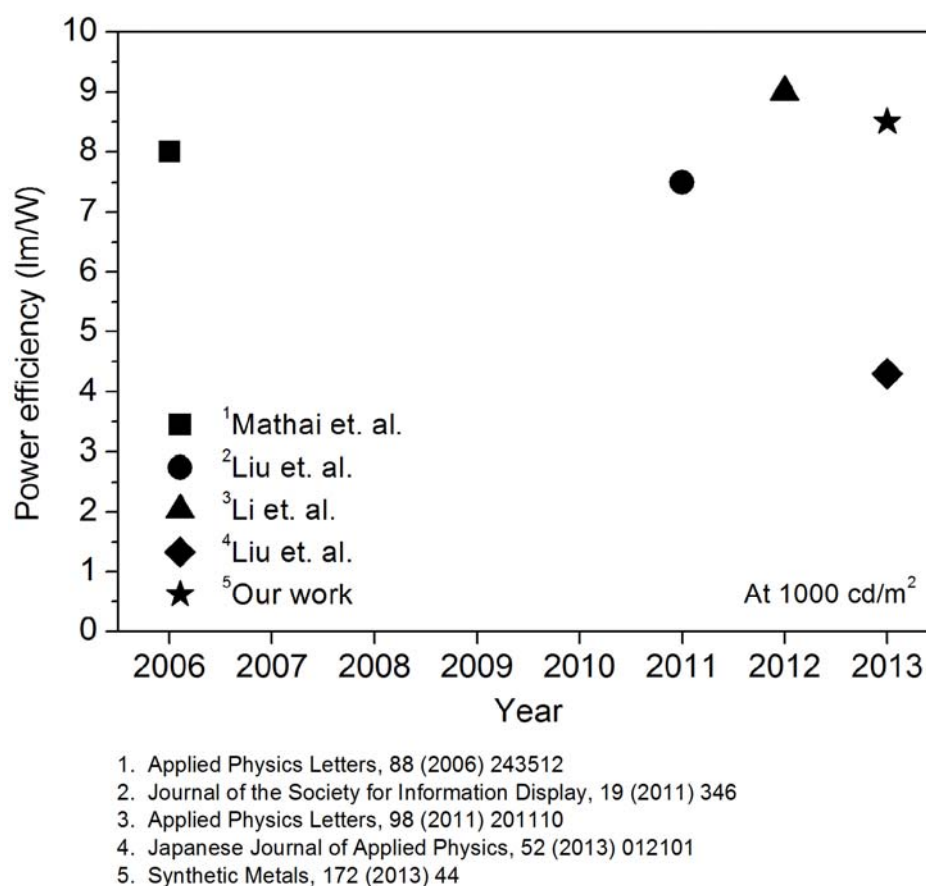


**Figure 4.1:** Some of the best single layer solution processed blue PHOLED reported to date. The efficiencies are benchmarked at 1000 cd/m<sup>2</sup>.

Poly(vinylcarbazole) (PVK) is often the preferred choice of host for solution processed blue PHOLED due to its ability to form good quality film. Previously the triplet energy of PVK is widely debated at either 2.5 eV (F. C. Chen et al., 2003; Noh, Lee, Kim, & Yase, 2003) or close to 2.9 eV (Burkhart & Chakraborty, 1990). However recently (Jankus & Monkman, 2011) carried out detailed studies and clarified that the low triplet energy of PVK is caused by the low energy traps states in the form of physical dimers. These dimers are formed when the carbazole units are spatially close which permits large  $\pi$ - $\pi^*$  overlapping (Jankus & Monkman, 2011). The lowest triplet energy of these dimers are found to be 2.5 eV. This low triplet energy can quench the emission of phosphorescent blue heavy metal complex due to triplet back energy transfer through Dexter mechanism. Dexter energy transfer occurs at short distance i.e.  $\sim 1.5$  nm. To eliminate back energy transfer, (S. P. Huang et al., 2008) suggested increasing the distance or reducing the contact between the guest-host. By doing so, triplet energy transfer of guest-host via Dexter mechanism can be minimized. For example, Chen's group (Y. K. Huang et al., 2010) introduced branched alcohol to provide shielding for triplet energy transfer from high triplet green phosphor to low triplet polymer host. In this chapter, we attempt to improve the efficiency of PVK based blue PHOLED by reducing back energy transfer from high triplet FIrpic ( $E_T$ : 2.7 eV) guest to low triplet PVK ( $E_T$ : 2.5 eV) host. Using Triton X-100 as shielding agent, the power efficiency of the blue PHOLED increased from 4.9 lm/W to 8.5 lm/W at brightness of 1000 cd/m<sup>2</sup>. The addition of Triton X-100 also roughened the film surface at the EML /cathode interface causing electric field localization and surface area enlargement which favours electron injection. This studies suggest that low cost commercially available PVK is still feasible in the development of high efficiency solution processed blue PHOLED.

## 4.2 Experimental

The hole injection material, PEDOT:PSS (P VP AI4083) was purchased from H.C. Starck. PVK (average Mw = 1 100 000) and Cs<sub>2</sub>CO<sub>3</sub> were purchased from Sigma-Aldrich. Electron transporting compound 1,3-bis[(4-tertbutylphenyl) -1,3,4-oxadiazolyl] phenylene (OXD-7) and blue phosphorescent dye, Flrpic were purchased from Luminescence Technology, Taiwan. Triton X-100 was purchased from Acros Organics. All materials were used as received without further purification. The device structure consists of ITO (100 nm)/ PEDOT:PSS (40 nm)/PVK: OXD-7:Flrpic: Triton X-100 (70 nm)/ Cs<sub>2</sub>CO<sub>3</sub> (1 nm) / Al (100 nm). Figure 4.2 shows the energy level diagram and the chemical structures of the material used in this work. The EML layer i.e. PVK:OXD-7:Flrpic:Triton X-100 was blended in 100:40:10:X weight ratio where X was varied from 0 to 10. ITO coated glass substrates were patterned using standard lithography method. The substrates were ultrasonically cleaned using DI water, acetone, isopropyl alcohol and DI water again for 10 minutes, followed by oxygen plasma treatment for 5 minutes. Next 40nm of PEDOT:PSS was spin coated on the substrates and immediately baked in N<sub>2</sub> environment for 10 minutes at 150°C. The EML layer was dissolved in chlorobenzene and spin coated on top of the PEDOT:PSS coated substrates to give a 70 nm thick film. Then the samples were baked at 80°C for 30 minutes. Following that, 1 nm of Cs<sub>2</sub>CO<sub>3</sub> and 100 nm Al was vacuum deposited at base pressure of 2.5X10<sup>-6</sup> mbar without breaking the vacuum. All the devices were encapsulated using UV curable epoxy and glass lid. The devices current-brightness-voltage characteristics were measured using Konica Minolta CS-200 integrated with Keithley 276 SMU. PL was measured using Perkin Elmer LS50B spectrometer. Photocurrents of OLED were measured under illumination of a simulated AM1.5 light source at 100 mW/cm<sup>2</sup> (Newport 67005 ). FTIR ATR measurements of the EML film were carried out using Perkin Elmer ATR Spectrum 400 spectrometer. All solution



processed films thickness was measured by P-6 profilometer (KLA Tencor ). AFM images were taken using NT- MDT NTEGRA-Prima.

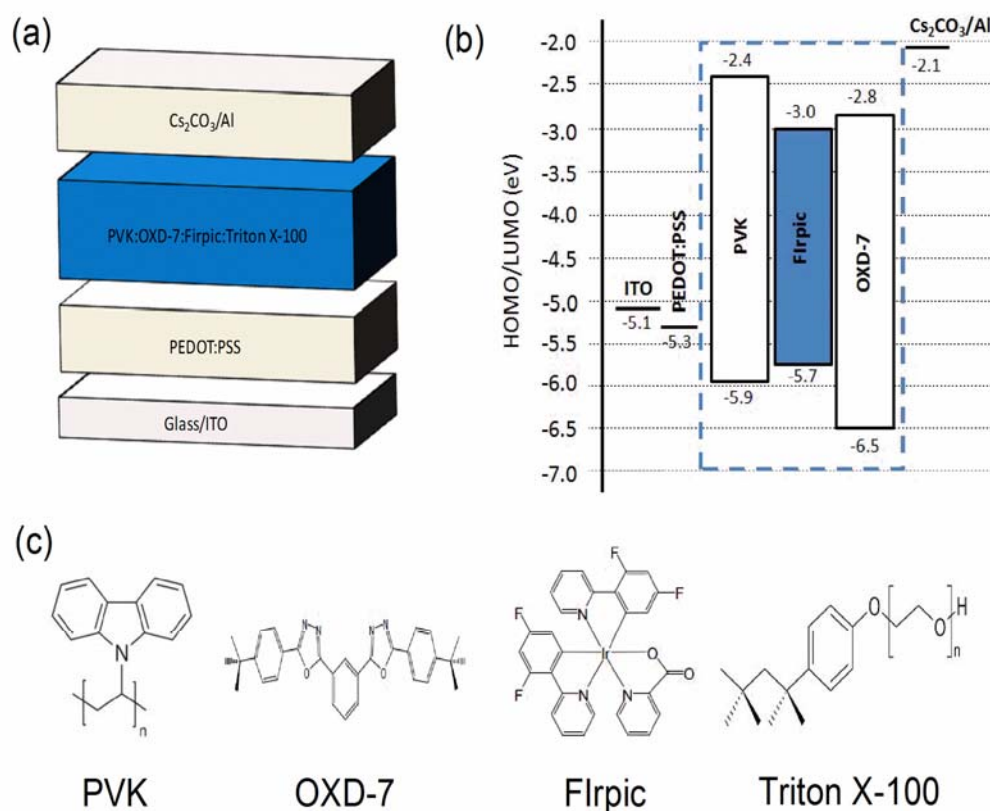


**Figure 4.2:** Schematic diagram of (a) device architecture (b) energy level diagram and (c) molecular structure of the materials used.

### 4.3 J- V –L and efficiency characteristics

In our blue devices, PVK is selected as host due to its good film formation property and moderate hole transporting capability. To balance the charge transport, oxadiazole compound OXD-7 was blended into PVK as the electron transport compound (X. H. Yang, Jaiser, et al., 2006). J-V-L curves of the PHOLED with different concentrations of Triton X-100 are shown in Figure 4.3. It is observed that the current injection increases with Triton X-100 concentration. Also the turn on voltage (defined at  $1 \text{ cd/m}^2$ ) reduced with the addition of Triton X-100. For instance, the turn

on voltage for device with 3.2 wt% Triton X-100 is reduced from 4.6 V to 3.5 V, suggesting the barrier height for carrier injection has reduced.

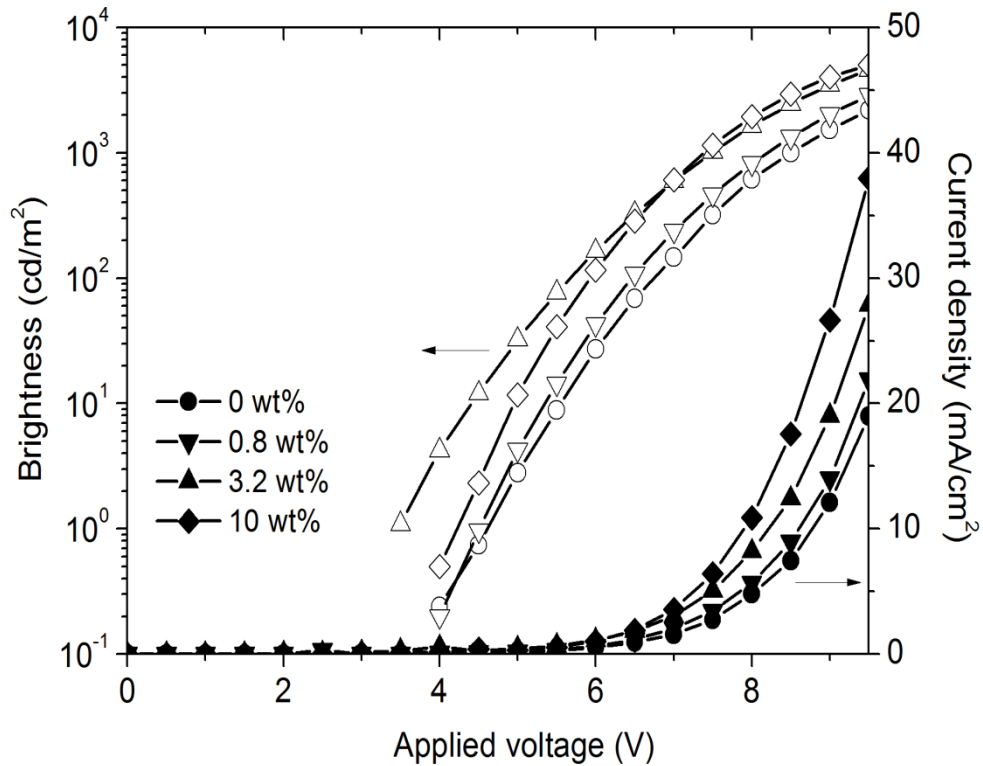


**Figure 4.3:** J-V-L characteristics of the blue devices with different concentrations of Triton X-100.

Figure 4.4a and Figure 4.4b show the current efficiencies and power efficiencies of the PHOLED devices at different brightness. Compared to the control device, the addition of 3.2 wt% Triton X-100 enhanced the power efficiency from 3.9 lm/W (8.4 cd/A) and 4.9 lm/W (13.4 cd/A) to 7 lm/W (12.7 cd/A) and 8.5 lm/W (20.1 cd/A) at 100 cd/m<sup>2</sup> and 1000 cd/m<sup>2</sup> respectively. This efficiency is comparable to the best power efficiency reported to date at brightness 1000 cd/m<sup>2</sup> for a single layer solution processed blue PHOLED (L. Li et al., 2011). The blue devices performances are summarized in Table 4.1.

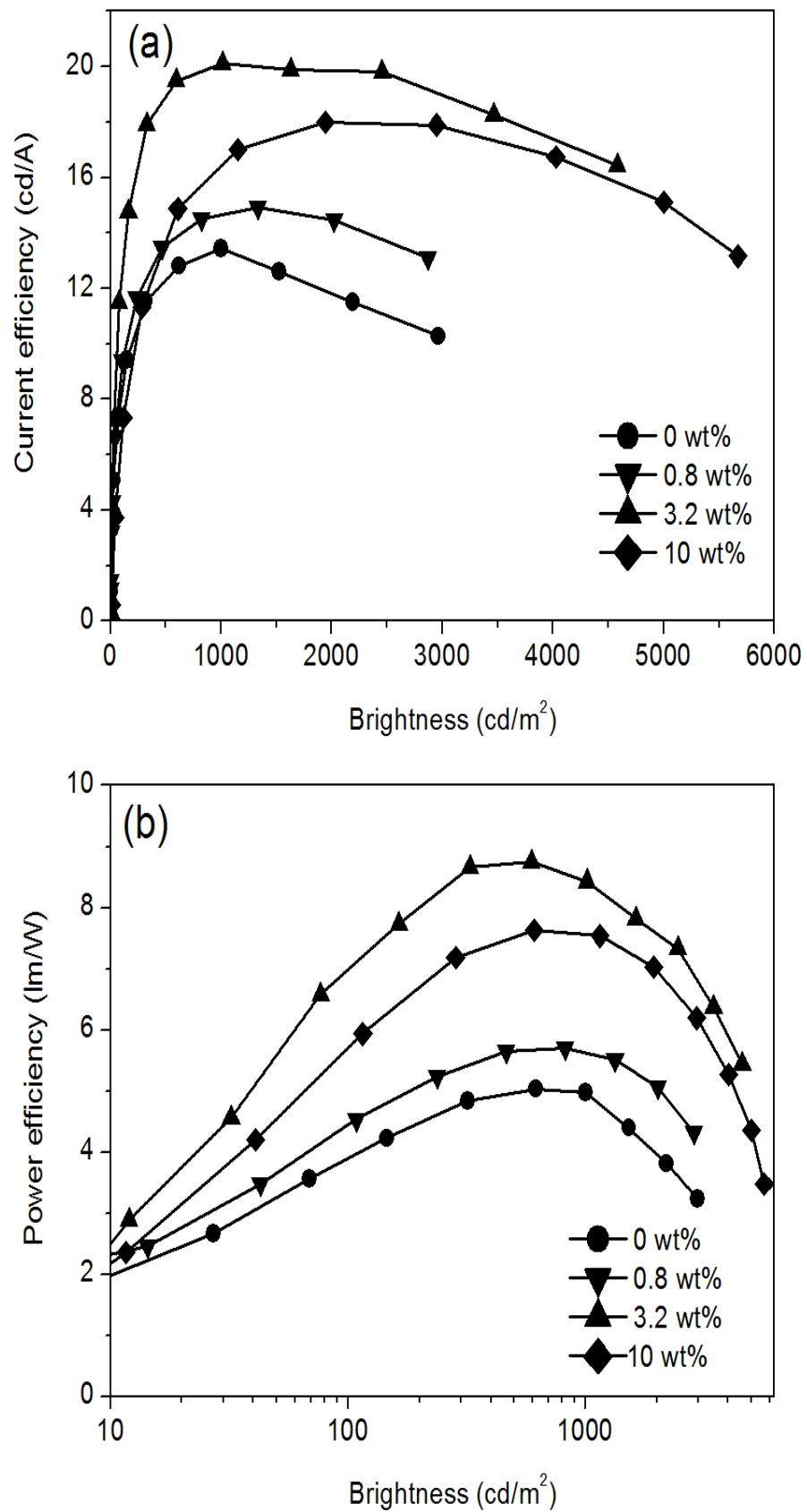


**Figure 4.4 :** (a) Current efficiency and (b) power efficiency vs brightness of blue PHOLEDs doped with different concentrations Triton X-100.

**Table 4.1:** Blue PHOLEDs performances at different concentrations of Triton X-100 doping

Triton X-100 concentration (wt%)	$V_{ON}$ (1cd/m <sup>2</sup> )	<sup>1</sup> $V_{ON}$	<sup>1</sup> PE (lm/W)	<sup>1</sup> CE (cd/A)	<sup>2</sup> $V_{ON}$	<sup>2</sup> PE (lm/W)	<sup>2</sup> CE (cd/A)
0	4.6	6.7	3.9	8.4	8.5	4.9	13.4
0.8	4.5	6.4	4.4	9.2	8.2	5.7	14.7
3.2	3.5	5.6	7.0	12.7	7.3	8.5	20.1
10	4.2	5.9	5.7	6.9	7.3	7.6	16.5

<sup>1</sup>At brightness of 100 cd/m<sup>2</sup>

<sup>2</sup>At brightness of 1000 cd/m<sup>2</sup>

#### 4.4 Shielding of triplet energy transfer by Triton X-100

The PL spectra of the blue devices with different concentrations of Triton X-100 are shown in Figure 4.5. The emission is centred at 479 nm with vibrational peak at 500 nm which are the typical characteristics of FIrplic emission. The peak around 380 nm is attributed to the host emission. Closer inspections on the PL curves reveal that the host emission increased with the concentration of Triton X-100 doping. In this case, the excess of Triton X-100 will provide separation between guest-host which in turn reduced the Förster energy transfer from host to guest (Y. K. Huang et al., 2010). This observation could provide an explanation on the reduction of device efficiency when the concentration of Triton X-100 is increased to 10 wt%. On the other hand, the close contact of the polymer host and blue phosphrescent guest will induce exciton quenching through Dexter mechanism. The excitons are back transferred from the high triplet FIrplic ( $E_T$ : 2.7 eV) to the low triplet PVK ( $E_T$ : 2.5 eV) which results in exciton quenching. The presence of Triton X-100 blocks the direct contact between guest-host in such a way that the exothermic energy transfer from guest to host can be suppressed.

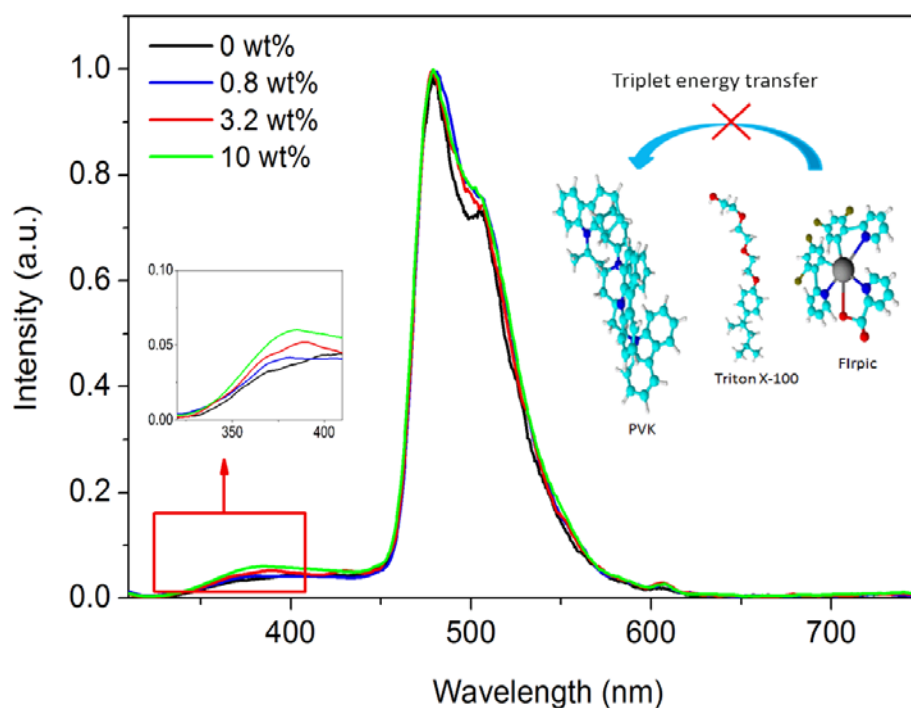


**Figure 4.5:** Normalized PL spectra of PVK:OXD-7:FIrpic thin film doped with different concentration of Triton X-100. Inset is the expanded view of PL in region of 320 nm to 400 nm.

Literature ascribed that the guest-host separation is assisted by the formation of hydrogen bond between the O-H group of the shielding agent and the electron donating group of the guest and polymer host (Y. K. Huang et al., 2010). The formation of hydrogen bond can cause absorbance wave number shift in the electron donating functional group (Maeda, Kubota, & Yamauchi, 2007; Pimentel & McClellan, 1960). For instance when acetone is added into alcohol, the C=O stretching mode can be red shifted by  $31\text{ cm}^{-1}$  (Pimentel & McClellan, 1960). Another example is that a  $20\text{ cm}^{-1}$  red-shift can be observed in C-O group when water is added into poly(2-methoxyethyl vinyl ether) (Maeda, Yamauchi, Fujisawa, Sugihara, & Ikeda, 2007). These shifts is caused by the bond lengthening or contraction when the hydrogen bond is formed (Joseph & Jemmis, 2006). Therefore FTIR measurement on the control device (PVK:OXD-7:FIrpic, 100:40:10 wt/wt/wt ) and the optimized blue device (PVK:OXD-7:FIrpic:Triton X-100 (100:40:10:3.2 wt/wt/wt/wt) were carried out. It is observed that there are no obvious shift in the absorption wavenumber of the electron donating groups

(i.e. C-O, C=O, C-N, C=N, C-F) (See Figure 4.6). This could be due to the bulky alkyl group of Triton X-100 in maintaining hydrogen bonding in thin film or the shift is too small to be observed in FTIR, consistent with the observation from (Y. K. Huang et al., 2010)

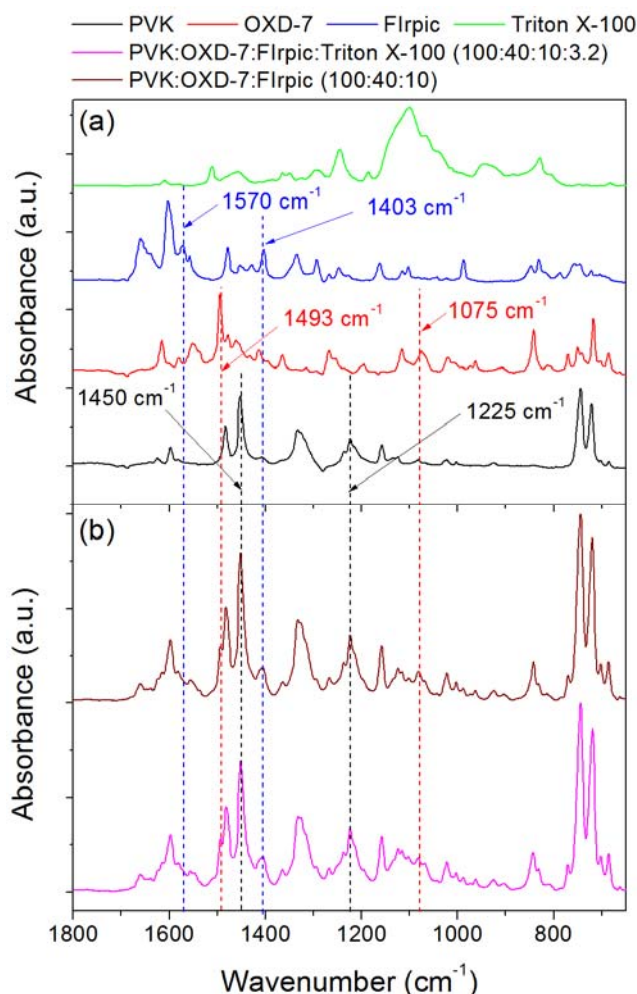


**Figure 4.6:** FTIR absorbance spectra on (a) PVK, OXD-7, Flrpic, Triton X-100, and (b) PVK:OXD-7:Flrpic (100:40:10 wt/wt/wt) and PVK:OXD-7:Flrpic:Triton X-100 (100:40:10:3.2 wt/wt/wt/wt).

The FTIR wave number assignments for the functional groups that are possible sites for hydrogen bond formation with O-H group in Triton X-100 are summarized in Table 4.2. Briefly, for PVK wave number  $1450\text{ cm}^{-1}$  and  $1225\text{ cm}^{-1}$  are assigned to C-N aromatic and C-N aliphatic respectively (Kumru, Springer, Sarac, & Bismarck, 2001; Lampman, Pavia, Kriz, & Vyvyan, 2010). The absorption band due to C=N and C-O-C for OXD-7

are  $1493\text{ cm}^{-1}$  and  $1075\text{ cm}^{-1}$  respectively (Liou, Huang, & Yang, 2006). FIrpic wave number  $1570\text{ cm}^{-1}$  and  $1403\text{ cm}^{-1}$  are attributed to O=C-O and C-F group respectively (S. M. Park et al., 2012; Popova, Chesalov, & Andrushkevich, 2004; Williams & Fleming, 2008).

Table 4.2: FTIR data for the functional groups that give the possibly of forming hydrogen bond with O-H group in Triton X-100.

Material	Assignment	Wavenumber ( $\text{cm}^{-1}$ )
PVK	C-N (aromatic)	1450
	C-N (aliphatic)	1225
OXD-7	C=N	1493
	C-O-C	1075
FIrpic	C=O-O	1570
	C-F	1403

Besides the -OH group, the ethylene oxide in Triton X-100 may also react with the metal ligand of the FIrpic complex (Funahashi, 2014). However, significant changes on the FIrpic PL spectrum was not observed (see Figure 4.5). It could be due to the amount of Triton X-100 is too low to initiate any substantial changes of the FIrpic PL spectrum.

#### 4.5 Effects of surface morphology in device efficiency enhancement

The surface morphology of the EML film was examined using AFM. Figure 4.7a, 4.7d, 4.7g and 4.7j show the AFM images of the surface roughness for control sample and sample with 0.8 wt%, 3.2 wt% and 10 wt% of Triton X-100. The surface morphology of the doped film is significantly different from the control film and as the concentrations of the Triton X-100 increases, the surface become rougher. For example the control sample film roughness is 0.443 nm rms and increased to 3.23 nm rms when the film is doped with 10 wt% Triton X-100. These observations suggest that Triton X-100 has phase separated in the film. With 0.8 wt% Triton X-100, nano-pores are



formed on the EML film surface and the concentrations of these pores increases slightly when the Triton X-100 concentration increase to 3.2 wt% as shown in Figure 4.7e and Figure 4.7

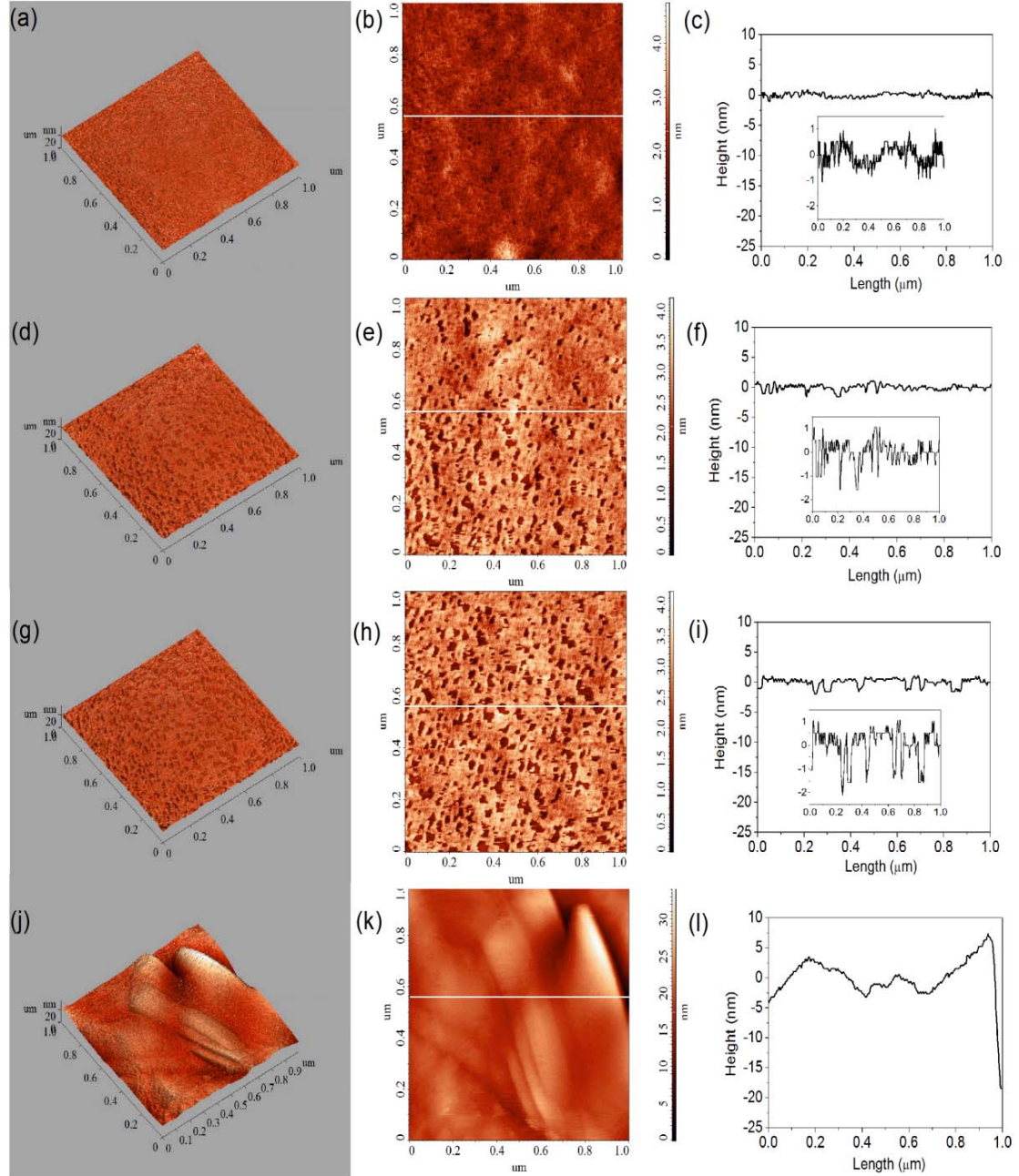


**Figure 4.7:** AFM topographical height images and cross-sectional line profile of the solution processed EML film doped with: (a)-(c) 0 wt% (d)-(f) 0.8 wt%, (g)-(i) 3.2 wt% and (j)- (l) 10 wt% of Triton X-100. The surface roughness of the EML films for 0 wt%, 0.8 wt%, 3.2 wt% and 10 wt% is 0.443 nm rms, 0.64 nm rms, 0.703 nm rms and 3.23 nm rms respectively. The white line in (b), (e), (h), (k) indicate the location where the cross sectional line profile is taken. Inset in (c), (f), (i) is the expanded view of the corresponding graphs.



The EML film cross-sectional profile (see Figure 4.7c, 4.7f, 4.7i and 4.7l) could provide some explanations on this observation. At higher concentration i.e. 10 wt% Triton X-100 nano-pores no longer exist, instead the line cross sectional profile of the film fluctuates dramatically as shown in Figure 4.7l.

For a better quantitative description on the films morphology, 2D PSD of the film surface is computed. PSD is often used in to study adhesion phenomenon, tribology and morphology of film surface (J. F. G. Martinez, Nieto-Carvajal, Abad, & Colchero, 2012). In contrast to the commonly used rms, PSD function able to describe the surface lateral distance over which the surface morphology start to change and the surface height distribution from a mean plane (Senthilkumar, Sahoo, Thakur, & Tokas, 2005). The 2D PSD of the EML film surface is computed using the following equation (Gavrila, Dinescu, & Mardare, 2007).

$$PSD(f_x, f_y) = L^2 \left[ \frac{1}{N^2} \sum_{n=0}^N \sum_{m=0}^N z(x_m, y_n) e^{(2\pi i \cdot (x_m \cdot f_x + y_n \cdot f_y))} \right]^2 \quad (4.1)$$

where  $x_m = m \cdot \frac{L}{N}$ ,  $y_n = n \cdot \frac{L}{N}$  and spatial frequency  $f_x, f_y = \frac{1}{L}, \frac{2}{L}, \dots, \frac{N}{2L}$ . The topography height at discrete point  $x_m, y_n$  is denoted by  $z(x_m, y_n)$ . L is the scan length which is equal to x and y direction. The 2D PSD plot characteristics are shown in Figure 4.8.

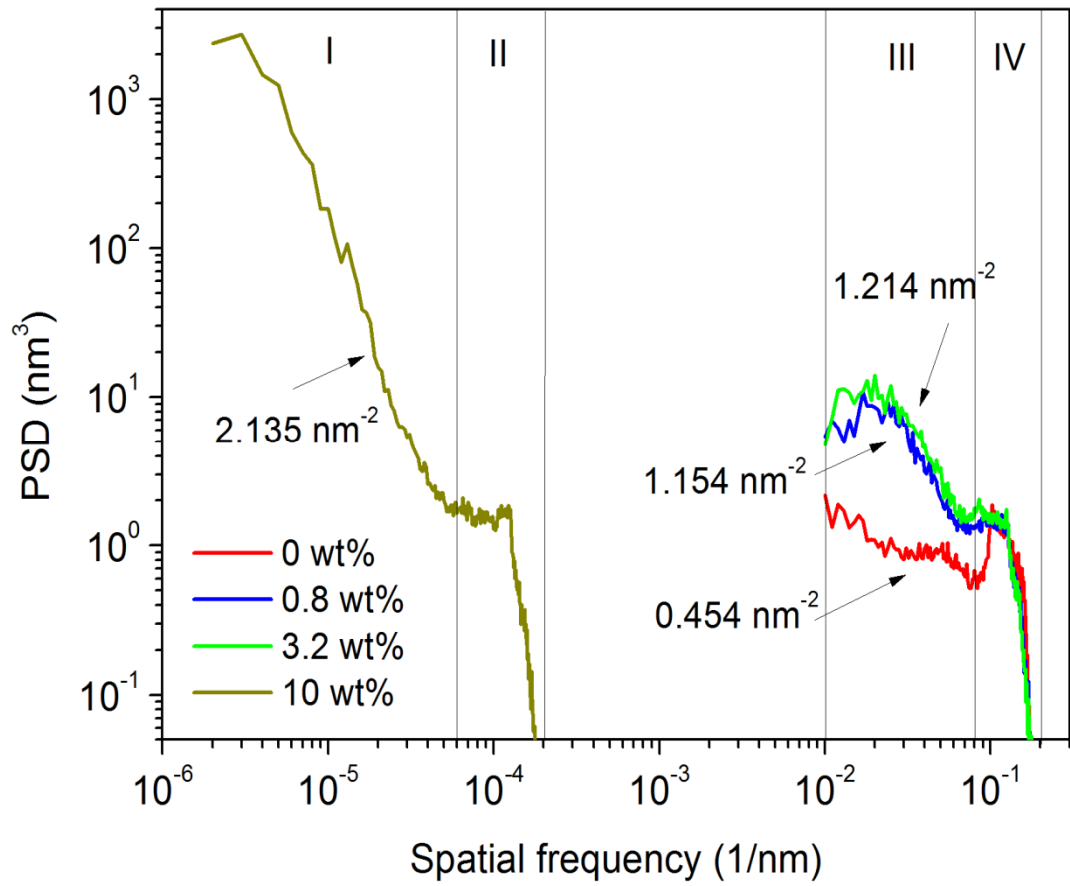


**Figure 4.8:** 2D PSD curves of the EL film doped with Triton X-100. Arrows indicate the slope of the PSD curves.

The PSD curves in Figure 4.8 can be explained as follow:

- a. Device with 10 wt% Triton X-100 significantly shifted to the low frequency region compared to the rest. Low frequency component correspond to aggregate or large structure present on the film. The presence of these large structures increases the surface roughness. This observation is consistent with the AFM image (see Figure 4.7j) and the line cross sectional profile (see Figure 4.7l) of the EML with 10 wt% Triton X-100.
- b. The slope for 10 wt% (region I), 3.2 wt%, 0.8 wt% and 0 wt% (region III) reduced from  $2.135 \text{ nm}^{-2}$  to  $0.454 \text{ nm}^{-2}$ . A lower slope indicates self-consistent roughness scaling (Lita & Sanchez, 1999) or the surface roughness is consistent over the plane. Also at these regions, the PSD for 10

wt% sample is the highest followed by the 3.2 wt%, 0.8 wt% and the control sample. Accordingly, the surface roughness decreases from 3.23 nm (10 wt% Triton X-100) to 0.44 nm (control sample). At spatial frequency above  $0.1 \text{ nm}^{-1}$  (Region IV), the PSD for 3.2 wt%, 0.8 wt% and 0 wt% sample starts to converge and drop drastically. The PSD for 10 wt% starts to drop in a similar manner at about  $1.25 \times 10^{-4} \text{ nm}^{-1}$  (Region II). This trend is commonly observed in PSD curve. It is because at higher spatial frequency, the domain of interest become smaller and hence surface profile variation lower leading to the decrease of PSD.

High EL film surface roughness on the cathode side is beneficial to the OLED performance (Hussain et al., 2009; D. Liu et al., 2009; Niu et al., 2005). The suggested reasons for this are as follows: First, with higher surface roughness the total surface area of the EML film/cathode interface increased. Second, rough surface promotes localization of electric field. Both of these attributes may ease the electron injection at the cathode.

Another possible reason for the efficiency improvement upon adding Triton X-100 could be due to the interaction of lone pair electron in Triton X-100 with Al which facilitates the formation of  $\text{Al}^{3+}$ . This process leads to excessive negative charge which n-doped the EML/cathode interface thus results in lowering the barrier height for electron injection (F. C. Chen et al., 2008; Deng et al., 2004; Lu Li et al., 2013). To further investigate the effects of EML surface modification by Triton X-100, photocurrent measurement was carried out on the devices under the illumination of AM1.5 light source at  $100 \text{ mW/cm}^2$ . The photocurrent responses of the PHOLED at different Triton X-100 concentrations are presented in Figure 4.9. Clearly, the open circuit voltage ( $V_{\text{OC}}$ ) increased with Triton X-100 doping. Without Triton X-100, the  $V_{\text{OC}}$  was 0.23 V and increased to 0.7 V at 10 wt% Triton X-100 doping. The

enhancement of  $V_{OC}$  shows that the electron injection at the cathode side has improved (Zhao et al., 2012).

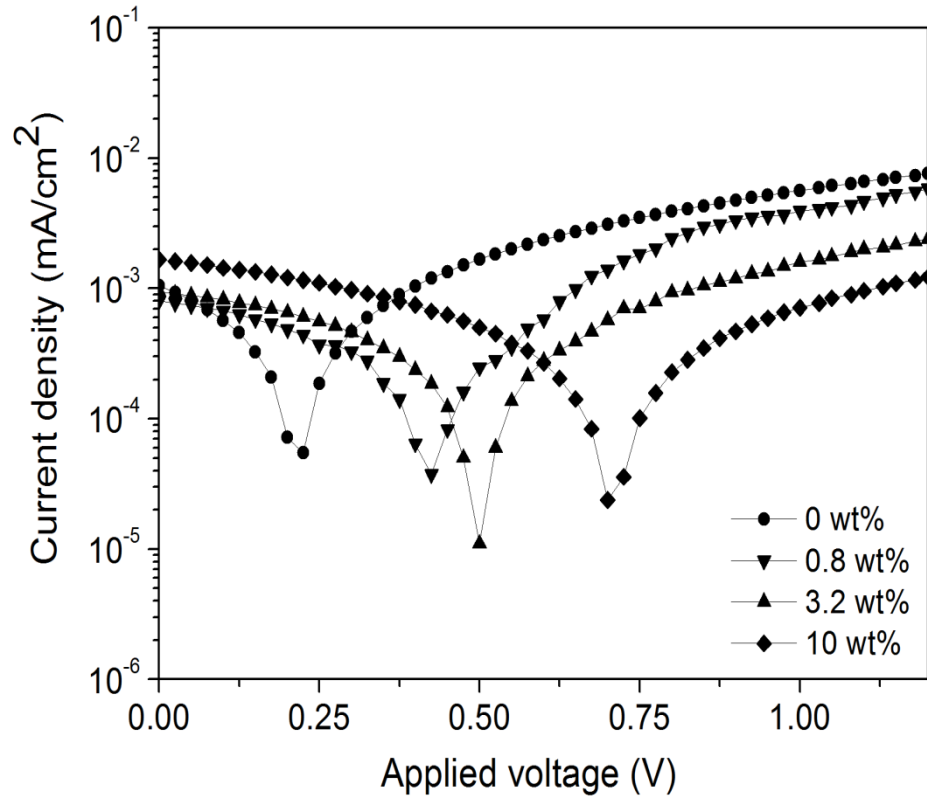


**Figure 4.9:** Photovoltaic characteristics of the blue devices with different concentrations of Triton X-100 in the EMLs.

Electron dominated (ITO/LiF/PVK:OXD-7:FIrpic:Triton X-100/Cs<sub>2</sub>CO<sub>3</sub>/Al) and hole (ITO/PEDOT:PSS/ PVK:OXD-7:FIrpic:Triton X-100/Au) dominated devices were fabricated. Au has high work function which can block off electron injection at the cathode. Similarly, ITO/LiF has low work function which retard hole injection at the anode. From Figure 4.10, it is shown that the addition of Triton X-100 improves the electron injection. In contrast, the hole injection for both devices are comparable. These results again indicate that the addition of Triton X-100 improves the electron injection at the cathode.

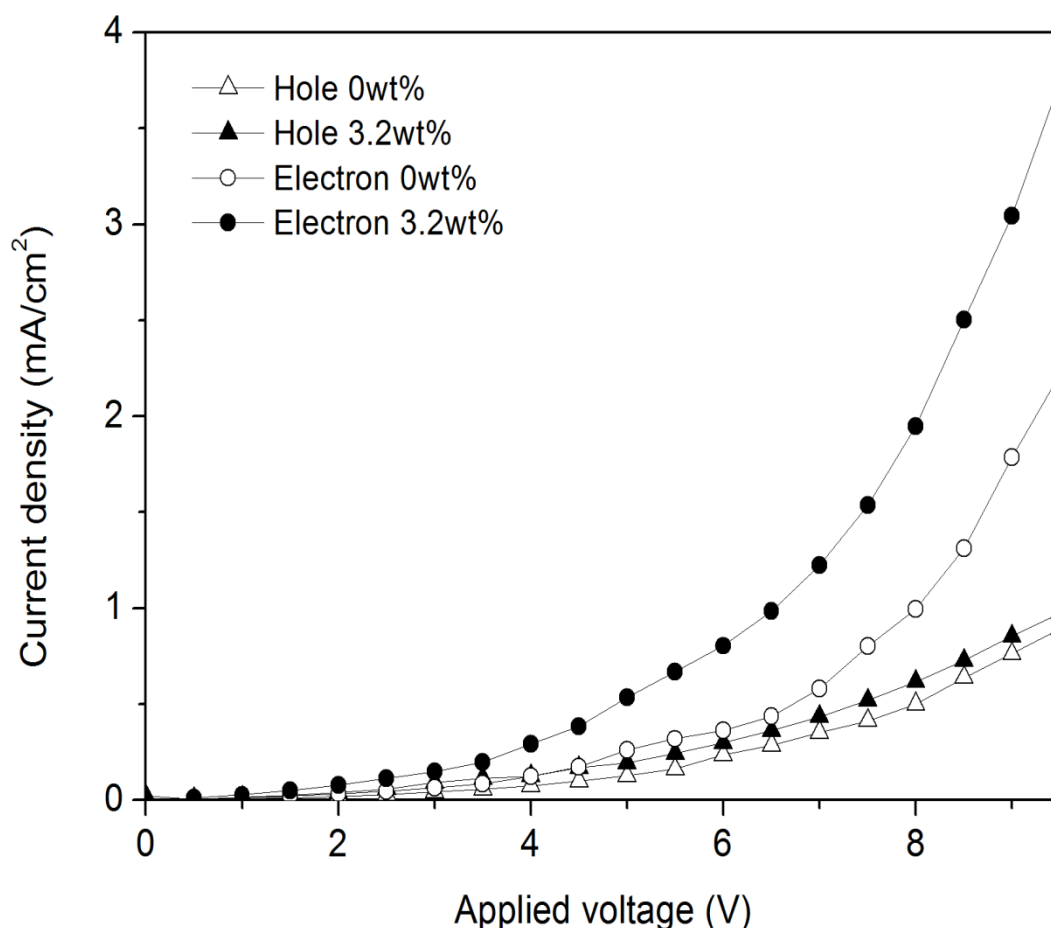


**Figure 4.10:** Current density-voltage characteristics of electron dominated and hole dominated devices of the blue PHOLEDs with 0 wt% and 3.2 wt% of Triton X-100.

#### 4.6 Summary

In summary, investigations of triplet energy shielding and surface modifications by Triton X-100 on blue PHOLED were carried out. By using this simple and cost effective method, the efficiency of a single layer solution processed blue PHOLED can be improved from 4.9 lm/W to 8.5 lm/W at brightness of 1000 cd/m<sup>2</sup>. The insertion of Triton X-100 increased the distance between guest-host thus reducing exothermic energy transfer from high triplet FIrpic to low triplet PVK. From the AFM images, EMLs cross-sectional line profiles and PSD spectrums, it is shown that the addition of Triton X-100 results in the formation of nano-pores on the EML surface. With higher Triton X-100, large aggregates start to form on the EML surface which effectively

enhanced the film roughness. The device efficiency enhancements are attributed to the collective effects of reduced back energy transfer from guest-host and also EML film surface roughness enhancement induced by Triton X-100. This simple and cost effective method will pave way towards large scale manufacturing of OLED for display and lighting applications.

## **CHAPTER 5: Efficiency enhancement of a single layer solution processed phosphorescent organic light emitting diodes via hole injection layer modification**

### **5.1 Introduction**

The performance of solution processed PHOLED can be improved by anode engineering which typically consists of ITO and HIL. PEDOT:PSS is commonly used as HIL since PEDOT:PSS solution can easily form high quality visible transparent thin film which can smoothen the surface of ITO (Xia & Ouyang, 2010; Y. F. Zhou et al., 2007). It also serves as a buffer layer to reduce hole barrier injection from ITO to OLED active layer. Recently there have been significant efforts dedicated to tuning the work function of PEDOT:PSS. By doing so, the hole injection and charge balance of the PHOLED can be controlled. For example, UV and/or ozone treatment was found to be able to change the resistivity and work function of PEDOT:PSS (Benor et al., 2009; Benor, Takizawa, Perez-Bolivar, & Anzenbacher, 2010; Helander et al., 2009; Lin et al., 2007; Moujoud, Oh, Shin, & Kim, 2010; Nagata et al., 2011). The resistivity change was attributed to the decomposition of chemical bond upon UV irradiation while the work function increment was due to surface dipoles induced by ozone exposure (Nagata et al., 2011). Zou et. al. reported mild oxygen plasma treatment on PEDOT:PSS which can reduce the OLED driving voltage and increase the device lifetime. These improvement was attributed to the formation of nanoislands on the PEDOT:PSS surface which can improve the contact with the HTL (Y. F. Zhou et al., 2006). Recently (T. H. Han, Choi, et al., 2012; T. H. Han, Lee, et al., 2012; T. W. Lee et al., 2005; J. K. Park, Hwang, Chin, Kang, & Lee, 2012) has demonstrated that the OLED efficiency can be enhanced by incorporation of PFI into PEDOT:PSS. It was found that the PFI concentration increased gradually from the ITO to the surface of the PEDOT:PSS. As a

results the work function of the PEDOT:PSS increases in a gradient manner. Using this technique, the PEDOT:PSS surface work function can be tuned from 5.55 eV to 5.95 eV by simply changing the concentration of PFI (T. W. Lee et al., 2007). However to the best of our knowledge, there are no reports on the investigation of PFI doped PEDOT:PSS in solution processed blue PHOLED which is highly needed for lighting applications.

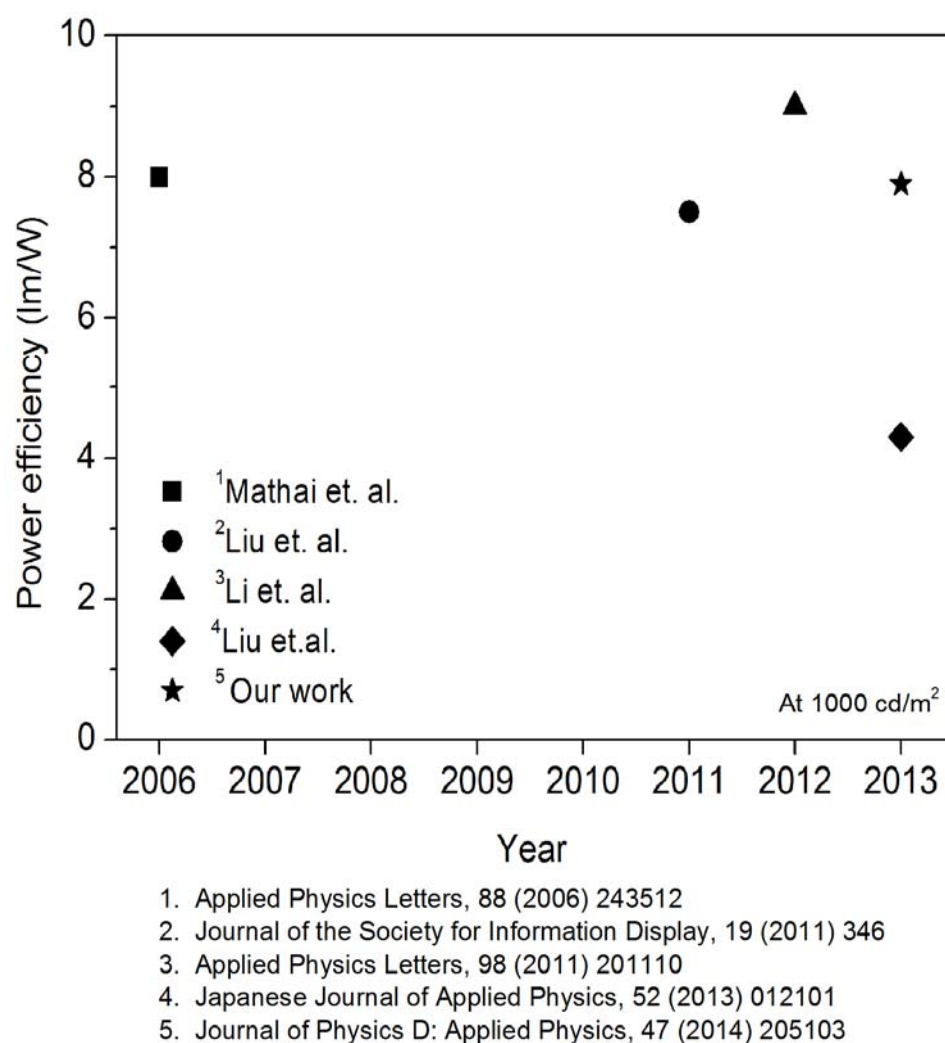


**Figure 5.1:** Some of the best single layer solution processed blue PHOLED reported to date. The efficiencies are benchmarked at 1000 cd/m<sup>2</sup>.

In this chapter, we studied the effects of PFI modified PEDOT:PSS on a single layer solution processed blue PHOLED. Using this techniques, our optimized blue device efficiencies improved from 7.3 lm/W (15.4 cd/A) and 5.9 lm/W (16.5 cd/A) to



9.4 lm/W (18.2 cd/A) and 7.9 lm/W (20.4 cd/A) at 100 cd/m<sup>2</sup> and 1000 cd/m<sup>2</sup> respectively. Some of the best solution processed single layer blue PHOLED devices reported to date are already discussed in section 4.1. Comparisons between our blue device efficiency and other reported works on single layer solution processed blue PHOLED are summarized in Figure 5.1.

## 5.2 Experimental

All materials were purchased and used as received without further purification. PVK (Mw = 1 100 000) and PFI (Nafion® perfluorinated resin solution) in a mixture of water and alcohol (4.5:5.5 v/v) were purchased from Sigma Aldrich. OXD-7 and FIrpic were purchased from Luminescence Technology Corp. PEDOT:PSS (AI4083) was purchased from H.C. Starck. The HIL consists of PFI blended into PEDOT:PSS at different concentrations as shown in Table 5.1.

**Table 5.1:** PEDOT:PSS work function with different concentrations of PFI. Taken from (T. W. Lee et al., 2007).

Device	PEDOT:PSS:PFI (wt/wt/wt)	Work function (eV)
I	1/6/0	5.20
II	1/6/6.3	5.72
III	1/6/12.7	5.79
IV	1/6/25.4	5.95

The device structure consists of ITO/PEDOT:PSS:PFI (40 nm)/PVK (60 wt %) :OXD-7 (30 wt %):FIrpic (10 wt %) (75 nm)/CsF (~1 nm)/Al (100 nm). ITO substrates were patterned using standard lithography method. The substrates were ultrasonically cleaned using DI water, acetone, isopropyl alcohol and DI water again for 10 minutes, followed by oxygen plasma treatment for 5 minutes. PEDOT:PSS:PFI blend was spin coated on top of the ITO substrate to form a 40 nm thin film and then immediately

baked at 150°C for 10 minutes in N<sub>2</sub> environment. Following that, EML which consists of PVK (60 wt %) :OXD-7 (30wt%):Flrpic (10 wt %) was dissolved in mixed solvent of toluene: chlorobenzene (3:2 v/v). The solution was spin coated on to the substrate to give a 75 nm film. Then the substrates were annealed at 100°C for 10 minutes. Finally ~1 nm of CsF and 100 nm of Al was vacuum deposited at base pressure of 2.5x10<sup>-6</sup> mbar. Devices were encapsulated in N<sub>2</sub> environment using glass lid and UV curable epoxy. Current density (J) –voltage (V) - luminance (L) characteristics were measured using Konica Minolta CS-200. All solution processed films thickness was measured by P-6 profilometer (KLA-Tencor). AFM images were taken using NT- MDT NTEGRA-Prima. The PFI doped PEDOT:PSS conductivity was measured using Jandel Universal 4-point probe. The transmittance spectra were measured using Perkin Elmer PE750. The device structure, energy level diagram and the chemical structures of the material used in this work are shown in Figure 5.2.

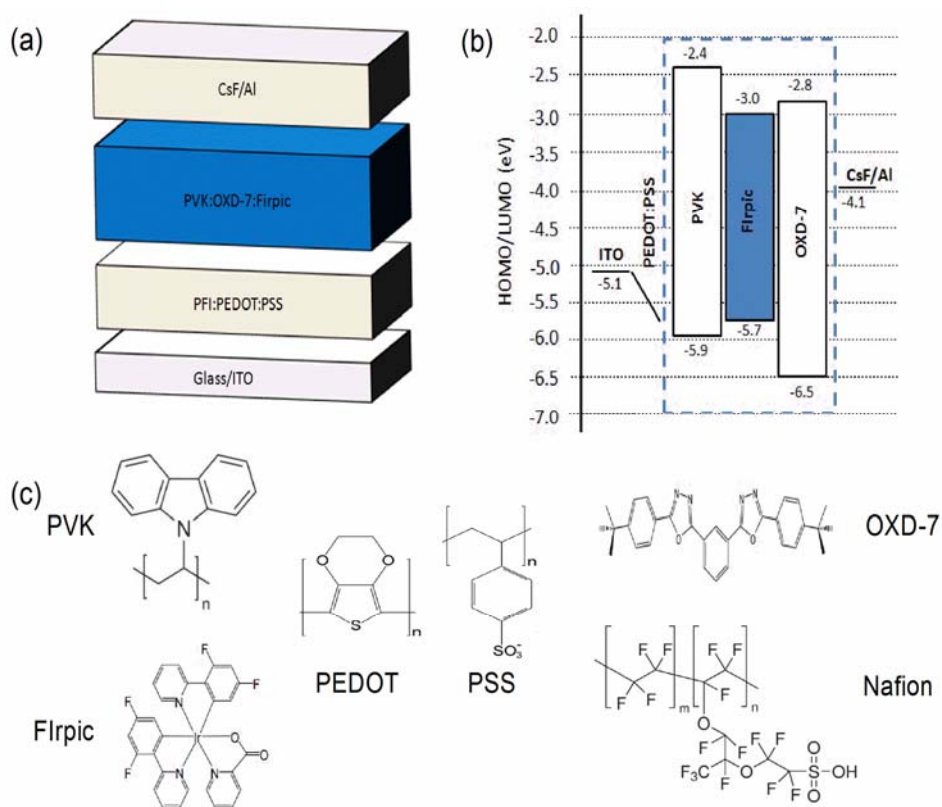


**Figure 5.2:** Schematic diagram of (a) device architecture (b) energy level diagram and (c) molecular structure of the materials used.

### 5.3 J-V-L and efficiency characteristics

Figure 5.3 shows the J-L-V characteristics of the devices with different concentrations of PFI blended into PEDOT:PSS. From the L-V characteristics, all the devices with PFI doped PEDOT:PSS show lower turn on voltage ( defined at 1  $\text{cd/m}^2$ ). For examples, compared to the control device, the optimized device (Device III) shows reduction of turn on voltage from 4.4 V to 3.7 V. In addition to this, devices with PFI doped PEDOT:PSS show higher current injection.

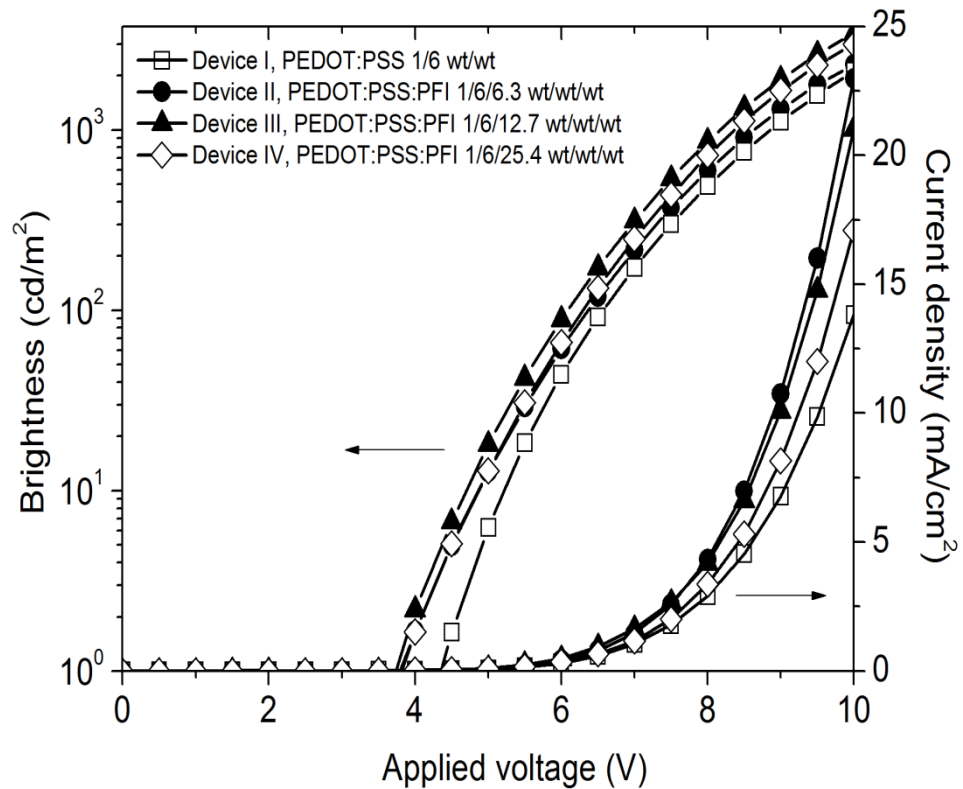


**Figure 5.3:** J-L-V characteristics of the blue devices with different amount of PFI doped into PEDOT:PSS.

Literature ascribes that the work function of PEDOT:PSS increased with PFI concentrations in a gradient manner from bottom to the top of the film surface. The work function enhancement is due to the high ionization potential of fluorinated sulfonic acid in PFI which creates high dipole moment on the PFI doped PEDOT:PSS film surface (T. W. Lee et al., 2007). It is reported that the surface work function of the

PFI doped PEDOT:PSS thin film with concentrations similar to Device II, III and IV gave 5.72 eV, 5.79 eV and 5.92 eV respectively (T. W. Lee et al., 2007). Therefore, the improvement of current injection and turn-on voltage of the blue devices can be attributed to the reduction of the anodic barrier height.

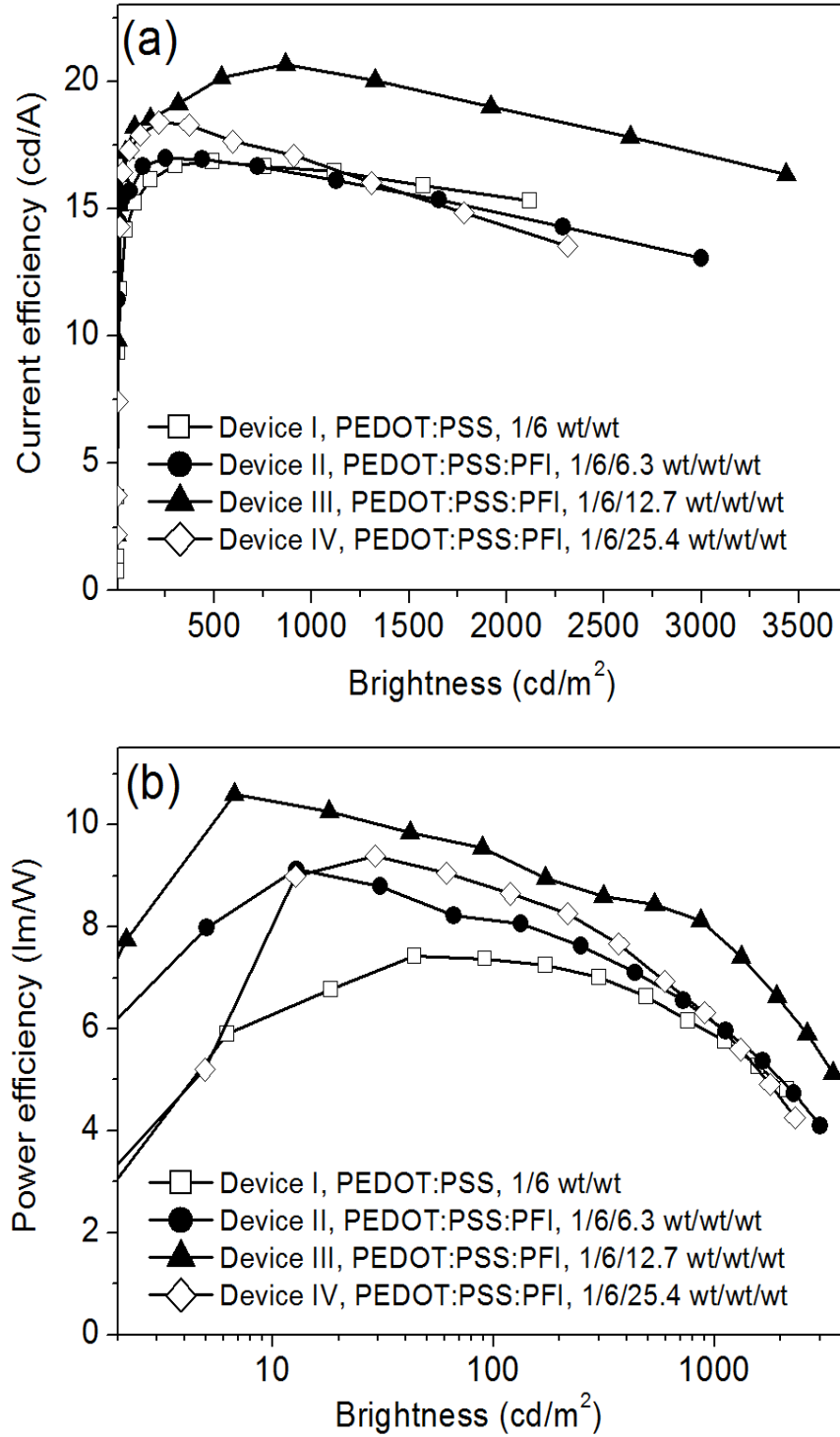


**Figure 5.4:** (a) Current efficiency and (b) power efficiency of the blue devices.

Figure 5.4 shows the efficiencies of the blue devices. Compared to the control device, our optimized blue device efficiency (Device III) improves from 7.3 lm/W (15.4 cd/A) and 5.9 lm/W (16.5 cd/A) to 9.4 lm/W (18.2 cd/A) and 17.9 lm/W (20.4 cd/A) at 100 cd/m<sup>2</sup> and 1000 cd/m<sup>2</sup> respectively. More important, PFI doped PEDOT:PSS improves the device efficiency markedly especially at low brightness, i.e.  $\sim 100$  cd/m<sup>2</sup>. This is due to the insulating and inert characteristics of PFI which can suppress excitons quenching at the HIL/EML interface as proposed by (T. H. Han, Choi, et al., 2012). The efficiencies improved when the amount of PFI increases. However HIL with higher concentration of PFI (i.e. Device IV) yield somewhat reduced efficiency. . The blue devices efficiencies are summarized in Table 5.2.

**Table 5.2:** Blue PHOLEDs performances with different amount of PFI blended into PEDOT:PSS.

Device	V <sub>ON</sub> (1cd/m <sup>2</sup> )	<sup>1</sup> V <sub>ON</sub>	<sup>1</sup> PE (lm/W)	<sup>1</sup> CE (cd/A)	<sup>2</sup> V <sub>ON</sub>	<sup>2</sup> PE (lm/W)	<sup>2</sup> CE (cd/A)
I	4.4	6.6	7.3	15.4	8.8	5.9	16.5
II	3.8	6.3	8.1	16.3	8.4	6.1	16.2
III	3.7	6.1	9.4	18.2	8.2	7.9	20.4
IV	3.8	6.4	8.7	17.7	8.7	6.1	16.7

<sup>1</sup>At brightness of 100 cd/m<sup>2</sup>

<sup>2</sup>At brightness of 1000 cd/m<sup>2</sup>

Hole current dominated devices (ITO/PEDOT:PSS:PFI/PVK:OXD-7:FIrpic/Au) were fabricated and the results are shown in Figure 5.5. Au has relatively high work function compared to the LUMO level of the EML. Therefore, Au cathode is expected to retard electron injection. With the exception of the HIL layer, all the blue devices have the same device architecture and processing conditions. Therefore any changes on the current injection will be solely attributed to the addition of PFI into the PEDOT:PSS. The J-V characteristics of the hole dominated devices exhibits the similar

trend with the device J-V characteristics in Figure 5.3. Control device (Device I) has the lowest current injection. The hole current increases with the concentrations of PFI. However, when PEDOT:PSS:PFI ratio reaches 1/6/25.4 (Device IV), the current injection reduces. The improvement in current injection and efficiency of the blue devices can be attributed to the reduction of barrier height for hole injection. On the other hand, the decrease of current density and efficiency at higher concentrations of PFI i.e. Device IV required further analysis which will be discussed in the following section.

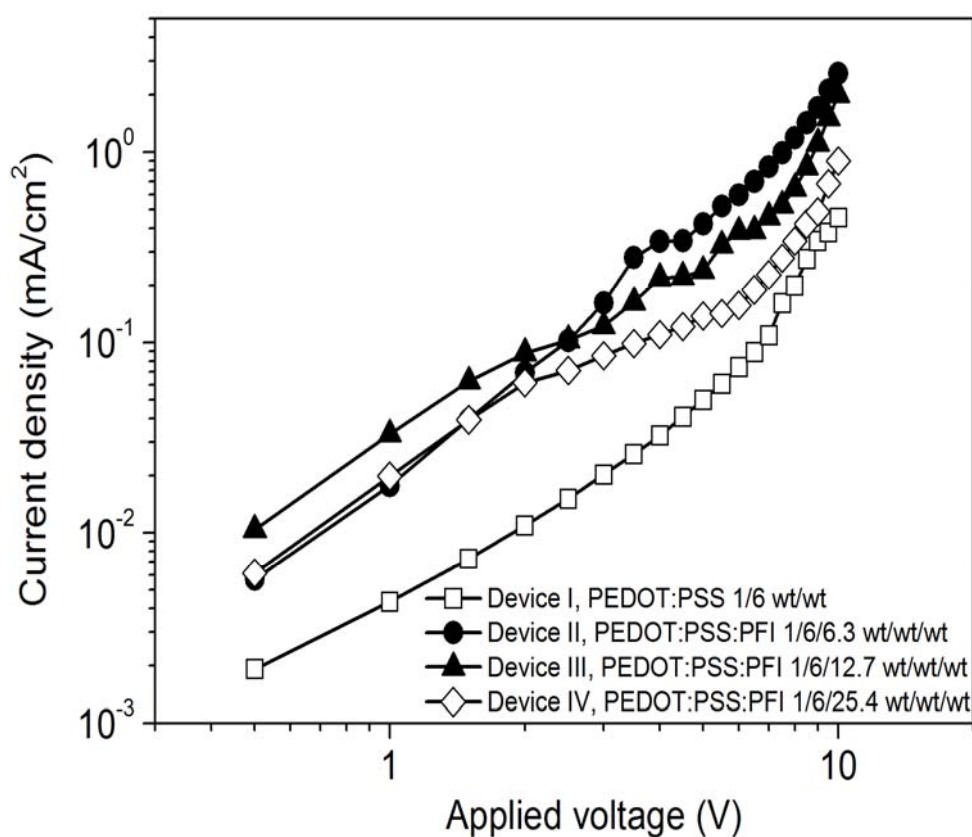


**Figure 5.5:** J-V characteristics of hole dominated devices of the blue PHOLEDs with different concentrations of PFI doping in the PEDOT:PSS.

#### 5.4 Conductivity characterizations.

Figure 5.6 presents the conductivity of the PFI modified PEDOT:PSS film. The pristine PEDOT:PSS film has conductivity of  $1.41 \times 10^{-4}$  S/cm which is comparable to the reported PEDOT:PSS (AI4083) conductivity in (Y. K. Han et al., 2011; Y. F. Xu et al., 2009).

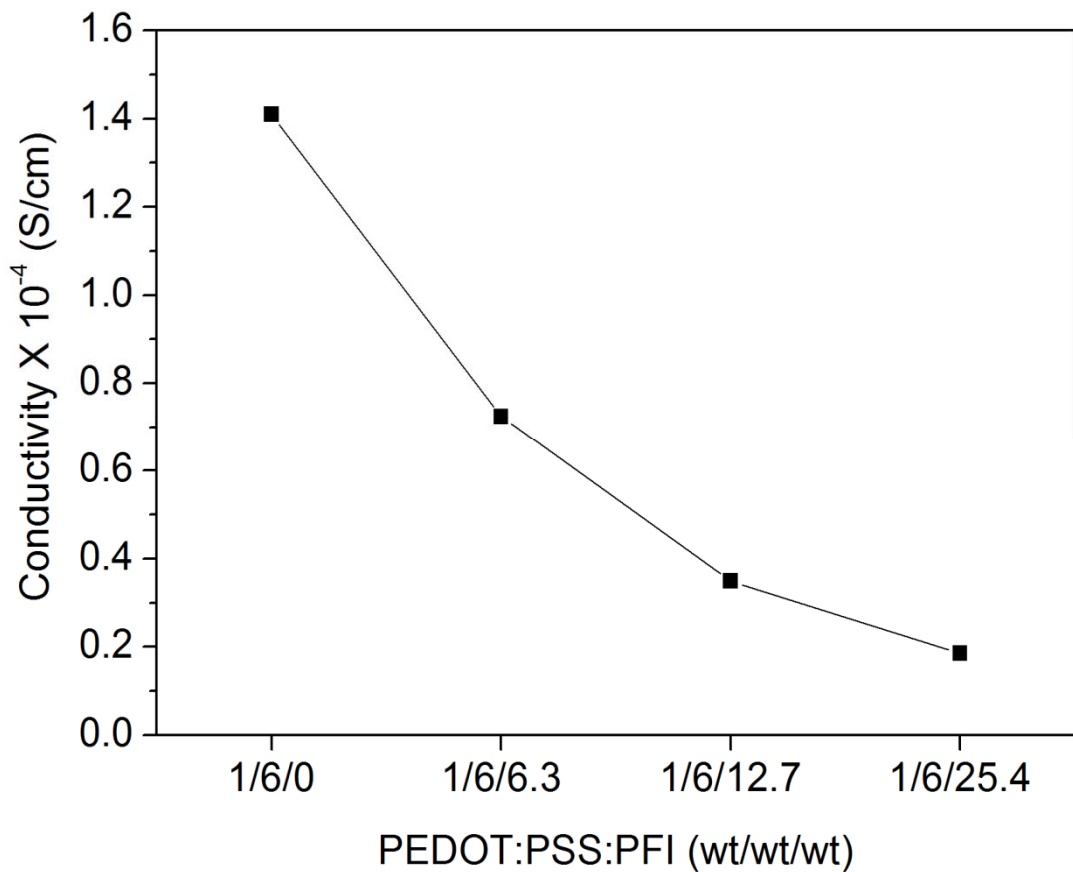


**Figure 5.6:** Conductivity of pristine PEDOT:PSS and PEDOT:PSS blended with different amount of PFI. The thin film conductivity was measured using 4-point probe.

The conductivity starts to decrease exponentially as the concentrations of PFI increases. At high concentration of PFI i.e. PEDOT:PSS:PFI 1/6/25.4 wt/wt/wt, the thin film conductivity drops to  $1.85 \times 10^{-5}$  S/cm which correspond to one order magnitude lower than the conductivity of the pristine PEDOT:PSS. This is not surprising as PFI is an ionic polymer with poor conductivity (J. K. Park et al., 2012). While PFI helps to

increase the PEDOT:PSS work function, it also enhances the film resistivity. Therefore at higher concentrations of PFI (Device IV), the current injection and device efficiency decreases as evident from the J-V and efficiency characteristics in Figure 5.3 and Figure 5.4.

## 5.5 Optical characterizations

The PFI modified PEDOT:PSS transmittance in visible range was measured and the results are presented in Figure 5.7.

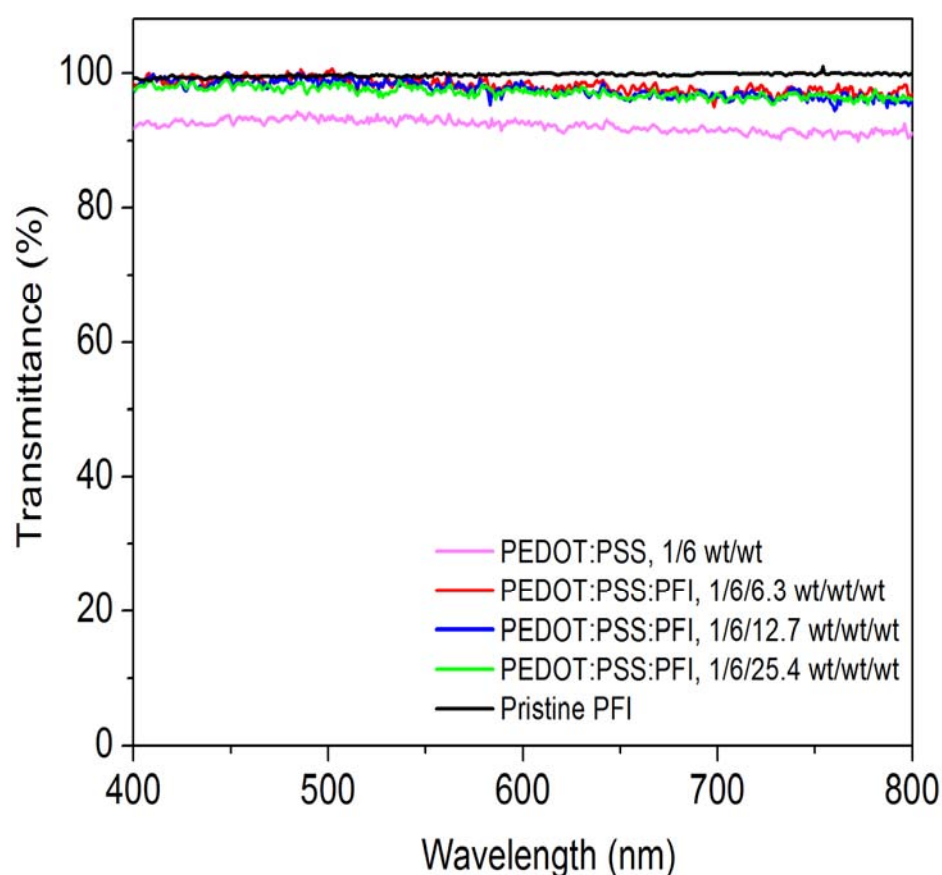


**Figure 5.7:** Transmittance spectra of pristine PEDOT:PSS film, PFI film and PFI doped PEDOT:PSS film.

The transmittance measurement was carried out on a 40 nm PEDOT:PSS:PFI film spin coated on quartz substrate. The pristine PEDOT:PSS shows 90%-94% transmittance across the whole visible range. When PFI is blended into the PEDOT:PSS, the transmittance further improved to 95%-98% due to the high transparency of the pristine



PFI film. The high transmittance of PFI doped PEDOT:PSS is beneficial to the device as it can reduced light loss due to the absorption of PEDOT:PSS.

The EML for all the devices are identical. It consists of PVK (60 wt%) : OXD-7 (30 wt%) : FIrpic (10 wt%). The EML absorption and PL spectra are shown in Figure 5.8. The absorption peak is at 232 nm which is consistent with the observation by (Xiong & Deng, 2011). On the other hand, the emission is centred at 479 nm with vibrational peak at 500 nm which are the typical characteristics of FIrpic emission.

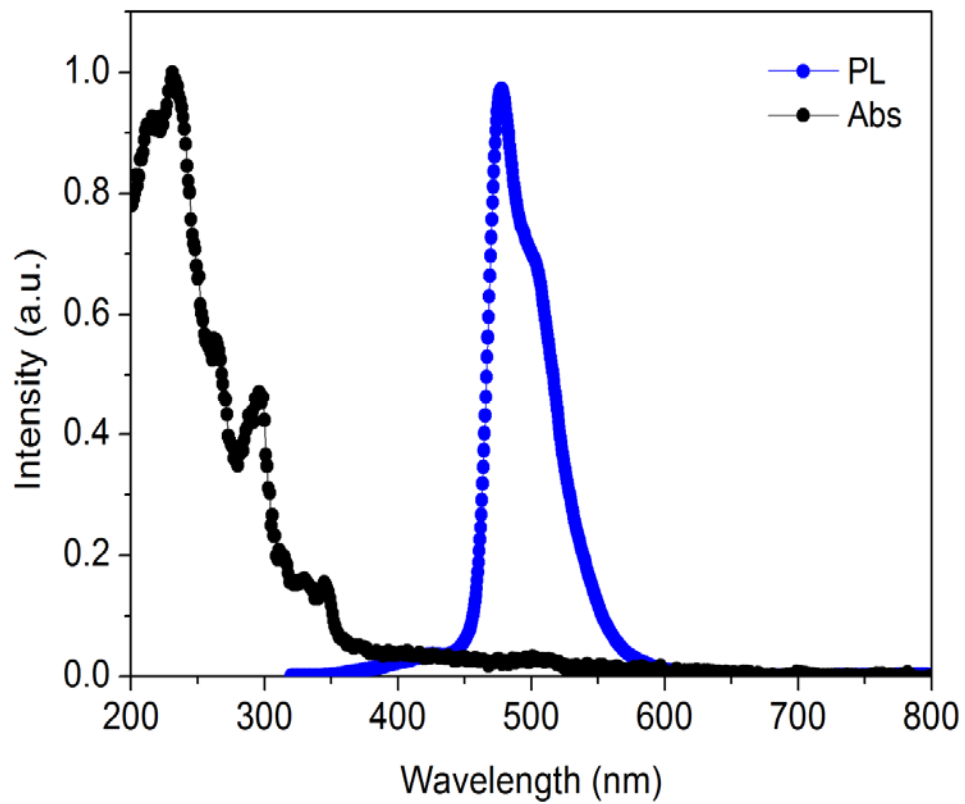


**Figure 5.8:** PL and absorption (Abs) spectra of the devices EML which consists of PVK (60 wt%):OXD-7 (30 wt%):FIrpic (10 wt%).

## 5.6 Surface morphology characterizations

The PFI modified PEDOT:PSS thin films were examined using AFM operating under tapping mode. The phase images are shown in Figure 5.9. Similar to the reported works by (Y. S. Hsiao, Whang, Chen, & Chen, 2008; J. Sun, Gerberich, & Francis,

2007), the bright region and dark region of the pristine PEDOT:PSS film correspond to PEDOT grain and PSS grain respectively as shown in Figure 5.9a

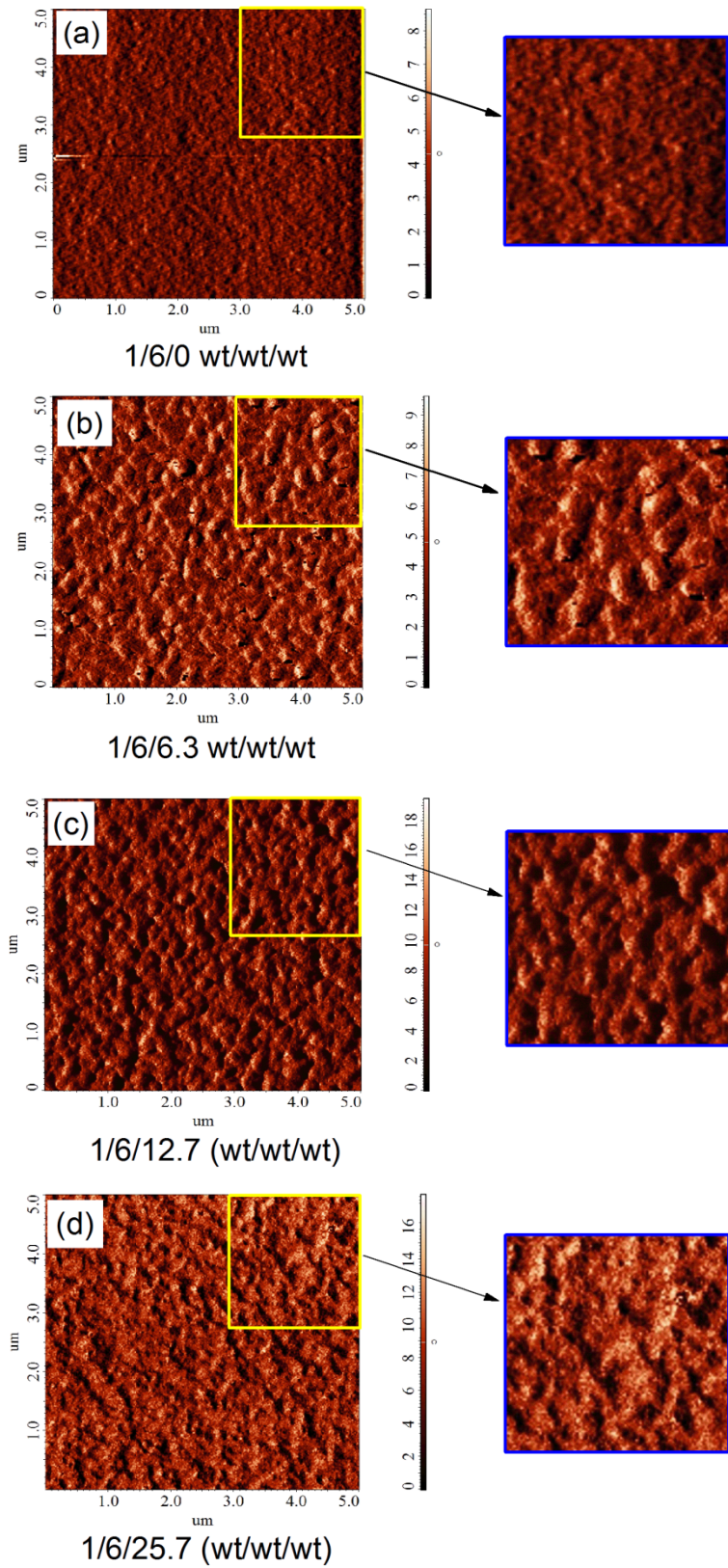


**Figure 5.9:** AFM phase images of the PEDOT: PSS:PFI (wt/wt/wt) film.

The AFM phase images of the PFI doped PEDOT:PSS indicate two possibilities. The first one is that the domains of PEDOT and PSS have become larger. The second possibility is that the PFI has phase segregated to the film surface. Recent XPS studies by Lee et. al. have shown that PFI phase segregated to the PEDOT:PSS:PFI film surface in a gradient manner with the highest concentration at the film surface (T. W. Lee et al., 2007). This leads to the work function enhancement when PFI is added into PEDOT:PSS.

## 5.7 Summary

In summary, for the first time we have demonstrated solution processed single layer blue PHOLED by using a mixture of PEDOT:PSS and PFI as HIL. Compared to the control device, our optimized blue device show efficiency enhancement from 7.3 lm/W (15.4 cd/A) and 5.9 lm/W (16.5 cd/A) to 9.4 lm/W (18.2 cd/A) and 7.9 lm/W (20.4 cd/A) at 100 cd/m<sup>2</sup> and 1000 cd/m<sup>2</sup> respectively. The device performance enhancements are due to reduction of barrier height for hole injection and high transparency of the PFI doped PEDOT:PSS film. In addition, the insulating and inert characteristics of PFI results in lower excitons quenching at the HIL/EML interface. With these observations and results, it is highly anticipated that the high concentration of PFI is beneficial to the OLED performance. In contrast, our results show that the conductivity of PFI doped PEDOT:PSS film reduces exponentially when the amount of PFI in PEDOT:PSS increases. Therefore, high amount of PFI in PEDOT:PSS can degrade the device performance, caused by the high resistivity of the PFI. Our work suggests that PFI is a cheap and effective method in enhancing the efficiency of a simple solution process single layer blue PHOLED which is highly needed especially for lighting applications.

## **CHAPTER 6: High efficiency solution processed single layer fluorescent yellow OLED through fluorinated alcohol treatment at the emissive layer/cathode interface**

### **6.1 Introduction**

Considerable efforts have been dedicated in developing high efficiency yellow OLED using solution processed method. Yellow emission OLED find its applications in lithography lab, traffic light, RGBY-TV and combined with blue emission, it can produce white emission for lighting applications (Jou et al., 2012). Some examples of high efficiency solution processed yellow PHOLED are reported by Jou's group which yielded 25 lm/W at 1000 cd/m<sup>2</sup> (J. H. Jou et al., 2013) and Zhang et. al. has achieved 19.7 lm/W at 1000 cd/m<sup>2</sup> (B. H. Zhang et al., 2012). Wu et. al. produced a yellow device with efficiency up to 11.9 lm/W at 1000 cd/m<sup>2</sup> (H. B. Wu et al., 2009). Recently, Jou's group reported the highest efficiency solution processed yellow PHOLED to date which gave a record-breaking of 52.3 lm/W at 1000 cd/m<sup>2</sup> (J.-H. Jou et al., 2013). On the other hand, the progress on fluorescent yellow OLED development is relatively slow. This is due to the discovery of phosphorescent dyes which enable both the singlet and triplet exciton to be harvested (Kappaun, Slugovc, & List, 2008; Tao, Yang, & Qin, 2011; Yersin et al., 2011). Some of the notable work on fluorescent yellow OLED are from Jou's group (Jou et al., 2012). They reported a nearly non-roll off yellow device with efficiency of 18.3 lm/W at 1000 cd/m<sup>2</sup> using vacuum deposition method. Although fluorescent device has lower quantum efficiency compared to phosphorescent device, the development of fluorescent is still relevant especially when high brightness is required for application such as large panel displays. This is because PHOLED suffers from severe efficiency roll-off when operating at high

brightness due to triplet-polaron quenching and triplet-triplet annihilation (C. Murawski, K. Leo, & M. C. Gather, 2013a; Okumoto, Kanno, Hamada, Takahashi, & Shibata, 2006). The efficiencies of some of the best processed blue yellow fluorescent OLED reported to date are summarized in Figure 6.1.

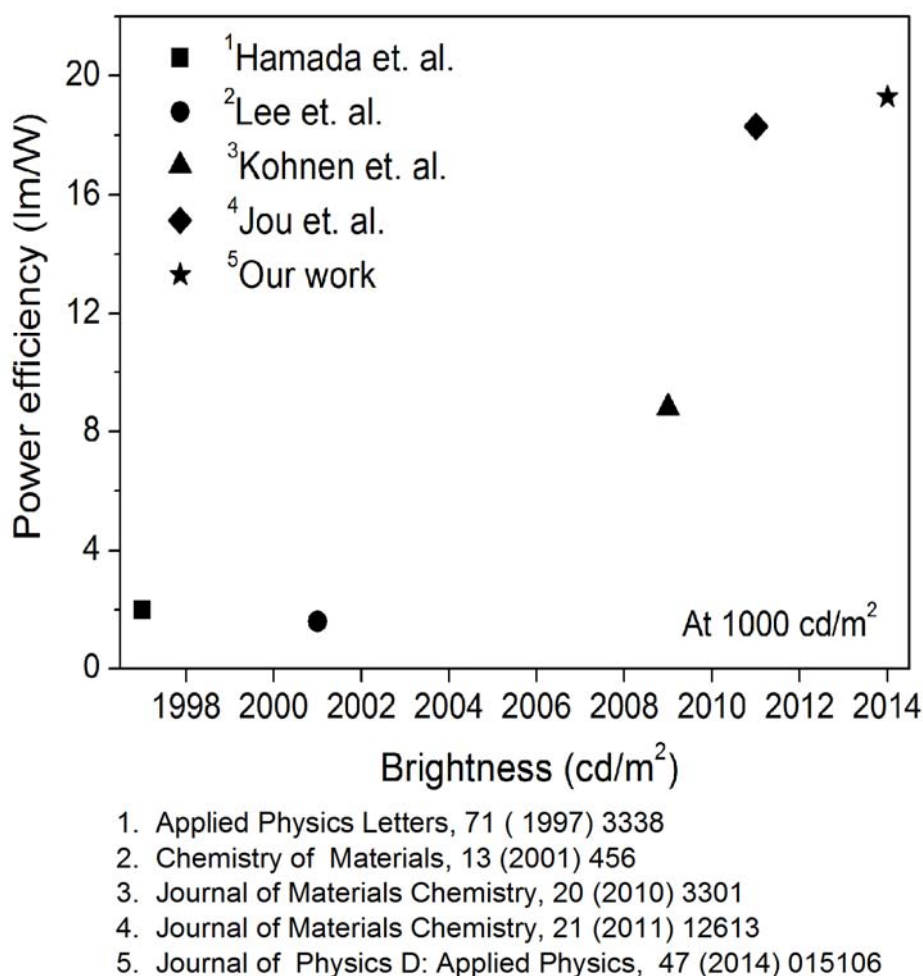


**Figure 6.1:** Some of the best solution processed yellow fluorescent OLED reported to date. The efficiencies are benchmarked at 1000 cd/m².

In this chapter, we report a simple method in enhancing the efficiency of a commercially available super yellow PPV (SY-PPV) OLED by treating the surface of the EML using 2,2,3,3,4,4,5,5-Octafluoro-1-pentanol. By using this method, we have increased the efficiency of the fluorescent yellow device from 11.7 lm/W (11.1 cd/A) and 11 lm/W (14 cd/A) to 19.7 lm/W (16.5 cd/A) and 19.2 lm/W (20.9 cd/A) at brightness of 100 cd/m² and 1000 cd/m² respectively. To the best of our knowledge,

this power efficiency is on par with the best reported yellow fluorescent OLED (Jou et al., 2012) and even comparable to some of the best solution processed yellow PHOLED reported to date (Moujoud et al., 2010; B. H. Zhang et al., 2012).

## 6.2 Experimental

The basic device structure consists of ITO/ PEDOT:PSS (40 nm)/ SY-PPV (80 nm)/LiF (0.8 nm)/Al (100 nm). Figure 6.2b and Figure 6.2c shows the energy level diagram and the chemical structures of the 2,2,3,3,4,4,5,5-Octafluoro-1-pentanol used in this work. ITOs were patterned using standard lithography method. The substrates were cleaned sequentially using DI water, acetone, isopropyl alcohol and DI water again followed by oxygen plasma treatment for 5 minutes. For the device fabrication, 40 nm of PEDOT:PSS was spin coated onto the ITO and then the substrates were baked at 150°C for 10 minutes in N<sub>2</sub> environment. Following that, SY-PPV (Merck) was spin coated on top of the PEDOT:PSS to form a 80 nm film. Then the substrates were baked at 100°C for 10 minutes. The EML treatment was carried out by either spin coating fluorinated alcohol i.e. 2,2,3,3,4,4,5,5-Octafluoro-1-pentanol (Sigma-Aldrich) or ethanol at 2000 rpm for 30s and then baked at 100°C for 10 minutes. Finally, the device cathode which consists of LiF (0.8 nm) and Al (100 nm) was vacuum deposited through a shadow mask, which defined the device active area. All the devices were encapsulated using UV curable epoxy and glass lid. The current (J) –voltage (V) – brightness (L) characteristics were measured using Konica Minolta CS-200. The photocurrents of the OLEDs were measured under the illumination of a simulated AM1.5 light source at 100 mW/cm<sup>2</sup> (Newport 67005). The film thickness was measured using P-6 profilometer (KLA-Tencor). The absorption spectra were measured using Perkin Elmer PE750 UV-Vis-NIR. Photoluminescence (PL) was measured using Perkin Elmer LS50B spectrometer. AFM images were taken using NX10 (Park Systems).

XPS measurements were carried out at the photoemission beamline of the Synchrotron Light Research Institute (SLRI) of Thailand (Nakajima et al., 2013). The photon energy of the excitation was 771.6 eV. The photoelectron spectra were collected by using a Thermo Scientific Alpha110 energy analyzer.

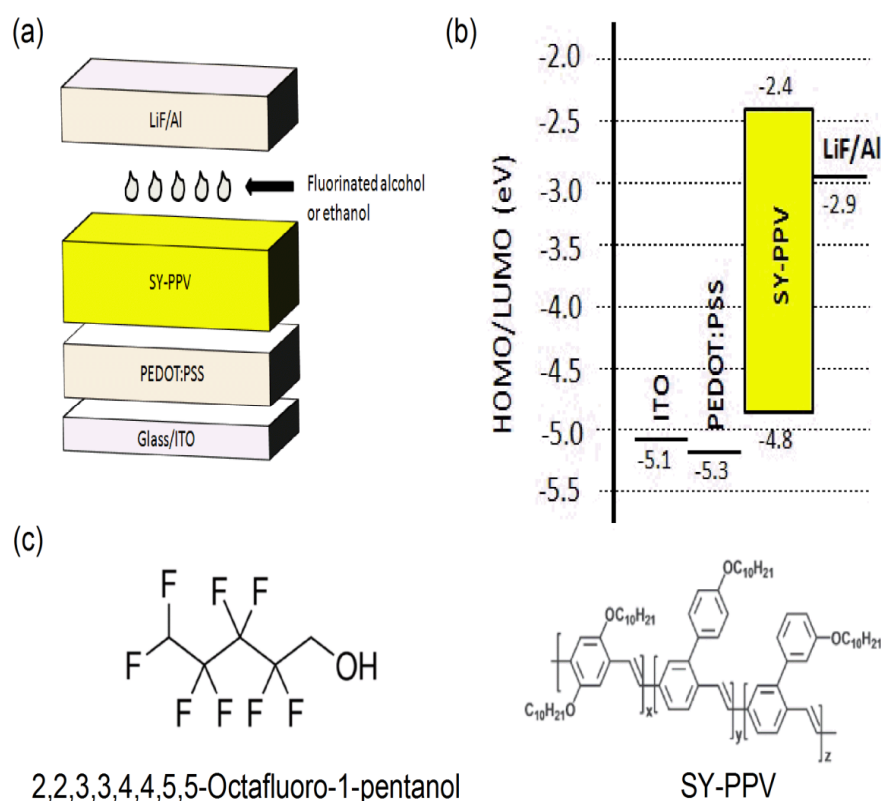


**Figure 6.2:** (a) Device structure, (b) energy level diagram of the yellow device and (c) molecular structure of 2,2,3,3,4,4,5,5-Octafluoro-1-pentanol and SY-PPV.

### 6.3 J-V-L and efficiency characteristics

Figure 6.3 shows the J-V-L characteristics of yellow devices. It can be seen that the fluorinated alcohol treated device shows the highest current injection, followed by the ethanol treated device and control device. Similarly, with fluorinated alcohol treatment the yellow device exhibits higher light output for the whole range of applied voltage. For example at 4 V, the brightness of the fluorinated alcohol treated device increases from 1027 cd/m<sup>2</sup> to 2508 cd/m<sup>2</sup>. Also, both devices with ethanol and fluorinated alcohol treatment show a reduction of turn-on voltage (defined at 1cd/m<sup>2</sup>)

from  $2.21 \pm 0.01$  V (control device) to  $2.14 \pm 0.02$  V (ethanol treated device) and  $2.11 \pm 0.04$  V (fluorinated alcohol treated device).

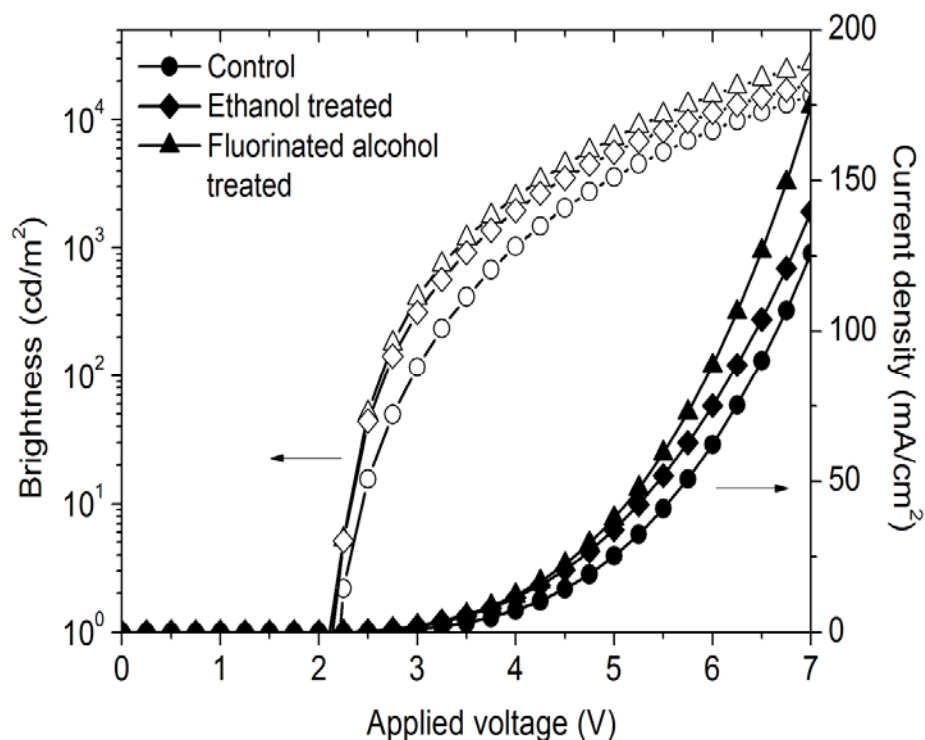


**Figure 6.3:** J-V-L characteristics of the yellow OLEDs.

Figure 6.4a and Figure 6.4b show the current efficiency and power efficiency of the yellow OLEDs. It is obvious that the efficiency of the control device is inferior to that of the treated devices, with the fluorinated alcohol treated device yielded the best efficiencies. For instance, the control device gave maximum power efficiency of 12.2 lm/W at 235 cd/m<sup>2</sup> and at 1000 cd/m<sup>2</sup> the power efficiency reduced to 11 lm/W. It is worth mentioning that our control device efficiency is comparable to the SY-PPV OLED efficiency reported recently (Kohnen et al., 2010). With fluorinated alcohol treatment, the device maximum power efficiency is 21.3 lm/W at 410 cd/m<sup>2</sup> and at 1000 cd/m<sup>2</sup> the efficiency dropped slightly to 19.2 lm/W.



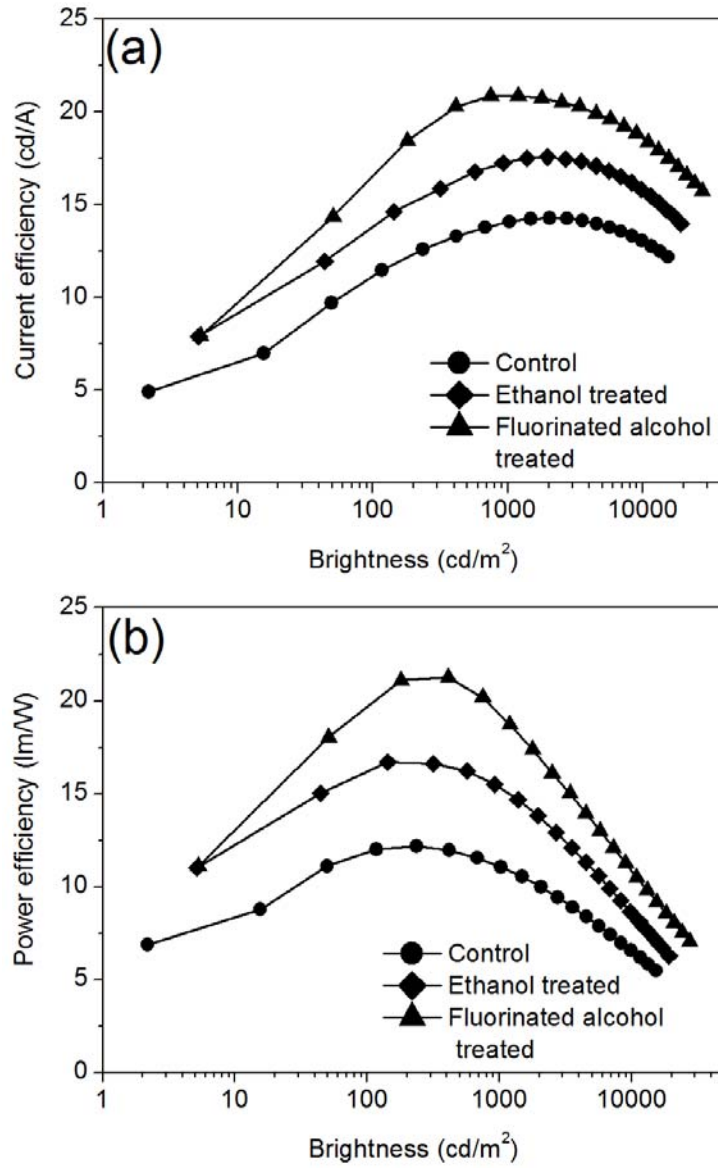


**Figure 6.4:** (a) Current efficiency and (b) power efficiency of the SY-PPV devices.

The yellow devices performances are summarized in Table 6.1.

**Table 6.1:** Yellow OLEDs performances with different type of alcohol treatment.

Treatment	V <sub>ON</sub> (1cd/m <sup>2</sup> )	<sup>1</sup> V <sub>ON</sub>	<sup>1</sup> PE (lm/W)	<sup>1</sup> CE (cd/A)	<sup>2</sup> V <sub>ON</sub>	<sup>2</sup> PE (lm/W)	<sup>2</sup> CE (cd/A)
Control	2.2	2.9	11.7	11.1	3.9	11.0	14.0
Ethanol	2.1	2.7	16.2	13.8	3.6	15.3	17.3
Fluorinated alcohol	2.1	2.6	19.7	16.5	3.4	19.2	20.9

<sup>1</sup>At brightness of 100 cd/m<sup>2</sup>

<sup>2</sup>At brightness of 1000 cd/m<sup>2</sup>

Recent works by (Q. Wang et al., 2013; Q. Wang et al., 2011; H. Q. Zhou et al., 2013) revealed that a simple treatment using alcohol on polymer can increase the surface potential of the film. This improvement is due to the interface dipole formed on the organic film surface induced by the solvent intrinsic dipole. Especially in the case of OLED, the ability to control the surface potential is very important as this opens up the possibility for us to control the charge injection at the cathode/organic layer or anode/organic layer interface. Realizing the fact that the intrinsic dipole of the solvent plays an important role in enhancing the surface potential of the organic film, it is not a surprise that fluorinated alcohol can further improve the device efficiency compared to ethanol. This is due to the presence of the high electronegativity of F (3.98) in the fluorinated alcohol. To further clarify the origin of this improvement, we calculated the dipole moment of the fluorinated alcohol using Gaussian 09 software by employing Hartree–Fock *ab initio* with a 6-31G\*\* basis set. A permanent dipole moment of 2.27D is obtained. The higher dipole moment of the fluorinated alcohol (2.27D) compared to ethanol (1.67D) could provide a good explanation on the inferior performance of the ethanol treated device compared to the fluorinated alcohol treated device. The interface dipole shifts the vacuum level at the SY-PPV/cathode interface which can reduce the barrier height for electron injection as shown in Figure 6.5.

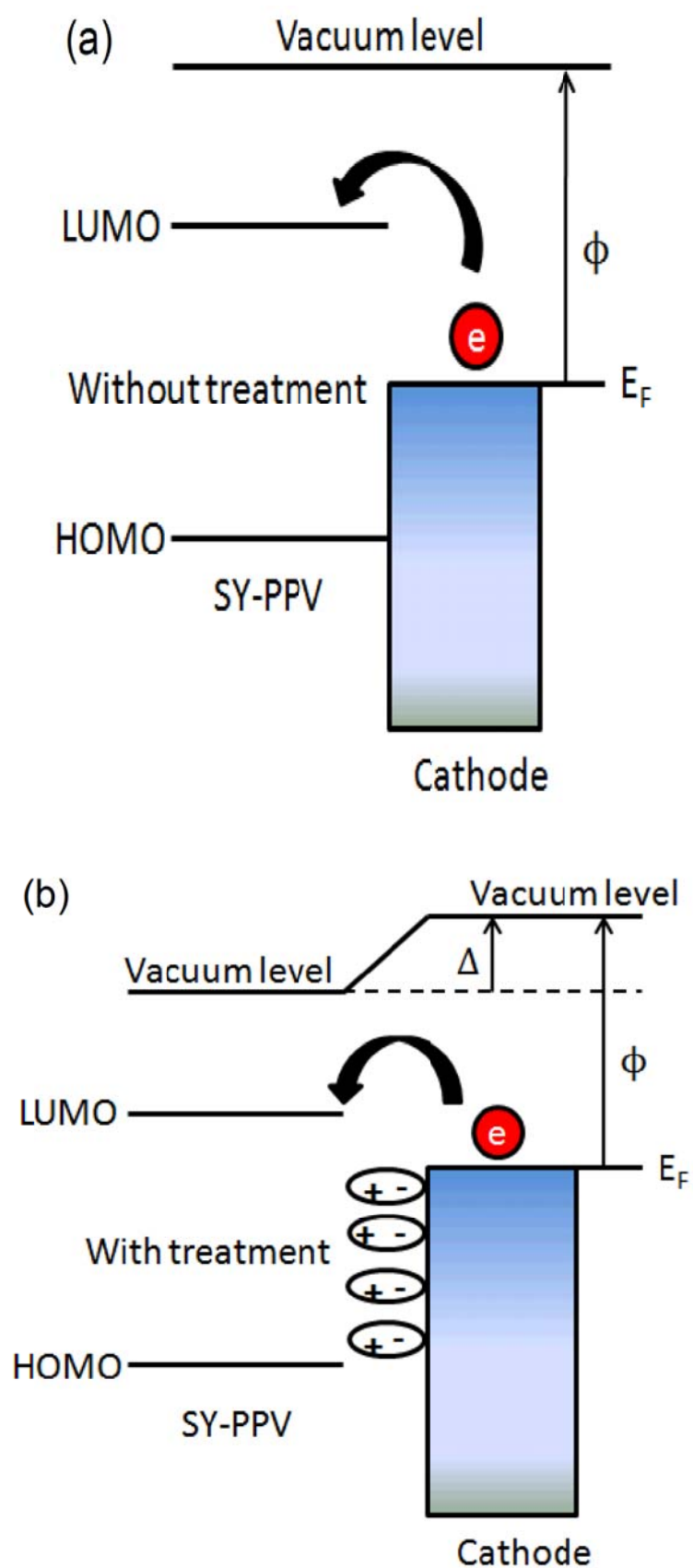


**Figure 6.5:** Energy level diagram at the SY-PPV/cathode interface for (a) device without treatment and (b) device with ethanol or fluorinated alcohol treatment.  $\Delta$  and  $\phi$  denotes the vacuum level shift and cathode work function respectively.

#### 6.4 Photovoltaic measurement and single carrier devices

In order to study the effects of EML surface modification by the alcohol solvents, photovoltaic measurement was carried out by illuminating the devices with a simulated AM1.5 light source at  $100 \text{ mW/cm}^2$ . The open circuit voltage ( $V_{OC}$ ) is a direct indication of the device built-in-potential (Niu et al., 2005). A high  $V_{OC}$  shows that either the anode or cathode barrier for carrier injection has reduced. Since the ethanol or fluorinated alcohol is spin coated at the EML/cathode interface, any changes on the  $V_{OC}$  will be solely attributed to the changes at the energy barrier between the EML and cathode. The photovoltaic response of the devices is shown in Figure 6.6.

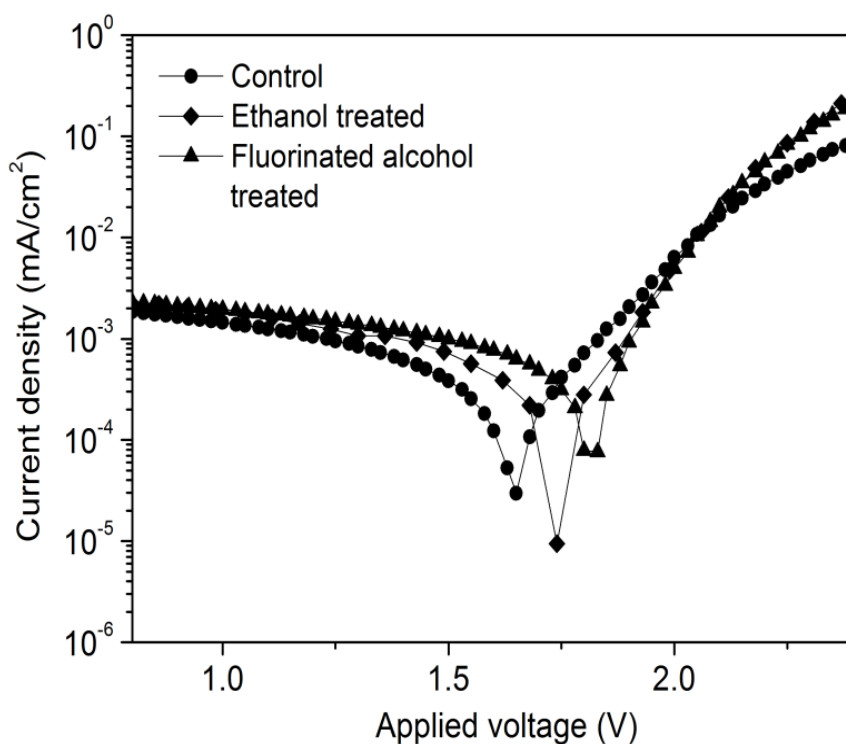


**Figure 6.6:** Photovoltaic response of the yellow OLED devices.

The  $V_{OC}$  for the devices increased gradually from  $1.65 \pm 0.02 \text{ V}$  to  $1.74 \pm 0.03 \text{ V}$  and  $1.82 \pm 0.02 \text{ V}$ , a shift of  $0.09 \text{ V}$  and  $0.17 \text{ V}$  for ethanol and fluorinated alcohol treatment respectively. This is an indication that the energy barrier for electron injection at the cathode has reduced upon adding ethanol or fluorinated alcohol into the

EML/cathode interface. In this case, fluorinated alcohol treatment gave the largest  $V_{OC}$  shift, suggesting that the fluorinated alcohol is more efficient in reducing the cathodic barrier height compared to ethanol.

To further elucidate the reduction of electron injection barrier, we fabricated electron dominated and hole dominated devices. The hole dominated device consists of ITO/PEDOT:PSS/EML/Au whereas the electron dominated device consists of ITO/LiF/EML/LiF/Al. Au has high work function which can block off electron injection at the cathode. Similarly, ITO/LiF has low work function which retard hole injection at the anode. The J-V characteristics for electron/hole dominated devices are shown in Figure 6.7.

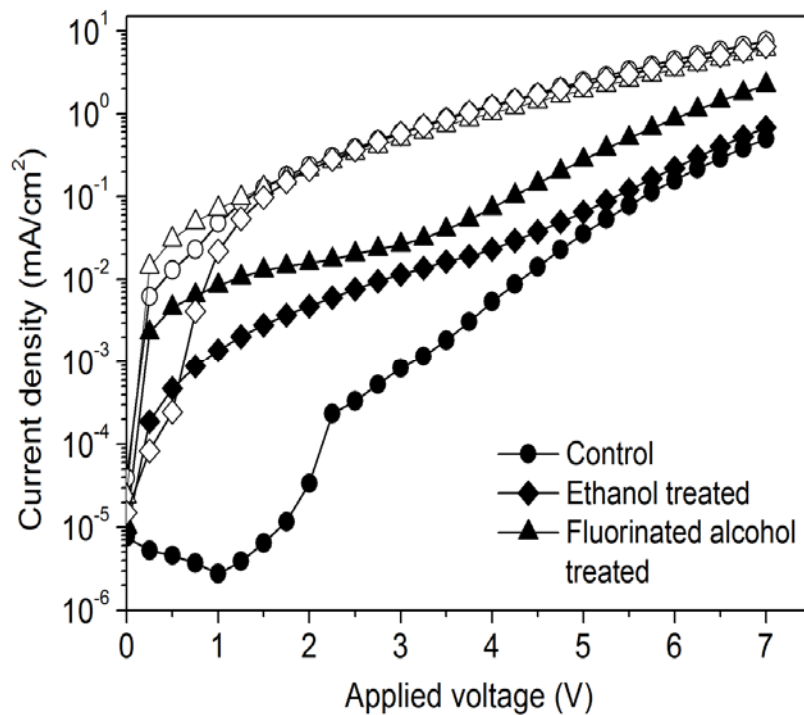


**Figure 6.7:** J-V characteristics of the electron/hole current dominated devices. Hollow symbols denote hole current dominated devices whereas solid symbols denote electron current dominated devices.

The hole current for all the devices are comparable. On the other hand, the electron current for the fluorinated alcohol treated device is the highest followed by the device with ethanol treatment. From these J-V characteristics, we can deduce two

important points. First, the charge balance for the fluorinated alcohol treated device is better compared to the rest of the devices. Second, the higher electron current injection of the treated devices is another indication that the electron injection barrier at the device cathode has improved. More important, these photovoltaic measurement results suggest that fluorinated alcohol treatment gives lower electron injection barrier compared to the ethanol counterpart.

The J-V characteristics of the electron dominated devices are plotted on a double logarithmic scale and the slopes are obtained by fitting the experimental data with power law as shown in Figure 6.8.

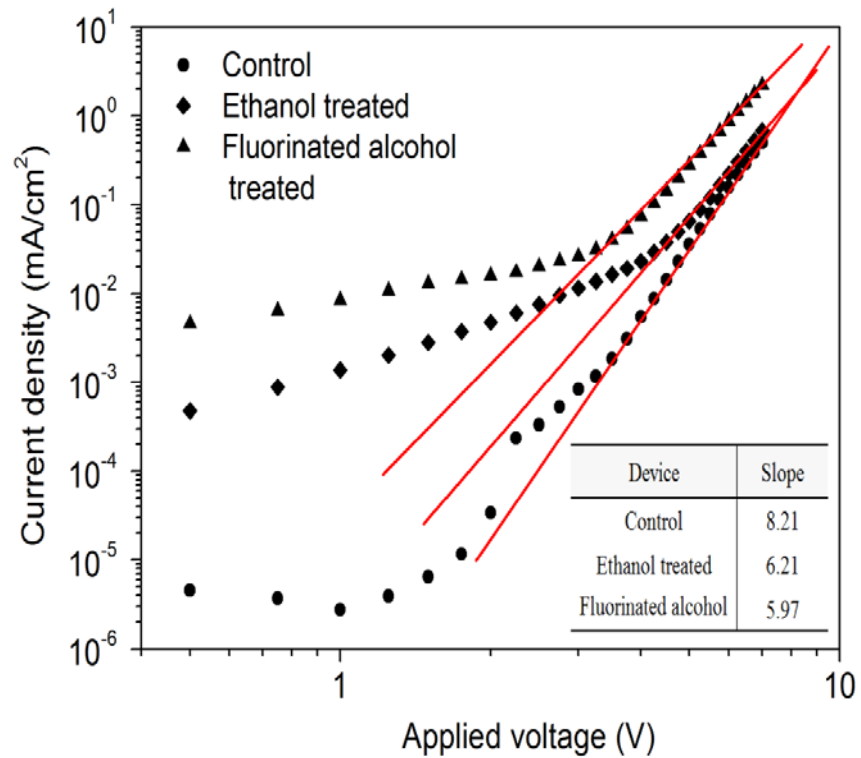


**Figure 6.8:** J-V characteristics of the electron current dominated devices. Inset is the slope calculated from the device J-V curves plotted on the double logarithmic scale. Red lines are only guide to eyes only.

The values of the slope obtained are 8.21, 6.21 and 5.97 for the control, ethanol treated and fluorinated treated device respectively. When bias is applied to the device, carriers are trapped in the trap states and with a wider distribution of traps the probability of a

carrier being trapped is higher. As the bias increased, more traps are being filled. With deep traps, the detrapping of the carrier become less probable and with a larger distribution of traps states the probability of the detrapped carrier being trapped again is higher. In other words, if the traps are deep and the distribution is wide, most of the trapped are being filled as the voltage increased. Consequently, a steep rise of current is observed across the applied voltage if the traps are deep and their distribution is wide. Therefore a steeper slope corresponds to deeper traps or a wider distribution of trap states (Nicolai, Mandoc, & Blom, 2011). Here a clear trend can be observed, suggesting the solvent treatments results in a smaller distribution of the trap states which could be due to traps passivation by the solvents. This is not surprising as recent works by Zhou et. al. showed that traps on a polymer film can be passivated by merely spin coating alcohol solvent on top of it (H. Q. Zhou et al., 2013). Our analysis clearly demonstrates that the reduced trap states are another possible reason for the enhancement of electron current in the treated devices.

## **6.5 XPS characterizations**

Wang et. al has shown that for a polymer film treated with alcohol, the solvent can only be removed by vacuuming the samples at  $10^{-4}$  Pa for 12 hours followed by vacuum baking at  $50^{\circ}\text{C}$  for 2 hours (Q. Wang et al., 2011). These findings suggest that the complete removal of alcohol solvent on the polymer film surface is not an easy task. In our case, we annealed the samples at  $100^{\circ}\text{C}$  for 10 minutes and vacuumed our samples to  $3 \times 10^{-4}$  Pa for 1.5 hours prior to the cathode deposition. Therefore, we expect this process should not remove the fluorinated alcohol completely. Moreover fluorinated alcohol has a relatively high boiling point of  $141^{\circ}\text{C}$  to  $142^{\circ}\text{C}$  ("Material Safety Data Sheet for 2,2,3,3,4,4,5,5-Octafluoro-1-pentanol," 2012 ). In order to validate this, we prepared three sets of samples: (a) SY-PPV films as control sample (b)

SY-PPV films treated with fluorinated alcohol (denoted as fluorinated non vacuumed) and (c) SY-PPV films treated with fluorinated alcohol and vacuumed at  $3 \times 10^{-4}$  Pa for 1.5 hours (denoted as fluorinated vacuumed). All these samples were annealed at  $100^{\circ}\text{C}$  for 10 minutes. We characterized these samples using XPS and Fluorine 1s (F 1s) peak can be detected on all samples treated with fluorinated alcohol (see Figure 6.9). The F1s signal is rather weak because prior to running the XPS measurement the samples were loaded in a load-lock chamber for almost 8-10 hours at about  $1.3 \times 10^{-4}$  Pa. During measurement, the sample was transferred to the analysis chamber under Ultra High Vacuum (UHV) condition with pressure below  $2.7 \times 10^{-8}$  Pa. This UHV condition could remove some of the F on the polymer film surface. Nevertheless, this suggests that the interface dipole induced by the fluorinated alcohol is strongly pinned on the EML surface and only can be partially removed under UHV condition.

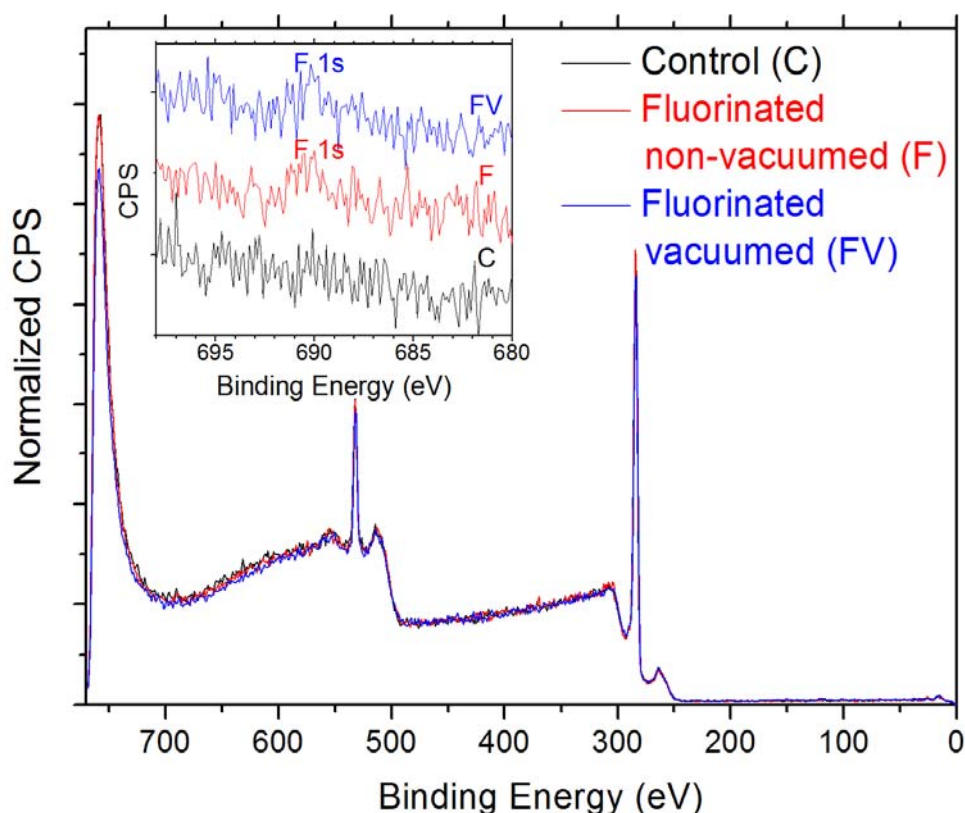


**Figure 6.9:** XPS spectra of the SY-PPV thin samples. Inset is the expanded view of the spectra in the region of 680 eV to 698 eV. The F 1s can be detected for the samples treated with fluorinated alcohol.



## 6.6 Optical characterizations

Absorption and PL measurements were carried on the SY-PPV films spin coated on glass substrate. The absorption and PL spectra are shown in Figure 6.10. The absorption and PL spectra peak at 445 nm and 560 nm respectively which is the typical characteristics of SY-PPV film (Kohnen et al., 2010). There are no significant changes on the absorption and emission properties after the SY-PPV treated with alcohol solvents. Therefore the fluorinated alcohol and ethanol treatment did not change the optical properties of the SY-PPV film.

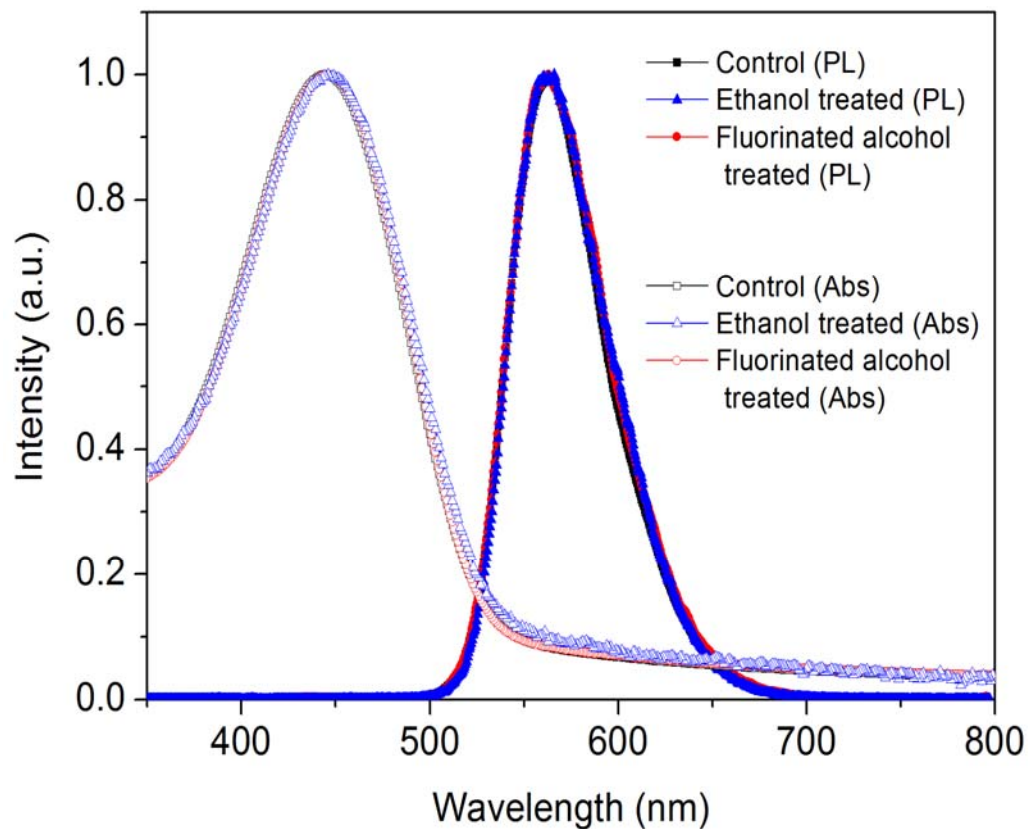


**Figure 6.10:** Absorption (hollow symbol) and PL (filled symbol) of the SY-PPV thin film.

## 6.7 Surface morphology

The surface morphology of the pristine and treated SY-PPV films was inspected using AFM as shown in Figure 6.11. We did not observe any morphology changes nor pin-holes formation on the SY-PPV films upon alcohol treatment.

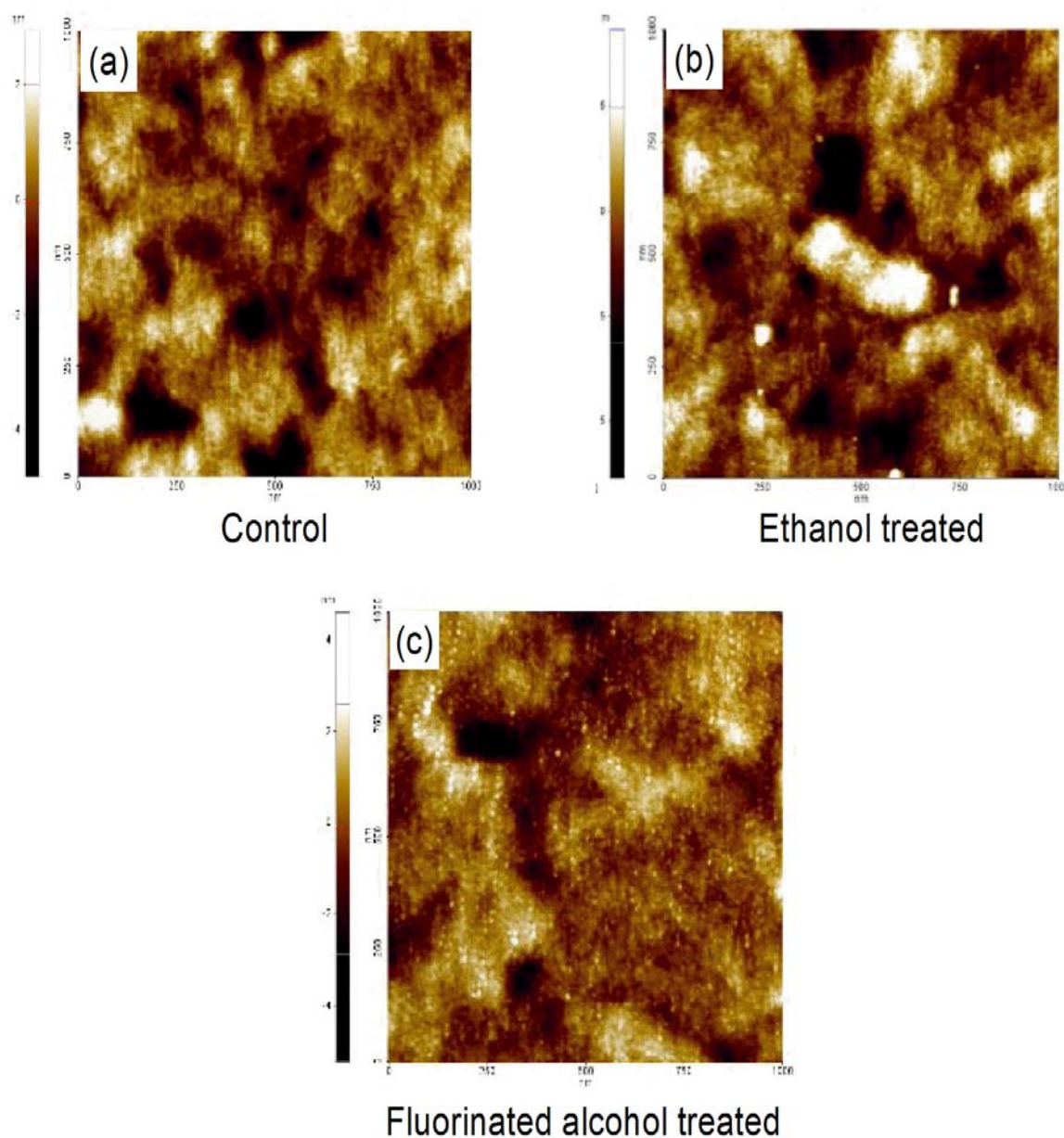


**Figure 6.11:** AFM images of the (a) pristine, (b) ethanol treated and (c) fluorinated alcohol treated SY-PPV thin film.

## 6.8 Summary

In summary, high efficiency yellow fluorescent device with efficiency 19.2 lm/W (20.9 cd/A) at brightness 1000 cd/m<sup>2</sup> was demonstrated by treating the SY-PPV/cathode interface with fluorinated alcohol. A comparison was made between ethanol, a widely used polar solvent and fluorinated alcohol in enhancing the device efficiency. It is shown that the intrinsic dipole of the polar solvent plays a crucial role in improving the device efficiency. Our studies show that the device efficiency enhancement is attributed to the (i) cathode barrier lowering induced by the solvents intrinsic dipole and (ii) the ability of the solvents to passivate traps on the film surface. This simple approach may be extended to the fabrication of high efficiency white OLED for flat panel display and energy saving lighting applications.

## CHAPTER 7: High efficiency double emissive solution processed blue PHOLED

### 7.1 Introduction

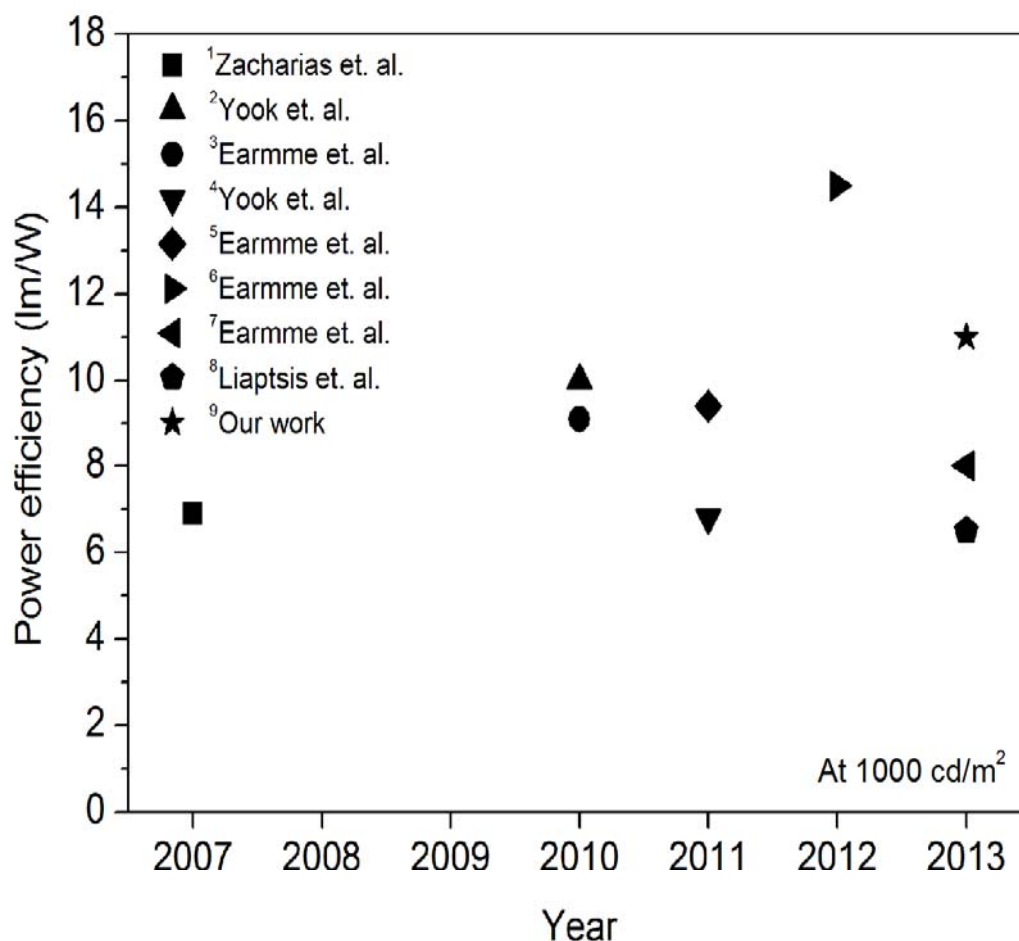
High performance PHOLED required multiple stacking of electron/hole transport layers, emissive layers and carrier blocking layers to confine excitons in the emissive layer, balance the electron /hole injection and prevent excitons quenching at the electrodes. Nevertheless, multilayer PHOLED are very difficult to achieve using wet process because solvent that used to deposit the top layer will dissolve the underlying layer resulting in intermixing (Duan et al., 2010a).

Thermally or UV crosslinkable HTL has shown to be an interesting approach to fabricate multilayer OLED. For example Jen's group has synthesized a series of thermally cross-linkable HTL i.e. 4,4',4''-tris(N-carbazolyl)triphenylamine (TCTA) by incorporating phenyl trifluorovinyl ether (TFV) which act as crosslinker (M. S. Liu et al., 2008). Very recently Kido's group has demonstrated that commercially available hole transport OLED material 4,4'-bis(carbazol-9-yl)biphenyl (CBP) can be thermally crosslinked by adding vinylbenzyl ether group as crosslinking agent (Aizawa, Pu, Sasabe, & Kido, 2013). Another interesting work is the thermal assisted UV crosslinkable 1-Bis[4-[N, N-di(4-tolyl)amino]phenyl]-cyclohexane (TAPC), a widely used hole transport material which reported by Meerholz's group (Liaptsis & Meerholz, 2013). Crosslinking is achieved by: (a) incorporating oxetane units into the TAPC molecular structure and (b) blending photoinitiator into the oxetane modified TAPC solution. Other examples of crosslinkable materials are reported in (Choulis, Choong, Patwardhan, Mathai, & So, 2006; Yook & Lee, 2012; Zuniga et al., 2013).

Another approach is to use orthogonal solvent where the solvent used to dilute the material for the top layer will not dissolve the underneath layer. One fine example

is the use of phosphine oxide (PO) base material (S. O. Jeon & Lee, 2012; Yook, Jang, et al., 2010; Yook, Jeon, Kim, & Lee, 2010). This material can be dissolved into alcohol thanks to the polar nature of P-O group. In addition to that, most host transporting OLED material is alcohol insoluble, rendering PO based material an excellent candidate as ETL in multilayer solution processed OLED. It is also worth mentioning that blade coating method has been successfully demonstrated to be able to coat polymer (Syu et al., 2010; Tseng et al., 2008) and small molecule (Chao et al., 2011; Ko et al., 2010; Z. Y. Liu et al., 2011) film for multi layer OLED as discussed in section 2.5.2.3.

Recently some research groups have developed high efficiency solution processed blue PHOLED using multilayer structure which is highly desirable for lighting application. However, these devices usually consist of a layer of solution processed emissive layer followed by a layer of ETL deposited using vacuum deposition method (Doh et al., 2012; Fu et al., 2012; Jou, Wang, et al., 2010). Research works on fully solution processed multilayer PHOLED are not widely reported. Some of the notable works on fully solution process multilayer PHOLED are reported in (Ahmed et al., 2011; Earmme et al., 2010; Earmme & Jenekhe, 2012a; Earmme & Jenekhe, 2013; Yook, Jang, et al., 2010). For example, Lee's group reported double emissive solution processed blue PHOLED with efficiency 19.3 cd/A at 1000cd/m<sup>2</sup> using alcohol soluble phosphine oxide based material in the second emissive layer (Yook, Jang, et al., 2010). By blending 4,7-diphenyl-1,10-phenanthroline (BPhen ) with Cs<sub>2</sub>CO<sub>3</sub> in the mixture of formic acid and water as ETL, Jenekhe's group has reported blue device with efficiency up to 14.5 lm/W at 1000 cd/m<sup>2</sup> (Earmme & Jenekhe, 2012b). Figure 7.1 shows the recent works done by other research groups compared to our work on fully solution processed multi layer blue PHOLED.



1. Angewandte Chemie International Edition, 46 (2007) 4388
2. Advance Materials, 22 (2010) 4479
3. Advance Materials, 22 (2010) 4744
4. Electrochemical and Solid-State Letters, 136 (2011) J71
5. Advance Functional Materials, 21 (2011) 3889
6. Advance Functional Material, 22 (2012) 5126
7. Applied Physics Letters, 102 (2013) 233305
8. Advanced Functional Materials, 23 (2013) 359
9. Phys. Status Solidi RRL, 7 (2013) 421

**Figure 7.1:** Efficiencies of fully solution processed multi layer blue PHOLED reported to date. The efficiencies are benchmarked at 1000 cd/m<sup>2</sup>.

In this chapter, we demonstrate an effective method in enhancing the power efficiency of a double emissive solution processed blue PHOLED. The first emissive layer consists of PVK and FIrpic mixed with either TCTA or OXD-7. The second layer consists of alcohol soluble 2,7-bis(diphenylphosphoryl)-9,9'-spirobi(fluorine) (SPPO13) and FIrpic blend. The efficiency improvement for OXD-7 based device is attributed to the reduction of carrier accumulation at the hetero-junction thus widening the

recombination zone. For TCTA based device, the efficiency improvement was due to the reduction of barrier height for hole injection. The device with 40 wt% TCTA showed power efficiency of 11 lm/W, which correspond to 37.5% increment compared to the control device at brightness of 1000 cd/m<sup>2</sup>, comparable to the best solution processed blue PHOLED reported to date at the same brightness (Earmme & Jenekhe, 2012b; Yook, Jang, et al., 2010). These results could pave way for the realization of large panel OLED lighting since lighting sources are typically benchmark by their power efficiency (B. H. Zhang et al., 2012).

## 7.2 Experimental

All materials were purchased and used as received without further purification. PVK (average Mw = 1 100 000) were purchased from Sigma-Aldrich. OXD-7, TCTA, SPPO13 and FIrpic were purchased from Luminescence Technology Corp. Figure 7.2 shows the device structure, energy level diagram of the devices and the chemical structures of the materials used in this work. Pre-patterned ITOs were cleaned sequentially using deionized water, acetone, isopropyl alcohol and deionized water again followed by oxygen plasma treatment for 5 minutes. To fabricate OLED, 40 nm of PEDOT:PSS (AI4083) was spin coated on to the ITO and immediately baked at 150 °C for 10 minutes in N<sub>2</sub> environment. Then chlorobenzene diluted PVK:M (100:20 or 40 wt/wt):FIrpic 10 wt% (where M is OXD-7 or TCTA) was spin coated on top of the PEDOT:PSS to form 40 nm polymer film. The substrates were baked at 100 °C for 10 minutes. Following that, 50 nm of ETL was obtained by spin-coating SPPO13:FIrpic (100:10 wt/wt) in isopropyl alcohol on to the samples. The samples were annealed and at 100°C for 10 minutes again. Finally LiF (0.8 nm) and Al (100 nm) was vacuum deposited at base pressure of 2.5x10<sup>-6</sup> mbar. All the devices were encapsulated using UV curable epoxy and glass lid. The devices current density (J) – brightness (L) –

voltage (V) characteristics were measured using Konica Minolta chroma-meter CS-200. Films thickness was measured by P-6 profilometer (KLA-Tencor). Photocurrents of PHOLED were measured under illumination of a simulated AM1.5 light source at 100 mW/cm<sup>2</sup> (Newport 67005). The absorption spectra were measured by Perkin Elmer PE750 UV-Vis. PL measurement was carried out using Perkin Elmer LS50B spectrometer.

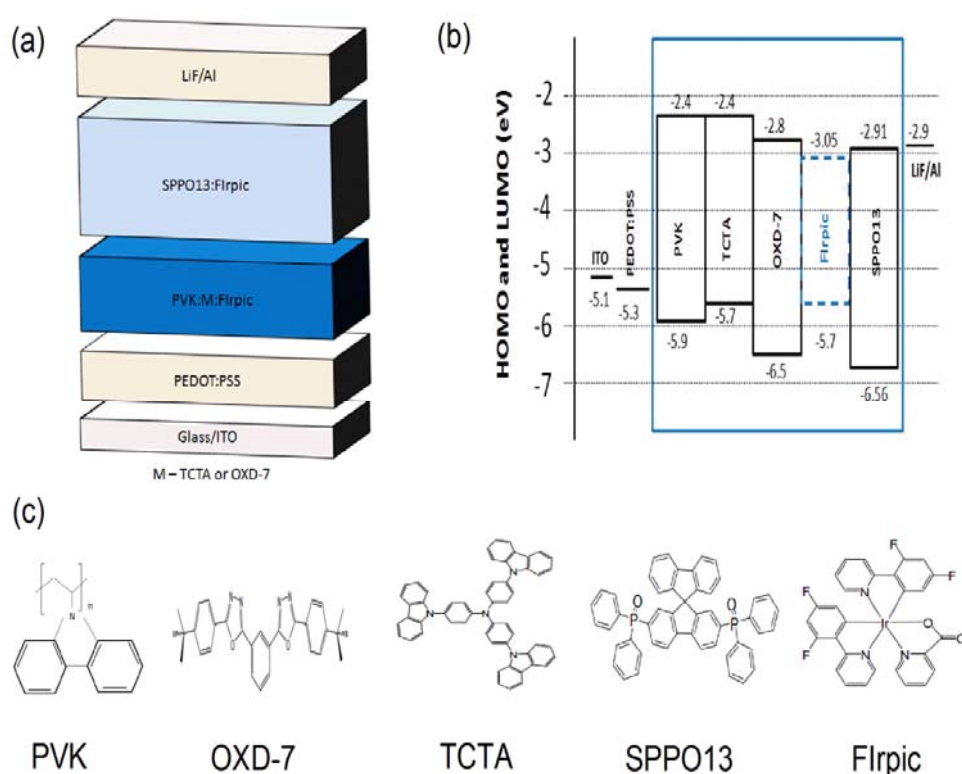


**Figure 7.2:** Schematic diagram of (a) device architecture (b) energy level diagram and (c) molecular structure of the materials used.

### 7.3 J-V-L characteristics and efficiencies of the TCTA doped devices

The first emissive layer is PVK:Flrpic blended with either TCTA or OXD-7 of different concentrations. Specifically, we choose TCTA and OXD-7 in our study. Each of these materials has different carrier transport behaviour: TCTA is a hole transport compound and OXD-7 is an electron transport compound. Common to these



materials are all of them have sufficiently high triplet energy to prevent back energy transfer from high triplet FIrpic. The triplet energies of the materials used in this study are 2.7 eV for OXD-7 and TCTA (J. Lee et al., 2008; J. J. Park et al., 2009).

Figure 7.3 shows the J-L-V characteristics of the blue devices doped with different concentrations of TCTA. The current densities increase substantially when the TCTA concentration increased to 40 wt%. It is interesting to note that the turn on voltage (defined at 1 cd/m<sup>2</sup>) reduces as the concentration of TCTA increased to 40 wt%. Therefore it is reasonable to suggest that the barrier for hole injection has reduced upon the addition of TCTA into the first emissive layer.

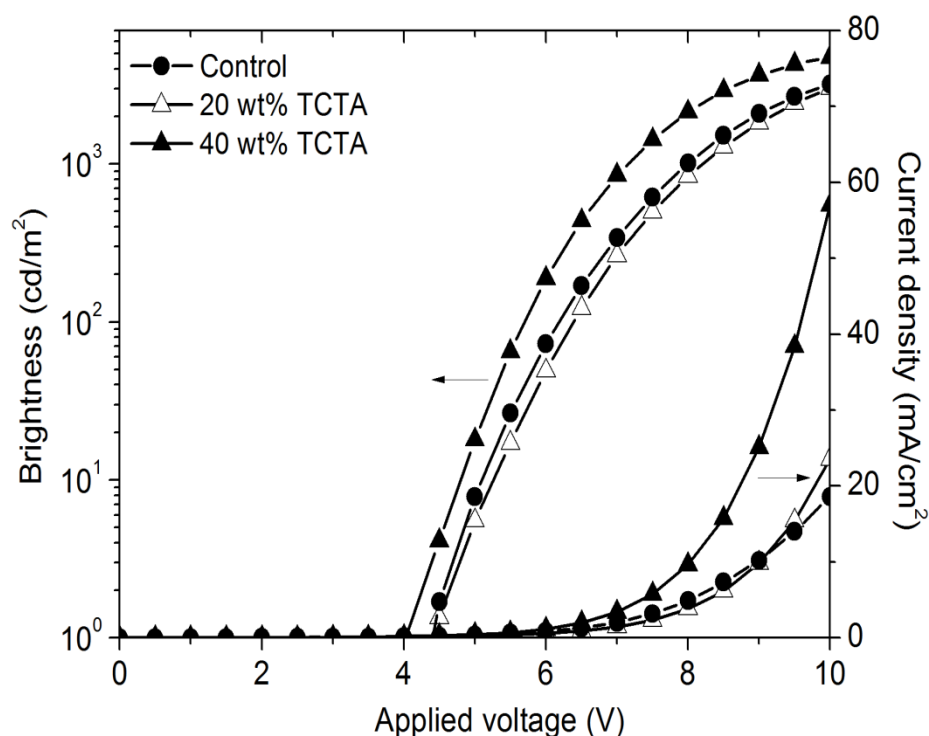


**Figure 7.3:** J-L-V characteristics of the blue devices doped with different concentrations of TCTA.

The reduction of barrier height is beneficial to the device efficiency as shown in Figure 7.4. The control device without any TCTA in the first emissive layer shows 8 lm/W power efficiency and 20.6 cd/A current efficiency at 1000 cd/m<sup>2</sup>. These efficiencies are increased to 11 lm/W and 25 cd/A at the same brightness when 40 wt% TCTA is

added into the first emissive layer. The device performance enhancement can be explained by the favourable energy level alignment of TCTA with respect to PEDOT:PSS and PVK. The HOMO level of TCTA lies between PEDOT:PSS and PVK HOMO level. This effectively reduces the barrier height for hole injection. The blue OLED device performance is summarized in Table 7.1.

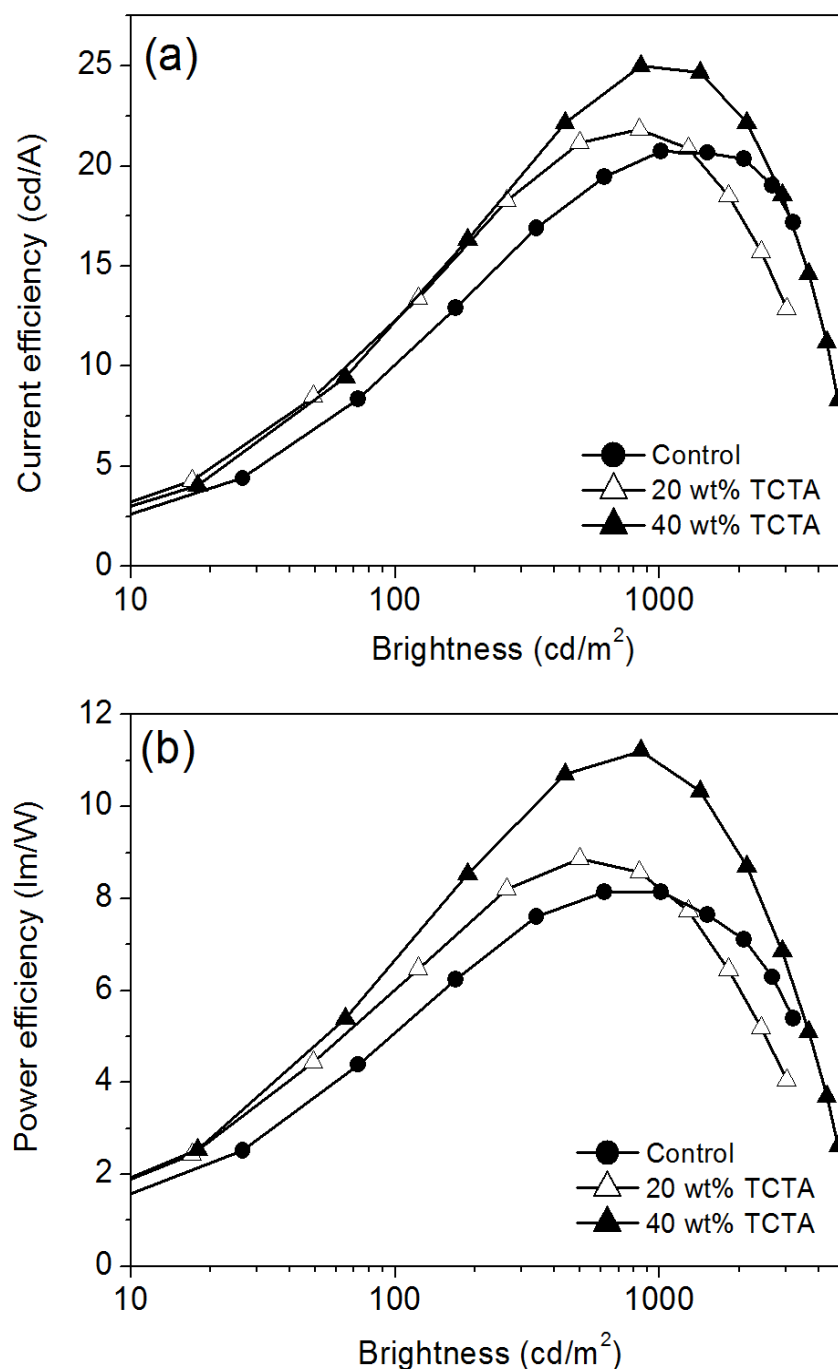


**Figure 7.4:** (a) Power efficiency and (b) current efficiency vs brightness of blue PHOLED with different concentrations of TCTA.

**Table 7.1:** Blue PHOLEDs performances with different concentrations of TCTA.

TCTA concentration (wt%)	$V_{ON}$ (1cd/m <sup>2</sup> )	<sup>1</sup> $V_{ON}$	<sup>1</sup> PE (lm/W)	<sup>1</sup> CE (cd/A)	<sup>2</sup> $V_{ON}$	<sup>2</sup> PE (lm/W)	<sup>2</sup> CE (cd/A)
0	4.4	6.2	5.1	10.2	8.0	8.0	20.6
20	4.4	6.4	6.1	12.3	8.2	8.0	21.5
40	4.0	5.7	6.6	12.3	7.1	11.0	25.0

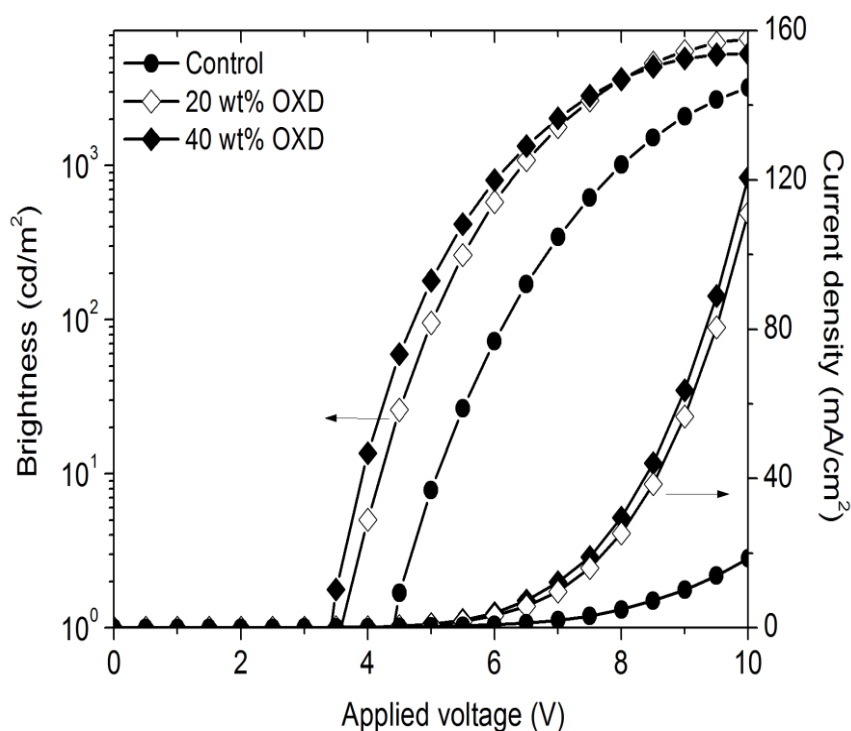
<sup>1</sup>At brightness of 100 cd/m<sup>2</sup>

<sup>2</sup>At brightness of 1000 cd/m<sup>2</sup>

It is worth mentioning that in contrast to 40 wt% TCTA, the 20 wt% TCTA device show an interesting trend where the turn-on voltage (at 1 cd/m<sup>2</sup>) does not show any changes compared to control device. In fact, the  $V_{ON}$  for efficiency at 100 cd/m<sup>2</sup> and 1000 cd/m<sup>2</sup> increases compared to the control device. As of now it is not clear why the 20 wt% TCTA device shows a different trend. Our initial explanations are as follows: TCTA acts as trap due to its HOMO level is 0.2 eV lower compared to PVK. At 20 wt% TCTA doping, injected holes are trapped in the TCTA, therefore causing the  $V_{ON}$  higher or same as the control device. Increasing the TCTA to 40 wt% causes the spatial separation of the TCTA induced trap states become closer, thus easing the hole hopping in TCTA.

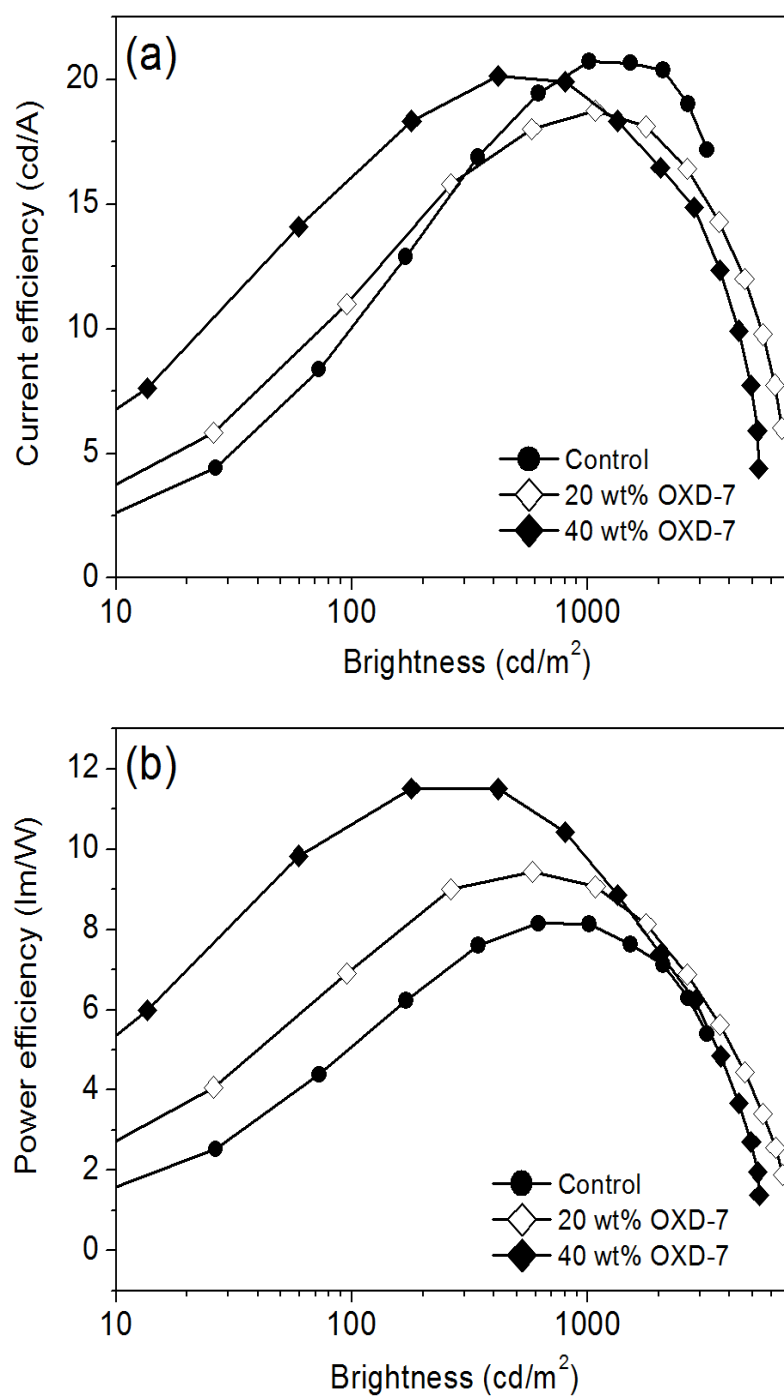
#### 7.4 J-V -L characteristics and efficiencies of the OXD-7 doped devices.

Figure 7.5 shows the J-V-L characteristics of the multilayer blue devices with OXD-7 varied from 0 wt% to 40 wt%. The J-V results indicate that the current injection is enhanced with the addition to OXD-7. Following the same trend as the TCTA devices, the turn on voltage (defined at 1 cd/m<sup>2</sup>) of the devices reduces from 4.4 V to 3.4 V when the OXD-7 concentration reaches 40 wt%.



**Figure 7.5:** J-L-V characteristics of the blue devices doped with different concentrations of OXD-7.

The efficiency of the blue devices with different concentrations of OXD-7 is presented in Figure 7.6. It is apparent that the addition of OXD-7 into the first emissive layer helps to improve the power efficiency. For example, the power efficiency of the devices are increased from 5.1 lm/W and 8 lm/W to 10.7 lm/W and 10 lm/W at 100 cd/m<sup>2</sup> and 1000 cd/m<sup>2</sup> respectively with the addition of 40 wt% OXD-7. The power efficiency improvement is attributed to the blurring effects which will be discussed in the following section. The blue PHOLEDs performance are summarized in Table 7.2



**Figure 7.6:** (a) Power efficiency and (b) current efficiency vs brightness of blue PHOLED with different concentrations of OXD-7.

**Table 7.2:** Blue PHOLEDs performances with different concentrations of OXD-7.

OXD-7 concentration (wt%)	$V_{ON}$ (1cd/m <sup>2</sup> )	$^1V_{ON}$	$^1PE$ (lm/W)	$^1CE$ (cd/A)	$^2V_{ON}$	$^2PE$ (lm/W)	$^2CE$ (cd/A)
0	4.4	6.2	5.1	10.2	8.0	8.0	20.6
20	3.6	5.0	7.0	11.3	6.4	9.1	18.6
40	3.4	4.7	10.7	16.0	6.2	10	19.3

<sup>1</sup>At brightness of 100 cd/m<sup>2</sup><sup>2</sup>At brightness of 1000 cd/m<sup>2</sup>

### 7.5 Blurring effects and reduction of hole injection barrier

The HOMO level alignment of TCTA with respect to PEDOT:PSS and PVK clearly favors hole injection as shown in Figure 7.7b. The TCTA HOMO level is between the PEDOT:PSS work function and the HOMO level of PVK, thus providing a lower energetic path for hole injection. On the other hand, the addition of OXD-7 reduces electron accumulation in heterojunction formed by the first and second emissive layer. Considering the LUMO level of OXD-7 and SPPO13 are very close to each other, the inclusion of OXD-7 provides additional path for the electron to leak from the SPPO13 to the first emissive layer as shown in Figure 7.7c. With this electron leakage path, less electron will be accumulated at the device heterojunction. This effect is known as blurring effect which was pointed out by (C. H. Hsiao, Tseng, & Lee, 2006; J. H. Lee, Wu, Liu, Huang, & Chang, 2005). In this case, the addition of OXD-7 into PVK blurs the interface between the two emissive layers and widens the recombination zone. This effect improves the efficiency of the OXD-7 device. Therefore the driving voltage was reduced. This effect can be directly observed from the J-V-L plot in Figure 7.5.

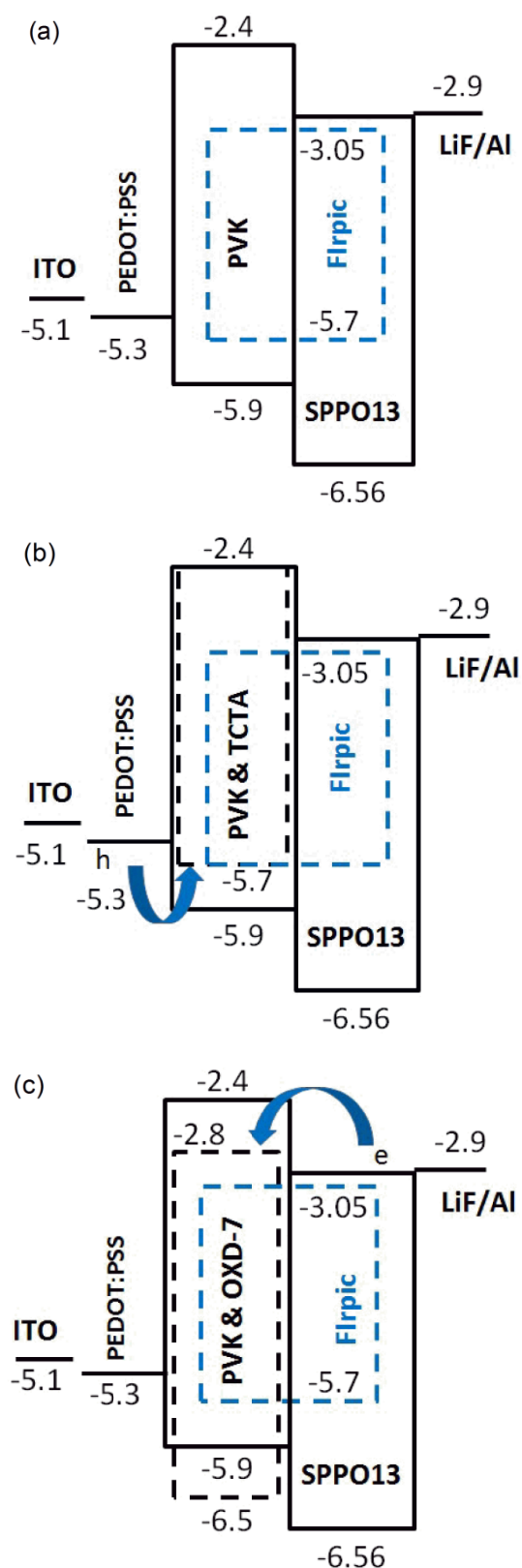


**Figure 7.7:** Energy level diagram (a) of the control devices, (b) device with 40 wt% TCTA doped into the first emissive layer. The effective hole barrier height is reduced due to the favourable HOMO level alignment. (c) The addition of 40 wt% of OXD-7 provides an additional path for electron to hop into the first emissive layer. Black dotted line in (b) and (c) indicate HOMO/LUMO level of TCTA and OXD-7 respectively. The HOMO/LUMO of Flrpic is denoted by blue dotted line.

From Figure 7.6a, it can be seen that the current efficiency of the OXD-7 doped devices starts to drop below the control device at brightness beyond  $300 \text{ cd/m}^2$  -  $700 \text{ cd/m}^2$ . The blurring effect at the heterojunction could provide an explanation on this observation. Although blurring effect can improve the device efficiency by widening the recombination zone, it also enhances the electron current leakage through the anode as the applied bias increases. Consequently, the efficiency of the device drops. On the other hand, at low applied bias the efficiency of OXD-7 devices are relatively good. It is because the leakage of electron current is less severe and a better charge balance between electron and hole can be achieved. This is confirmed by single carrier device as illustrated in Figure 7.9.

## 7.6 Photovoltaic measurement and single carrier devices

Photovoltaic measurement of the devices was measured to determine the  $V_{OC}$  by illuminating the devices with simulated AM1.5 light source at  $100 \text{ mW/cm}^2$  (Guo et al., 2006; Zhao et al., 2012). The photovoltaic characteristics are shown in Figure 7.8. The  $V_{OC}$  for control device is 0.25 V whereas with 40 wt% doping of TCTA into the first emissive layer, the  $V_{OC}$  increased to 0.47 V. The increment of  $V_{OC}$  indicates that the hole injection barrier has decreased (Choulis et al., 2006; Fu et al., 2012) since the TCTA HOMO level is in between PEDOT:PSS than PVK HOMO level. This suggest that the addition of TCTA assists hole injection from the PEDOT:PSS into the first emissive layer. Following the same trend, the  $V_{OC}$  for device with 40 wt% of OXD-7 increased to 0.8 V when TCTA was replaced by OXD-7. It is unlikely that OXD-7 helps hole injection since its HOMO level (-6.5 eV) is much deeper than PVK (-5.9 eV). The high  $V_{OC}$  of the OXD-7 device could be to the role of OXD-7 in blurring the heterojunction. This blurring effects decrease the barrier for electron injection into the first emissive layer.



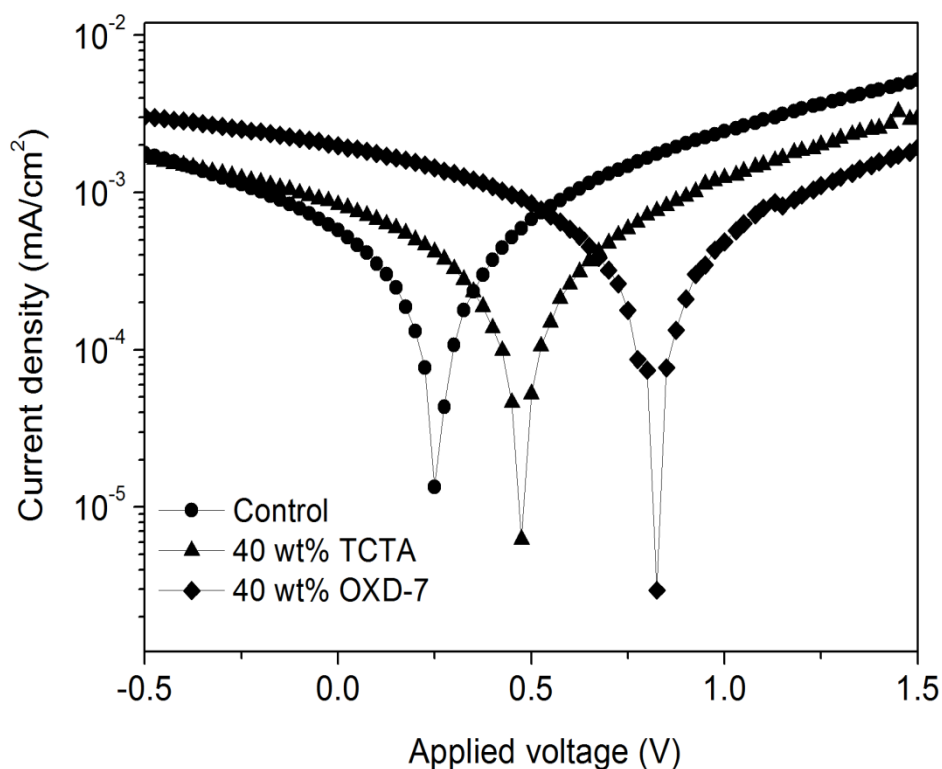


**Figure 7.8:** Photovoltaic response of the blue devices.

To gain insight to the charge balance of the devices, hole-dominated and electron-dominated devices were fabricated. The hole-dominated device consists of ITO/PEDOT:PSS/first EML/second EML/Au. Au has large function and it is expected it will block the electron injection. For electron-dominated device, following device structure was fabricated: ITO/LiF/first EML/second EML/LiF/Al. Similarly ITO/LiF has relatively small work function compared to the HOMO level of the first EML. This can shield off hole injection. The hole and electron-dominated current densities characteristics are shown in Figure 7.9.

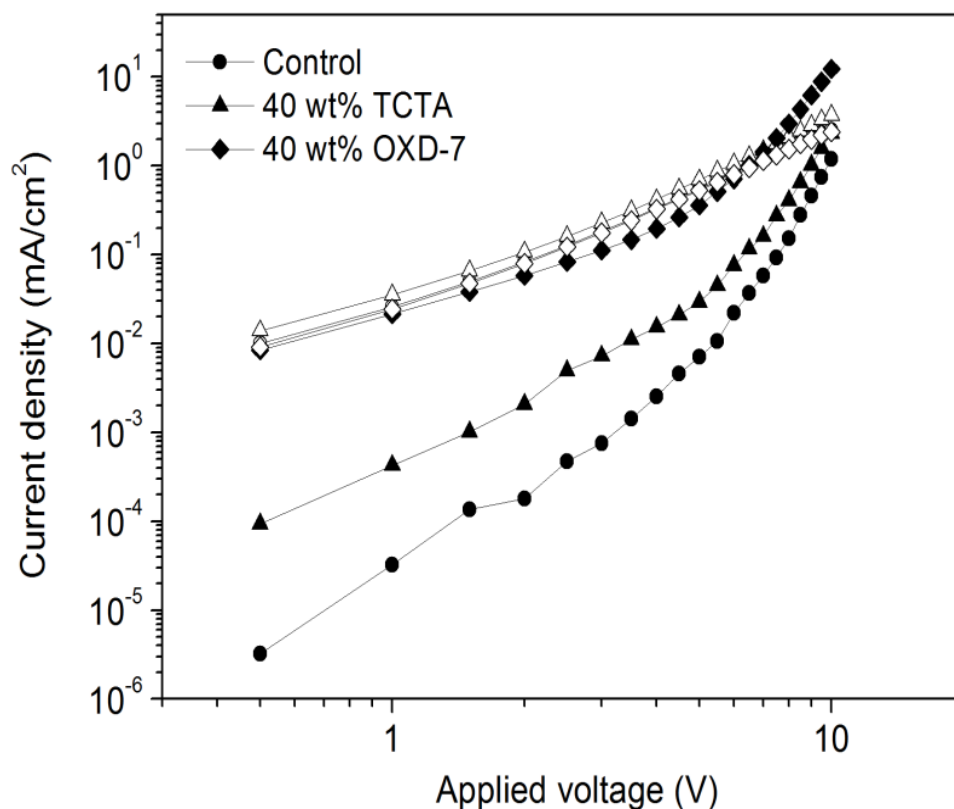


**Figure 7.9:** Current density characteristics of the hole-dominated (empty symbols) ITO/PEDOT:PSS/first EML/second EML/Au and electron-dominated ITO/LiF/first EML/second EML/LiF/Al (filled symbols) devices.

In the control device there is a significant imbalance in the charge transport. The hole current density is 1 to 2 order higher than the electron current over a wide range of voltage. The charge balance further improved when TCTA or OXD-7 was added to form trinary blend in the first emissive layer. The charge balance improvement could explain the improvement of TCTA and OXD-7 device performance compared to the control device. The electron-dominated current density is the highest in OXD-7 device due to the incorporation of OXD-7 into the PVK:Flrpic layer which assists electron current flow from SPP013:Flrpic into the first emissive layer, consistent with the J-V characteristics in Figure 7.5.

## 7.7 Validation of orthogonal film formation

As discussed in section 7.1, the blue devices presented in this chapter consists of two layers. The first layer consists of either PVK:FIrpic, PVK:TCTA:FIrpic or PVK:OXD-7:FIrpic whereas SPPO13:FIrpic was used as the second layer. In order to form a double layer structure, the solvent that is used to dissolve the second layer should not dissolve the first layer. In our case, PVK, OXD-7, TCTA and FIrpic are soluble in aromatic solvent such as chlorobenzene or chloroform. On the other hand, SPPO13 can be easily dissolved in alcohol e.g. IPA thanks to the high polar nature of phosphine oxide group in SPPO13. The FIrpic dopant also can be dissolved using IPA due to the high electronegativity of F in the ligand structure. It is expected that IPA will not washed off the first layer of our devices. In order to validate this, we spin coated the first layer on the quartz substrates and baked the samples at 100°C for 10 minutes. The films thickness and absorbance were measured. Next the samples were washed with IPA and dried at 100°C for 10 minutes. The film thickness and absorbance were measured again. We did not observed any significant changes in the films thickness after we washed them using IPA (see Table 7.3 and Figure 7.10).

**Table 7.3:** Comparison of the first layer film thickness after being washed by IPA

First layer	Before wash	After wash
	Thickness (nm)	
PVK:FIrpic (100:10 wt/wt)	30.4	28.98
PVK: TCTA: FIrpic (100:40:10 wt/wt/wt)	30.95	30.58
PVK: OXD-7: FIrpic (100:40:10 wt/wt/wt)	30.32	29.24

Similarly no significant changes were observed on the thin films absorbance spectra after we washed the films with IPA as evident from Figure 7.10. Therefore, we expect that the combination of SPPO13:FIrpic (100:10 wt/wt) can form a orthogonal layer with the first layer which consists of either PVK:FIrpic (100:10 wt/wt),

PVK:TCTA:FIrpic (100:40:10 wt/wt/wt) or PVK:OXD-7:FIrpic (100:40:10 wt/wt/wt)

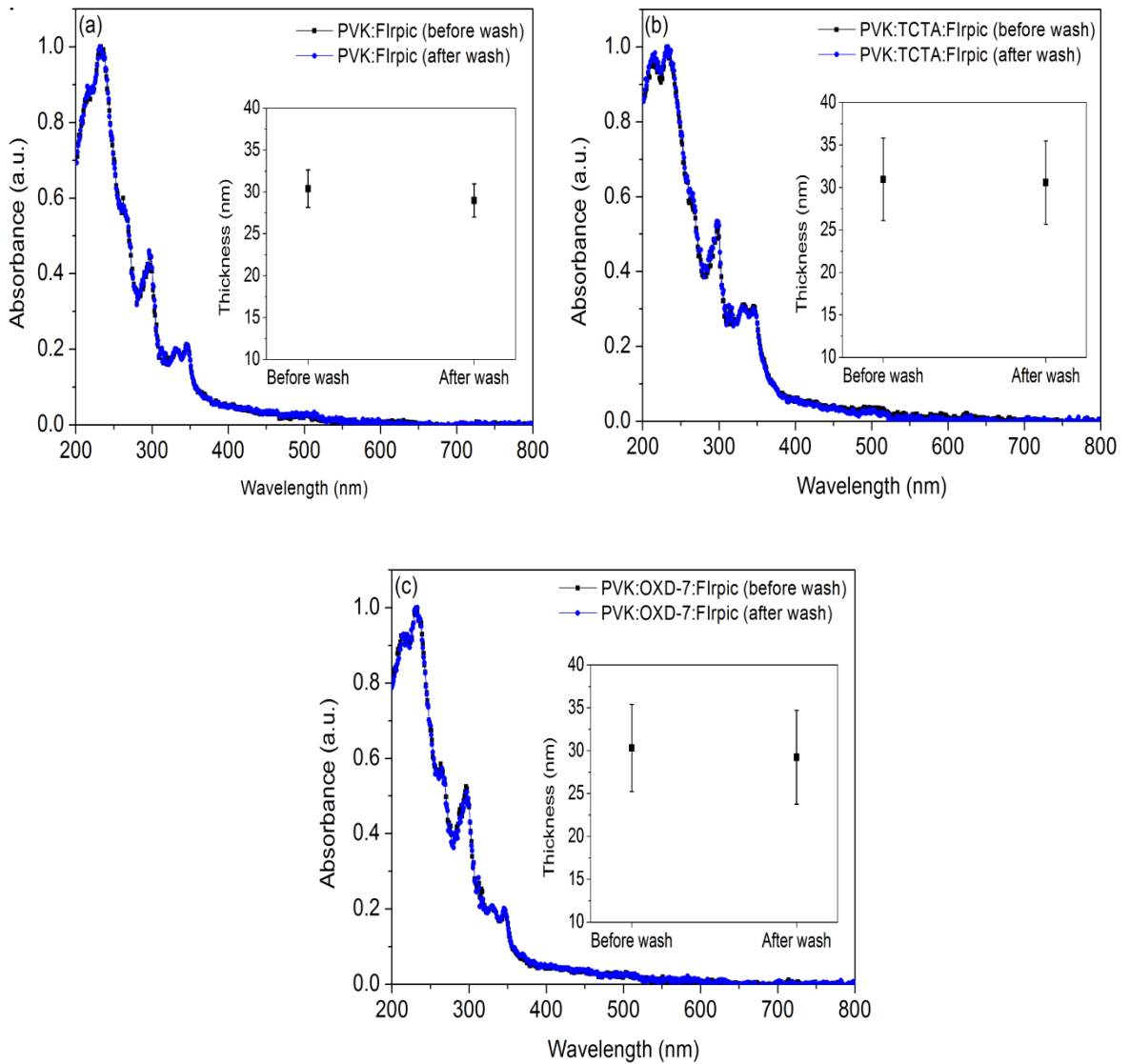


**Figure 7.10:** Comparison of the thin films absorbance and thickness after being washed with IPA. The film consists of (a) PVK:FIrpic (100:10 wt/wt) (b) PVK:TCTA:FIrpic (100:40:10 wt/wt/wt) and (c) PVK:OXD-7:FIrpic (100:40:10 wt/wt/wt).

## 7.8 Optical characterizations

The absorption and PL spectra of control device, OXD-7 and TCTA blue PHOLEDs are shown in Figure 7.11. All the absorption peaks are below 350 nm. The emission is centred at 479 nm with vibrational peak at 500 nm which are the typical characteristics of FIrpic emission. Also the addition of 40 wt% OXD-7 or TCTA into the first emissive layer does not change the EML emission spectra.

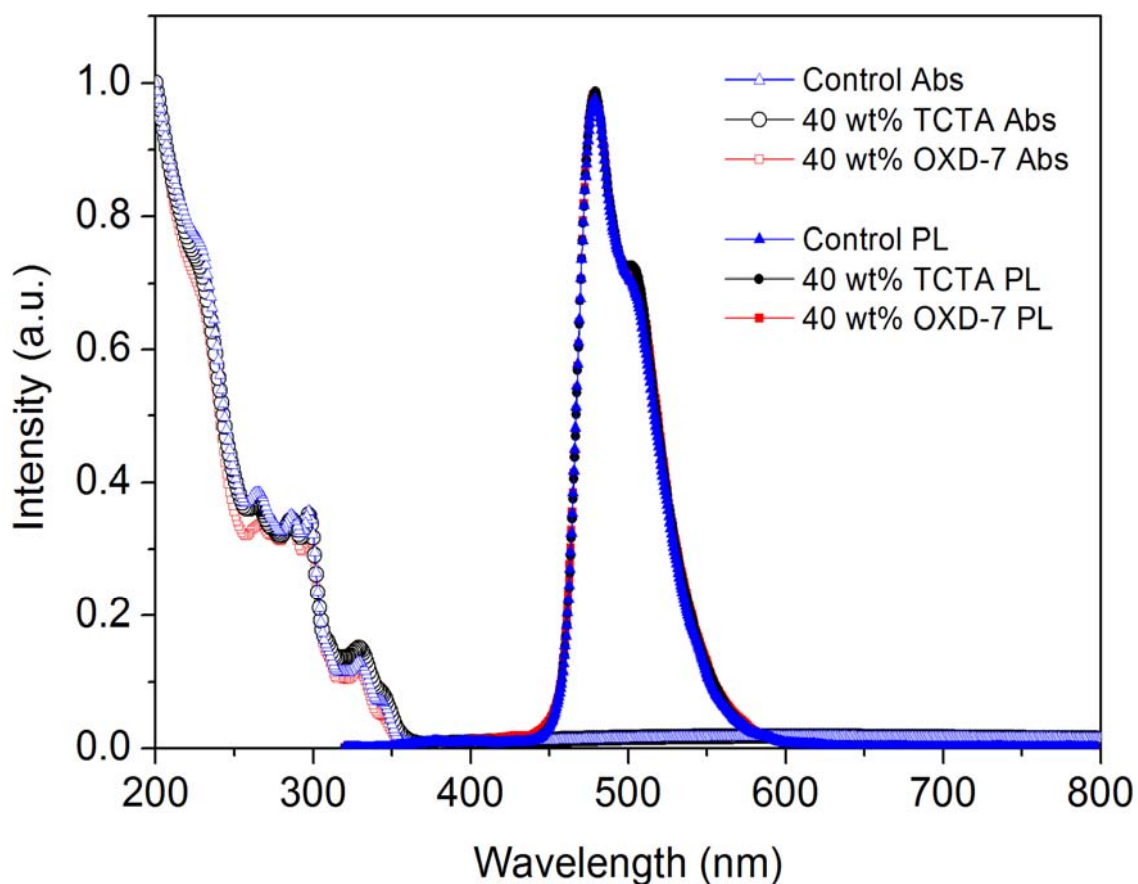


**Figure 7.11:** Absorption (hollow symbols) and PL (filled symbols) spectra of control, 40 wt% TCTA and 40 wt% blue PHOLEDs.

## 7.9 Summary

In summary, high efficiency Irpic based double emissive solution processed blue PHOLED were fabricated by controlling the charge transport in the emissive layer and heterojunction. By introducing OXD-7 into the first emissive layer, power efficiency of 10 lm/W at 1000 cd/m<sup>2</sup> has been achieved. This is due to the widening of recombination zone induced by blurring effect. On the other hand, the incorporation of TCTA ease hole injection from PEDOT:PSS to the first emissive layer. Using this approach, the efficiency was found to be 11 lm/W at 1000 cd/m<sup>2</sup>. Our results could contribute to the realization and optimization of solution processed high efficiency multilayer blue PHOLED which is highly needed in lighting application.

## CHAPTER 8: Summary and future works

### 8.1 Summary

In this thesis several methods have been investigated and developed in enhancing the efficiency of solution processed OLED. The mechanisms of the device efficiency enhancement were systematically studied and implemented. Our main findings are summarized in the following.

In Chapter 4, it was demonstrated that Triton X-100 can improve the efficiency of a solution processed blue PVK based PHOLED. PVK has been extensively used as host in solution processed PHOLED because it is cheap and can easily form high quality thin film using solution processed method. However when PVK is used as host in blue PHOLED, it quenches the excitons in the blue phosphor guest due to the back energy transfer from the high triplet energy of blue dopant to the lower triplet energy of PVK. Our findings showed that Triton X-100 can provide spatial separation between PVK (host) and the blue dopant FIrpic (guest), thus reducing the excitons quenching brought by the exothermic energy transfer from guest to host. It was further demonstrated that Triton X-100 can increase the roughness of the EML surface. A rough EML surface is beneficial for electron injection at the OLED cathode because it can enhance electric field localization and increase the surface area for electron injection from the cathode. By using this method, blue OLED with efficiency 8.5 lm/W (at 1000 cd/m<sup>2</sup>) was achieved. This efficiency is comparable to the best reported single layer solution process blue PHOLED reported to date at the brightness of 1000 cd/m<sup>2</sup>.

In Chapter 5, the interplay between the PFI doped PEDOT:PSS work function and conductivity in enhancing the efficiency of solution processed blue PHOLED was

systematically studied. It is widely known that the work function of PEDOT:PSS can be enhanced by increasing the amount of PFI in PEDOT:PSS. However the excess of PFI doping can degrade the device power efficiency. This phenomenon was attributed to the high power loss in the device induced by high resistivity of PFI, which in turn reduced the device efficiency. Moreover, PFI can enhance the transmittance of the PEDOT:PSS thin film from 93% to nearly 100%. The high transparency of PFI doped PEDOT:PSS thin film can reduce light loss from the operating device. As a result, the device efficiency can be further improved.

In Chapter 6, solvent treatment between fluorinated alcohol (2,2,3,3,4,4,5,5-octafluoro-1-pentanol) and ethanol in improving the efficiency of a yellow fluorescent SY-PPV OLED was compared. The efficiency improvement is due to the interface dipole formed on the EML/cathode interface which induced by the solvent intrinsic dipole. In this case, fluorinated alcohol with higher dipole moment (2.27D) was shown to be a better solvent in enhancing the device performance compared to ethanol which has a lower dipole moment (1.67D). The presence of the surface dipole at the EML/cathode interface lifts the vacuum level and lowered the cathode barrier for electron injection. It was further demonstrated that solvent with higher dipole moment is better in passivating traps on the EML surface. This could be another reason for the high efficiency yellow OLED achieved using fluorinated alcohol treatment. The solvent treatment by fluorinated alcohol on the SY-PPV based OLED results in efficiency reaching as high as 19.2 lm/W at brightness of 1000 cd/m<sup>2</sup>. To the best our knowledge, this efficiency is one of the best efficiency for fluorescent yellow OLED reported to date.

Finally in Chapter 7, high efficiency fully solution processed double layer blue PHOLEDs were demonstrated. The essence of the proposed design concept was to reduced the barrier height for hole injection at the first emissive layer. This was

achieved by incorporating embedded ladder type energy level concept into the first emissive layer. Another key feature in the device design was blurring the device heterojunction which effectively reduced carrier accumulations thus widening the recombination zone. Our best device yielded efficiency of 11 lm/W (1000 cd/m<sup>2</sup>) which is comparable to the best fully solution processed blue PHOLED reported to date at the same brightness.

The efficiency enhancement methods carried out in this research work are summarized in Table 8.1.

**Table 8.1:** Summary of the OLED devices performance and optimization techniques carried out in this research work. The efficiency are benchmarked at 1000 cd/m<sup>2</sup>.

Device	Initial efficiency (lm/w)	Optimized efficiency (lm/W)	Optimization technique
I	4.9	8.5	Using Triton X-100 to reduce back energy transfer of excitons from guest to host and enhancing the electron injection at the cathode
II	5.9	7.9	Using PFI in reducing the barrier height for hole injection, reducing excitons quenching and improving the transmittance of PEDOT:PSS film
III	11	19.2	Reduction of cathodic barrier height and traps passivation by using fluorinated alcohol
IV	8	10	Blurring the heterojunction by using OXD-7.
V	8	11	Introducing embedded ladder energy level at the first emissive layer by incorporating TCTA.

Device I: ITO/PEDOT:PSS/PVK:OXD-7:FIrpic:Triton X-100/Cs<sub>2</sub>CO<sub>3</sub>/Al

Device II: ITO/PEDOT:PSS:PFI/PVK:OXD-7:FIrpic/CsF/Al

Device III: ITO/PEDOT:PSS/SY-PPV/Fluorinated alcohol/LiF/Al

Device IV: ITO/PEDOT:PSS/PVK:OXD-7:FIrpic/SPPO13:FIrpic/LiF/Al

Device V: ITO/PEDOT:PSS/PVK:TCTA:FIrpic/SPPO13:FIrpic/LiF/Al



## 8.2 Future works

Based on the understanding acquired in these studies, following are worth investigating in the future for OLED development:

1. Fluorinated alcohol treatment reported in this thesis can be extended to blue OLED since OLED lighting applications are currently bottlenecked at blue emission.
2. Our research works showed that the ability of alcohol solvent in passivating surface traps is depending on its intrinsic dipole moment. It is worth investigating the mechanisms and effects of solvent dipole moment in passivating surface traps of organic semiconductor thin film.
3. Throughout our studies, PEDOT:PSS was HIL for all the devices. It is widely known that PEDOT:PSS can reduce the OLED lifetime due to its acidic and hygroscopic nature. Recently TMO has shown to be a better alternative to PEDOT:PSS. However, TMO is usually vacuum deposited. Although there are several research groups that successfully demonstrated solution processed TMO, its coating process usually required high temperature annealing and the applications are limited to photovoltaic applications. Reports on room temperature solution process TMO and its application in OLED are not widely reported. Future works could be done in synthesizing room temperature TMO to replace PEDOT:PSS as HIL in OLED.
4. Most of the reported fully solution processed PHOLED incorporated PVK as host. As discussed in Chapter 4, PVK has low triplet which limit its use in blue PHOLED. Moreover, PVK is polymer, making it difficult to purify compared to small molecule. To date, not many research groups are investigating fully solution processed all small molecule PHOLED.

Further study is needed in the development of fully solution processed all small molecule multi layer PHOLED.

5. Future works could be done on blue devices combining various optimization methods discussed in this work. For example, it is worth investigating the efficiency of the following device stack:  
ITO/PEDOT:PSS:PFI/PVK:TCTA:FIrpic: Triton X-100/SPPO13:FIrpic/  
fluorinated alcohol/LiF/Al.

## REFERENCES

- Adachi, C., Baldo, M. A., Forrest, S. R., Lamansky, S., Thompson, M. E., & Kwong, R. C. (2001). High-efficiency red electrophosphorescence devices. *Applied Physics Letters*, 78(11), 1622-1624. doi: Doi 10.1063/1.1355007
- Adachi, C., Tokito, S., Tsutsui, T., & Saito, S. (1988). Organic Electroluminescent Device with a 3-Layer Structure. *Japanese Journal of Applied Physics Part 2-Letters*, 27(4), L713-L715. doi: Doi 10.1143/Jjap.27.L713
- Ahmed, E., Earmme, T., & Jenekhe, S. A. (2011). New Solution-Processable Electron Transport Materials for Highly Efficient Blue Phosphorescent OLEDs. *Advanced Functional Materials*, 21(20), 3889-3899. doi: DOI 10.1002/adfm.201100848
- Aizawa, N., Pu, Y. J., Sasabe, H., & Kido, J. (2012). Solution-processable carbazole-based host materials for phosphorescent organic light-emitting devices. *Organic Electronics*, 13(11), 2235-2242. doi: DOI 10.1016/j.orgel.2012.06.036
- Aizawa, N., Pu, Y. J., Sasabe, H., & Kido, J. (2013). Thermally cross-linkable host materials for enabling solution-processed multilayer stacks in organic light-emitting devices. *Organic Electronics*, 14(6), 1614-1620. doi: DOI 10.1016/j.orgel.2013.03.028
- Atkins, P. W., & Friedman, R. S. (1997). *Molecular Quantum Mechanics* (3 ed.). Oxford: Oxford University Press.
- Baldo, M., & Segal, M. (2005). *Physics of Organic Semiconductors* (1 ed.). Weinheim: Wiley-VCH.
- Baldo, M. A., Lamansky, S., Burrows, P. E., Thompson, M. E., & Forrest, S. R. (1999). Very high-efficiency green organic light-emitting devices based on electrophosphorescence. *Applied Physics Letters*, 75(1), 4-6. doi: Doi 10.1063/1.124258
- Baldo, M. A., O'Brien, D. F., You, Y., Shoustikov, A., Sibley, S., Thompson, M. E., & Forrest, S. R. (1998). Highly efficient phosphorescent emission from organic electroluminescent devices. *Nature*, 395(6698), 151-154.
- Baldo, M. A., Thompson, M. E., & Forrest, S. R. (1999). Phosphorescent materials for application to organic light emitting devices. *Pure and Applied Chemistry*, 71(11), 2095-2106. doi: DOI 10.1351/pac199971112095
- Benor, A., Takizawa, S. Y., Chen, P., Perez-Bolivar, C., & Anzenbacher, P. (2009). Dramatic efficiency improvement in phosphorescent organic light-emitting diodes with ultraviolet-ozone treated poly(3,4-ethylenedioxythiophene):poly(styrenesulfonate). *Applied Physics Letters*, 94(19). doi: Artn 193301 Doi 10.1063/1.3132059
- Benor, A., Takizawa, S. Y., Perez-Bolivar, C., & Anzenbacher, P. (2010). Efficiency improvement of fluorescent OLEDs by tuning the working function of PEDOT:PSS using UV-ozone exposure. *Organic Electronics*, 11(5), 938-945. doi: DOI 10.1016/j.orgel.2010.02.014
- Bernius, M., Inbasekaran, M., Woo, E., Wu, W. S., & Wujkowski, L. (2000). Fluorene-based polymers-preparation and applications. *Journal of Materials Science-Materials in Electronics*, 11(2), 111-116. doi: Doi 10.1023/A:1008917128880
- Blochwitz, J., Pfeiffer, M., Fritz, T., & Leo, K. (1998). Low voltage organic light emitting diodes featuring doped phthalocyanine as hole transport material. *Applied Physics Letters*, 73(6), 729-731. doi: Doi 10.1063/1.121982
- Braun, D., & Heeger, A. J. (1991). Visible-Light Emission from Semiconducting Polymer Diodes. *Applied Physics Letters*, 58(18), 1982-1984. doi: Doi 10.1063/1.105039

- Brown, T. M., Friend, R. H., Millard, I. S., Lacey, D. J., Butler, T., Burroughes, J. H., & Cacialli, F. (2003). Electronic line-up in light-emitting diodes with alkali-halide/metal cathodes. *Journal of Applied Physics*, 93(10), 6159-6172. doi: Doi 10.1063/1.1562739
- Burkhart, R. D., & Chakraborty, D. K. (1990). Binding-Energies of Triplet Excimers in Poly(N-Vinylcarbazole) Solid Films from Laser-Based Kinetic Spectroscopy between 15-K and 55-K. *Journal of Physical Chemistry*, 94(10), 4143-4147. doi: Doi 10.1021/J100373a049
- Burroughes, J. H., Bradley, D. D. C., Brown, A. R., Marks, R. N., Mackay, K., Friend, R. H., . . . Holmes, A. B. (1990). Light-Emitting-Diodes Based on Conjugated Polymers. *Nature*, 347(6293), 539-541. doi: Doi 10.1038/347539a0
- Cao, X. A., & Zhang, Y. Q. (2012). Performance enhancement of organic light-emitting diodes by chlorine plasma treatment of indium tin oxide. *Applied Physics Letters*, 100(18). doi: Artn 183304 Doi 10.1063/1.4709426
- Chan, I. M., Cheng, W. C., & Hong, F. C. (2002). Enhanced performance of organic light-emitting devices by atmospheric plasma treatment of indium tin oxide surfaces. *Applied Physics Letters*, 80(1), 13-15. doi: Doi 10.1063/1.1428624
- Chan, M. M.-Y., Tao, C.-H., & Yam, V. W.-W. (2010). *WOLEDs and Organic Photovoltaics Recent Advances and Applications* (First ed.). Heidelberg: Springer.
- Chang, Y.-L., & Lu, Z.-H. (2013). White Organic Light-Emitting Diodes for Solid-State Lighting. *JOURNAL OF DISPLAY TECHNOLOGY*, 9(6), 10. doi: 10.1109/JDT.2013.2248698
- Chao, Y. C., Huang, S. Y., Chen, C. Y., Chang, Y. F., Meng, H. F., Yen, F. W., . . . Horng, S. F. (2011). Highly efficient solution-processed red organic light-emitting diodes with long-side-chained triplet emitter. *Synthetic Metals*, 161(1-2), 148-152. doi: DOI 10.1016/j.synthmet.2010.11.013
- Chen, C. Y., Chang, H. W., Chang, Y. F., Chang, B. J., Lin, Y. S., Jian, P. S., . . . Tseng, M. R. (2011). Continuous blade coating for multi-layer large-area organic light-emitting diode and solar cell. *Journal of Applied Physics*, 110(9). doi: Artn 094501 Doi 10.1063/1.3636398
- Chen, F. C., Chang, S. C., He, G. F., Pyo, S., Yang, Y., Kurotaki, M., & Kido, J. (2003). Energy transfer and triplet exciton confinement in polymeric electrophosphorescent devices. *Journal of Polymer Science Part B-Polymer Physics*, 41(21), 2681-2690. doi: Doi 10.1002/Polb.10648
- Chen, F. C., & Chien, S. C. (2009). Nanoscale functional interlayers formed through spontaneous vertical phase separation in polymer photovoltaic devices. *Journal of Materials Chemistry*, 19(37), 6865-6869. doi: Doi 10.1039/B907773a
- Chen, F. C., Chien, S. C., & Lee, S. W. (2008). High-performance single-layer polymer electrophosphorescent devices with polymer oxides. *Electrochemical and Solid State Letters*, 11(6), J50-J53. doi: Doi 10.1149/1.2902166
- Chen, J. S., Shi, C. S., Fu, Q., Zhao, F. C., Hu, Y., Feng, Y. L., & Ma, D. G. (2012). Solution-processable small molecules as efficient universal bipolar host for blue, green and red phosphorescent inverted OLEDs. *Journal of Materials Chemistry*, 22(11), 5164-5170. doi: Doi 10.1039/C2jm16463a
- Chiba, T., Pu, Y. J., Hirasawa, M., Masuhara, A., Sasabe, H., & Kido, J. (2012). Solution-Processed Inorganic-Organic Hybrid Electron Injection Layer for Polymer Light-Emitting Devices. *Acs Applied Materials & Interfaces*, 4(11), 6104-6108. doi: Doi 10.1021/Am301732m
- Chino, M. (2008). World's First OLED Lamp from Ingo Maurer, from <http://inhabitat.com/osram-oled-lamp-ingo-maurer/>

- Chopra, N., Lee, J., Xue, J. G., & So, F. (2010). High-Efficiency Blue Emitting Phosphorescent OLEDs. *Ieee Transactions on Electron Devices*, 57(1), 101-107. doi: Doi 10.1109/Ted.2009.2035028
- Choulis, S. A., Choong, V. E., Patwardhan, A., Mathai, M. K., & So, F. (2006). Interface modification to improve hole-injection properties in organic electronic devices. *Advanced Functional Materials*, 16(8), 1075-1080. doi: DOI 10.1002/adfm.200500443
- de Jong, M. P., van IJzendoorn, L. J., & de Voigt, M. J. A. (2000). Stability of the interface between indium-tin-oxide and poly(3,4-ethylenedioxythiophene)/poly(styrenesulfonate) in polymer light-emitting diodes. *Applied Physics Letters*, 77(14), 2255-2257. doi: Pii [S0003-6951(00)05040-3] Doi 10.1063/1.1315344
- Deng, X. Y., Lau, W. M., Wong, K. Y., Low, K. H., Chow, H. F., & Cao, Y. (2004). High efficiency low operating voltage polymer light-emitting diodes with aluminum cathode. *Applied Physics Letters*, 84(18), 3522-3524. doi: Doi 10.1063/1.1739510
- Dexter, D. L. (1953). A Theory of Sensitized Luminescence in Solids. *Journal of Chemical Physics*, 21. doi: 10.1063/1.1699044
- Ding, X. M., Hung, L. M., Cheng, L. F., Deng, Z. B., Hou, X. Y., Lee, C. S., & Lee, S. T. (2000). Modification of the hole injection barrier in organic light-emitting devices studied by ultraviolet photoelectron spectroscopy. *Applied Physics Letters*, 76(19), 2704-2706. doi: Doi 10.1063/1.126449
- Divayana, Y., Liu, S. W., Kyaw, A. K. K., & Sun, X. W. (2011). Efficient extraction of singlet-triplet excitons for high-efficient white organic light-emitting diode with a multilayer emission region. *Organic Electronics*, 12(1), 1-7. doi: DOI 10.1016/j.orgel.2010.10.005
- Doh, Y. J., Park, J. S., Jeon, W. S., Pode, R., & Kwon, J. H. (2012). Soluble processed low-voltage and high efficiency blue phosphorescent organic light-emitting devices using small molecule host systems. *Organic Electronics*, 13(4), 586-592. doi: DOI 10.1016/j.orgel.2012.01.003
- Duan, L. A., Hou, L. D., Lee, T. W., Qiao, J. A., Zhang, D. Q., Dong, G. F., . . . Qiu, Y. (2010a). Solution processable small molecules for organic light-emitting diodes. *Journal of Materials Chemistry*, 20(31), 6392-6407. doi: Doi 10.1039/B926348a
- Duan, L. A., Hou, L. D., Lee, T. W., Qiao, J. A., Zhang, D. Q., Dong, G. F., . . . Qiu, Y. (2010b). Solution processable small molecules for organic light-emitting diodes (vol 20, pg 6392, 2010). *Journal of Materials Chemistry*, 20(48), 10946-10946.
- Earmme, T., Ahmed, E., & Jenekhe, S. A. (2010). Solution-Processed Highly Efficient Blue Phosphorescent Polymer Light-Emitting Diodes Enabled by a New Electron Transport Material. *Advanced Materials*, 22(42), 4744-+. doi: DOI 10.1002/adma.201001585
- Earmme, T., & Jenekhe, S. A. (2012a). High-performance multilayered phosphorescent OLEDs by solution-processed commercial electron-transport materials. *Journal of Materials Chemistry*, 22(11), 4660-4668. doi: Doi 10.1039/C2jm14347j
- Earmme, T., & Jenekhe, S. A. (2012b). Solution-Processed, Alkali Metal-Salt-Doped, Electron-Transport Layers for High-Performance Phosphorescent Organic Light-Emitting Diodes. *Advanced Functional Materials*, 22(24), 5126-5136. doi: DOI 10.1002/adfm.201201366
- Earmme, T., & Jenekhe, S. A. (2013). Improved electron injection and transport by use of baking soda as a low-cost, air-stable, n-dopant for solution-processed phosphorescent organic light-emitting diodes. *Applied Physics Letters*, 102(23). doi: Atrn 233305 doi: 10.1063/1.4811087

- Ford, T. A., Ohkita, H., Cook, S., Durrant, J. R., & Greenham, N. C. (2008). Direct observation of intersystem crossing in charge-pair states in polyfluorene polymer blends. *Chemical Physics Letters*, 454(4-6), 237-241. doi: DOI 10.1016/j.cplett.2008.02.021
- Förster, T. (1959). Transfer mechanisms of electronic excitation. *Discussions of the Faraday Society*, 27, 7-17. doi: 10.1039/DF9592700007
- Fu, Q., Chen, J., Shi, C., & Ma, D. (2013). Room-Temperature Sol–Gel Derived Molybdenum Oxide Thin Films for Efficient and Stable Solution-Processed Organic Light-Emitting Diodes. *Acs Applied Materials & Interfaces*. doi: doi: dx.doi.org/10.1021/am4007319
- Fu, Q., Chen, J. S., Shi, C. S., & Ma, D. G. (2012). Solution-Processed Small Molecules As Mixed Host for Highly Efficient Blue and White Phosphorescent Organic Light-Emitting Diodes. *Acs Applied Materials & Interfaces*, 4(12), 6579-6586. doi: Doi 10.1021/Am301703a
- Funahashi, M. (2014). [External examiner comment to K.H. Yeoh PhD. thesis].
- Gao, C. H., Cai, S. D., Gu, W., Zhou, D. Y., Wang, Z. K., & Liao, L. S. (2012). Enhanced Hole Injection in Phosphorescent Organic Light-Emitting Diodes by Thermally Evaporating a Thin Indium Trichloride Layer. *Acs Applied Materials & Interfaces*, 4(10), 5211-5216. doi: Doi 10.1021/Am3011324
- Gavrila, R., Dinescu, A., & Mardare, D. (2007). A power spectral density study of thin films morphology based on AFM profiling. *Romanian Journal of Information Science and Technology*, 10(3), 291-300.
- Gesquiere, A. J., Park, S. J., & Barbara, P. F. (2005). Hole-induced quenching of triplet and singlet excitons in conjugated polymers. *Journal of the American Chemical Society*, 127(26), 9556-9560. doi: Doi 10.1021/Ja051271i
- Goushi, K., Yoshida, K., Sato, K., & Adachi, C. (2012). Organic light-emitting diodes employing efficient reverse intersystem crossing for triplet-to-singlet state conversion. *Nature Photonics*, 6(4), 253-258. doi: DOI 10.1038/nphoton.2012.31
- Gray, G. P. (2010). *Phosphorescent Organic Light Emitting Devices*. Master of Science, University of California Santa Cruz, USA.
- Greczynski, G., Fahlman, M., & Salaneck, W. R. (2000). An experimental study of poly(9,9-dioctyl-fluorene) and its interfaces with Li, Al, and LiF. *Journal of Chemical Physics*, 113(6), 2407-2412. doi: Pii [S0021-9606(00)70230-3] Doi 10.1063/1.482056
- Guilbault, G. G. (1973). *Practical Fluorescence Theory, Methods, and Techniques* (First ed.). New York: Marcel Dekker.
- Guo, T. F., Yang, F. S., Tsai, Z. J., Wen, T. C., Wu, C. I., & Chung, C. T. (2006). Organic oxide/Al composite cathode in small molecular organic light-emitting diodes. *Applied Physics Letters*, 89(5). doi: Artn 053507 Doi 10.1063/1.2266571
- Han, E. M., Do, L. M., Yamamoto, N., & Fujihira, M. (1996). Crystallization of organic thin films for electroluminescent devices. *Thin Solid Films*, 273(1-2), 202-208. doi: Doi 10.1016/0040-6090(95)06782-5
- Han, T. H., Choi, M. R., Woo, S. H., Min, S. Y., Lee, C. L., & Lee, T. W. (2012). Molecularly Controlled Interfacial Layer Strategy Toward Highly Efficient Simple-Structured Organic Light-Emitting Diodes. *Advanced Materials*, 24(11), 1487-1493. doi: DOI 10.1002/adma.201104316
- Han, T. H., Lee, Y., Choi, M. R., Woo, S. H., Bae, S. H., Hong, B. H., . . . Lee, T. W. (2012). Extremely efficient flexible organic light-emitting diodes with modified graphene anode. *Nature Photonics*, 6(2), 105-110. doi: Doi 10.1038/Nphoton.2011.318

- Han, Y. K., Chang, M. Y., Huang, W. Y., Pan, H. Y., Ho, K. S., Hsieh, T. H., & Pan, S. Y. (2011). Improved Performance of Polymer Solar Cells Featuring One-Dimensional PEDOT Nanorods in a Modified Buffer Layer. *Journal of the Electrochemical Society*, 158(3), K88-K93. doi: Doi 10.1149/1.3534201
- Hatwar, T. K., & Spindler, J. (2008). *Luminescent Materials and Applications* (1 ed.). Singapore: John Wiley & Sons.
- Heil, H., Steiger, J., Karg, S., Gastel, M., Ortner, H., von Seggern, H., & Stossel, M. (2001). Mechanisms of injection enhancement in organic light-emitting diodes through an Al/LiF electrode. *Journal of Applied Physics*, 89(1), 420-424. doi: Doi 10.1063/1.1331651
- Helander, M. G., Wang, Z. B., Greiner, M. T., Liu, Z. W., Lian, K., & Lu, Z. H. (2009). The effect of UV ozone treatment on poly(3,4-ethylenedioxythiophene):poly(styrenesulfonate). *Applied Physics Letters*, 95(17). doi: Artn 173302 Doi 10.1063/1.3257382
- Helander, M. G., Wang, Z. B., Qiu, J., Greiner, M. T., Puzzo, D. P., Liu, Z. W., & Lu, Z. H. (2011). Chlorinated Indium Tin Oxide Electrodes with High Work Function for Organic Device Compatibility. *Science*, 332(6032), 944-947. doi: DOI 10.1126/science.1202992
- Helfrich, W., & Schneider, W. G. (1964). Recombination Radiation in Anthracene Crystals. *Physical Review Letters*, 14(7), 4.
- Hofle, S., Do, H., Mankel, E., Pfaff, M., Zhang, Z. H., Bahro, D., . . . Colmann, A. (2013). Molybdenum oxide anode buffer layers for solution processed, blue phosphorescent small molecule organic light emitting diodes. *Organic Electronics*, 14(7), 1820-1824. doi: DOI 10.1016/j.orgel.2013.04.017
- Hong, Y. J. (2007). *Luminescent Materials for Organic Light-Emitting Diodes (OLEDs) and Bioimaging*. Doctor of Science, National University of Singapore, Singapore.
- Hsiao, C. H., Tseng, C. A., & Lee, J. H. (2006). Aging-induced recombination zone shift in mixed-host organic light-emitting devices - art. no. 63331A. *Organic Light Emitting Materials and Devices X*, 6333, A3331-A3331. doi: Artn 63331a Doi 10.1117/12.678317
- Hsiao, Y. S., Whang, W. T., Chen, C. P., & Chen, Y. C. (2008). High-conductivity poly(3,4-ethylenedioxythiophene):poly(styrene sulfonate) film for use in ITO-free polymer solar cells. *Journal of Materials Chemistry*, 18(48), 5948-5955. doi: Doi 10.1039/B813079e
- Huang, J. S., Hou, W. J., Li, J. H., Li, G., & Yang, Y. (2006). Improving the power efficiency of white light-emitting diode by doping electron transport material. *Applied Physics Letters*, 89(13). doi: Artn 133509 Doi 10.1063/1.2357938
- Huang, J. S., Xu, Z., & Yang, Y. (2007). Low-work-function surface formed by solution-processed and thermally deposited nanoscale layers of cesium carbonate. *Advanced Functional Materials*, 17(12), 1966-1973. doi: DOI 10.1002/adfm.200700051
- Huang, S. P., Jen, T. H., Chen, Y. C., Hsiao, A. E., Yin, S. H., Chen, H. Y., & Chen, S. A. (2008). Effective shielding of triplet energy transfer to conjugated polymer by its dense side chains from phosphor dopant for highly efficient electrophosphorescence. *Journal of the American Chemical Society*, 130(14), 4699-4707. doi: Doi 10.1021/Ja076413i
- Huang, Y. K., Jen, T. H., Chang, Y. T., Yang, N. J., Lu, H. H., & Chen, S. A. (2010). Enhancing Shielding of Triplet Energy Transfer to Poly(p-phenylene)s from Phosphor Dopant by Addition of Branched Alcohol for Highly Efficient Electrophosphorescence. *Acs Applied Materials & Interfaces*, 2(4), 1094-1099. doi: Doi 10.1021/Am900878f

- Hung, L. S., Tang, C. W., & Mason, M. G. (1997). Enhanced electron injection in organic electroluminescence devices using an Al/LiF electrode. *Applied Physics Letters*, 70(2), 152-154. doi: Doi 10.1063/1.118344
- Hung, L. S., Tang, C. W., Mason, M. G., Raychaudhuri, P., & Madathil, J. (2001). Application of an ultrathin LiF/Al bilayer in organic surface-emitting diodes. *Applied Physics Letters*, 78(4), 544-546. doi: Doi 10.1063/1.1327273
- Hussain, A. M., Neppolian, B., Kim, S. H., Kim, J. Y., Choi, H. C., Lee, K., . . . Heeger, A. J. (2009). Improved performance of polymer light-emitting diodes with nanocomposites. *Applied Physics Letters*, 94(7). doi: Artn 073306 Doi 10.1063/1.3086275
- Irfan, I., Graber, S., So, F., & Gao, Y. L. (2012). Interplay of cleaning and de-doping in oxygen plasma treated high work function indium tin oxide (ITO). *Organic Electronics*, 13(10), 2028-2034. doi: DOI 10.1016/j.orgel.2012.05.036
- Jabbour, G. E., Kippelen, B., Armstrong, N. R., & Peyghambarian, N. (1998). Aluminum based cathode structure for enhanced electron injection in electroluminescent organic devices. *Applied Physics Letters*, 73(9), 1185-1187. doi: Doi 10.1063/1.122367
- Jain, S. C., Willander, M., & Kumar, V. (2007). *Conducting Organic Materials and Devices* (1 ed.). USA: Elsevier.
- Jang, S., Chae, H. Y., Jung, D. G., Kim, H. G., & Kim, C. K. (2007). Simultaneous oxygen plasma and thermal treatments of an ITO surface to improve the electrical characteristics of organic light-emitting diodes. *Journal of the Korean Physical Society*, 51(3), 956-962.
- Jang, S. E., Joo, C. W., & Lee, J. Y. (2010). High quantum efficiency in simple blue phosphorescent organic light-emitting diodes without any electron injection layer. *Thin Solid Films*, 519(2), 906-910. doi: DOI 10.1016/j.tsf.2010.08.143
- Jang, S. E., Yook, K. S., & Lee, J. Y. (2010). High power efficiency in simplified two layer blue phosphorescent organic light-emitting diodes. *Organic Electronics*, 11(6), 1154-1157. doi: DOI 10.1016/j.orgel.2010.04.004
- Jankus, V., & Monkman, A. P. (2011). Is Poly(vinylcarbazole) a Good Host for Blue Phosphorescent Dopants in PLEDs? Dimer Formation and Their Effects on the Triplet Energy Level of Poly(N-vinylcarbazole) and Poly(N-Ethyl-2-Vinylcarbazole). *Advanced Functional Materials*, 21(17), 3350-3356. doi: DOI 10.1002/adfm.201100732
- Jeon, S. O., & Lee, J. Y. (2012). Phosphine oxide derivatives for organic light emitting diodes. *Journal of Materials Chemistry*, 22(10), 4233-4243. doi: Doi 10.1039/C1jm14832j
- Jeon, W. S., Park, T. J., Kim, S. Y., Pode, R., Jang, J., & Kwon, J. H. (2009). Ideal host and guest system in phosphorescent OLEDs. *Organic Electronics*, 10(2), 240-246. doi: DOI 10.1016/j.orgel.2008.11.012
- Jorgensen, M., Norrman, K., Gevorgyan, S. A., Tromholt, T., Andreasen, B., & Krebs, F. C. (2012). Stability of Polymer Solar Cells. *Advanced Materials*, 24(5), 580-612. doi: DOI 10.1002/adma.201104187
- Joseph, J., & Jemmis, E. D. (2006). Red-, Blue-, or No-Shift in Hydrogen Bonds: A Unified Explanation. *Journal of the American Chemical Society*, 129(15), 4620-4632. doi: 10.1021/ja067545z
- Jou, J.-H., Lin, Y.-X., Peng, S.-H., Li, C.-J., Yang, Y.-M., Chin, C.-L., . . . Hu, J.-P. (2013). Highly Efficient Yellow Organic Light Emitting Diode with a Novel Wet- and Dry-Process Feasible Iridium Complex Emitter. *Advanced Functional Materials*. doi: DOI: 10.1002/adfm.201302013
- Jou, J. H., Peng, S. H., Chiang, C. I., Chen, Y. L., Lin, Y. X., Jou, Y. C., . . . Wang, C. W. (2013). High efficiency yellow organic light-emitting diodes with a solution-



- processed molecular host-based emissive layer. *Journal of Materials Chemistry C*, 1(8), 1680-1686. doi: Doi 10.1039/C2tc00249c
- Jou, J. H., Shen, S. M., Chen, S. H., Wu, M. H., Wang, W. B., Wang, H. C., . . . Shyue, J. J. (2010). Highly efficient orange-red phosphorescent organic light-emitting diode using 2,7-bis(carbazol-9-yl)-9,9-ditolylfluorene as the host. *Applied Physics Letters*, 96(14). doi: Artn 143306 Doi 10.1063/1.3374326
- Jou, J. H., Wang, W. B., Chen, S. Z., Shyue, J. J., Hsu, M. F., Lin, C. W., . . . Liu, S. W. (2010). High-efficiency blue organic light-emitting diodes using a 3,5-di(9H-carbazol-9-yl) tetraphenylsilane host via a solution-process. *Journal of Materials Chemistry*, 20(38), 8411-8416. doi: Doi 10.1039/C0jm01163k
- Jou, J. H., Wang, W. B., Shen, S. M., Kumar, S., Lai, I. M., Shyue, J. J., . . . Wu, C. C. (2011). Highly efficient blue organic light-emitting diode with an oligomeric host having high triplet-energy and high electron mobility. *Journal of Materials Chemistry*, 21(26), 9546-9552. doi: Doi 10.1039/C1jm10609k
- Jou, J. H., Wang, Y. S., Lin, C. H., Shen, S. M., Chen, P. C., Tang, M. C., . . . Chen, C. T. (2012). Nearly non-roll-off high efficiency fluorescent yellow organic light-emitting diodes (vol 21, pg 12613, 2011). *Journal of Materials Chemistry*, 22(48), 25482-25482.
- Kalinowski, J., Stampor, W., Mezyk, J., Cocchi, M., Virgili, D., Fattori, V., & Di Marco, P. (2002). Quenching effects in organic electrophosphorescence. *Physical Review B*, 66(23). doi: Artn 235321 Doi 10.1103/Physrevb.66.235321
- Kalyani, N. T., & Dhoble, S. J. (2012). Organic light emitting diodes: Energy saving lighting technology-A review. *Renewable & Sustainable Energy Reviews*, 16(5), 2696-2723. doi: DOI 10.1016/j.rser.2012.02.021
- Kappaun, S., Slugovc, C., & List, E. J. W. (2008). Phosphorescent organic light-emitting devices: Working principle and iridium based emitter materials. *International Journal of Molecular Sciences*, 9(8), 1527-1547. doi: Doi 10.3390/Ijms9081527
- Kemerink, M., Kramer, J. M., Gommans, H. H. P., & Janssen, R. A. J. (2006). Temperature-dependent built-in potential in organic semiconductor devices. *Applied Physics Letters*, 88(19). doi: Artn 192108 Doi 10.1063/1.2205007
- Kepler, R. G., Caris, J. C., Avakian, P., & Abramson, E. (1963). Triplet excitons and Delayed Fluorescence in Anthracene Crystals. *Physical Review Letters*, 10, 3. doi: 10.1103/PhysRevLett.10.400
- Kido, J., & Iizumi, Y. (1998). Fabrication of highly efficient organic electroluminescent devices. *Applied Physics Letters*, 73(19), 2721-2723. doi: Doi 10.1063/1.122570
- Kido, J., Kimura, M., & Nagai, K. (1995). Multilayer White Light-Emitting Organic Electroluminescent Device. *Science*, 267(5202), 1332-1334. doi: DOI 10.1126/science.267.5202.1332
- Kim, B. S., & Lee, J. Y. (2014). Phosphine Oxide Type Bipolar Host Material for High Quantum Efficiency in Thermally Activated Delayed Fluorescent Device. *Acs Applied Materials & Interfaces*, 6(11), 8396-8400. doi: 10.1021/am501301g
- Kim, H., Byun, Y., Das, R. R., Choi, B. K., & Ahn, P. S. (2007). Small molecule based and solution processed highly efficient red electrophosphorescent organic light emitting devices. *Applied Physics Letters*, 91(9). doi: Artn 093512 Doi 10.1063/1.2776016
- Kim, J. S., Cacialli, F., Cola, A., Gigli, G., & Cingolani, R. (1999). Increase of charge carriers density and reduction of Hall mobilities in oxygen-plasma treated indium-tin-oxide anodes. *Applied Physics Letters*, 75(1), 19-21. doi: Doi 10.1063/1.124263
- Ko, L. C., Liu, T. Y., Chen, C. Y., Yeh, C. L., Tseng, S. R., Chao, Y. C., . . . Horng, S. F. (2010). Multi-layer organic light-emitting diodes processed from solution

- using phosphorescent dendrimers in a polymer host. *Organic Electronics*, 11(6), 1005-1009. doi: DOI 10.1016/j.orgel.2010.03.014
- Kohler, A., & Bassler, H. (2009). Triplet states in organic semiconductors. *Materials Science & Engineering R-Reports*, 66(4-6), 71-109. doi: DOI 10.1016/j.mser.2009.09.001
- Kohnen, A., Irion, M., Gather, M. C., Rehmann, N., Zacharias, P., & Meerholz, K. (2010). Highly color-stable solution-processed multilayer WOLEDs for lighting application. *Journal of Materials Chemistry*, 20(16), 3301-3306. doi: Doi 10.1039/B924968k
- Kouki, F., Karsi, N., Lang, P., Horowitz, G., & Bouchriha, H. (2012). Effect of self assembled monolayers on charge carrier photogeneration in sexithiophene based diodes. *Synthetic Metals*, 162(19-20), 1741-1745. doi: DOI 10.1016/j.synthmet.2011.09.028
- Krummacher, B. C., Mathai, M., So, F., Choulis, S., & Choong, V. E. (2007). Light extraction from solution-based processable electrophosphorescent organic light-emitting diodes. *JOURNAL OF DISPLAY TECHNOLOGY*, 3(2), 200-210. doi: Doi 10.1109/Jdt.2007.895361
- Kumru, M. E., Springer, J., Sarac, A. S., & Bismarck, A. (2001). Electrografting of thiophene, carbazole, pyrrole and their copolymers onto carbon fibers: electrokinetic measurements, surface composition and morphology. *Synthetic Metals*, 123(3), 391-402. doi: Doi 10.1016/S0379-6779(01)00338-1
- Lai, S. L., Chan, M. Y., Lee, C. S., & Lee, S. T. (2003). Investigation of calcium as high performance cathode in small-molecule based organic light-emitting devices. *Journal of Applied Physics*, 94(11), 7297-7299. doi: Doi 10.1063/1.1623326
- Lampman, G. M., Pavia, D. L., Kriz, G. S., & Vyvyan, J. R. (2010). *Spectroscopy* (4 ed.). Canada: Brooks/Cole.
- Le, Q. T., Yan, L., Gao, Y. G., Mason, M. G., Giesen, D. J., & Tang, C. W. (2000). Photoemission study of aluminum/tris-(8-hydroxyquinoline) aluminum and aluminum/LiF/tris-(8-hydroxyquinoline) aluminum interfaces. *Journal of Applied Physics*, 87(1), 375-379. doi: Doi 10.1063/1.371870
- Lee, C. W., & Lee, J. Y. (2013). High Quantum Efficiency in Solution and Vacuum Processed Blue Phosphorescent Organic Light Emitting Diodes Using a Novel Benzofuopyridine-Based Bipolar Host Material. *Advanced Materials*, 25(4), 596-600. doi: DOI 10.1002/adma.201203180
- Lee, C. W., Yook, K. S., & Lee, J. Y. (2013). Synthesis and device application of hybrid host materials of carbazole and benzofuran for high efficiency solution processed blue phosphorescent organic light-emitting diodes. *Organic Electronics*, 14(3), 1009-1014. doi: DOI 10.1016/j.orgel.2013.01.025
- Lee, J., Chopra, N., Eom, S. H., Zheng, Y., Xue, J. G., So, F., & Shi, J. M. (2008). Effects of triplet energies and transporting properties of carrier transporting materials on blue phosphorescent organic light emitting devices. *Applied Physics Letters*, 93(12). doi: Artn 123306 Doi 10.1063/1.2978235
- Lee, J., Lee, J. I., Lee, J. Y., & Chu, H. Y. (2009). Enhanced efficiency and reduced roll-off in blue and white phosphorescent organic light-emitting diodes with a mixed host structure. *Applied Physics Letters*, 94(19). doi: Artn 193305 Doi 10.1063/1.3136861
- Lee, J., Shizu, K., Tanaka, H., Nomura, H., Yasuda, T., & Adachi, C. (2013). Oxadiazole- and triazole-based highly-efficient thermally activated delayed fluorescence emitters for organic light-emitting diodes. *Journal of Materials Chemistry C*, 1(30), 4599-4604. doi: Doi 10.1039/C3tc30699b

- Lee, J. H., Wu, C. I., Liu, S. W., Huang, C. A., & Chang, Y. (2005). Mixed host organic light-emitting devices with low driving voltage and long lifetime. *Applied Physics Letters*, 86(10). doi: Artn 103506 Doi 10.1063/1.1879093
- Lee, K. H., Jang, H. W., Kim, K. B., Tak, Y. H., & Lee, J. L. (2004). Mechanism for the increase of indium-tin-oxide work function by O-2 inductively coupled plasma treatment. *Journal of Applied Physics*, 95(2), 586-590. doi: Doi 10.1063/1.1633351
- Lee, S. Y., Yasuda, T., Nomura, H., & Adachi, C. (2012). High-efficiency organic light-emitting diodes utilizing thermally activated delayed fluorescence from triazine-based donor-acceptor hybrid molecules. *Applied Physics Letters*, 101(9). doi: Artn 093306 Doi 10.1063/1.4749285
- Lee, T. W., Chung, Y., Kwon, O., & Park, J. J. (2007). Self-organized gradient hole injection to improve the performance of polymer electroluminescent devices. *Advanced Functional Materials*, 17(3), 390-396. doi: DOI 10.1002/adfm.200600278
- Lee, T. W., Kwon, O., Kim, M. G., Park, S. H., Chung, J., Kim, S. Y., . . . Pu, L. (2005). Hole-injecting conducting-polymer compositions for highly efficient and stable organic light-emitting diodes. *Applied Physics Letters*, 87(23). doi: Artn 231106 Doi 10.1063/1.2132072
- Li, C. L., Su, Y. J., Tao, Y. T., Chou, P. T., Chien, C. H., Cheng, C. C., & Liu, R. S. (2005). Yellow and red electrophosphors based on linkage isomers of phenylisoquinolinyridium complexes: Distinct differences in photophysical and electroluminescence properties. *Advanced Functional Materials*, 15(3), 387-395. doi: DOI 10.1002/adfm.200305100
- Li, L., Liu, J., Yu, Z., & Pei, Q. (2013). Single-Layer White Polymer Phosphorescent Light-Emitting Diodes Employing Poly(Ethylene Glycol) Dimethyl Ether Blended in the Emissive Layer as Functional Interlayer. *JOURNAL OF DISPLAY TECHNOLOGY*, 9, 483-489. doi: 10.1109/JDT.2012.2234436
- Li, L., Liu, J., Yu, Z. B., & Pei, Q. B. (2011). Highly efficient blue phosphorescent polymer light-emitting diodes by using interfacial modification. *Applied Physics Letters*, 98(20). doi: Artn 201110 Doi 10.1063/1.3593380
- Liaptsis, G., & Meerholz, K. (2013). Crosslinkable TAPC-Based Hole-Transport Materials for Solution-Processed Organic Light-Emitting Diodes with Reduced Efficiency Roll-Off. *Advanced Functional Materials*, 23(3), 359-365. doi: DOI 10.1002/adfm.201201197
- Lin, Y. J., Yang, F. M., Huang, C. Y., Chou, W. Y., Chang, J., & Lien, Y. C. (2007). Increasing the work function of poly(3,4-ethylenedioxythiophene) doped with poly(4-styrenesulfonate) by ultraviolet irradiation. *Applied Physics Letters*, 91(9). doi: Artn 092127 Doi 10.1063/1.2777147
- Liou, G. S., Huang, N. K., & Yang, Y. L. (2006). Synthesis, photoluminescent and electrochromic properties of new aromatic poly(amine-hydrazide)s and poly(amine-1,3,4-oxadiazole)s derived from 4,4'-dicarboxy-4"-methyltriphenylamine. *European Polymer Journal*, 42(10), 2283-2291. doi: DOI 10.1016/j.eurpolymj.2006.06.021
- Lita, A. E., & Sanchez, J. E. (1999). Characterization of surface structure in sputtered Al films: Correlation to microstructure evolution. *Journal of Applied Physics*, 85(2), 876-882. doi: Doi 10.1063/1.369206
- Liu, B., Xu, M., Tao, H., Ying, L., Zou, J., Wu, H., & Peng, J. (2013). Highly efficient red phosphorescent organic light-emitting diodes based on solution processed emissive layer. *Journal of Luminescence*, 142, 35-39. doi: dx.doi.org/10.1016/j.jlumin.2013.03.032

- Liu, D., Fina, M., Guo, J. H., Chen, X. B., Liu, G., Johnson, S. G., & Mao, S. S. (2009). Organic light-emitting diodes with carbon nanotube cathode-organic interface layer. *Applied Physics Letters*, 94(1). doi: Artn 013110 Doi 10.1063/1.3049605
- Liu, M. S., Niu, Y. H., Ka, J. W., Yip, H. L., Huang, F., Luo, J. D., . . . Jen, A. K. Y. (2008). Thermally Cross-Linkable Hole-Transporting Materials for Improving Hole Injection in Multilayer Blue-Emitting Phosphorescent Polymer Light-Emitting Diodes. *Macromolecules*, 41(24), 9570-9580. doi: Doi 10.1021/Ma801374w
- Liu, S. W., Chang, Y. T., Lee, C. C., Yuan, C. H., Liu, L. A., Chen, Y. S., . . . Chen, C. T. (2013). Single-Layer Blue Electrophosphorescent Organic Light-Emitting Diodes Based on Small-Molecule Mixed Hosts: Comparison between the Solution and Vacuum Fabrication Processes. *Japanese Journal of Applied Physics*, 52(1). doi: Artn 012101 Doi 10.7567/Jjap.52.012101
- Liu, S. W., Yuan, C. H., Yeh, S. J., Wu, M. F., Chen, C. T., & Lee, C. C. (2011). Efficiency enhancement of solution-processed single-layer blue-phosphorescence organic light-emitting devices having co-host materials of polymer (PVK) and small-molecule (SimCP2). *Journal of the Society for Information Display*, 19(4), 346-352. doi: Doi 10.1889/Jsid19.4.346
- Liu, Z. Y., Tseng, S. R., Chao, Y. C., Chen, C. Y., Meng, H. F., Horng, S. F., . . . Chen, S. H. (2011). Solution-processed small molecular electron transport layer for multilayer polymer light-emitting diodes. *Synthetic Metals*, 161(5-6), 426-430. doi: DOI 10.1016/j.synthmet.2010.12.021
- Lu, H. T., & Yokoyama, M. (2004). Plasma preparation on indium-tin-oxide anode surface for organic light emitting diodes. *Journal of Crystal Growth*, 260(1-2), 186-190. doi: DOI 10.1016/j.jcrysgro.2003.08.032
- Lu, J. H., Ma, Z. H., Meng, B., Sui, D., Zhang, B. H., Xie, Z. Y., . . . Wang, L. X. (2011). Phosphonate functionalized oxadiazole derivative as an efficient electron transporting material for solution-processed blue electrophosphorescent devices. *Optics Express*, 19(23), A1241-A1249.
- Luo, Y. C., Aziz, H., Popovic, Z. D., & Xu, G. (2006). Electric-field-induced fluorescence quenching in dye-doped tris(8-hydroxyquinoline) aluminum layers. *Applied Physics Letters*, 89(10). doi: Artn 103505 Doi 10.1063/1.2337269
- Maeda, Y., Kubota, T., & Yamauchi, H. (2007). Hydration changes of poly(2-(2-methoxyethoxy)ethyl methacrylate) during thermosensitive phase separation in water. *Langmuir*, 23(22), 11259-11265. doi: Doi 10.1021/La7016006
- Maeda, Y., Yamauchi, H., Fujisawa, M., Sugihara, S., & Ikeda, I. (2007). Infrared Spectroscopic Investigation of Poly(2-methoxyethyl vinyl ether) during Thermosensitive Phase Separation in Water. *Langmuir*, 23(12), 6561-6566. doi: 10.1021/la700387w
- Malliaras, G. G., Salem, J. R., Brock, P. J., & Scott, J. C. (1998). Photovoltaic measurement of the built-in potential in organic light emitting diodes and photodiodes. *Journal of Applied Physics*, 84(3), 1583-1587. doi: Doi 10.1063/1.368227
- Martinez, J. F. G., Nieto-Carvajal, I., Abad, J., & Colchero, J. (2012). Nanoscale measurement of the power spectral density of surface roughness: how to solve a difficult experimental challenge. *Nanoscale Research Letters*, 7. doi: Artn 174 Doi 10.1186/1556-276x-7-174
- Martinez, N. F., & Garcia, R. (2006). Measuring phase shifts and energy dissipation with amplitude modulation atomic force microscopy. *Nanotechnology*, 17(7), S167-S172. doi: Doi 10.1088/0957-4484/17/7/S11
- Mason, M. G., Tang, C. W., Hung, L. S., Raychaudhuri, P., Madathil, J., Giesen, D. J., . . . Bredas, J. L. (2001). Interfacial chemistry of Alq(3) and LiF with reactive

- metals. *Journal of Applied Physics*, 89(5), 2756-2765. doi: Doi 10.1063/1.1324681
- . Material Safety Data Sheet for 2,2,3,3,4,4,5,5-Octafluoro-1-pentanol. (2012 12 April 2012) Retrieved 3 October, 2013, from <http://www.sigmaaldrich.com/catalog/product/aldrich/269433?lang=en&region=MY>
- Mathai, M. K., Choong, V. E., Choulis, S. A., Krummacher, B., & So, F. (2006). Highly efficient solution processed blue organic electrophosphorescence with 14 lm/W luminous efficacy. *Applied Physics Letters*, 88(24). doi: Artn 243512 Doi 10.1063/1.2212060
- Méhes, G., Goushi, K., Potscavage Jr., W. J., & Adachi, C. (2014). Influence of host matrix on thermally-activated delayed fluorescence: Effects on emission lifetime, photoluminescence quantum yield, and device performance. *Organic Electronics*, 15(9), 2027–2037. doi: 10.1016/j.orgel.2014.05.027
- Mertens, R. (2012). A Brief History of OLED Lighting, from <http://lighting.com/history-oled-lighting/>
- Meyer, J., Hamwi, S., Kroger, M., Kowalsky, W., Riedl, T., & Kahn, A. (2012). Transition Metal Oxides for Organic Electronics: Energetics, Device Physics and Applications. *Advanced Materials*, 24(40), 5408-5427. doi: DOI 10.1002/adma.201201630
- Meyer, J., Zilberberg, K., Riedl, T., & Kahn, A. (2011). Electronic structure of Vanadium pentoxide: An efficient hole injector for organic electronic materials. *Journal of Applied Physics*, 110(3). doi: Artn 033710 Doi 10.1063/1.3611392
- Mi, B. X., Gao, Z. Q., Liao, Z. J., Huang, W., & Chen, C. H. (2010). Molecular hosts for triplet emitters in organic light-emitting diodes and the corresponding working principle. *Science China-Chemistry*, 53(8), 1679-1694. doi: DOI 10.1007/s11426-010-4043-7
- Mikhnenko, O. V. (2012). *Singlet and Triplet Excitons in Organic Semiconductors*. PhD, University of Groningen, Netherlands.
- Monkman, A. P. (2013). Singlet Generation from Triplet Excitons in Fluorescent Organic Light-Emitting Diodes. *ISRN Materials Science*, 2013, 19. doi: dx.doi.org/10.1155/2013/670130
- Moujoud, A., Oh, S. H., Shin, H. S., & Kim, H. J. (2010). On the mechanism of conductivity enhancement and work function control in PEDOT:PSS film through UV-light treatment. *Physica Status Solidi a-Applications and Materials Science*, 207(7), 1704-1707. doi: DOI 10.1002/pssa.200983711
- Murawski, C., Leo, K., & Gather, M. C. (2013a). Efficiency Roll-Off in Organic Light-Emitting Diodes. *Advanced Materials*. doi: DOI: 10.1002/adma.201301603
- Murawski, C., Leo, K., & Gather, M. C. (2013b). Efficiency Roll-Off in Organic Light-Emitting Diodes. *Advanced Materials*, 1-27. doi: DOI: 10.1002/adma.201301603
- Nagata, T., Oha, S., Chikyow, T., & Wakayama, Y. (2011). Effect of UV-ozone treatment on electrical properties of PEDOT:PSS film. *Organic Electronics*, 12(2), 279-284. doi: DOI 10.1016/j.orgel.2010.11.009
- Nakagawa, T., Ku, S. Y., Wong, K. T., & Adachi, C. (2012). Electroluminescence based on thermally activated delayed fluorescence generated by a spirobifluorene donor-acceptor structure. *Chemical Communications*, 48(77), 9580-9582. doi: Doi 10.1039/C2cc31468a
- Nakajima, H., Tong-on, A., Sumano, N., Sittisard, K., Rattanasuporn, S., Euaruksakul, C., . . . Songsiriritthigul, P. (2013). Photoemission Spectroscopy and Photoemission Electron Microscopy Beamline at the Siam Photon Laboratory.

- 11th International Conference on Synchrotron Radiation Instrumentation (Sri 2012)*, 425. doi: Unsp 132020 Doi 10.1088/1742-6596/425/13/132020
- Nakanotani, H., Masui, K., Nishide, J., Shibata, T., & Adachi, C. (2013). Promising operational stability of high-efficiency organic light-emitting diodes based on thermally activated delayed fluorescence. *Scientific Reports*, 3. doi: Artn 2127 Doi 10.1038/Srep02127
- Nicolai, H. T., Mandoc, M. M., & Blom, P. W. M. (2011). Electron traps in semiconducting polymers: Exponential versus Gaussian trap distribution. *Physical Review B*, 83(19). doi: Artn 195204 Doi 10.1103/Physrevb.83.195204
- Niu, Y. H., Ma, H., Xu, Q. M., & Jen, A. K. Y. (2005). High-efficiency light-emitting diodes using neutral surfactants and aluminum cathode. *Applied Physics Letters*, 86(8). doi: Artn 083504 Doi 10.1063/1.1865327
- Noh, Y. Y., Lee, C. L., Kim, J. J., & Yase, K. (2003). Energy transfer and device performance in phosphorescent dye doped polymer light emitting diodes. *Journal of Chemical Physics*, 118(6), 2853-2864. doi: Doi 10.1063/1.1535211
- Okumoto, K., Kanno, H., Hamada, Y., Takahashi, H., & Shibata, K. (2006). Green fluorescent organic light-emitting device with external quantum efficiency of nearly 10% (vol 89, art no 063504 2006). *Applied Physics Letters*, 89(16). doi: Artn 169901 Doi 10.1063/1.2359696
- Padmaperuma, A. B., Sapochak, L. S., & Burrows, P. E. (2006). New charge transporting host material for short wavelength organic electrophosphorescence: 2,7-bis(diphenylphosphine oxide)-9,9-dimethylfluorene. *Chemistry of Materials*, 18(9), 2389-2396. doi: Doi 10.1021/Cm0600677
- Park, J. J., Park, T. J., Jeon, W. S., Pode, R., Jang, J., Kwon, J. H., . . . Chae, M. Y. (2009). Small molecule interlayer for solution processed phosphorescent organic light emitting device. *Organic Electronics*, 10(1), 189-193. doi: DOI 10.1016/j.orgel.2008.08.014
- Park, J. K., Hwang, G. S., Chin, B. D., Kang, N. S., & Lee, T. W. (2012). Electrophosphorescent devices with solution processible emitter and hole transport layer stack. *Current Applied Physics*, 12, E38-E41. doi: DOI 10.1016/j.cap.2011.04.030
- Park, S. M., Yu, H., Park, M. G., Han, S. Y., Kang, S. W., Park, H. M., & Kim, J. W. (2012). Quantitative analysis of an organic thin film by XPS, AFM and FT-IR. *Surface and Interface Analysis*, 44(2), 156-161. doi: Doi 10.1002/Sia.3786
- Park, Y., Choong, V., Gao, Y., Hsieh, B. R., & Tang, C. W. (1996). Work function of indium tin oxide transparent conductor measured by photoelectron spectroscopy. *Applied Physics Letters*, 68(19), 2699-2701. doi: Doi 10.1063/1.116313
- Parker, I. D., Cao, Y., & Yang, C. Y. (1999). Lifetime and degradation effects in polymer light-emitting diodes. *Journal of Applied Physics*, 85(4), 2441-2447. doi: Doi 10.1063/1.369564
- Parker, I. D., & Kim, H. H. (1994). Fabrication of Polymer Light-Emitting-Diodes Using Doped Silicon Electrodes. *Applied Physics Letters*, 64(14), 1774-1776. doi: Doi 10.1063/1.111804
- Pereira, L. (2012). Organic Light-Emitting Diodes The Use of Rare-Earth and Transition Metals (pp. 343).
- Perepichka, D. F., Meng, H., & Ling, M.-M. (2007). *Organic Light-Emitting Materials and Devices*. USA: CRC Press.
- Pimentel, G. C., & McClellan, A. L. (1960). *The Hydrogen Bond* (1 ed.). san Francisco: W.H. Freeman.
- Piromreun, P., Oh, H., Shen, Y. L., Malliaras, G. G., Scott, J. C., & Brock, P. J. (2000). Role of CsF on electron injection into a conjugated polymer. *Applied Physics*

- Letters*, 77(15), 2403-2405. doi: Pii [S0003-6951(00)04341-2] Doi 10.1063/1.1317547
- Poon, C. Y., & Bhushan, B. (1995). Comparison of surface roughness measurements by stylus profiler, AFM and non-contact optical profiler. *Wear*, 190(1), 76-88. doi: Doi 10.1016/0043-1648(95)06697-7
- Popova, G. Y., Chesalov, Y. A., & Andrushkevich, T. V. (2004). In situ FTIR study of pyridine-3-carbaldehyde adsorption on TiO<sub>2</sub> (anatase) and V-Ti-O catalyst. *Reaction Kinetics and Catalysis Letters*, 83(2), 353-360. doi: Doi 10.1023/B:Reac.0000046097.85909.B2
- Rao, M. V. M., Su, Y. K., & Huang, T. S. (2013). Cesium Carbonate as an Effective Interfacial Layer on the High Performance of Polymer Light-Emitting Devices. *Ecs Solid State Letters*, 2(1), R5-R7. doi: Doi 10.1149/2.002302ssl
- Ray, D., Patankar, M. P., Periasamy, N., & Narasimhan, K. L. (2005). Measurement of built-in voltage of organic semiconductor devices. *Synthetic Metals*, 155(2), 349-351. doi: DOI 10.1016/j.synthmet.2005.09.011
- Reineke, S., & Baldo, M. A. (2012). Recent progress in the understanding of exciton dynamics within phosphorescent OLEDs. *Physica Status Solidi a-Applications and Materials Science*, 209(12), 2341-2353. doi: DOI 10.1002/pssa.201228292
- Reineke, S., Lindner, F., Schwartz, G., Seidler, N., Walzer, K., Lussem, B., & Leo, K. (2009). White organic light-emitting diodes with fluorescent tube efficiency. *Nature*, 459(7244), 234-U116. doi: Doi 10.1038/Nature08003
- Reineke, S., Thomschke, M., Lussem, B., & Leo, K. (2013). White organic light-emitting diodes: Status and perspective. *Reviews of Modern Physics*, 85(3), 1245-1293. doi: DOI 10.1103/RevModPhys.85.1245
- Reineke, S., Walzer, K., & Leo, K. (2007). Triplet-exciton quenching in organic phosphorescent light-emitting diodes with Ir-based emitters. *Physical Review B*, 75(12). doi: Artn 125328 Doi 10.1103/Physrevb.75.125328
- Remmers, M., Neher, D., Gruner, J., Friend, R. H., Gelinck, G. H., Warman, J. M., . . . Bredas, J. L. (1996). The optical, electronic, and electroluminescent properties of novel poly(p-phenylene)-related polymers. *Macromolecules*, 29(23), 7432-7445. doi: Doi 10.1021/Ma960599g
- Sasabe, H., & Kido, J. (2011). Multifunctional Materials in High-Performance OLEDs: Challenges for Solid-State Lighting. *Chemistry of Materials*, 23(3), 621-630. doi: Doi 10.1021/Cm1024052
- Schlaf, R., Parkinson, B. A., Lee, P. A., Nebesny, K. W., Jabbour, G., Kippelen, B., . . . Armstrong, N. R. (1998). Photoemission spectroscopy of LiF coated Al and Pt electrodes. *Journal of Applied Physics*, 84(12), 6729-6736. doi: Doi 10.1063/1.369000
- Scholes, G. D. (2003). Long-range resonance energy transfer in molecular systems. *Annual Review of Physical Chemistry*, 54, 57-87. doi: DOI 10.1146/annurev.physchem.54.011002.103746
- Schroder, D. K. (2006). *Semiconductor Material and Device Characterization* (Third ed.). New Jersey: John Wiley & Sons.
- Schroegel, P., Tomkeviciene, A., Strohriegl, P., Hoffmann, S. T., Kohler, A., & Lennartz, C. (2011). A series of CBP-derivatives as host materials for blue phosphorescent organic light-emitting diodes. *Journal of Materials Chemistry*, 21(7), 2266-2273. doi: Doi 10.1039/C0jm03321a
- Segal, M., Baldo, M. A., Holmes, R. J., Forrest, S. R., & Soos, Z. G. (2003). Excitonic singlet-triplet ratios in molecular and polymeric organic materials. *Physical Review B*, 68(7). doi: Artn 075211 Doi 10.1103/Physrevb.68.075211

- Segal, M., Singh, M., Rivoire, K., Difley, S., Van Voorhis, T., & Baldo, M. A. (2007). Extrafluorescent electroluminescence in organic light-emitting devices. *Nature Materials*, 6(5), 374-378. doi: Doi 10.1038/Nmat1885
- Senthilkumar, M., Sahoo, N. K., Thakur, S., & Tokas, R. B. (2005). Characterization of microroughness parameters in gadolinium oxide thin films: A study based on extended power spectral density analyses. *Applied Surface Science*, 252(5), 1608-1619. doi: DOI 10.1016/j.apsusc.2005.02.122
- Seo, C. W., & Lee, J. Y. (2011). High efficiency in two color and three color phosphorescent white organic light-emitting diodes using a 2,7-substituted 9-phenylcarbazole derivative as the host material. *Organic Electronics*, 12(9), 1459-1464. doi: DOI 10.1016/j.orgel.2011.05.026
- Shirota, Y. (2005). Photo- and electroactive amorphous molecular materials - molecular design, syntheses, reactions, properties, and applications. *Journal of Materials Chemistry*, 15(1), 75-93. doi: Doi 10.1039/B413819h
- So, F., & Kondakov, D. (2010). Degradation Mechanisms in Small-Molecule and Polymer Organic Light-Emitting Diodes. *Advanced Materials*, 22(34), 3762-3777. doi: DOI 10.1002/adma.200902624
- So, F., Krummacher, B., Mathai, M. K., Poplavskyy, D., Choulis, S. A., & Choong, V. E. (2007). Recent progress in solution processable organic light emitting devices. *Journal of Applied Physics*, 102(9). doi: Artn 091101 Doi 10.1063/1.2804122
- Sokolik, I., Priestley, R., Walser, A. D., Dorsinville, R., & Teng, C. W. (1996). Bimolecular reactions of singlet excitons in tris(8-hydroxyquinoline) aluminum. *Applied Physics Letters*, 69(27), 4168-4170. doi: Doi 10.1063/1.116974
- Song, Y. H., Yeh, S. J., Chen, C. T., Chi, Y., Liu, C. S., Yu, J. K., . . . Lee, G. H. (2004). Bright and efficient, non-doped, phosphorescent organic red-light-emitting diodes. *Advanced Functional Materials*, 14(12), 1221-1226. doi: DOI 10.1002/adfm.200400137
- Sonoyama, T., Ito, M., Seki, S., Miyashita, S., Xia, S., Brooks, J., . . . Brown, J. J. (2008). Ink-jet-printable phosphorescent organic light-emitting-diode devices. *Journal of the Society for Information Display*, 16(12), 1229-1236. doi: Doi 10.1889/Jsid16.12.1229
- Spreitzer, H., Becker, H., Kluge, E., Kreuder, W., Schenk, H., Demandt, R., & Schoo, H. (1998). Soluble phenyl-substituted PPVs - New materials for highly efficient polymer LEDs. *Advanced Materials*, 10(16), 1340-+. doi: Doi 10.1002/(Sici)1521-4095(199811)10:16<1340::Aid-Adma1340>3.0.Co;2-G
- Sun, J., Gerberich, W. W., & Francis, L. F. (2007). Transparent, conductive polymer blend coatings from latex-based dispersions. *Progress in Organic Coatings*, 59(2), 115-121. doi: DOI 10.1016/j.porgcoat.2007.01.019
- Sun, Y. R., Giebink, N. C., Kanno, H., Ma, B. W., Thompson, M. E., & Forrest, S. R. (2006). Management of singlet and triplet excitons for efficient white organic light-emitting devices. *Nature*, 440(7086), 908-912. doi: Doi 10.1038/Nature04645
- Syu, W. S., Lin, S. C., Tseng, S. R., Chen, C. Y., Liu, C. Y., Chao, Y. C., . . . Horng, S. F. (2010). Efficient multilayer red fluorescent polymer light-emitting diodes by host and guest blend system. *Synthetic Metals*, 160(9-10), 871-875. doi: DOI 10.1016/j.synthmet.2010.01.037
- Tanaka, H., Shizu, K., Miyazaki, H., & Adachi, C. (2012). Efficient green thermally activated delayed fluorescence (TADF) from a phenoxazine-triphenyltriazine (PXZ-TRZ) derivative. *Chemical Communications*, 48(93), 11392-11394. doi: Doi 10.1039/C2cc36237f



- Tang, C. W., & Vanslyke, S. A. (1987). Organic Electroluminescent Diodes. *Applied Physics Letters*, 51(12), 913-915. doi: Doi 10.1063/1.98799
- Tao, Y. T., Yang, C. L., & Qin, J. G. (2011). Organic host materials for phosphorescent organic light-emitting diodes. *Chemical Society Reviews*, 40(5), 2943-2970. doi: Doi 10.1039/C0cs00160k
- Tokito, S., Iijima, T., Suzuri, Y., Kita, H., Tsuzuki, T., & Sato, F. (2003). Confinement of triplet energy on phosphorescent molecules for highly-efficient organic blue-light-emitting devices. *Applied Physics Letters*, 83(3), 569-571. doi: Doi 10.1063/1.1594834
- Tsai, M. H., Hong, Y. H., Chang, C. H., Su, H. C., Wu, C. C., Matoliukstyte, A., . . . Hsu, C. P. (2007). 3-(9-carbazolyl)carbazoles and 3,6-di(9-carbazolyl)carbazoles as effective host materials for efficient blue organic electrophosphorescence. *Advanced Materials*, 19(6), 862-+. doi: DOI 10.1002/adma.200600822
- Tse, S. C., Cheung, C. H., & So, S. K. (2010). Charge Transport and Injection in Amorphous Organic Semiconductors. In F. So (Ed.), *Electronics Materials, Processing, Devices and Applications* (First edition ed., pp. 61-109). Boca Raton: CRC Press.
- Tseng, S. R., Meng, H. F., Lee, K. C., & Horng, S. F. (2008). Multilayer polymer light-emitting diodes by blade coating method. *Applied Physics Letters*, 93(15). doi: Artn 153308 Doi 10.1063/1.2999541
- Tsutsui, T. (1997). Progress in electroluminescent devices using molecular thin films. *Mrs Bulletin*, 22(6), 39-45.
- Tyan, Y.-S. (2011). Organic light-emitting-diode lighting overview. *Journal of Photonics for Energy*, 1(1), 15. doi: 10.1117/1.3529412
- Ulman, A. (2010). *Characterization of Organic Thin films*. New York: Momentum Press.
- Uoyama, H., Goushi, K., Shizu, K., Nomura, H., & Adachi, C. (2012). Highly efficient organic light-emitting diodes from delayed fluorescence. *Nature*, 492(7428), 234-+. doi: Doi 10.1038/Nature11687
- Walker, B., Tamayo, A., Yang, J. H., Brzezinski, J. Z., & Nguyena, T. Q. (2008). Solution-processed small molecule-based blue light-emitting diodes using conjugated polyelectrolytes as electron injection layers. *Applied Physics Letters*, 93(6). doi: Artn 063302 Doi 10.1063/1.2968189
- Walzer, K., Maennig, B., Pfeiffer, M., & Leo, K. (2007). Highly efficient organic devices based on electrically doped transport layers. *Chemical Reviews*, 107(4), 1233-1271. doi: Doi 10.1021/Cr050156n
- Wang, H., Xie, L., Peng, Q., Meng, L., Wang, Y., Yi, Y., & Wang, P. (2014). Novel Thermally Activated Delayed Fluorescence Materials–Thioxanthone Derivatives and Their Applications for Highly Efficient OLEDs. *Advanced Materials*, 1-7. doi: 10.1002/adma.201401393
- Wang, Q., Chen, Y. W., Zheng, Y. N., Ai, N., Han, S. H., Xu, W., . . . Cao, Y. (2013). Solvent treatment as an efficient anode modification method to improve device performance of polymer light-emitting diodes. *Organic Electronics*, 14(2), 548-553. doi: DOI 10.1016/j.orgel.2012.11.025
- Wang, Q., Zhou, Y., Zheng, H., Shi, J., Li, C. Z., Su, C. M. Q., . . . Cao, Y. (2011). Modifying organic/metal interface via solvent treatment to improve electron injection in organic light emitting diodes. *Organic Electronics*, 12(11), 1858-1863. doi: DOI 10.1016/j.orgel.2011.07.021
- Wang, Z. B., Helander, M. G., Qiu, J., Puzzo, D. P., Greiner, M. T., Hudson, Z. M., . . . Lu, Z. H. (2011). Unlocking the full potential of organic light-emitting diodes on flexible plastic. *Nature Photonics*, 5(12), 753-757. doi: DOI 10.1038/nphoton.2011.259

- Williams, D., & Fleming, I. (2008). *Spectroscopic Methods in Organic Chemistry* (6 ed.). UK: McGraw Hill.
- Wohlgenannt, M., Tandon, K., Mazumdar, S., Ramasesha, S., & Vardeny, Z. V. (2001). Formation cross-sections of singlet and triplet excitons in pi-conjugated polymers. *Nature*, 409(6819), 494-497. doi: Doi 10.1038/35054025
- Wu, C. C., Wu, C. I., Sturm, J. C., & Kahn, A. (1997). Surface modification of indium tin oxide by plasma treatment: An effective method to improve the efficiency, brightness, and reliability of organic light emitting devices. *Applied Physics Letters*, 70(11), 1348-1350. doi: Doi 10.1063/1.118575
- Wu, C. I., Lin, C. T., Chen, Y. H., Chen, M. H., Lu, Y. J., & Wu, C. C. (2006). Electronic structures and electron-injection mechanisms of cesium-carbonate-incorporated cathode structures for organic light-emitting devices. *Applied Physics Letters*, 88(15). doi: Artn 152104 Doi 10.1063/1.2192982
- Wu, H. B., Zhou, G. J., Zou, J. H., Ho, C. L., Wong, W. Y., Yang, W., . . . Cao, Y. (2009). Efficient Polymer White-Light-Emitting Devices for Solid-State Lighting. *Advanced Materials*, 21(41), 4181-+. doi: DOI 10.1002/adma.200900638
- Wu, W. S., Inbasekaran, M., Hudack, M., Welsh, D., Yu, W. L., Cheng, Y., . . . O'Brien, J. (2004). Recent development of polyfluorene-based RGB materials for light emitting diodes. *Microelectronics Journal*, 35(4), 343-348. doi: DOI 10.1016/j.mejo.2003.07.001
- Xia, Y. J., & Ouyang, J. Y. (2010). Significant Conductivity Enhancement of Conductive Poly(3,4-ethylenedioxythiophene): Poly(styrenesulfonate) Films through a Treatment with Organic Carboxylic Acids and Inorganic Acids. *Acs Applied Materials & Interfaces*, 2(2), 474-483. doi: Doi 10.1021/Am900708x
- Xia, Y. J., Sun, K., & Ouyang, J. Y. (2012). Highly conductive poly(3,4-ethylenedioxythiophene):poly(styrene sulfonate) films treated with an amphiphilic fluoro compound as the transparent electrode of polymer solar cells. *Energy & Environmental Science*, 5(1), 5325-5332. doi: Doi 10.1039/C1ee02475b
- Xiong, Y., & Deng, F. (2011). Efficient white polymer light-emitting diodes based on a phosphorescent iridium complex and a fluorescent silole and carbazole copolymer. *Journal of Physics and Chemistry of Solids*, 72(9), 1077-1080. doi: DOI 10.1016/j.jpcs.2011.06.002
- Xu, Y. F., Wang, Y., Liang, J. J., Huang, Y., Ma, Y. F., Wan, X. J., & Chen, Y. S. (2009). A Hybrid Material of Graphene and Poly (3,4-ethyldioxythiophene) with High Conductivity, Flexibility, and Transparency. *Nano Research*, 2(4), 343-348. doi: DOI 10.1007/s12274-009-9032-9
- Xu, Z. Q., Li, J., Yang, J. P., Cheng, P. P., Zhao, J., Lee, S. T., . . . Tang, J. X. (2011). Enhanced performance in polymer photovoltaic cells with chloroform treated indium tin oxide anode modification. *Applied Physics Letters*, 98(25). doi: Artn 253303 Doi 10.1063/1.3601853
- Yamamori, A., Adachi, C., Koyama, T., & Taniguchi, Y. (1998). Doped organic light emitting diodes having a 650-nm-thick hole transport layer. *Applied Physics Letters*, 72(17), 2147-2149. doi: Doi 10.1063/1.121304
- Yang, L. (2008). *Materials Characterization Introduction to Microscopic and Spectroscopic Methods* (First ed.). Singapore: John Wiley & Sons.
- Yang, X. H., Jaiser, F., Klinger, S., & Neher, D. (2006). Blue polymer electrophosphorescent devices with different electron-transporting oxadiazoles. *Applied Physics Letters*, 88(2). doi: Artn 021107 Doi 10.1063/1.2162693

- Yang, X. H., Muller, D. C., Neher, D., & Meerholz, K. (2006). Highly efficient polymeric electrophosphorescent diodes. *Advanced Materials*, 18(7), 948-+. doi: DOI 10.1002/adma.200501867
- Yersin, H., Rausch, A. F., Czerwieniec, R., Hofbeck, T., & Fischer, T. (2011). The triplet state of organo-transition metal compounds. Triplet harvesting and singlet harvesting for efficient OLEDs. *Coordination Chemistry Reviews*, 255(21-22), 2622-2652. doi: DOI 10.1016/j.ccr.2011.01.042
- Yook, K. S., Jang, S. E., Jeon, S. O., & Lee, J. Y. (2010). Fabrication and Efficiency Improvement of Soluble Blue Phosphorescent Organic Light-Emitting Diodes Using a Multilayer Structure Based on an Alcohol-Soluble Blue Phosphorescent Emitting Layer. *Advanced Materials*, 22(40), 4479-4483. doi: DOI 10.1002/adma.201002034
- Yook, K. S., Jeon, S. O., Kim, O. Y., & Lee, J. Y. (2010). Solution Processed Blue Phosphorescent Organic Light Emitting Diodes Using a Phosphine Oxide Host Material. *Electrochemical and Solid State Letters*, 13(6), J71-J73. doi: Doi 10.1149/1.3367630
- Yook, K. S., & Lee, J. Y. (2012). Solution Processed p-Doped Hole Transport Layer for Polymer Light-Emitting Diodes. *Electrochemical and Solid State Letters*, 15(3), J11-J13. doi: Doi 10.1149/2.004203esl
- You, J. D., Tseng, S. R., Meng, H. F., Yen, F. W., Lin, I. F., & Horng, S. F. (2009). All-solution-processed blue small molecular organic light-emitting diodes with multilayer device structure. *Organic Electronics*, 10(8), 1610-1614. doi: DOI 10.1016/j.orgel.2009.06.020
- Zhang, B. H., Tan, G. P., Lam, C. S., Yao, B., Ho, C. L., Liu, L. H., . . . Wang, L. X. (2012). High-Efficiency Single Emissive Layer White Organic Light-Emitting Diodes Based on Solution-Processed Dendritic Host and New Orange-Emitting Iridium Complex. *Advanced Materials*, 24(14), 1873-1877. doi: DOI 10.1002/adma.201104758
- Zhang, Q., Li, B., Huang, S., Nomura, H., Tanaka, H., & Adachi, C. (2014). Efficient blue organic light-emitting diodes employing thermally activated delayed fluorescence. *Nature Photonics*, 8(4), 326-332. doi: 10.1038/NPHOTON.2014.12
- Zhang, Q. S., Li, J., Shizu, K., Huang, S. P., Hirata, S., Miyazaki, H., & Adachi, C. (2012). Design of Efficient Thermally Activated Delayed Fluorescence Materials for Pure Blue Organic Light Emitting Diodes. *Journal of the American Chemical Society*, 134(36), 14706-14709. doi: Doi 10.1021/Ja306538w
- Zhang, S., Li, L., & Kumar, A. (2009). *Materials Characterization Techniques* (1 ed.). Boca Raton: CRC Press.
- Zhao, Y., Duan, L., Zhang, D. Q., Hou, L. D., Qiao, J., Wang, L. D., & Qiu, Y. (2012). Small molecular phosphorescent organic light-emitting diodes using a spin-coated hole blocking layer. *Applied Physics Letters*, 100(8). doi: Artn 083304 Doi 10.1063/1.3688300
- Zheng, S. Z., & Wong, K. Y. (2013). Enhanced performance in polymer solar cells by the use of a halogenated indium tin oxide anode. *Applied Physics Letters*, 102(5). doi: Artn 053302 Doi 10.1063/1.4790624
- Zhong, C. M., Duan, C. H., Huang, F., Wu, H. B., & Cao, Y. (2011). Materials and Devices toward Fully Solution Processable Organic Light-Emitting Diodes. *Chemistry of Materials*, 23(3), 326-340. doi: Doi 10.1021/Cm101937p
- Zhou, H. Q., Zhang, Y., Seifert, J., Collins, S. D., Luo, C., Bazan, G. C., . . . Heeger, A. J. (2013). High-Efficiency Polymer Solar Cells Enhanced by Solvent Treatment. *Advanced Materials*, 25(11), 1646-1652. doi: DOI 10.1002/adma.201204306

- Zhou, X., He, J., Liao, L. S., Lu, M., Ding, X. M., Hou, X. Y., . . . Lee, S. T. (2000). Real-time observation of temperature rise and thermal breakdown processes in organic LEDs using an IR imaging and analysis system. *Advanced Materials*, 12(4), 265-269. doi: Doi 10.1002/(Sici)1521-4095(200002)12:4<265::Aid-Adma265>3.0.Co;2-L
- Zhou, Y. F., Yuan, Y. B., Cao, L. F., Zhang, J., Pang, H. Q., Lian, J. R., & Zhou, X. (2007). Improved stability of OLEDs with mild oxygen plasma treated PEDOT : PSS. *Journal of Luminescence*, 122, 602-604. doi: DOI 10.1016/j.jlumin.2006.01.236
- Zhou, Y. F., Yuan, Y. B., Lian, J. R., Zhang, J., Pang, H. Q., Cao, L. F., & Zhou, X. (2006). Mild oxygen plasma treated PEDOT : PSS as anode buffer layer for vacuum deposited organic light-emitting diodes. *Chemical Physics Letters*, 427(4-6), 394-398. doi: DOI 10.1016/j.cplett.2006.06.035
- Zhu, M. R., Ye, T. L., He, X., Cao, X. S., Zhong, C., Ma, D. G., . . . Yang, C. L. (2011). Highly efficient solution-processed green and red electrophosphorescent devices enabled by small-molecule bipolar host material. *Journal of Materials Chemistry*, 21(25), 9326-9331. doi: Doi 10.1039/C1jm10987a
- Zilberberg, K., Meyer, J., & Riedl, T. (2013). Solution Processed Metal-Oxides for Organic Electronic Devices. *Journal of Materials Chemistry C*. doi: DOI: 10.1039/c0xx00000x
- Zuniga, C. A., Abdallah, J., Haske, W., Zhang, Y. D., Coropceanu, I., Barlow, S., . . . Marder, S. R. (2013). Crosslinking Using Rapid Thermal Processing for the Fabrication of Efficient Solution-Processed Phosphorescent Organic Light-Emitting Diodes. *Advanced Materials*, 25(12), 1739-1744. doi: DOI 10.1002/adma.201204518

## LIST OF PUBLICATIONS AND PAPERS PRESENTED

The author has contributed to the following publications:

### Journals

1. **K.H. Yeoh**, C.L. Chua and K.L. Woon, “Effects of nanoscale surface modification and triplet energy shielding of a singlelayer solution processed blue phosphorescent organic light emitting diode by using Triton X-100”, *Synthetic Metals*, 172 (2013) 44-48.  
*(Highlighted by the front cover of Synthetic Metals)*
2. **K.H. Yeoh**, C.Y.B. Ng, C.L. Chua, N.A. Talik and K.L. Woon, “High power efficiency solution-processed double-layer blue phosphorescent organic light-emitting diode by controlling charge transport at the emissive layer and heterojunction”, *Physica Status Solidi: Rapid Research Letters*, 7 (2013) 421-424.
3. **K.H. Yeoh**, N.A. Talik, T.J. Whitcher, C.Y.B. Ng, K.L. Woon, “Effects of hole injection layer modification on efficiency of a single layer solution processed blue phosphorescent organic light emitting diodes”, *Journal Physics D: Applied Physics*, 47 (2014) 205103.

The following papers finished during this period are either overlap or the subjects are outside the scope of this thesis.

4. C.Y.B. Ng, **K.H. Yeoh**, T.J. Whitcher, N.A. Talik, K.L. Woon, T. Saisopa, H. Nakajima, R. Supruangnet and P. Songsiriritthigul, “High Efficiency Solution Processed Fluorescent Yellow Organic Light Emitting Diode through Fluorinated Alcohol Treatment at the Emissive Layer/cathode Interface”, *Journal Physics D: Applied Physics*, 46 (2014) 015106.

*(C.Y.B Ng and **K.H. Yeoh** contribute equally to this work)*

5. T. J. Whitcher, **K. H. Yeoh**, C.Y.B. Ng, N.A. Talik, C. L. Chua, K. L. Woon, N. Chanlek, H. Nakajima, T. Saisopa, P. Songsiriritthigul, T. Saisopa, S. Oswald and B.K. Yap, “Enhancement of the work function of indium tin oxide by surface modification using caesium fluoride”, *Journal of Physics D: Applied Physics*, 46 (2013) 475102.
6. T.J. Whitcher, **K.H. Yeoh**, C.L. Chua, K.L. Woon, N. Chanlek, H. Nakajima, T. Saisopa and P. Songsiriritthigul, “The effect of carbon contamination and argon ion sputtering on the work function of chlorinated indium tin oxide”, *Current Applied Physics*, 14 (2014) 472.
7. Malcolm S.Y. Tang, T. J. Whitcher, **K.H. Yeoh**, C.L. Chua, K.L. Woon, P.L. Show, Y.K. Lin and T.C. Ling, “The removal of metallic single-walled carbon nanotubes using an aqueous two-phase system”, *Journal of Nanoscience and Nanotechnology*, 14 (2014) 3398.

### **Paper presented in international conference:**

1. **K.H. Yeoh** and K.L. Woon, “Efficiency enhancement of solution processed single layer blue phosphorescent organic light emitting diodes by using Polyethylene glycol mono [4-(1,1,3,3-tetramethylbutyl)phenyl] ether (Triton X-100)” in *16th International Workshop on Inorganic and Organic Electroluminescence 2012 (EL 2012)*, Hong Kong Baptist University (HKBU), Hong Kong.
2. **K.H. Yeoh**, N.A. Talik, C.Y.B. Ng and K.L. Woon, “Efficiency enhancement of solution processed blue phosphorescent organic light emitting diodes by using perfluorinated ionomer doped PEDOT:PSS” in *3<sup>rd</sup> International Conference on the Advancement of Materials and Nanotechnology 2013 (ICAMN III 2013)*, Penang, Malaysia.

**(Best poster award)**

### **Patent**

1. Enhanced Electron Injection Organic Light Emitting Diode, Patent, PI2013003279, 2013.